Towards optimal maintenance planning of existing structures based on time-dependent reliability analysis

Morteza Ahmadivala

No d'ordre : 0000

EDSPIC : 0000

Université Clermont Auvergne

École Doctorale

Sciences pour l'Ingénieur de Clermont-Ferrand

THÈSE

présentée par

Morteza Ahmadivala

en vue d'obtenir le grade de

Docteur d'Université

(Spécialité : Génie Mécanique)

Vers une planification optimale de la maintenance des structures existantes sur la base d'une analyse de fiabilité en fonction du temps

soutenue le **lundi 14 decembre 2020**, à Sigma Clermont, devant un jury composé de:

Pr. Franck Schoefs,	Université de Nantes	Rapporteur
Pr. Alan O'Connor,	Trinity College Dublin	Rapporteur
Pr. John Dalsgaard Sørensen,	Aalborg University	Examinateur
Dr. David Clair,	Université Clermont Auvergne	Examinateur
Pr. Nicolas Gayton,	SIGMA Clermont	Co-directeur
Dr. André Orcesi,	Université Gustave	Co-directeur
Dr. Cécile Mattrand,	SIGMA Clermont	Encadrante
Dr. Thierry Yalamas,	Phimeca Engineering	Encadrant
Mr. Jacques Berthellemy,	Cerema	Membre invité

Université Clermont Auvergne,CNRS, SIGMA Clermont, Institut Pascal

F-63000 Clermont-Ferrand, France

Towards optimal maintenance planning of existing structures based on time-dependent reliability analysis

Morteza Ahmadivala

A thesis submitted for the degree of

Doctor of Philosophy

Mechanical Engineering

Jury

Pr. Franck Schoefs,	Université de Nantes	Reviewer
Pr. Alan O'Connor,	Trinity College Dublin	Reviewer
Pr. John Dalsgaard Sørensen,	Aalborg University	Examiner
Dr. David Clair,	Université Clermont Auvergne	Examiner
Pr. Nicolas Gayton,	SIGMA Clermont	Thesis co-director
Dr. André Orcesi,	Université Gustave Eiffel	Thesis co-director
Dr. Cécile Mattrand,	SIGMA Clermont	Academic supervisor
Dr. Thierry Yalamas,	Phimeca Engineering	Industrial supervisor
Mr. Jacques Berthellemy,	Cerema	Invited member

Université Clermont Auvergne, CNRS, SIGMA Clermont, Institut Pascal

F-63000 Clermont-Ferrand, France

Synthèse Des Travaux

INFRASTAR, projet européen

INFRASTAR signifie "Innovation and Networking for Fatigue and Reliability Analysis of Structures - Training for Assessment of Risk". Ce projet a reçu un financement du programme de recherche et d'innovation Horizon 2020 de l'Union européenne dans le cadre des actions Marie Skłodowska-Curie. INFRASTAR a impliqué douze ESR (Early Stage Researcher), travaillant dans différents instituts de recherche, universités et entreprises dans cinq pays européens (France, Allemagne, Suisse, Danemark et Pologne). La société d'accueil de ce doctorat était PHIMECA Engineering en France, en coopération avec l'Université Clermont Auvergne et l'IFSTTAR (aujourd'hui Université Gustave Eiffel).

L'objectif principal de l'INFRASTAR était d'améliorer les connaissances, les compétences, l'expertise et de proposer des solutions innovantes pour une maintenance et une gestion optimales des ouvrages civils contre la fatigue (en particulier pour les ponts et les éoliennes). Trois défis majeurs ont été abordés dans le cadre de ce programme: 1) la modélisation avancée du comportement en fatigue du béton, 2) de nouvelles méthodes d'essais non destructifs pour la détection précoce des dommages vieillis, et 3) une approche probabiliste de la fiabilité des structures en fatigue. À cet égard, trois lots de travaux peuvent être reconnus où quatre ESR travaillaient sous chaque lot de travaux. Le premier lot de travaux était lié à «la surveillance et l'auscultation ». Le deuxième groupe de travail portait sur les « modèles de structure et d'action » et le

troisième sur les « approches fondées sur la fiabilité pour la prise de décision ».

Pour atteindre cet objectif, une expérience croisée et une coopération interdisciplinaire entre les ESR au sein de différents centres de recherche étaient nécessaires. Pour cette raison, différents détachements en plus des semaines de formation ont été envisagés pour chaque ESR, afin de visiter les autres centres de recherche du programme afin de pouvoir collaborer avec d'autres ESR et centres de recherche. Deux détachements (chacun d'une durée de trois mois) ont été envisagés pour ce projet. Le premier détachement a eu lieu à l'EPFL, département de génie civil, et le second a été réalisé à l'IFSTTAR et au Cerema. En outre, trois semaines de formation ont été suivies au cours de ce doctorat respectivement au BAM Berlin, à l'EPFL et à l'Université d'Aalborg.

Synthèse générale

L'entretien des structures est une partie importante de la Gestion du Cycle de Vie (GCV) des structures. Il est considéré comme un ensemble de pratiques mises en œuvre pour garantir qu'une structure remplit ses fonctions avec un niveau adéquat de service et de sécurité pendant sa durée de vie. Une bonne planification de la maintenance peut aider à éviter les défaillances imprévues. Par conséquent, il peut être considéré comme un outil permettant d'assurer le retour sur investissement des propriétaires de structures après une période de temps prévue. Les pratiques visant à optimiser la planification de la maintenance des structures civiles ont gagné plus d'attention au cours des dernières décennies, car le nombre de structures vieillissantes augmente alors que le budget de maintenance est limité.

Les structures peuvent être confrontées à divers modes de défaillance au cours de leur durée de vie. Les informations statistiques sur les structures métalliques montrent que l'affouillement des pieux / fondations, le flambage, la fatigue, l'impact et la fracture sont parmi les modes de défaillance les plus courants. Bien que l'affouillement soit un mode de défaillance important pour tous les ponts, la rupture par fatigue semble être

la plus critique pour les ponts en acier. Il est évident qu'une bonne planification de la maintenance devrait impliquer plusieurs actions pour atténuer l'occurrence de défaillance par n'importe quel mode de défaillance. Cependant, les modes de défaillance les plus susceptibles de se produire recevront une plus grande attention dans le cadre de la maintenance. On peut donc dire que la maintenance contre la fatigue a la priorité pour les structures en acier.

La fatigue est l'un des principaux processus de dégradation des structures métalliques soumises à des charges cycliques (par exemple, le trafic et les charges environnementales). Le processus de fatigue commence par l'amorçage de la fissure. Les fissures initiales peuvent alors se propager sous chargement cyclique, jusqu'à atteindre des longueurs critiques si elles ne sont pas contrôlées, ce qui peut mettre la structure dans une situation critique. Un défi dans l'évaluation de la fatigue est lié à l'incertitude impliquée dans le problème qui peut provenir de différentes sources, telles que la charge de fatigue, les propriétés du matériau, la géométrie (par exemple, la géométrie de la soudure), les modèles d'accumulation de fatigue ou de croissance de fissure, la géométrie de la soudure, etc. Un autre défi peut être lié aux outils et méthodes pour étudier l'initiation et la propagation des fissures afin d'identifier les stratégies de réparation efficaces.

Afin de faire face aux incertitudes liées à la fatigue, certains indicateurs tels que la fiabilité et le risque peuvent être utilisés pour évaluer la probabilité de défaillance par fatigue et les conséquences associées. Effectuer une analyse de fiabilité de la fatigue dans un cadre dépendant du temps semble plus raisonnable, puisque la fatigue est un processus de dégradation dépendant du temps associé à des paramètres d'entrées stochastiques. Une analyse de fiabilité en fonction du temps diffère fondamentalement d'une analyse indépendante du temps puisque l'objectif de la première est de trouver la probabilité de défaillance cumulée pour une période de temps donnée. Trouver cette probabilité de défaillance est particulièrement difficile pour les problèmes avec des fonctions de performance non monotones et coûteuses en calcul.

Les enquêtes sur l'efficacité des actions de réparation de la fatigue sur une struc-

ture donnée dans le cadre de la planification de la maintenance structurelle nécessitent la réalisation d'expériences de propagation des fissures. L'exécution d'expériences de fatigue en laboratoire peut prendre beaucoup de temps et nécessiter des ressources financières considérables. En conséquence, les expériences basées sur la simulation par l'Analyse par Éléments Finis (AEF) peuvent être très fructueuses pour alléger les dépenses requises. Il convient de souligner que la réalisation d'une telle analyse à l'aide des Méthodes des Éléments Finis (MEF) classiques peut nécessiter un coût de calcul très élevé, en raison de la limitation de ces méthodes qui exigent une mise à jour de l'ensemble du maillage après l'application de chaque cycle de charge. Pour résoudre ce problème, des méthodes avancées comme la XFEM (eXtended Finite Element Method) ont été développées afin d'effectuer l'analyse de propagation des fissures avec des ressources de calcul plus faibles.

Par rapport aux nouvelles structures, les structures existantes ont déjà expérimenté les conditions de chargement réelles. La Surveillance de l'État des Structures (SES) peut donc être utilisée sur des structures existantes pour évaluer leurs états. La SES est un processus axé sur l'observation, la mesure, l'enregistrement et le traitement des données liées à la structure en temps réel. Il fournit des informations précieuses aux propriétaires de structures et aux décideurs. Ces informations peuvent être utilisées pour mettre à jour des indicateurs de performance, tels que la fiabilité et le risque pour une structure donnée, afin de proposer une meilleure planification de la maintenance. Outre les défis tels que l'acquisition et le stockage de données, le traitement des données et l'utilisation des informations SES dans le contexte de la planification de la maintenance structurelle peuvent être un défi. La SES peut parfois conduire à une énorme quantité de données qui peuvent également être très complexes. Le traitement et l'interprétation de ces données sur une structure donnée nécessitent l'utilisation d'outils avancés de statistique et de science des données, tels que les méthodes de séries chronologiques, l'apprentissage en profondeur, etc.

D'après ce qui a été brièvement discuté ci-dessus, on peut facilement se rendre compte que l'amélioration des méthodes et des stratégies dans le cadre d'une planific-

ation optimale de la maintenance des structures existantes est une tâche très complexe et exhaustive. Cela implique de nombreux défis provenant de différentes sources qui doivent être traités correctement afin d'améliorer les pratiques actuelles en matière de planification de la maintenance structurelle. En conséquence, les objectifs et les contributions de cette recherche à une planification optimale de l'entretien des structures sont décrits dans la section suivante.

Objectif et portée de la recherche doctorale

L'objectif global de cette thèse est d'apporter des contributions au domaine de recherche de la planification optimale de la maintenance des structures existantes. En considérant un cadre d'optimisation de la maintenance basé sur la fiabilité, l'objectif est de relever les défis liés aux problématiques suivantes :

1. Approche de fiabilité en fonction du temps pour l'analyse de la fiabilité en fatigue
2. Modélisation de la croissance des fissures de fatigue pour caractériser les projets de réparation
3. Évaluation de la fiabilité en fonction du temps de propagation des fissures de fatigue
4. Traitement des données de surveillance à long terme pour l'analyse de fatigue

Relever ces défis conduit à identifier quatre tâches principales, comme décrit ci-après.

Comme mentionné précédemment, une évaluation de la fiabilité de la fatigue en fonction du temps permet d'évaluer la probabilité cumulée de défaillance d'une structure due à la fatigue pendant un intervalle de temps donné. Effectuer une telle évaluation peut être très difficile. D'une part, la fonction de performance associée peut être très irrégulière et non monotone, ce qui peut affecter la précision du résultat final. D'autre part, l'évaluation de la fonction de performance associée peut être coûteuse

en calcul, car elle peut être effectuée via un AEF qui affecte l'efficacité des méthodes existantes. Par conséquent, de nouvelles approches de fiabilité en fonction du temps sont nécessaires pour évaluer la probabilité de défaillance cumulative avec un compromis raisonnable entre précision et efficacité. Par conséquent, une nouvelle approche de fiabilité en fonction du temps est développée dans ce contexte, appelée AK-SYS-t. Cette méthode associe le problème de fiabilité en fonction du temps au problème de fiabilité du système connecté en série, puis elle utilise l'efficacité des méthodes avancées de fiabilité du système comme AK-SYS pour l'évaluation de la fiabilité en fonction du temps. Pour cette raison, la méta-modélisation Krigeage est utilisée pour remplacer les fonctions de performance coûteuses à évaluer, et la fonction d'apprentissage d'AK-SYS est utilisée pour enrichir efficacement les méta-modèles initiaux. Un autre objectif ici est lié à la proposition d'une stratégie pour construire la courbe complète de la probabilité cumulée de défaillance pour un intervalle de temps donné par AK-SYS-t. Cette courbe est un outil essentiel pour les décideurs pour décider du temps et des types d'actions de maintenance.

L'évaluation de la durée de vie à la fatigue est généralement traitée soit dans le cadre d'une approche de durée de vie sûre reposant sur des courbes S-N, soit d'une approche de tolérance aux dommages reposant sur le mécanisme de fracture. L'analyse de fatigue utilisant le mécanisme de fracture semble appropriée pour les structures existantes puisqu'elles peuvent avoir déjà développé des fissures de fatigue à divers endroits critiques. La propagation de fissures nécessite des outils et des techniques avancés tels que la méthode XFEM pour pouvoir gérer la complexité ajoutée au modèle par les fissures de fatigue. En particulier, en considérant un détail de soudure nervure-pont dans les plaques de pont orthotropes, une stratégie est proposée pour étudier l'utilité de la méthode XFEM pour un problème de fissuration indésirable dans ce détail qui est lié à la situation où les fissures commencent à se développer vers la plaque de pont. De telles fissures peuvent atteindre une longueur critique sans être détectées. De plus, l'efficacité de deux solutions de réparation sur un tel problème de fissuration est étudiée en effectuant des analyses de propagation de fissure en utilisant la méthode XFEM.

Le prochain objectif de cette étude est d'examiner la fonctionnalité de la méthode de fiabilité en fonction du temps proposée, AK-SYS-t, sur les modèles de propagation des fissures de fatigue. L'évaluation de la fiabilité en fonction du temps pour les modèles probabilistes de propagation des fissures est difficile car la fonction de performance associée est hautement non linéaire. De plus, l'évaluation de la fiabilité en fonction du temps pour les modèles de propagation de fissures est exigeante en termes de calcul, car elle nécessite un calcul cycle par cycle du Facteur d'Intensité de Contrainte (FIC). Cela nécessite encore plus de ressources de calcul si le FIC est approché par AEF. À cet égard, il pourrait être nécessaire de formuler des hypothèses et des étapes de simplification pour être en mesure de résoudre ces problèmes. Par conséquent, l'application d'AK-SYS-t sur des modèles probabilistes de propagation de fissures associés à des étapes et des hypothèses de simplification est étudiée sur deux études de cas d'application.

La dernière partie de cette thèse propose une approche pour employer des méthodes de séries chronologiques sur des données de surveillance à long terme pour l'analyse de fatigue. Pour cette raison, les données de suivi à long terme des viaducs de Chillon sont utilisées. Les données sont collectées pendant près de deux ans à l'aide de jauges de contrainte avec une fréquence de 50, 100 ou 200 Hz. Les difficultés ici peuvent être liées aux effets de saisonnalité disponibles dans les données de surveillance et à l'immense taille des données de surveillance. Les modèles conventionnels pour la modélisation de la charge de fatigue tels que le rainflow et les chaînes de Markov sont incapables de gérer l'effet saisonnier en raison des hypothèses de stationnarité. En conséquence, des méthodes de séries chronologiques telles que l'ARIMA saisonnière (Auto Regressive Integrated Moving Average, ou moyenne mobile intégrée auto-régressive) peuvent être utilisées pour résoudre ce problème. La difficulté ici peut être liée à la taille des données de surveillance à long terme. À cet égard, une approche est proposée pour traiter ce problème en transformant les données de surveillance de grande taille en un petit ensemble d'observations. A cet égard, la durée de surveillance est d'abord divisée en intervalles de temps plus petits. On peut alors adapter une distribution aux données de surveillance pour chaque intervalle de temps. Ensuite, les paramètres des distributions

associées peuvent être utilisés pour remplacer les observations dans chaque intervalle de temps. Par conséquent, toutes les données de surveillance peuvent être remplacées par une série chronologique avec moins d'observations. L'ARIMA saisonnière peut ensuite être facilement appliquée sur le nouvel ensemble de données pour fournir un modèle de charge pour l'analyse de fatigue. Ce modèle de charge peut être utilisé dans l'approche S-N ou le mécanisme de fracture avec quelques ajustements.

Résumé

Selon ce qui a été décrit ci-dessus, cinq chapitres sont considérés pour cette thèse comme suit :

- Le chapitre 1 sert d'introduction.
- Le chapitre 2 est consacré aux concepts et pratiques généraux au sein du GCV structurel pour résoudre les problèmes de fatigue.
- Le chapitre 3 est lié à l'analyse de fiabilité en fonction du temps. Une nouvelle méthodologie pour résoudre les problèmes dépendant du temps est présentée dans ce chapitre, appuyée par quelques exemples tirés de la littérature.
- Le chapitre 4 se concentre sur la fourniture de stratégies pour étudier l'utilité de méthodes avancées telles que XFEM pour évaluer les problèmes de fatigue structurelle et caractériser les solutions de réparation possibles dans un contexte de propagation de fissures. De plus, les stratégies proposées sont appliquées sur un détail de fatigue de cas réel.
- Le chapitre 5 se concentre sur la connexion de la méthode de fiabilité en fonction du temps proposée aux problèmes de propagation des fissures en décrivant les étapes et les hypothèses nécessaires sur deux exemples d'application.

Une étude supplémentaire présentée dans cette thèse est liée à l'application de méthodes de séries chronologiques sur des données de surveillance structurelle à long

terme. Ce travail a été réalisé sous la direction du professeur Eugen Brühwiler à l'EPFL. Ce travail est présenté à l'annexe A car il n'a pas été utilisé en relation avec d'autres approches dans le cadre de cette thèse.

Abstract

Civil engineering structures play an important role in any country for improving the economy together with the social and environmental welfare. An unwanted failure might cause significant impacts at different levels for the structure owner and for users. Fatigue is one of the main degradation processes on steel structures that causes structural failure before the end of the designed service life. To avoid unexpected failures due to fatigue, a comprehensive structural Life Cycle Management (LCM) is required to minimize the life-cycle cost and maximize the structural service life. One of the main objectives within the LCM can be related to optimizing the structural maintenance planning. Achieving this goal is a challenging task which requires to address some challenges such as predicting the structural performance under uncertainty, employing Structural Health Monitoring (SHM) data to reduce uncertainties, taking into account crack propagation behavior for given components, reliability- and cost-informed decision making, and effect of maintenance actions among others. Accordingly, following contributions are considered in this research to improve the capabilities of structural LCM which are explained shortly in the sequel.

1. Developing a new time-dependent reliability method for fatigue reliability analysis.

2. Investigating the effectiveness of advanced crack propagation tools to study unwanted fatigue cracking problems and characterizing some possible repair actions on a real case study.

3. Introducing the assumptions and simplification steps required to integrate the

proposed time-depend reliability method with crack propagation models to approximate the time-dependent fatigue reliability.

As the first contribution of this thesis a new time-dependent reliability method called AK-SYS-t is proposed. This method provides an efficient and accurate tool to evaluate time-dependent reliability of a component compared to other available methods. AK-SYS-t relates the time-dependent reliability to system reliability problems and tries to exploit the efficient system reliability methods such as AK-SYS towards time-dependent reliability analysis. It is worth mentioning that time-dependent reliability analysis is necessary in this context since the performance deterioration (such as fatigue) is a time-dependent process associated with time-dependent parameters such as fatigue loading.

Another related topic is the study of crack propagation phenomenon with advanced modeling tools such as Finite Element Method (FEM) and Extended Finite Element Method (XFEM). For illustration purposes, the crack in the root of a fillet weld is considered (common fatigue detail in bridges with orthotropic deck plates). One important issue investigated herein is the influence of the transversal tension in the deck plate on the direction of the crack propagation. It is shown how increasing the transversal tension in the deck plate may change the crack propagation towards the deck plate. Such cracks are considered dangerous since they are hard to inspect and detect. In the end, XFEM is used to investigate the effectiveness of two possible repair solutions.

A supplementary contribution is related to introducing the required steps in order to integrate the newly developed time-depend reliability method with crack propagation problems through some applicational examples. This is a challenging task since performing the time-dependent reliability analysis for such problems requires a cycle-by-cycle calculation of stress intensity factors which requires huge computational resources. Therefore, the aim here is to introduce the assumptions and simplification steps in order to adopt the AK-SYS-t for fatigue reliability analysis. Accordingly, two

examples are considered. The first example considers an analytical model to calculate the stress intensity factors while the second example AK-SYS-t is coupled with a finite element model (Code_Aster) and the stress intensity factors are calculated by XFEM method.

In the end, an additional contribution of this study to the structural LCM is added in annex. This work is related to employing time series methods such as seasonal ARIMA to provide a load model for long-term fatigue loading that can capture more details of the loading scenario regarding the seasonal effects in traffic loading. This is an important advantage of this method compared to other methods (e.g. rain-flow counting) since they are unable of dealing with problems with seasonality effect. This approach can be used for long-term monitoring data that are recorded with high frequency. It should be noted that employing time series methods for such data is not a straightforward task. Therefore, some data treatment is required first to be able to apply such methods for long-term monitoring data.

Acknowledgments

Hereby, I would like to show my gratitude and appreciation to those from whom I received a great deal of help and support to accomplish this thesis.

I would first like to thank my supervisors, Pr. Nicolas Gayton, Dr. Cécile Mattrand, Dr. André Orcesi, and Dr. Thierry Yalamas. I really appreciate your invaluable support to fulfill my PhD. Your insightful feedback pushed me to sharpen my thinking and brought my research skills to a higher level.

I would like to acknowledge my colleagues during this PhD at the research and development group of Phimeca Engineering especially Antoine Dumas, Gillaume Causse and Barbara Heinter for assisting me during my PhD in Phimeca.

In addition to that, I would like to thank Mr. Jacques Berthellemy from Cerema for his great help during this PhD. Moreover, I would like to thank the EMGCU lab of IFSTTAR in Marne-la-Vallée and MCS lab of EPFL for providing me great conditions in order to perform my research during the secondments of this PhD.

It should also be mentioned that this research has been performed under INFRASTAR program that has received funding from the European Union's Horizon 2020 research and innovation program. Therefore, I would like to show my appreciation for such programs that are devoted to train researchers for a better future.

Finally, I would like to thank my parents for their wise counsel and sympathetic ear. You are always there for me.

List of abbreviations

AERS Adaptive Extreme Response Surface

AK-MCS Adaptive Kriging using Monte-Carlo Simulation

ARIMA Auto-Regressive Integrated Moving Average

AK-SYS Active learning and Kriging-based SYStem reliability method

ARMA Auto-Regressive Moving Average

BAM Bundesanstalt für Materialforschung und -prüfung

CDF Cumulative Distribution Function

COV Coefficient of Variation

DoE Design of Experiment

EDF Électricité de France

EGO Efficient Global Optimization

EI Expected Improvement

EICS Equivalent Initial Crack Size

EPFL École polytechnique fédérale de Lausanne

ESR Early Stage Researchers

EVB Extreme-Value Based

FEA Finite Element Analysis

FEM Finite Element Method

FORM First Order Reliability Method

GTA Gas Tungsten Arc

IFSTTAR Institut français des sciences et technologies des transports, de l'aménagement et des réseaux

INFRASTAR Innovation and Networking for Fatigue and Reliability Analysis of Structures - Training for Assessment of Risk

IQOA Image de la Qualité des Ouvrages d'Art: Image of the Quality of Bridges

IS Importance Sampling

ITSEOA l'Instruction Technique pour la Surveillance et l'Entretien des Ouvrages d'Art

KL Karhunen-Loeve

LCM Life Cycle Management

LEFM Linear Elastic Fracture Mechanism

LHS Latin Hypercube Sampling

MCMC Markov Chain Monte Carlo

MCS Monte Carlo Simulation

MPP Most Probable Point

MTS Maximum Tangential Stress

NBI National Bridge Inventor

NERS Nestd Extreme Response Surface

NTPM Nested Time Prediction Model

OCB Out-Crossing Based

OSD Orthotropic Steel Deck

PCA Principle Component Analysis

PCE Polynomial Chaos Expansion

PDF Probability Density Function

RAM Random Access Memory

SHM Structural Health Monitoring

SIF Stress Intensity Factor

SILK SIngle-Loop Kriging method

SORM Second Order Reliability Method

SS Subset Simulation

XFEM Extended Finite Element Method

Contents

List of Figures

List of Tables

Chapter 1 : Introduction

1.1 INFRASTAR, European project

INFRASTAR stands for "Innovation and Networking for Fatigue and Reliability Analysis of Structures - Training for Assessment of Risk". It has received funding from the European Union's Horizon 2020 research and innovation program under the Marie Skłodowska-Curie actions. INFRASTAR involved twelve Early Stage Researchers (ESR) working in different research institutes, universities, and companies in five European countries (France, Germany, Switzerland, Denmark, and Poland). The host company for this PhD was PHIMECA Engineering in France in cooperation with the Université Clermont Auvergne and IFSTTAR (now Université Gustave Eiffel).

The main goal of INFRASTAR was to improve the knowledge, skills, expertise, and to propose innovative solutions toward optimal maintenance and management of civil structures against fatigue (particularly for bridges and wind turbines). Three major challenges have been addressed within this program: 1) advanced modeling of concrete fatigue behavior, 2) new non-destructive testing methods for early aged damage detection, and 3) probabilistic approach of structure reliability under fatigue. With this respect three workpackages can be recognized where four ESRs were working under each workpackage.The first workpackage was related to "monitoring and auscultation". The second workpackage dealt with "structure and action models", and the third one covered "reliability-based approaches for decision making".

To achieve this goal, a cross-experience and inter-disciplinary cooperation between

ESRs within different research centers was necessary. For this reason different secondments in addition to training weeks were considered for each ESR to visit the other research centers within the program to be able to collaborate with other ESRs and research centers. Two secondments (each one three month long) were considered for this project. The first secondment took place at École polytechnique fédérale de Lausanne (EPFL), department of civil engineering and the second one was carried out at IFSTTAR and Cerema. Also, three training weeks were completed during this PhD in BAM Berlin, EPFL, and University of Aalborg respectively.

1.2 Overview

Maintenance of structures is an important part of the structural Life Cycle Management (LCM). It is considered as a set of practices performed to ensure that a structure fulfills its duties with an adequate level of serviceability and safety during its service life. A proper maintenance planning can help to prevent unexpected failures. Therefore, it can be seen as a tool to ensure the return of investment for the owners of structures after an expected period of time. Practices to optimize maintenance planning of civil structures have gained more attention during past decades since the number of the aging structures is increasing while the budget for the maintenance is limited.

To well understand the importance of maintenance planning for a given structure, e.g. a bridge, one can study the consequences of different failures on the structure. Local failures on bridges can cause traffic disruption for carrying out some emergency repair actions. This can bring loss of capital and reputation for the bridge owner in one hand and waste of time and inconvenience for the road users in the other hand. At a higher level, the failure can lead to catastrophic damage including collapse of the structure, loss of lives, and environmental and social damage. Therefore, a proper maintenance planning is crucial for owners of structures to prevent unexpected adverse events on the structure.

Structures may face various modes of failure during their service life. Statistical

information of metallic structures show that scour of piles/foundations, buckling, fatigue, impact, and fracture are among the most common failure modes. Although, scour is an important failure mode for all bridges, fracture by fatigue appears to be the most critical one for steel bridges. It is obvious that a proper maintenance planning should involve several actions to mitigate the failure occurrence by any failure mode. However, failure modes that are more likely to happen will receive higher attention within the maintenance framework. Therefore, one can say that maintenance against fatigue has the priority for steel structures.

Fatigue is one of the main degradation processes on metallic structures subjected to cyclic loading (e.g. traffic and environmental loading). Fatigue process starts with crack initiation. Initial cracks may then propagate under cyclic loading until they reach critical lengths, if not controlled, which can put the structure in a critical situation. One challenge in fatigue assessment is related to the involved uncertainty in the problem which can be originated from different sources such as fatigue loading, material properties, geometry (e.g. weld geometry), fatigue accumulation or crack growth models, weld geometry, etc. Another challenge can be related to the tools and methods to study the crack initiation and propagation in order to identify the effective repair strategies.

In order to deal with fatigue related uncertainties, some indicators like reliability and risk can be used to evaluate the fatigue failure probability and associated consequences. Performing fatigue reliability analysis in a time-dependent framework seems more reasonable since fatigue is a time-dependent degradation process associated with stochastic input parameters. A time-dependent reliability analysis basically differs from a time-independent analysis since the objective of the former is to find the cumulative failure probability for a given period of time. Finding this failure probability is challenging particularly for problems with non-monotonic and computationally expensive performance functions.

Investigations on the effectiveness of the repair actions for fatigue on a given structure in the context of structural maintenance planning requires performing crack

propagation experiments. Executing fatigue experiments in the laboratory can take a very long time and it might need considerable financial resources. Accordingly, simulation-based experiments through Finite Element Analysis (FEA) can be very fruitful to alleviate the required expenses. It should be pointed out that performing such analysis using classic FEMs can require a very high computational cost due to the limitation of such methods which requires an update of entire mesh grid after applying each load cycle. To tackle this issue, advanced methods like XFEM have been developed in order to perform the crack propagation analysis with lower computational resources.

Compared to new structures, existing structures have already experienced the real life loading conditions. Structural Health Monitoring (SHM) can therefore be employed on existing structures to evaluate their states. SHM is a process focusing on observing, measuring, recording, and processing of the data related to the structure in real time. It provides valuable information for owners of structures and decision makers. This information can be used to update performance indicators such as reliability and risk for a given structure to propose a better maintenance planning. Apart from challenges like data acquisition and data storage, data processing and employing the SHM information in the context of structural maintenance planning can be a challenge. SHM can sometimes lead to a huge amount of data which can be very complex as well. Processing and interpreting such data on a given structure requires employing advanced statistical and data science tools such as time series methods, deep learning, etc.

Previously mentioned practices such as fatigue reliability assessment, identification of repair actions, and application of SHM can be introduced into the structural LCM. This can help to search for the optimal maintenance planning in order to ensure the adequate level of safety and serviceability for a given structure under given financial limitations. Such maintenance planning is mainly aiming at minimizing the maintenance, inspection, and monitoring cost, and/or maximizing the structural service life. This can be done by searching among available maintenance, inspection, and monitoring actions in order to define the best type and time of interventions which lead

to the minimum cost. It should be noted that preparing an appropriate cost model for the structure of interest is another challenging task.

According to what has been shortly discussed above, it can easily be realized that improving methods and strategies within the context of optimal maintenance planning of existing structures is a very complex and exhaustive task. It involves many challenges coming from different sources which are required to be addressed properly in order to improve the current practices in structural maintenance planning. Accordingly, the objectives and contributions of this research towards optimal maintenance planning of structures are described in the next section.

1.3 Objective and scope of the PhD research

The overall goal of this PhD is to bring contributions to the research field of optimal maintenance planning of existing structures. Considering a reliability-based maintenance optimization framework, the objective is to address challenges related to:

- Time-dependent reliability approach for fatigue reliability analysis
- Fatigue crack growth modelling for characterizing repair projects
- Fatigue crack propagation time-dependent reliability assessment
- long-term monitoring data processing for fatigue analysis

Addressing these challenges leads to identify four main tasks, as described hereafter.

As mentioned previously, a time-dependent fatigue reliability assessment helps to evaluate the cumulative probability of failure of a structure due to fatigue for a given time interval. Performing such assessment can be very challenging. On the one hand, associated performance function can be highly irregular and non-monotonic which can affect the accuracy of the final result. On the other hand, evaluating the associated

performance function can be computationally expensive since it might be done through a FEA that affects the efficiency of existing methods. Accordingly, new time-dependent reliability approaches are required to evaluate the cumulative failure probability with a reasonable trade-off between accuracy and efficiency. Hence, a new time-dependent reliability approach is developed in this context that is called AK-SYS-t. This method relates the time-dependent reliability problem with serially connected system reliability problem then it employs the efficiency of advanced system reliability methods like AK-SYS (Fauriat and Gayton, 2014) for time-dependent reliability assessment. On that account, Kriging meta-modeling is used to replace the costly-to-evaluate performance functions and the learning function of AK-SYS is used to efficiently enrich the initial meta-models. Another goal here is related to proposing a strategy to construct the full curve of the cumulative probability of failure for a given time interval by AK-SYS-t. This curve is an essential tool for decision makers to decide upon the time and types of maintenance actions.

Fatigue life assessment is usually addressed either under a safe-life approach relying on S-N curves or a damage tolerance approach relying on fracture mechanism. Fatigue analysis using fracture mechanism seems appropriate for existing structures since they may have already developed some fatigue cracks in various critical locations. Performing crack propagation requires advanced tools and techniques such as XFEM method to be able to handle the complexity added to the model by fatigue cracks. In particular, considering a rib-to-deck welding detail in orthotropic deck plates, a strategy is proposed to investigate the usefulness of XFEM method for an unwanted cracking problem in this detail which is related to the situation when cracks start growing towards the deck plate. Such cracks can reach a critical length without being detected. Additionally, the effectiveness of two repair solutions on such cracking problem is investigated by performing crack propagation analyses using XFEM method.

The next objective of this study is to examine the functionality of the proposed time-dependent reliability method, AK-SYS-t, on fatigue crack propagation models. Time-dependent reliability assessment for probabilistic crack propagation models is

challenging since the associated performance function is highly nonlinear. Additionally, time-dependent reliability assessment for crack propagation models is computationally demanding since it requires a cycle-by-cycle calculation of the Stress Intensity Factor (SIF). This requires even more computational resources if the SIF is approximated by FEA. With this respect, one might need to make some assumptions and simplifications steps to be able to address such problems. Accordingly, application of AK-SYS-t on probabilistic crack propagation models associated with simplification steps and assumptions is investigated on two applicational case studies.

The last part of this PhD proposes an approach to employ time series methods on long-term monitoring data for fatigue analysis. For this reason, the long-term monitoring data of Chillon viaducts is used. The data is collected for almost two years using strain gauges with the frequency of 50, 100, or 200 Hz. The difficulties here can be related to the seasonality effects available within the monitoring data and huge size of the monitoring data. Conventional models for fatigue load modeling such as rainflow counting, and Markov chains are unable to deal with the seasonal effect due to the stationarity assumptions. Accordingly, time series methods such as seasonal ARIMA (Auto-Regressive Integrated Moving Average) can be employed to address this issue. The difficulty here can be related to the size of the long-term monitoring data. With this respect, an approach is proposed to deal with this issue by transforming the large-sized monitoring data to a small set of observations. With this respect, the monitoring duration is divided into smaller time intervals first. One can then fit a distribution to the monitoring data for each time interval. Afterwards, the parameters of associated distributions can be used to replace the observations in each time interval. Therefore, the entire monitoring data can be replaced by a time series with fewer observations. Seasonal ARIMA can then be easily applied on the new data set to provide a load model for fatigue analysis. This load model can be employed within S-N approach or fracture mechanism with some adjustments.

1.4 Summary

According to what has been described above, five chapters are considered for this thesis as follows:

- **Chapter 1** serves as introduction.
- **Chapter 2** is devoted to the general concepts and practices within the structural LCM to tackle fatigue problems.
- **Chapter 3** is related to time-dependent reliability analysis. A new methodology to address time-dependent problems is introduced in this chapter supported by some examples from the literature.
- **Chapter 4** focuses on providing strategies to investigate the usefulness of advance methods like XFEM for assessing structural fatigue problems and characterizing possible repair solutions in a crack propagation context. Moreover, proposed strategies are applied on a real case fatigue detail.
- **Chapter 5** concentrates on connecting the proposed time-dependent reliability method to crack propagation problems by describing the necessary steps and assumptions on two applicational examples.

An additional study that is presented in this thesis is related to the application of time series methods on long-term structural monitoring data. This work has been done under the supervision of professor Eugen Brühwiler at EPFL. This work is presented in Appendix A since it has not been further employed in connection with other approaches within this thesis.

Chapter 2: Background: Fatigue life-cycle management of deteriorating structures and performance indicators

2.1 Introduction

This chapter aims to provide some general information regarding common practices for Life Cycle Management (LCM) of structures that are vulnerable to fatigue (e.g. steel bridges, off-shore structures, wind turbines, etc.). The challenges of structural LCM is highlighted to integrate the work that is further conducted in this thesis. Structural LCM is composed of different blocks in which an optimal maintenance and/or inspection planning can be derived as a result. The LCM introduced here is incorporated with the information from Structural Health Monitoring (SHM) and probabilistic modeling. This will lead to a more realistic outcomes that is very resourceful for decision makers. For this reason, the objectives and strategies of structural maintenance are introduced first. Then, models for structural performance deterioration and performance indicators are reviewed. Common methods for fatigue life assessment of steel structures accompanied with uncertainty modeling in fatigue and performance functions for fatigue reliability analysis are investigated subsequently. In the next step, some methods for monitoring, inspection, and maintenance for fatigue are summarized. In the end, life-cycle optimization of structures associated with inspection, monitoring, and maintenance is characterized.

2.2 Structural life-cycle management

Civil engineering structures are built to perform their desired functions for decades. They play a crucial task to improve the economy in addition to social and environmental welfare. However, these national assets are exposed to different aging processes (e.g. fatigue and corrosion for steel structures), random loading and environmental conditions (e.g. storms, snow, etc.), and some other natural extreme events such as earthquakes and those resulting from humans such as accidents and terrorist attacks. Apart from the unexpected accidents, deterioration is one of the inevitable processes that happens to any structure with time, no matter how well it is designed. A sudden failure in civil structures (due to hidden cracks) can have major economic, environmental, and social impacts, see e.g. collapse of Genoa bridge. Besides, the cost of a failure can be significantly higher than the cost required only for rebuilding or replacing the structure (Dong et al., 2013; Bocchini et al., 2014). In order to ensure the long-term functionality of structures, it is then crucial to plan some interventions to reduce the number of unexpected failures. These interventions can involve periodic inspections, SHM, and maintenance actions.

The number of scheduled interventions has to be defined with care during the service life of a structure since it can lead to a large financial burden. Proposing an integrated framework which aims at evaluating the conflicting safety and financial requirements altogether in the context of structural LCM is inevitable. Life-cycle cost optimization is one important step in LCM process since financial limitations can significantly impact further decisions. A rational trade-off between the minimization of the life-cycle cost and the maximization of the expected service life is sought. The optimization part can be a computationally expensive process especially when it is performed in a probabilistic framework to account for associated uncertainties. However, recent advances in processing tools make it easier to conduct such calculations in a large-scale simulation (Okasha and Frangopol, 2010a, 2011; Orcesi and Frangopol, 2011b).

A comprehensive LCM is composed of different modules that work in an integrated

way to minimize the life-cycle cost, and maximize the extended service life, etc. Figure 2.1 illustrates the general framework for LCM for deteriorating structures. It starts with analyzing the structure under investigation to determine the potential deteriorating mechanisms. In this step, one should specify some details such as the type of structure, the type of material, and the details of components. Depending on the type of structure and material, several types of deterioration processes can be considered. For instance, corrosion is an important deterioration process that can happen in both steel and concrete structures. Fatigue is a common process that causes deterioration in steel structures while carbonation and chloride penetration are common in concrete structures. Considering each process, structural performance can be evaluated using appropriate approaches. For instance, S-N approach and fracture mechanism can be used to model the fatigue damage in steel structures. Since this thesis concentrates more on steel structures, S-N curves and fracture mechanism are further elaborated in Section 2.6.

It should be noted that the structural performance is a concept which corresponds to the protection of human life and property. The structural performance is usually divided into two categories according to the serviceability limit state and the ultimate limit state. Structures can reach their serviceability limit state due to some issues like deflection, cracks, vibration, etc. while the ultimate limit state can occur due to some problems such as bending, shear, compression, and overturning among others (Yusof, 2014; Akiyama et al., 2000). Several indicators have been proposed in literature such as reliability, risk, availability, hazard, etc. in order to evaluate the structural performance. Such indicators are described with more details in Section 2.4.

Another step in structural LCM is to use SHM data in order to reduce the uncertainty in predicting structural performance. Afterwards, to make the decision making process easier some performance indicators such as reliability or risk are required in the next step. After predicting the deterioration of performance indicators over time, appropriate maintenance actions are chosen to improve the structural performance. The effect of maintenance actions associated with their costs are used in the optimization

step to be able to propose appropriate outcomes such as optimum maintenance and inspection strategy, optimum expected extended service life, etc. Such framework has been presented in Frangopol (2011); Frangopol et al. (2012); Miyamoto and Motoshita (2015) that is already applied on different types of structures such as bridges (Kim and Frangopol, 2011b, 2012; Kwon and Frangopol, 2011; Okasha and Frangopol, 2010b; Orcesi and Frangopol, 2011a) and sea vessels (Kim and Frangopol, 2011c,a; Frangopol, 2012; Kwon and Frangopol, 2012).

It is obvious that providing a comprehensive LCM framework facilitates the process of inspection and maintenance planning for structures within the financial restrictions. However, it can be considered as an extensive mission that requires schooling in many other fields such as structural analysis, reliability assessment, data analysis, etc. Addressing challenges in the related fields, of course, can help to improve the results of LCM approaches. For such purposes, some studies focus on new methods and approaches to approximate the performance indicators such as reliability or risk indices in a time-dependent or time independent framework, while others are searching for more appropriate cost models. Quantifying uncertainties is another active field in this domain that can be helpful to improve the practices in structural LCM. Thus, the goal of this chapter is to describe different steps in structural LCM against fatigue with more details to clarify the objectives and challenges in this framework.

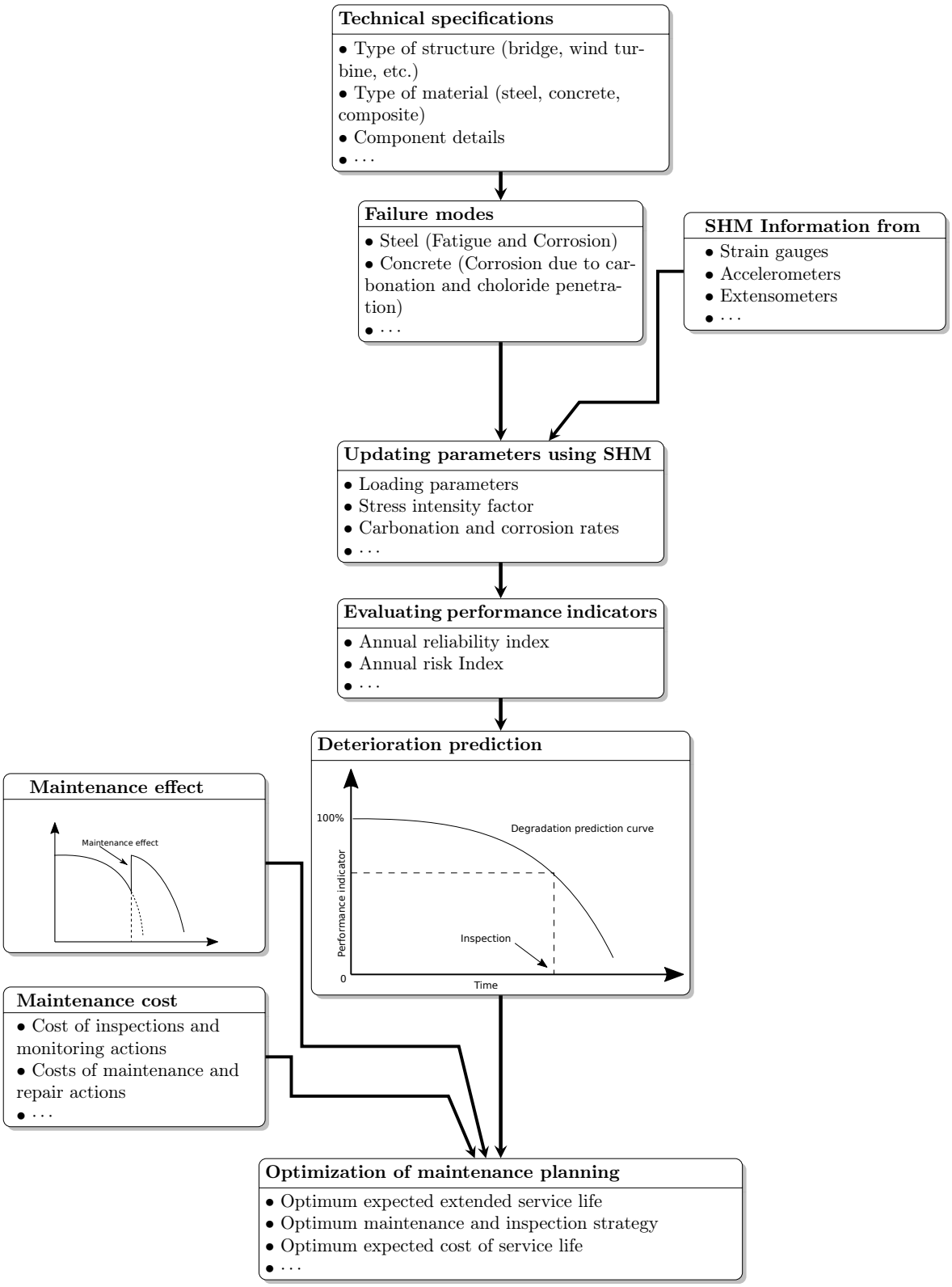

Figure 2.1: LCM framework incorporating SHM data

2.3 Structural maintenance objectives and strategies

Simply speaking, structural maintenance means "to retain a structure in a good condition so that it can accomplish its expected tasks" (van der Toorn, 1994). This definition may imply that all the components of a structure should be in a condition so a structure can fulfill all intended duties. However, financial and physical limitations force the managers to find more sophisticated solutions for maintaining structures in which the targets and the limitations are clearly specified and addressed. Some targets for the structural maintenance can be expressed in terms of reliability, availability, durability, serviceability, etc. Finally, the maintenance can be defined as: "All technical activities on the component level linked to each other in order to keep the structure in a condition to perform its duties properly for a specified period of time to satisfy maintenance targets (e.g. sufficient reliability, or availability, etc.)" (van der Toorn, 1994).

Maintenance targets such as reliability rely on measurements that evaluate the performance of a structure which deteriorates over time due to different degradation processes. Therefore, the main goal of maintenance actions is to improve the performance of structures to meet those targets. As those measurements inherently deteriorate through time due to different aging processes, one main goal of maintenance actions is to restore the initial properties of the structure completely or at least partially in order to meet the requirements expressed in terms of maintenance targets. The cost of maintenance represents a non-negligible portion in total the life-cycle cost of a structure since maintenance actions are meant to apply frequently during its service life and it can even be higher than the original cost of construction (Estes and Frangopol, 2001). Therefore, another objective is to search for an economically balanced maintenance allocation. In other words, this can be considered as another target that defines the financial limitations for the maintenance planning. Optimizing the maintenance planning is of paramount importance as it looks for the best maintenance strategies for given level of targets and financial constraints.

Maintenance actions are generally employed to change the course of the structural

deterioration. They can mainly be grouped in two categories namely preventive and corrective actions , see Figure 2.2. The goal of preventive maintenance interventions is either to stop or slow down the aging process which can help to extend the service life of a structure. Preventive maintenance actions are usually applied based on a planned schedule. However, sometimes according to the condition of the structure, preventive maintenance can be recommended. The second category of maintenance interventions are called corrective actions since they are performed to restore the performance of some components of the structure partially or totally. Corrective maintenance is usually performed when the performance indicators reach a predefined threshold. This kind of maintenance can be planned or unplanned due to some unwanted accidents on the structure (Barone and Frangopol, 2014).

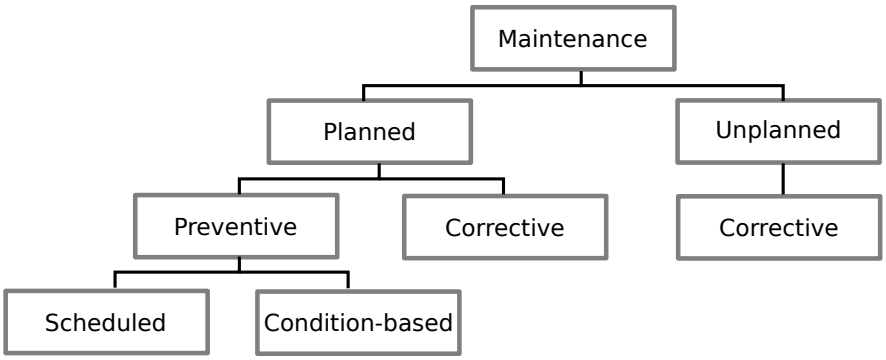

Figure 2.2: Different types of maintenance actions

The effect of preventive and corrective maintenance actions on the structural performance is illustrated in Figure 2.3 in addition to the cumulative cost of maintenance. The service life of a structure can be defined when the structural performance reaches its threshold. Preventive and corrective maintenance actions are applied to keep the structural performance above the threshold and therefore to extend the structural service life (Kong and Frangopol, 2003a,b; Neves et al., 2006). Implementation times of preventive maintenance actions can be preplanned considering the structural performance evolution and the cost of maintenance (Okasha and Frangopol, 2010b). The preventive maintenance actions can lead to small improvements on the performance of a structure at a lower cost compared to the corrective actions. Corrective maintenance interventions are usually performed when the performance of the structure is reaching

some threshold and an essential improvement such as replacement is necessary which consequently leads to a higher cost of maintenance (Frangopol and Kim, 2019).

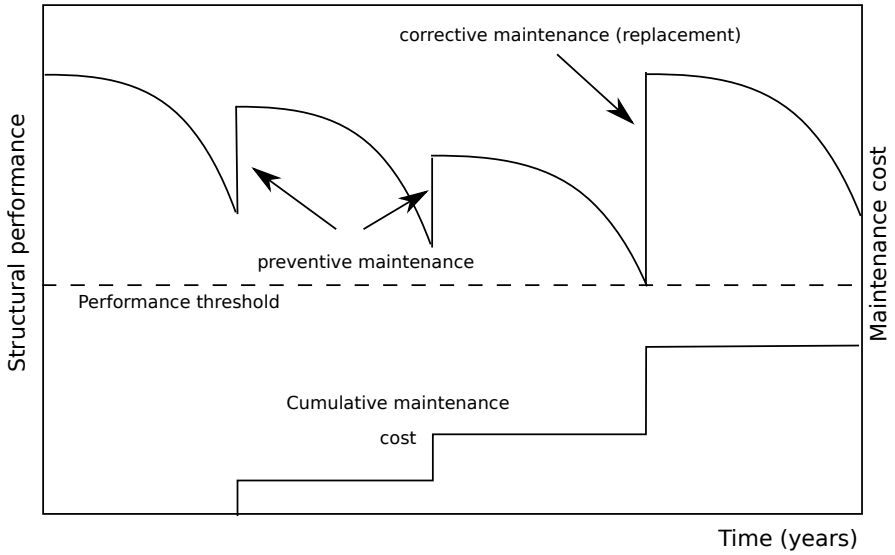

Figure 2.3: An illustration of effect of maintenance types on structural performance and cumulative maintenance cost.

2.4 Structural performance deterioration models

One of the most important steps in structural life-cycle analysis is the evaluation and prediction of the structural performance deterioration (Frangopol, 2011, 2018). Aging and degradation are some other terms that are usually used instead of deterioration. Combined effect of some drivers of operating environment (more or less harsh) and mechanical stressors trigger the structure to degrade over time (Frangopol and Kim, 2019). An accurate model for structural deterioration process can be a major tool for the life-cycle management of a structure. Fatigue and corrosion are the most common degradation processes on steel structures that cause the structural performance to gradually deteriorate over time. However, there are some other extreme events like earthquakes, floods, etc. that cause an unanticipated change in the structural performance (Frangopol and Soliman, 2016).

Performance degradation of structures can have different behavior depending on the governing failure mode. Figure 2.4 illustrates some of possible deterioration pat-

terns. For instance, the case one which is a linear degradation pattern can be used to model the corrosion process over time for many cases. Case 2 represents a process that slows down with time and can be used to represent the carbonation and chloride penetration in concrete structures. Fatigue behavior is similar to case 3 where the deterioration is caused by the cumulative load effect over time and the failure occurs by abruptly. In some cases, the degradation process has a stepwise behavior since it happens by collisions and extreme loads (case 4). In case 5, structure experiences a sudden failure since an unexpected extreme load exceeds the structural tolerance level. As many of the components in the civil engineering structures are covered with a protection layer, they may show a two-phase degradation process, see case 6 on Figure 2.4. The first phase is related to the degradation of the protection layer and in the second phase the component degrades (van der Toorn, 1994).

Maintenance strategy highly depends on the type of the degradation model. For instance, if defects or cracks are assumed to exist before the beginning of structural service life, which is the case in a damage tolerance analysis, cracks should be detected before reaching a critical value. Therefore, regular inspections should be planned during the service life of a structure. If a crack is detected in a critical fatigue detail by inspections, preventive or corrective maintenance actions should then be performed promptly since the stable crack growth phase is not so long compared to the total service life of a structure. For a two-phase degradation process (case 6), the aging process in the first phase that is related to the protection layer can be considered as a conditional parameter for the second phase which is related to the component deterioration. If there is only one degradation phase (case 1 to 5), it is important to properly predict the behavior of the process since it is the only indicator to decide about the inspection and maintenance actions. Fatigue as one of the most important aging process for steel structures is introduced in Section 2.6 because the aim here is to contribute to the optimal maintenance planning of structures against fatigue.

The existence of uncertainties within the aging processes increases the complexity of the problem for damage occurrence, propagation and detection. In general, uncer-

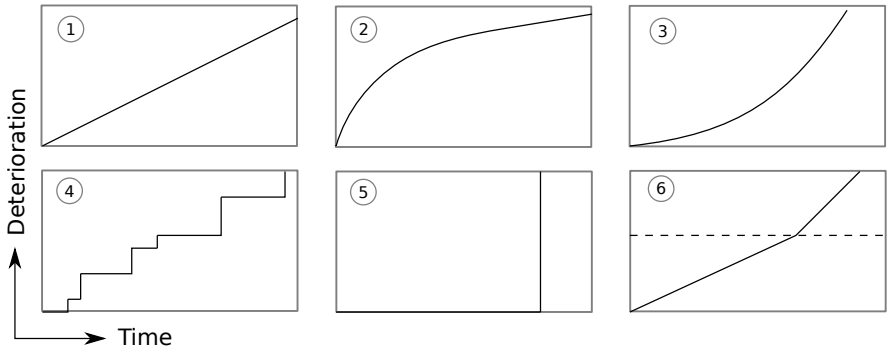

Figure 2.4: Different courses of structural performance degradation over time

tainties can be classified in two groups. The first group gathers randomness which is inherent to the parameters, and it is called aleatory uncertainty. The second group gathers uncertainties due to the lack of knowledge about a phenomenon and it is referred to epistemic uncertainties. (Rahman et al., 2018; Karanki et al., 2017; Ferchichi et al., 2017). Aleatory uncertainties are usually irreducible while epistemic uncertainties can be reduced by adding extra information to the problem (e.g with a more realistic modeling). Therefore, Structural performance indicators are better to be derived in a probabilistic framework which is suitable to account for uncertainties in the problem. One can refer to reliability, risk, availability, and hazard as indicators that take into account associated uncertainties in the problem. They are hence introduced in the next section.

2.5 Structural performance indicators for maintenance allocation

Structural performance indicators are crucial for maintenance allocation and optimization since they provide consistent criteria for decision making process (Ghosn et al., 2016). Performance indicators are time-dependent functions that can be measured and quantified. It is evident that a careful assessment of performance indicators over time can help for a better structural maintenance planning.

Condition index is one of the most common performance indicators that is attained

through visual inspections (Strauss et al., 2017; Frangopol and Kim, 2019). Using this performance indicator, the condition of the structure is rated in different scales after each inspection. For instance National Bridge Inventor (NBI) and Pontis are two condition rating methods that are used in the United states (Masciotta et al., 2016; Frangopol and Kim, 2019). NBI rates the condition of bridge components (such as deck, superstructures, etc) using a value ranging from 0 to 9 where 0 indicates the failing condition and 9 shows the excellent condition. In Pontis condition rating method, however, the rating is from 1 to 5 where 1 indicates "no evidence of damage in a bridge component" and 5 represents "severe damage which affect the serviceability of a bridge component". Table 2.1 describes the condition states in Pontis condition rating method (Frangopol and Kim, 2019). Other countries such as Austria and Croatia use the condition rating method that is similar to Pontis and the structural condition is described with 5 condition states (Strauss et al., 2017). Condition rating of components is prepared mostly by visual inspection within different methods and usually provides qualitative information about components of the structure (as it can be seen from Table 2.1 for Pontis condition rating). The quality of data is highly dependent on the inspector's skills, rush level of the inspector, accessibility to the inspections zone, etc.

Other relevant performance indicators can be used in the area of structural maintenance planning such as reliability, availability, hazard, and risk based indicators (Barone and Frangopol, 2014). These indicators provide quantitative information about the deterioration of structural performance that can be easier to interpret and evaluate the structural performance. Some countries like Netherlands and Denmark have started to employ those indicators more comprehensively in the field of structural maintenance planning and not only for research purposes (Strauss et al., 2017). Reliability and risk-based indicators rely on the failure probability, assessed in practice from the so-called performance function (which is described in Section 2.5.1), while availability and hazard are directly calculated according to the lifetime distribution. In the latter approach, the lifetime of a structure is considered as a random variable (Okasha and Frangopol, 2010c). A probabilistic framework for the life cycle management allows one to take into account uncertainties associated with structural resistance and loads,

Condition index	***Description***
1: Good	Painting quality is good as it is intended to protect the metal surface and no active corrosion is detected
2: Fair	The painting system is distressed meaning that it shows some peeling, curling, or chalking but the metal is still covered. There is a little or no evidence of corrosion
3: Paint failure	There is no evidence of an active corrosion that may cause loss of section but the metal surface is exposed and freckled rust is common
4: Paint failure with steel corrosion	Corrosion may be present but any section loss due to active corrosion does not yet warrant structural analysis of either the element or the bridge
5: Major section loss	Section loss due to corrosion has been detected which may be sufficient to warrant structural analysis to ascertain the impact on the ultimate strength and/or serviceability of either the element or the bridge

Table 2.1: Pontis condition rating for painted steel girder element (CDOT, 1998)

and therefore to compute those performance indicators. A short description for the indicators mentioned above is provided hereafter.

2.5.1 Reliability and risk indicators

Reliability measures the probability that a structure performs its duties properly for a given period of time under specified conditions. One goal of reliability analysis is to find the probability of failure of a structure from its behavior for a given failure mode that is formulated by means of a performance function $Z = G(\mathbf{X})$. $\mathbf{X}$ here denotes a vector of input random variables that encompasses for example mechanical properties, operational parameters, load characteristics, and geometry among others. $G(\mathbf{X}) = 0$ separates the safe domain $G(\mathbf{X}) > 0$ from the failure domain $G(\mathbf{X}) < 0$ and it is called the limit state function. The probability of failure for a given failure mode is expressed by the integration of the joint probability density function $f_{\mathbf{X}}(\mathbf{x})$ of the random vector $\mathbf{X}$ over the failure domain as it is usually formulated by Equation 2.1.

$$p_f = \mathrm{P}(G(\mathbf{X}) \leq 0) = \int ... \int_{G(\mathbf{X})<0} f_{\mathbf{X}}(\mathbf{x}) d\mathbf{x} \tag{2.1}$$

Calculating this failure probability is not an easy task and increasingly robust and efficient reliability methods have been proposed over the last decades to approximate this failure probability. This formulation is related to the time-independent reliability analysis and evaluates the failure probability for a given time instant. However, in many of engineering applications, time-dependent reliability analysis is necessary due to the temporal nature of material properties, loading, and geometrical parameters. Time-dependent reliability analysis is more complicated than time-independent analysis by introducing the time into the problem and it aims to calculate the cumulative failure probability for a given time interval. More information about methods and definitions for reliability analysis is provided in Chapter 3 where a new approach called AK-SYS-T for time-dependent reliability analysis is developed.

Risk is simply defined by multiplying the probability of failure with its associated consequences C as shown in Equation 2.2 (Barone and Frangopol, 2014). Methods and approaches for reliability assessment can also be used here to calculate the failure

probability in a risk-based framework. Risk-based decision making has become an important tool for structural maintenance optimization because, in most of the cases, it is necessary to put the consequences of structural failure into consideration.

$$R = p_f \times C \tag{2.2}$$

One way to evaluate consequences of a failure is to identify the losses associated with failure and their equivalent cost. The failure cost can be divided into direct and indirect costs. The direct cost, C_{dir}, is related to the monetary loss after failure while the indirect cost C_{ind} takes into account the cost related to the impacts on the environment, society, and etc. Therefore, the Risk can be formulated by Equation 2.3, as:

$$R = p_f \times (C_{dir} + C_{ind}) \tag{2.3}$$

In real life applications, reliability and risk are generally evaluated at constant time intervals. For instance, one year time interval can be used to evaluate the annual reliability index and annual risk Barone and Frangopol (2014).

2.5.2 Availability and hazard indicators

Another way to provide indicators for LCM is through structural lifetime distributions (Leemis, 1995). In this way, time to failure of a component or system is considered as a continuous random variable. The random time to failure T_f is defined as the amount of time that has elapsed since the beginning of the service life until the first failure happens (Rausand and Høyland, 2003). The Probability Density Function (PDF) of time to failure f_{T_f} should be determined using the statistical information of the degradation process. For a given time t and a small time interval Δt, this PDF measures the failure probability between t and $t + \Delta t$ as expressed in Equation 2.4.

$$f_{T_f} = \lim_{\Delta t \to \infty} \frac{\mathrm{P}(t \leq T_f \leq (t + \Delta t))}{\Delta t} \tag{2.4}$$

if Δt is small it can be rewritten as:

$$f_{T_F} \Delta t \approx \mathrm{P}(t \leq T_f \leq (t + \Delta t)) \tag{2.5}$$

With this respect multiple lifetime functions can be defined such as survivor, availability and hazard functions which have already been successfully employed for LCM of bridges (Orcesi and Frangopol, 2011b; Okasha and Frangopol, 2009b; Yang et al., 2004). Among different lifetime functions, availability and hazard are appropriate indicators that can be used for threshold-based approaches for LCM (Barone and Frangopol, 2014). Before introducing these functions, let us first introduce the survival function $S(t)$ which measures the probability that a component or system has not failed until time t, see Equation 2.6.

$$S(t) = \mathrm{P}(T_f \geq t) \tag{2.6}$$

The availability $A(t)$ function is based on the same definition as the survival function except that it is not monotonous with time, i.e. it can change over time by applying maintenance actions, whereas survivor function is a monotonically decreasing function over time.

The hazard function $h(t)$ is rather defined as the instantaneous failure rate of a component or system. It expresses that failure occurs between t and $t + \Delta t$ given that no failure has happened before t. It finds the probability of failure at time interval $[t, t+\Delta t]$ given that the component or system is surviving at time t while this probability is averaged over the same interval and Δt tends to zero. The hazard function can also be seen as the ratio between the derivative of survivor function $S'(t)$ and survivor function, see Equation 2.7.

$$h(t) = \lim_{\Delta t \to 0} \frac{\mathrm{P}[t \leq T_f \leq t + \Delta t | T_f \geq t]}{\Delta t} = -\frac{S'(t)}{S(t)} \tag{2.7}$$

Providing a closed form solution is the main advantage of the lifetime functions over performance-based indicators. However, this closed form solution can be obtained only for the systems in which the components are independent or fully correlated. Moreover, by resorting to lifetime distributions of components and therefore using availability and hazard functions, one cannot access to the sources of uncertainties. In the contrary, reliability and risk-based approaches or more generally probabilistic approaches allow one to study the effect or sensitivity of the model response, e.g. G,

to each input random variable. Any level of correlation between random variables can also be considered (Barone and Frangopol, 2014).

2.6 Fatigue assessment of steel structures

Fatigue is a multi-stage process that is caused and accumulates under cyclic loadings (Ye et al., 2014). It starts with initiation of cracks at a microscopic level in the first stage. The cracks propagate under cyclic loading in the next stage and it continues until the failure of components or specimen happens in the last stage. The separation of aforementioned stages is not well defined (Ellyin, 1997). Fatigue cracks usually initiate on the surface of a specimen due to several factors (surface roughness, surface treatment, etc.) and they propagate in the same direction of the maximum shear stress. Fatigue cracking mostly happens in the regions with high stress concentration e.g. near notches, pits, scratches, or notch like valleys on the surface. The main factors that affect the fatigue life can be related to material properties, processing and manufacturing of the material, loading condition, geometry of the components, and surrounding environment. Moreover, some of these factors can be correlated meaning that a change in one would lead to a change in another (Fisher et al., 1998).

Two main life-assessment procedures exist to predict fatigue failure. The first approach named safe-life approach is advised when inspections are impossible, very difficult, or costly. Cracks are not allowed and must not appear during the service life. This fatigue design approach mostly relies on S-N curves which basically provide a relationship between stress levels and number of stress cycles to failure. The second approach called damage-tolerance approach (Ye et al., 2014) assumes that components are potentially flawed before their use and therefore, cracks are assumed to exist in important structural details. In such an approach, inspections are mandatory and the objective is to ensure that the component does not fail between inspections. This approach resorts to fracture mechanics and crack growth theories. The basics of fatigue S-N curves and fracture mechanism approaches are briefly reviewed hereafter. More comprehensive information about those approaches can be found in Ellyin (1997);

Fisher et al. (1998); Lukic (1999) for example.

2.6.1 S-N curve based approach

S-N or Wöhler curves usually characterize the fatigue behavior of different materials (Susmel, 2009; Susmel et al., 2011). An illustration of S-N curve is provided in Figure 2.5. S-N curves show the relation between the level of stress ranges S and the associated number of cycles N to failure. For stress ranges higher than ultimate stress limit S_{ut}, few cycles are enough to cause fatigue failure. By contrast, if all stress ranges are smaller than the endurance limit S_e, failure due to fatigue never happens.

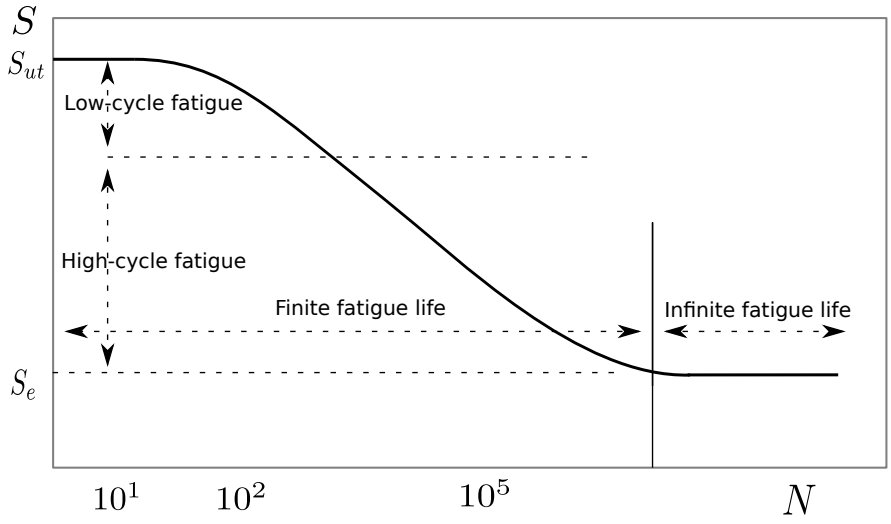

Figure 2.5: A typical S-N curve

S-N curves are obtained from fatigue test campaigns. In a fatigue test, a test specimen goes under a cyclic loading with a constant amplitude until fatigue failure happens. As the stress ranges are getting closer to the endurance limit, the number of cycles to failure increases, see Figure 2.5. The experiments are performed for some given test specimen and lab conditions. Therefore, the fatigue behavior of the fatigue details, components, or structures in real conditions might be different. A commonly used method to represent the finite fatigue life zone of the S-N curve is the Basquin model (Basquin, 1910) which can be expressed as:

$$NS^m = A \tag{2.8}$$

or

$$logN = -mlogS + logA \tag{2.9}$$

where m and A are material parameters.

One of the simplest and most common ways to calculate the cumulative damage caused by fatigue is the Miner's rule that is formulated in Equation 2.10 (Miner, 1945). Miner's rule states that the damage caused by a stress cycle belonging to a variable amplitude load history is equal to the damage caused by the same cycle in a constant amplitude load history. Therefore, the order of the cycles has no influence on fatigue damage accumulation. In the Miner's rule, n_i is the number of stress cycles for the stress range $\Delta\sigma_i$ extracted from the variable amplitude load history andvN_i denotes the number of cycles to failure for $\Delta\sigma_i$ in the constant amplitude load history that can be approximated using S-N curves. It is generally assumed that failure happens when the amount of the accumulative damage D is equal to 1.

$$D = \sum_i \frac{n_i}{N_i} \tag{2.10}$$

Simplicity is one main advantage of this fatigue design procedure that makes it very well-known and explains why it remains the mostly used method in industry (Lukic, 1999). However, one drawback is that this method ignores the effect of the load cycles under the endurance limit S_e (if defined) on fatigue damage, although a notable portion of fatigue damage comes from those stress cycles according to Marquis (2011); Lukic (1999). Another shortcoming of this approach is that it is not intended to incorporate some inspection results e.g. crack dimensions. This can be an issue for aging structures for which it is desirable to extend their service life or if cracks have to be considered before the beginning of the service life. For those purposes, fatigue damage approach based on fracture mechanism is introduced in the following.

2.6.2 Fracture mechanism-based approach

Fatigue in structures appears with cracking. Three modes of crack opening can be identified in literature such as tensile opening, sliding, and tearing. These types of

cracks are illustrated in Figure 2.6. A Stress Intensity Factor (SIF) can be defined at the tip of the crack for each opening mode as K_I, K_{II}, and K_{III} respectively. This parameter represents the amplitude of the stress fields near the crack tip which is a function of the loading on the cracked structure and the geometry of the component and the crack (Lukic, 1999).

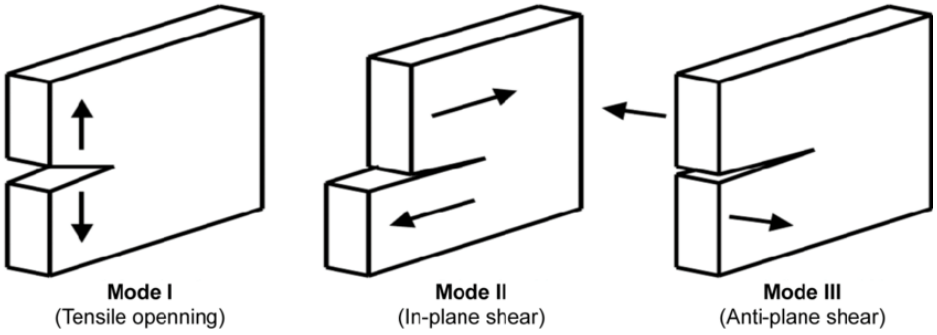

Figure 2.6: Crack opening modes

A common approach for fatigue assessment is based on Linear Elastic Fracture Mechanism (LEFM). LEFM can be applied under linear elastic assumptions and small scale yielding at the crack tip. According to Paris, the SIF is a driving force for crack expansion. Hence, Paris and Erdogan (1963) have proposed a model that links the crack growth speed (da/dN) to the SIF, K, see Equation 2.11.

$$\frac{da}{dN} = C(\Delta K)^m \tag{2.11}$$

where C and m are parameters related to the material and ΔK is the SIF range which is the difference between the maximum and minimum values of stress intensity for each stress range. SIF is usually given by Equation 2.12, where $Y(a)$ is defined based on the crack and component geometry and S denotes the stress range (Broek, 1986; Ritchie and Knott, 1973). Depending on the complexity of the geometry either closed form solutions exist for ΔK or Finite Element Analysis (FEA) is required to assess it (Li et al., 2019; Qian and Long, 1992).

$$\Delta K = SY(a)\sqrt{\pi a} \tag{2.12}$$

As it can be seen from Figure 2.7, crack propagation can be divided into three stages. In the first stage, for low values of ΔK near ΔK_{th} underlying mechanisms are

not continuous. Before ΔK_{th}, fatigue cracks are assumed to be inactive. In the second stage, the crack propagation shows a linear behavior and it can be described by Paris-Erdogan's law. In the third stage, the crack propagation has a nonlinear behavior when K_{max} gets closer to the fracture toughness K_C. Fatigue failure happens for $K_{max} > K_c$ (Ritchie, 1999).

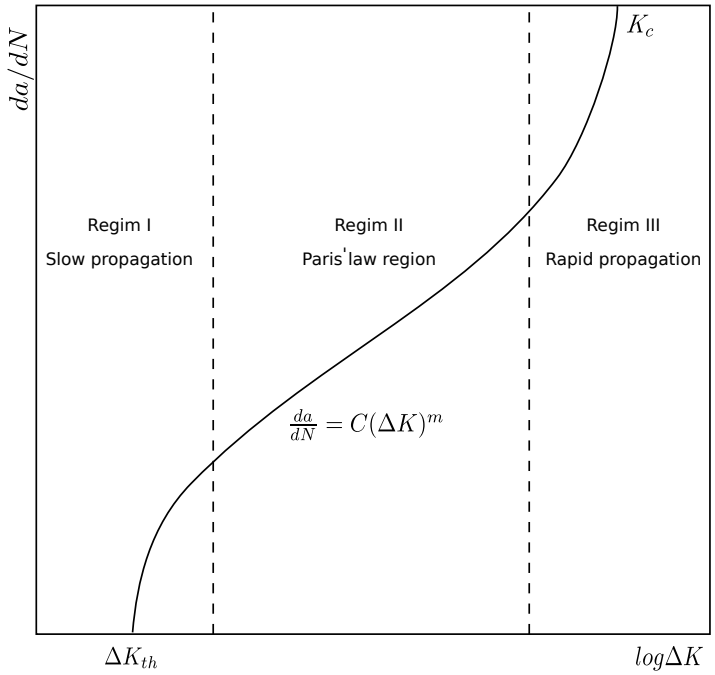

Figure 2.7: Paris law region

Fatigue crack propagation models based on fracture mechanism are appropriate tools to study structural fatigue life for existing structures since they have already experienced real life loading conditions and therefore may have developed cracks in critical locations. Characteristics of the crack, geometry, and loading conditions should be incorporated in this approach. Fracture mechanism provides a framework that allows to evaluate the time-dependent crack length which in turn can be used to decide the inspection schedule.

Before employing fatigue models, one should keep in mind that they are associated with significant amount of uncertainties. Consequently, uncertainty quantification and probabilistic modeling for fatigue life assessment is essential. In the next part, uncertainty modeling in fatigue life analysis is discussed.

2.6.3 Uncertainty modeling in fatigue

Fatigue life assessment is highly influenced by several sources of uncertainties which can be classified in three different types such as natural variability, data uncertainties, and model uncertainty. These sources of uncertainty can exist in both S-N approach and fracture mechanism. For instance, Table 2.2 represents some sources of uncertainty in fracture mechanism approach (Sankararaman et al., 2009; Ling et al., 2011). It is necessary therefore to rely on probabilistic modeling to take into account those sources of uncertainties. Performing a probabilistic fatigue life assessment requires to identify, quantify, and take them into account properly. Therefore, the aim of this section is to introduce some of the main sources of uncertainty in fatigue assessment.

Type	Sources of uncertainty
1: Natural variability	• Loading • Equivalent initial crack size • Material properties (fatigue limit, SIF threshold)
2: Data uncertainty	• Spares data (uncertain distribution parameters for material properties) • Output measurement error • Crack detection uncertainty
3: Model uncertainty / errors	• Crack growth law • Uncertainty in calculation of SIF (FE discretization error, surrogate model uncertainty)

Table 2.2: Sources of uncertainty in fatigue crack growth (Sankararaman et al., 2009)

Regarding the uncertainties in fatigue loading, previous experimental studies have shown that fatigue life and crack propagation behavior is highly influenced by the variability and uncertainty in the loading spectrum (Moreno et al., 2003; Zapatero et al., 2005). Uncertainties in loading can be originated by characteristics of a) operational environment such as temperature, wind, road profile, etc., b) mission type or service use that can be normal or emergency use, military or commercial use, etc., and c) human factors like traffic loading, maneuvers, and customer usage. Fatigue load spectrum is usually modeled by cycle counting and random process methods. Rainflow counting is the most common method among the cycle counting methods which extracts the counting matrices from the loading spectrum that include information about the number of load cycles, the range and the mean value of each load cycle (Dowling, 1971).

Methods based on random process try to model the load spectrum as a stochastic process. Markov chain method lies in this category in which the load spectrum is treated as a discrete time Markov chain that has a stationary probability matrix (Krenk and Gluver, 1989). Time domain and frequency domain based methods can be used to model a random process with a continuous state space. Time domain based methods are more appropriate to model load spectrum according to issues related to fatigue damage prognosis such as inspection and maintenance scheduling that are defined in the time domain (Ling et al., 2011). With this respect, time series methods such as Auto-Regressive Moving Average (ARMA) or Auto-Regressive Integrated Moving Average (ARIMA) are time domain based methods and they can be used to model the load spectrum (Benasciutti and Tovo, 2007). Ling et al. (2011) have investigated load models such as rainflow counting, discrete time Markov chain, and ARMA. They have assessed the predictive confidence of all models and the results show that all models work well. However, the overall confidence metric (computed by Bayesian hypothesis testing) based on the presented numerical example shows that ARMA has the best support from the loading data. They also have shown that additional information about the load spectrum on the structure obtained by SHM can help to update the model parameters. It should be mentioned that methods such as rainflow counting,

Markov chain, and ARMA are assuming that the load spectrum is a stationary process.

Providing suitable approaches to model the load spectrum is an important step for fatigue probabilistic modeling. However, another important issue with this respect is to calculate local stresses in the proximity of fatigue region. Local stresses are also influenced by some parameters such as overall loading, fatigue detail geometry, residual stresses, etc. Calculated stress ranges and number of stress cycles can directly be used in S-N approach to evaluate the remaining fatigue life. Within the fracture mechanism approach they are used to calculate SIF. FEA is a common way that is used to calculate local stresses. One of the important issues that affect the accuracy in this method is the mesh size (Sankararaman et al., 2011). Assuming that the boundary conditions are provided properly, a small mesh size will lead to almost accurate solutions. This, however, is very difficult to implement in practice since it needs a huge computation time.

Initial crack size is another source of uncertainty related to the natural variability. Some factors such as welding procedure, type of joint, fabrication yard, etc. affect the initial crack size. The crack propagation behavior for small cracks is not known very well. Introducing an Equivalent Initial Crack Size (EICS) is one way to avoid the analysis of crack propagation in microscopic scale (Sankararaman et al., 2009; Liu and Mahadevan, 2009). Therefore, in crack propagation models like Paris law, the propagation related to microscopic cracks is replaced with an EICS. This quantity cannot be measured by experiments therefore some researchers consider its value between 0.25 to 1 mm for metals (Merati and Eastaugh, 2007; Gallagher et al., 1984). Some studies consider EICS as a random variable in which they use lognormal distribution to model the uncertainty (Wirsching, 1984).

Uncertainties in the material properties is another source of uncertainty in fatigue assessment which can be either related to natural variability or data uncertainty which exist in both S-N curves and fracture mechanism approaches. This uncertainty can be related to the type of material, manufacturing and preparation, and test conditions. In S-N curves material characteristics are represented by parameters m and A. The large

scatter observed in number of cycles to failure in S-N curves is due to the uncertainty in material properties. Parameters m and A are highly correlated therefore it is useful to consider one of them as a fixed parameter and the other one as a random variable. Fatigue tests can be used to identify the parameters of the desired random variable. This is also the same for material parameters, m and C, in fracture mechanism approach. similarly, these two parameters are highly correlated. Therefore one of them can be considered as a fixed parameter and the other on as a random variable (Wirsching, 1984).

As mentioned previously, according to the Miner's hypothesis for linear damage accumulation using S-N curves, the fatigue failure occurs when the cumulative damage is equal to 1. Although fatigue tests under varying amplitude loading show a spread from this value which means that the Miner's sum (Δ) should be treated as random variable. This randomness can be caused because of the model error in Miner's assumptions. It has been proposed in some studies to treat the Miner's sum as a log-normal variable with the mean value of 1 (Wirsching, 1984). According to the crack growth model, plenty of crack propagation laws can be noticed in the literature (e.g. Paris law, Foreman's equation (Minguez, 1994), Weertman's equation (Weertman, 1984), etc.) which shows non of them can be applied commonly to all crack propagation problems. Apart from the uncertainties in the coefficients of the crack propagation model there is also a model error that needs to be considered. For instance if one uses Paris law for crack propagation, it can be formulated as in Equation 2.13 where ε_{cg} is the error for the crack growth model (Sankararaman et al., 2009).

$$\frac{da}{dN} = C(\Delta K)^m + \varepsilon_{cg} \tag{2.13}$$

2.6.4 Performance functions for fatigue reliability assessment

Fatigue life assessment being associated with large amount of uncertainties, a reliability-based fatigue life assessment is a rational way to treat uncertainties coming from natural randomness, modeling errors, and prediction imperfections (Byers et al., 1997). In this context one can define the probability of failure as the probability of violating one or

more limit states. Limit state is the boundary between the failure and the safe domain defined by a structural performance function (denoted G in Subsection 2.5.1) which mathematically expresses a given failure criterion. For many mechanical problems, a "stress-strength" definition is used. The "stress" (S) represents a given structural response, i.e. local Van Mises stresses, and the "strength" (R) denotes the material capacity of the structure, i.e. the yield stress. The "stress" and "strength" can be input and output variables, e.g. the results of the propagation of input uncertainties through a mechanical model. In both S-N and fracture based approaches performance function can be expressed by the difference between the "stress" and the "strength" (Melchers, 1999; Barone and Frangopol, 2014).

$$G(t) = R(t) - S(t) \tag{2.14}$$

S-N based approach performance function can be described in different forms. A common way to provide the performance function in this approach is in terms of damage. This can be expressed by Equation 2.15 where the cumulative damage D_L should be less than a target damage Δ_{target}. Parameter $\mathbf{X}$ here represents the associated input random variables.

$$Z(\mathbf{X}) = \Delta_{target} - D_L(\mathbf{X}) \tag{2.15}$$

Another way to express the performance function for this approach is based on the number of cycles to failure N_c. If the total number of stress cycles to failure under variable stress range is N_t then the performance function can be formulated as Equation 2.16. For further information about formulation of N_t and N_c refer to (Liu et al., 2010).

$$Z(\mathbf{X}) = N_t - N_c(\mathbf{X}) \tag{2.16}$$

As mentioned previously, it is common to assume the Miner's sum as unity and the failure happens when the cumulative damage is more than 1. The damage caused by each stress range can be estimated using S-N curves that are usually provided by performing a huge number of fatigue tests under constant amplitude loading conditions for different stress ranges (Szerszen et al., 1999). To make good conclusions about the fatigue failure using this approach, it is necessary to properly estimate the stress ranges and the number of stress cycles.

Fracture based approach has been used in many studies for fatigue reliability analysis, see e.g. Park et al. (2005); Ye et al. (2014). As far as fracture mechanism of steel structures is concerned, two failure modes can be considered. The first failure mode, named brittle failure, is derived under LEFM assumptions when a crack exists in the structure. In such a framework, a static failure can be defined when the crack driving force expressed in terms of SIF (K) exceeds the fracture toughness K_c:

$$K(a, \sigma) \geq K_c \tag{2.17}$$

The fracture toughness, also named tenacity, refers to material ability to withstand unstable cracking. This equation can be equivalently rewritten by:

$$K_r = \frac{K(a, \sigma)}{K_c} \leq 1 \tag{2.18}$$

In Equations 2.17 and 2.18, a stands for the current crack length and σ for the peak stress of the current fatigue cycle. The criterion K_r shows the proximity to the brittle failure.

The second failure mode, named ductile failure, happens on any structure, even on structures without cracks, subjected to an increasing loading. The criterion is expressed by Equation 2.19. Where P corresponds to the applied load, $P_L(a, \sigma_y)$ is the value of P corresponding to the plastic collapse of the material which naturally depends on the yield stress σ_y and crack length a, and L_r^{max} is the threshold value that is a function of the material flow stress and yield stress.

$$L_r = \frac{P}{P_L} \leq L_r^{max} \tag{2.19}$$

Interactions between brittle failure and pure plastic collapse (e.g. for structures without crack) for some material (i.e. with ductile behavior, for which LEFM assumptions do not apply) and/or under specific loading conditions lead to intermediate configurations known as ductile tearing. In such cases the performance function should encompass both criteria in Equations 2.18 and 2.19. One solution is to resort to the R6 curve based rule, see Figure 2.8, which has been originally proposed by Harrison

et al. (1977). The performance function $G(L_r, K_r)$ may have different closed-form expressions. According to Kunz (1992) $G(L_r, K_r)$ can be represented by Equation 2.20.

$$G(L_r, K_r) = \begin{cases} \frac{1}{\sqrt{1+0.5L_r^2}} - K_r & L_r \leq 1 \\ 0 & L_r > 1 \end{cases} \tag{2.20}$$

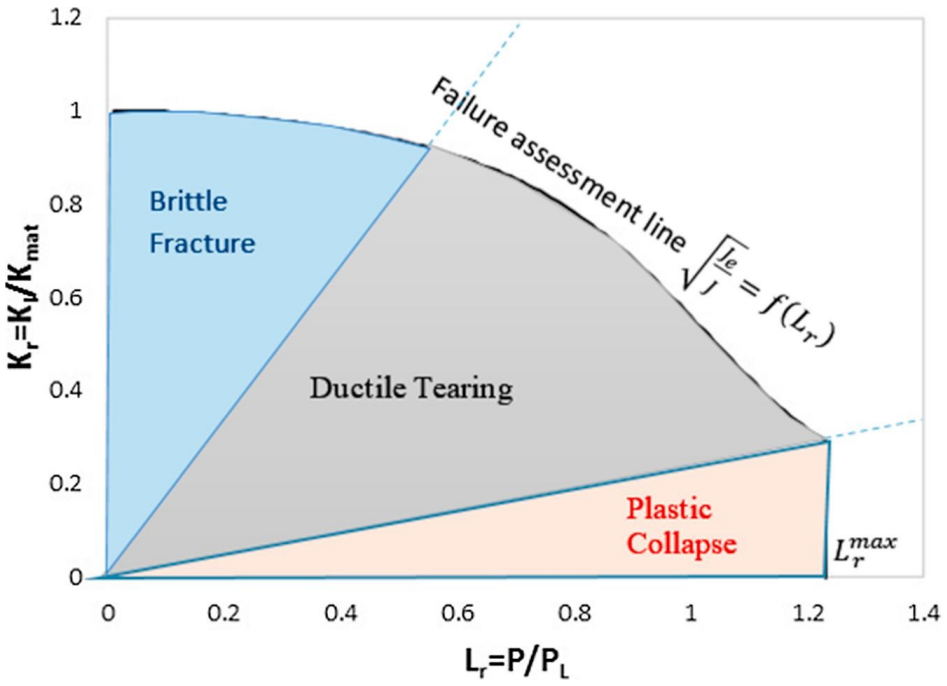

Figure 2.8: Schematic representation of different modes of failure in R6 (Sahu et al., 2019)

Another common way to formulate a performance function within the fracture based approach is according to the crack length. Under LEFM assumptions and given that the crack propagation occurs within the Paris' law region , the failure happens when the crack length at time t, $a(\mathbf{X}, t)$, is larger than a given critical crack length a_{cr}. The performance function hence can be formulated by Equation 2.21.

$$G(\mathbf{X}, t) = a_{cr} - a(\mathbf{X}, t) \tag{2.21}$$

In this section, several types of performance functions for fatigue reliability assessment (according to S-N and and fracture mechanism approaches) for steel structures have been reviewed. As said before, the main goal of fatigue reliability analysis is to compute the failure probability of components exposed to fatigue. An extensive review of

methods and approaches for evaluating the failure probability is provided in Chapter 3.

2.7 Monitoring, inspection and maintenance for fatigue

An accurate prediction of structural performance is the core of structural maintenance planning and LCM. With this respect inspections and SHM can play a crucial role. SHM provides real time information about the structural responses under the real loading conditions and inspections provide information about the actual fatigue damage level for the critical locations Frangopol (2011). An accurate knowledge about the fatigue behavior in critical locations of the structure is of paramount importance for decision makers to allocate proper maintenance strategies. Maintenance actions against fatigue usually try to reduce or stop the fatigue damage propagation. Table 2.3 summerizes some actions related to SHM, inspections, and maintenance for fatigue and the following part provides a brief introduction on some basic concepts of SHM, inspections, and maintenance for structures suffering from fatigue.

2.7.1 Structural health monitoring

SHM is a process focusing on observing, measuring, recording, and processing of actual data related to the structure. It provides valuable information about the current state of a structure under real loading conditions (e.g. loading, local stresses, crack geometry,etc.) (Cremona and Santos, 2018). During the past years, practices in SHM have significantly changed due to the developments in information technology. Advances in monitoring technology such as smart sensors, data storage, etc. make it possible to have a better snapshot of the structural behavior under different loading conditions (Cai and Mahadevan, 2016). Methods in SHM are mostly based on installing sensors on structures to continuously monitor and record their response which enables in turns to identify and localize the damage. SHM can generally be used for several reasons such as validation of design assumptions, recording the structural response under normal operating conditions, damage detection, and useful life estimation

Intervention type	Actions
1: SHM	• Acoustic emissions • Ultrasonic guided waves • Lamb waves
2: Inspection	• Visual inspection • Magnetic penetrant • Ultrasonic • Eddy current
3: Maintenance	• Surface treatment • Through thickness repair • modification of details

Table 2.3: Intervention types and related actions

(Zhu and Frangopol, 2013a,b). SHM can be very fruitful for fatigue life assessment by providing information about crack length, stress ranges and average number of cycles on a detail, etc. Acoustic emission, ultrasonic guided waves, and Lamb waves are among several SHM techniques that are commonly used to monitor and detect fatigue damage (Ciang et al., 2008). Acoustic emission has received more attention within the past decade. In this method, special sensors are used to record the stress waves that are expelled because of the changes inside the material. The recorded information can be used to detect some damage such as crack initiation and propagation, plastic deformation, corrosion, etc. (Anastasopoulos et al., 2009). Some other fatigue related monitoring systems employ strain gauges and accelerometers for example to measure stress levels and average number of load cycles on the critical fatigue locations. Before selecting a monitoring strategy for fatigue, one should consider material and geometry of the structure, potential defects, accuracy of the monitoring data, installation cost,

operation and maintenance of the monitoring system, etc. (Soliman et al., 2016).

2.7.2 Inspections

Inspections on the structures are usually performed visually on a regular basis. The time interval between inspection, for bridges for example, can be defined by different factors such as the volume of the traffic, age of the bridge, and the bridge condition. In the USA, 95 percent of the inspections are done at the intervals of 2 years or less. Road agencies in other countries, however, perform detailed inspections at intervals of 5 to 6 years along with less detailed check inspection at 1 to 3 year intervals (Transportation Research Board and National Academies of Sciences Engineering and Medicine, 2007). In France for instance, l'Instruction Technique pour la Surveillance et l'Entretien des Ouvrages d'Art (ITSEOA) is responsible for establishment of the procedure for inspection of most roadway infrastructures. Inspection planning for bridges according to regulations of ITSEOA is described in Table 2.4. Four types of inspections can be identified from this table such as routine visit, annual inspection, IQOA (Image de la Qualité des Ouvrages d'Art: Image of the Quality of Bridges) assessment, and detailed inspection (ITSEOA, 1979).

The simplest method to perform structural inspection is visual inspection that is done by human eyes and some optical devices. The quality of the inspection results are highly dependent on the visual acuity and color vision of the inspector, the hastiness level of the inspector, and accessibility to the inspection zone. Therefore, it is hard to ensure that inspections can detect fatal problems (Swartz and Lynch, 2009). By employing visual inspections for fatigue damage one could face notable limitations especially when fatigue cracks are small or if they occur in subsurface areas. For this reason, it is better to resort to more reliable techniques such as magnetic penetrant, ultrasonic, and eddy current methods for critical fatigue details (Fisher et al., 1998; Moan, 2005; Ciang et al., 2008).

In magnetic method, magnetic particles are used to detect discontinuities in steel plates. These can be indications for existence of cracks in smooth surfaces. The accur-

Table 2.4: Inspection types, France (ITSEOA, 1979)

Inspection type	Interval	Performed by	Description
Routine visit	Frequent	Road maintenance agents employed by DDE	Drive-by inspection
Annual	1 year	Road maintenance agents employed by DDE	Cursory examination during visit to bridge
IQOA	3 years	Inspection agent sometimes with certified inspector	Visual verification of conditions focusing on known defects
Detailed	9 years	Certified inspector	Robust bridges. Arms-length visual examination of all components and noting all defects
	6 years	Certified inspector	Normal bridges. Arms-length visual examination of all components and noting all defects
	3 years	Certified inspector	Ill bridges. Arms-length visual examination of all components and noting all defects
	1 year	Certified inspector	Very ill bridges. Arms-length visual examination of all components and noting all defects
Underwater	6 years	Certified inspector	Diver making arms-length touch and visual inspection

DDE: Direction Départementale de lEq uipment

acy of this method would decrease on welded surfaces (Demsetz, 1996). In penetrant methods, a liquid with low viscosity and high capillary is used. After cleaning the surface, this liquid with red color is applied (on the surface) and cracks become visible by spraying a developer on the surface. Like the previous method, this method is efficient on smooth surfaces (Fisher et al., 1998). High frequency sound waves are used in ultrasonic methods. A distortion in the reflected wave can be an indication of a crack. This method is good for steel plates with a thickness greater than 3 mm, but it requires high-skilled operators (Soliman et al., 2016). Eddy currents can also be used to detect cracks near surface in steel. Eddy current is produced by electromagnetic induction. Cracks then lead to some changes in the current that is detectable. Applying this method also requires well-trained inspectors (Hellier, 2012; Demsetz, 1996). Employing an inspection method to detect fatigue cracks is in general limited to a single critical location and it would be unfit to be used for scanning all the fatigue critical locations efficiently.However, monitoring systems make it possible to detect the

long-term fatigue damage in multiple critical regions efficiently and reliably (Antonaci et al., 2012).

It must be noted that one of the most important aspect of such inspection techniques is related to their failure detection reliability for applications out of lab conditions. With this respect, Probability of Detection (PoD) is an accepted quantitative measurement to evaluate the reliability of an inspection technique. The PoD is strongly connected to the topic of risk assessment and probabilistic analysis in the evaluation of the performance of components, and it provides the probability for the detection of certain flaw size. The PoD delivers the realistic, statistical assessment of the reliability for an inspection method, and the knowledge of the PoD of a certain defect allows assessing the consequences of this flaw in a probabilistic manner.

2.7.3 Maintenance

Maintenance against fatigue can be grouped into different categories such as surface treatments, through-thickness repair of cracks, and modification of details or structures (FHWA, 2013). Surface treatment usually involves grinding, applying Gas Tungsten Arc (GTA), and impact treatments. Grinding is used to remove a small portion of the fatigue detail that involves small cracks. Then, GTA is used to re-melt (a weld toe for example) to remove the small discontinuities and to reduce the stress concentration. Impact treatment is the last step that is used to reduce the crack initiation and propagation speed by applying a compressive residual stress on the weld toe, improving the geometry, or reshaping the weld toe (Fisher et al., 1998). Another common method to stop fatigue crack propagation through thickness is to drill a hole with a large-enough diameter at the tip of the crack. Depending on the size and location of the hole it can either be considered as long-term or short-term maintenance (Connor and Lloyd, 2017). Some repair actions aim to reproduce the same condition as before cracking. We can quote cutting out and re-fabricating some parts of components, where cracks through the thickness exist (Fisher et al., 1998). Another way to reduce fatigue crack propagation is to increase the cross sectional area by adding some cover plates.

In this way the stress concentration around the crack is decreased which mitigates the crack propagation speed.

2.8 Life-Cycle optimization with maintenance, monitoring, and inspection

An accurate evaluation of structural performance during its service life helps decision makers to decide about possible maintenance and repair actions. However, financial resources are limited and cannot cover all costs related to maintenance. Life-cycle cost is one of the most regular cost-based indicators that is used within many decision making processes to assess associated costs within the service life of a structure Frangopol et al. (1997). Including the cost of SHM (C_{mon}), the expected total life-cycle cost of a structure, C_{life}, can be formulated as:

$$C_{life} = C_{int} + C_{insp} + C_{mon} + C_{ma} + C_{fail} \tag{2.22}$$

where C_{int} is the initial cost; C_{insp} is the cost of inspection; C_{ma} is the cost of maintenance; and C_{fail} is the failure cost (Frangopol et al., 1997). According to the condition of a structure, different kinds of inspection, monitoring, and maintenance can be considered. Assuming that there are i types of inspections, j types monitoring, and k types of maintenance that are employed during the lifetime of a structure, their cost can be formulated as follows (Soliman et al., 2016).

$$C_{insp} = C^1_{insp} + ... + C^i_{insp} \tag{2.23}$$

$$C_{mon} = C^1_{mon} + ... + C^j_{mon} \tag{2.24}$$

$$C_{ma} = C^1_{ma} + ... + C^k_{ma} \tag{2.25}$$

Each type of inspection, maintenance, and monitoring can be applied for several times. Therefore, the cost for each type of inspection, monitoring, and maintenance can be calculated by following equations:

$$C^i_{insp} = \begin{cases} 0 & N^i_{insp} = 0 \\ \sum_{l=1}^{N^i_{insp}} \frac{C^i_{insp}}{(1+r)^{t^{(i,l)}_{insp}}} & N^i_{insp} \geq 1 \end{cases} \tag{2.26}$$

$$C^j_{mon} = \begin{cases} 0 & N^j_{mon} = 0 \\ \sum_{m=1}^{N^j_{mon}} \frac{C^j_{mon}}{(1+r)^{t^{(j,m)}_{mon}}} & N^j_{mon} \geq 1 \end{cases} \tag{2.27}$$

$$C^k_{ma} = \begin{cases} 0 & N^k_{ma} = 0 \\ \sum_{n=1}^{N^k_{ma}} \frac{C^k_{ma}}{(1+r)^{t^{(k,n)}_{ma}}} & N^k_{ma} \geq 1 \end{cases} \tag{2.28}$$

where C^i_{insp}, C^j_{mon}, and C^k_{ma} represent respectively the cost for single inspection of type i, monitoring of type j, and maintenance of type k. N^i_{insp}, N^j_{mon}, and N^k_{ma} are the number of applied inspection of type i, monitoring of type j, and maintenance of type k respectively. The annual discount rate for money is r and the time for applying lth inspection of type i, mth monitoring of type j, and nth maintenance of type k respectively are $t^{(i,l)}_{insp}$, $t^{(j,m)}_{mon}$, and $t^{(k,n)}_{ma}$. It is clear that the maintenance actions are applied to reduce the probability of failure p_f. Therefore, they can have a direct influence on the cost of failure. By taking the influence of maintenance actions into consideration one can formulate the cost of failure at year T by Equation 2.29 (Orcesi and Frangopol, 2011a).

$$C_{fail}(T) = C_{fail} \times p_f(0) + \sum_{t=1}^{T} \frac{C_{fail}(p_f(t) - p_f(t-1))}{(1+r)^t} \tag{2.29}$$

Life-cycle cost optimization is an important step within the LCM in which the optimum intervention times and types of maintenance and inspection interventions can be decided according to different objectives such as structural performance, cost, and service life (Liu and Frangopol, 2005; Frangopol and Liu, 2007). Figure 2.9 shows the relationship between the expected life-cycle cost and structural performance. It illustrates that the initial cost of a structure increases with a higher expected performance. By contrast, a high performance leads to lower costs for maintenance, and failure. An optimal maintenance and inspection strategy can be followed to maintain the structure performing its duties at a predefined performance level P^* while the expected total life-cycle cost is minimized to C^*. Decision makers usually search for the solutions that fall near this optimal value according to the owner's requirements (Frangopol et al., 1997).

Decision making process for maintenance and inspection planning should be per-

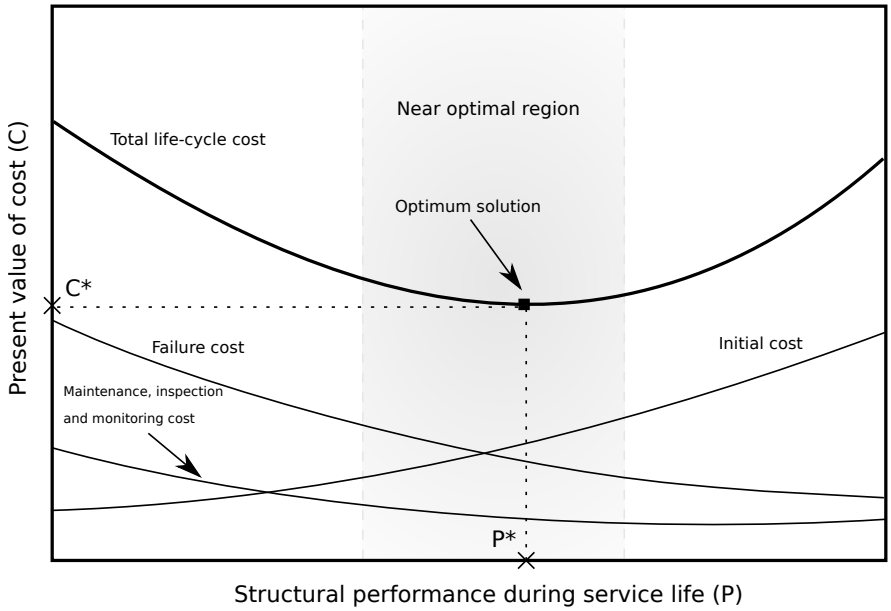

Figure 2.9: Relation between the life-cycle cost and structural performance (Frangopol, 2011)

formed through an optimization process. This can be formulated as a single or multi-objective model. Including more objectives within the optimization process makes it possible for more flexible decisions since multiple optimal solutions are provided for the problem according to the trade-off between the importance of each objective (Kim and Frangopol, 2017, 2018a). Different objectives that are considered for the multi-objective optimization can be related to the cost, reliability index, damage detection, and service life.

A multi-objective optimization problem can be generally formulated as following (Cheng, 1999; Augusto et al., 2012; Chang, 2015):

$$Minimize: \quad \mathbf{f(X)} \tag{2.30}$$

subject to

$$g_i(\mathbf{X}) \leq 0, \quad i = 1, ..., m \tag{2.31}$$

$$h_j(\mathbf{X}) = 0, \quad h = 1, ..., l \tag{2.32}$$

$$\mathbf{X}_{inf} \leq \mathbf{X} \leq \mathbf{X}_{inf} \tag{2.33}$$

where

$$\mathbf{f(X)} = [f_1, f_2, ..., f_k]^T \quad : \mathbf{X} \rightarrow \mathbb{R}^k \tag{2.34}$$

represents the vector containing the objective functions that are going to be minimized. Decision variables (or design variables) are collected in vector $\mathbf{X}$ and they are defined within the design space $\mathbb{R}^n$. Decision variables can be bounded between the lower bound $\mathbf{X}_{inf}$ and upper bound $\mathbf{X}_{inf}$. The three equations 2.31-2.33 define the feasible region for the optimal solutions where $g_i(\mathbf{X})$ represents the ith inequality constraint function and $h_j(\mathbf{X})$ is the jth equality constraint function. Inequality functions here are of type "less than or equal" functions that can represent functions of type "greater or equal" if they are multiplied by -1. likely, for the "minimization" of the functions that can be transformed to "maximization" in the same way as constraints.

Often, minimizing the cost is one of the main objectives within life-cycle optimization. With this respect some studies try to minimize life-cycle cost Lukic and Cremona (2001), and others search for the minimum maintenance cost (Orcesi et al., 2010). Other cost-related objectives can be linked to minimizing the failure, inspection, and monitoring costs (Soliman et al., 2013; Orcesi and Frangopol, 2011a). Improving the structural performance by maximizing reliability index (Kim and Frangopol, 2018b) or minimizing probability of failure (Kim and Frangopol, 2018a) is another objective for life-cycle optimization. Another objective that is defined in some studies is related to fatigue damage detection. Regarding to this Soliman et al. (2013) aims at maximizing the probability of fatigue damage detection whereas Kim and Frangopol (2011c) try to minimize the damage detection delay. Maximizing the extended service life can also be an objective within the multi-objective optimization process that has been considered in (Kim and Frangopol, 2018a; Soliman et al., 2016). Among possible decision variables that can be used in the multi-objective optimization, inspection times and types, maintenance times and types, monitoring starting times and durations are among the most used (Soliman et al., 2016; Kim and Frangopol, 2018a; Orcesi and Frangopol, 2011a).

An exemplary formulation for a bi-objective maintenance optimization can be

formulated as following (Okasha and Frangopol, 2009a).

• Find

$$Maintenance\ application\ times:\ \mathbf{t}_{ma} = \{t_1, t_2, ..., t_n\} \tag{2.35}$$

$$Maintenance\ types:\ ma_{t_1}, ma_{t_2}, ..., ma_{t_j} \tag{2.36}$$

• Objectives

$$Minimize\ the\ C_{life} \tag{2.37}$$

$$Maximize\ annual\ reliability\ index\ \beta\ or\ minimize\ P_f \tag{2.38}$$

• Such that

$$t_n - t_{n-1} \geq T_{min}\ years \tag{2.39}$$

$$\beta \geq \beta_{min} \tag{2.40}$$

The goals of the optimization process are a) to minimize the life-cycle cost C_{life} and b) to maximize the annual reliability index β. Decision variables for this problem are maintenance times, $\mathbf{t}_{ma} = \{t_1, t_2, ..., t_n\}$, and maintenance types $ma_{t_1}, ma_{t_2}, ..., ma_{t_j}$. The optimization algorithm should search for the optimal solutions under given conditions such as the minimum time between two consecutive repairs should be greater than a given minimum value T_{min}, and also it should search within annual reliability indices that are greater than a given minimum value β_{min}.

2.9 Conclusion and contributions of this thesis to LCM

As it was discussed in this chapter, Structural LCM is a framework combined by different steps and each step performs given duties to play a part in accomplishment of the overall LCM objectives. Optimizing the structural maintenance planning can be considered as one of the goals of the structural LCM. It is an exhaustive task in which different challenges and obstacles need to be properly addressed. To enumerate some of the challenges in steel structures one can refer to performance prediction under uncertainty, employing SHM data to reduce uncertainties, crack propagation behavior for given components, reliability- and cost-informed decision making, and effect of maintenance actions among others.

In this thesis, studies have been performed to enhance the capabilities of the structural LCM by proposing methods and approaches related to previously mentioned challenges. With this respect and as it was discussed in Chapter 1, a new time-dependent reliability method is proposed in Chapter 3 that is called AK-SYS-T. This method provides an efficient and accurate tool to evaluate time-dependent reliability of a component compared to other available methods. It is worth mentioning that time-dependent reliability analysis is necessary in this context since the performance deterioration (such as fatigue) is a time-dependent process associated with time-dependent parameters such as fatigue loading.

Another subject that is performed in this context is related to investigating the usefulness of advanced methods like XFEM and FEM methods for evaluating structural fatigue issues in Chapter 4. On that account, cracking problem in the root of a fillet weld that is a common fatigue detail in bridges with orthotropic deck plates is considered as an illustrative example. One important issue that is investigated here is the influence of the transversal tension in the deck plate on the direction of the crack propagation for the cracks initiated in such a location. Moreover, XFEM is used again to examine the effectiveness of two possible repair solutions an such fatigue cracking problems.

The objective in Chapter 5 is to provide a framework to employ the proposed time-dependent reliability method for fracture based time-dependent fatigue reliability problems. The performance function for such problems is highly irregular and requires a require a cycle-by-cycle calculation of SIFs. Hence, huge computational resources are needed in order to directly applying available methods like AK-SYS-t for such problems. Therefore, a strategy is proposed to simplify the underlying performance function in order to perform time-dependent reliability analysis using AK-SYS-t.

Finally, the last contribution of this study to structural LCM is to employ time-series methods such as seasonal ARIMA to provide a load model for long-term fatigue loading that can capture more details of the loading scenario regarding the seasonal effects in traffic loading which is an important advantage of this method compared

to other methods (e.g. rain-flow counting). This approach can be used for long-term monitoring data that are recorded with high frequency. It should be noted that employing time series methods for such data is not a straightforward task. More details for this method are provided in Appendix A.

Chapter 3: AK-SYS-t: a new approach for time-dependent reliability analysis

3.1 Introduction

Several steps of the structural LCM for structures suffering from fatigue have been introduced in Chapter 2. Fatigue is one of the dominant failure modes in metallic structures that can cause structural failure before reaching the designed service life. Fatigue is a time-dependent process due to the repetition of the applied loads which contribute to the degradation of material properties. Accordingly, dealing with such a deterioration process within the structural LCM requires some performance indicators which can take into account this time dependency. With this respect, time-dependent reliability can be employed to provide a well-suited indicator for structural LCM to tackle fatigue issues. It enables us to take into account the associated uncertainties in the phenomenon and to provide an estimation of cumulative failure probability for a given period of time. Accurate approximation of fatigue reliability is crucial for making decisions about structural maintenance and inspection planning to tackle fatigue problems. On that account, efficient approaches are indispensable to estimate the time-dependent reliability. The goal of this chapter is to propose a new time-dependent reliability method which tries to tackle this issue.

The new methodology is called AK-SYS-t that is aiming at accurately and efficiently evaluating the cumulative failure probability especially for time-dependent problems involving non-monotonic and costly-to-evaluate performance functions. The idea behind this method is to relate time-dependent reliability problems with system

reliability problems in order to take advantage of effective system reliability methods. This can be done by discretizing the desired time interval into a finite number of time nodes. AK-SYS (Fauriat and Gayton, 2014) is a recent and efficient system reliability method in which performance functions for components are replaced with Kriging meta-models and an active learning process is used for the enrichment of the Design of Experiment (DoE). AK-SYS owes its efficiency to its learning process due to the fact that it only searches among the most vulnerable components to update the DoEs. AK-SYS-t employs this learning process in order to address time-dependent reliability problems and it is introduced in this chapter.

Accordingly, the rest of this chapter is organized as follows. The general context of reliability analysis is provided in Section 3.2 which also includes a short summery of static, i.e time-independent, reliability approaches. Section 3.3 formulates a time-dependent reliability problem, introduces the main challenges, and reviews the available methods and approaches to handle such problems. Meta-model-based approaches for time-dependent reliability analysis are reviewed in Section 3.4 and the new method AK-SYS-t is presented in Section 3.5. Two numerical cases are employed in Section 3.6 to validate the proposed methodology. Section 3.7 proposes a crude approach to provide the whole curve of cumulative failure probability over time using AK-SYS-t. In the end, a short conclusion is provided in 3.8.

3.2 Time-independent reliability analysis

One main goal of a structural reliability analysis is to find the probability of failure of a component, structure or system under given conditions and for a given period of time. Failure mode is generally expressed by a so called performance function G. This function is used to mathematically describe the performance of a physical system by the following equation

$$G : \mathbf{X} \in \mathcal{D}_{\mathbf{X}} \subset \mathbb{R}^d \rightarrow Y = G(\mathbf{X}) \in \mathbb{R} \tag{3.1}$$

in which $\mathbf{X}$ is the vector of input random variables of dimension d and Y is the evaluation of the performance function on $\mathbf{X}$. According to the sign of $G(\mathbf{x})$, the input space, $\mathcal{D}_{\mathbf{X}}$, can be divided into a failure domain $\mathcal{D}_f$ and a safe domain $\mathcal{D}_f$. The failure domain refers to the region where for each realization of $\mathbf{X}$ in this region $G(\mathbf{x}) \leq 0$, while realizations of $\mathbf{X}$ within the safe domain lead to $G(\mathbf{x}) > 0$. The threshold separating the failure domain from the safe domain is called limit state function where $G(\mathbf{x}) = 0$.

Generally, two types of limit states can be realized for structures: 1) ultimate limit states and 2) serviceability limit states. Failure modes within the former limit states are related to the loss of load carrying capacity such as weld rupture, fatigue rupture, formation of plastic hinge, etc. The latter limit states include failure modes related to gradual deterioration, user's comfort, etc. Undesired deflections, corrosion, and excessive deformations are some examples of the failure modes related to serviceability limit states.

Given the general form of the performance function $G(\mathbf{X})$, the failure probability can be calculated by integrating the joint probability density function $f_{\mathbf{X}}(\mathbf{x})$ of the n-dimensional vector $\mathbf{X}$ of the input random variables over the failure domain $G(\mathbf{x}) \leq 0$ (see Equation 3.2).

$$P_f = \text{Prob}(G(\mathbf{X}) < 0) = \int ... \int_{G(\mathbf{x}) \leq 0} f_{\mathbf{X}}(\mathbf{x}) \mathrm{d}\mathbf{x} \tag{3.2}$$

where $\mathbf{x}$ is a realization of the random vector $\mathbf{X}$.

Solving the Equation 3.2 requires multi-dimensional integration which makes it very difficult to find an analytical solution for real cases. Several challenges are identified in literature to evaluate this failure probability such as a) estimating low probabilities of failure, b) dealing with computationally expensive performance functions, c) handling a high number of random variables, and d) combination of previous challenges. Many reliability methods have already been developed in literature over years with this respect to approximate the failure probability. Available methods can be classified into three groups: 1) simulation-based methods, 2) approximation-based methods, and

3) hybrid-based methods. A very brief state-of-the-art of common methods in those groups are reviewed hereafter.

3.2.1 Simulation-based methods

Crude Monte Carlo Simulation (MCS) is one of the most common direct simulation-based methods used to approximate the failure probability. Considering the indicator function formulated in Equation 3.4 and introducing it in Equation 3.2, the failure probability can be reformulated as Equation 3.3.

$$P_f = \int ... \int_{\mathbf{X}} I(\mathbf{x}) f_{\mathbf{X}}(\mathbf{x}) \mathrm{d}\mathbf{x} \equiv \mathbb{E}(I(\mathbf{X})) \tag{3.3}$$

$$I(\mathbf{x}) = \begin{cases} 1 & if \quad G(\mathbf{x}) \leq 0 \\ 0 & \text{Otherwise} \end{cases} \tag{3.4}$$

where $\mathbb{E}()$ denotes the expectation of a given random quantity. Accordingly, by generating a sample of N_{MCS} independent realizations of $\mathbf{X}$ from $f_{\mathbf{X}}(\mathbf{x})$ such as $\{\mathbf{x}^{(i)}, i = 1, ..., N_{MCS}\}$, Monte Carlo simulation approximates the failure probability as:

$$\hat{P}_f^{MCS} = \frac{1}{N_{MCS}} \sum_{i=1}^{N_{MCS}} I(\mathbf{X}^{(i)}) \tag{3.5}$$

The associated estimator is unbiased and it is a summation of N_{MCS} independent and identically Bernoulli distributed random variables. According to the central limit theorem, given that N_{MCS} is large enough, $\hat{P}_f^{MCS}$ follows a normal distribution meaning that:

$$[\hat{P}_f^{MCS} - P_f] \underset{N \to \infty}{\hookrightarrow} N(0, \sigma_{MCS}^2) \tag{3.6}$$

where its variance can be calculated using the following equation (Lemaire et al., 2009)

$$\sigma_{MCS}^2 = \frac{1}{N_{MCS}} P_f (1 - P_f) \tag{3.7}$$

It can be realized that by increasing the sample size (N_{MCS}) the variance of MCS prediction decreases. This means that the uncertainty in the prediction of failure probability using MCS is epistemic and reducible (using a larger Monte Carlo population). The Coefficient of Variation (COV) is generally used to evaluate the accuracy of MCS, see Equation 3.8. A lower COV indicates a higher confidence (less uncertainty) on the final prediction.

$$CoV_{P_f^{MCS}} = \frac{\sigma_{MCS}}{\hat{P}_f^{MCS}} = \sqrt{\frac{1 - \hat{P}_f^{MCS}}{N_{MCS} \times \hat{P}_f^{MCS}}} \tag{3.8}$$

Application of MCS is simple and straightforward. This method can be applied on any type of performance functions regardless of their shape and dimensionality. However, one basic problem in this method is related to the required sample size which drastically increases for calculating small failure probabilities for a sufficiently low COV. For instance, for a problem with failure probability of 10^{-n}, at least 10^{n+2} simulations are required to reach a COV of 10%. This becomes even more critical when costly-to-evaluate performance functions are involved.

Researchers have tried to sort out this issue by introducing advanced simulation-based methods such as Importance Sampling (IS) (Au and Beck, 1999; Melchers, 1999) and Subset Simulation (SS) methods (Au and Beck, 2001, 2003). The aim of these methods is to estimate the probability of failure by making fewer calls to the original performance function to reach the same variation of estimation.

Importance Sampling (IS) technique (Melchers, 1999; Au and Beck, 1999) is a variance reduction technique which is used to evaluate the probability of rare events more efficiently than MCS. The main idea here is to estimate the failure probability by sampling from a different distribution $q(\mathbf{x})$, called IS distribution or instrumental probability density function. Selecting an appropriate IS distribution would help to sample rare events more efficiently. In this way the probability of failure in Equation 3.3 can be reformulated as:

$$P_f = \int ... \int_{\mathbf{X}} I(\mathbf{x}) \frac{f_{\mathbf{X}}(\mathbf{x})}{q(\mathbf{x})} q(\mathbf{x}) \mathrm{d}\mathbf{x} = \mathbb{E}\big(I(\mathbf{x}) \frac{f_{\mathbf{X}}(\mathbf{x})}{q(\mathbf{x})}\big) \tag{3.9}$$

Accordingly, by applying the MCS and sampling N_{IS} independent realizations of $\mathbf{X}$ from $q(\mathbf{x})$ such as $\{\mathbf{x}^{(i)}, i = 1, ..., N_{IS}\}$, the failure probability can be approximated with the following equation

$$P_f^{IS} = \frac{1}{N_{IS}} \sum_{i=1}^{N_{IS}} I(\mathbf{x}^{(i)}) \frac{f_{\mathbf{X}}(\mathbf{x}^{(i)})}{q(\mathbf{x}^{(i)})} \tag{3.10}$$

Number of samples required in IS (N_{IS}) is theoretically less than the one required in MCS if an appropriate IS distribution is selected, i.e. if it allows one to generate samples in the vicinity of the failure region. The efficiency of IS method therefore depends on the choice of the IS distribution which requires a good knowledge about the failure region. It should be mentioned that the optimal IS distribution is

$$q_{opt}(\mathbf{x}) = \frac{I(\mathbf{x}) f(\mathbf{x})}{P_f} \tag{3.11}$$

which ensures that the variance of estimation in Equation 3.10 is equal to zero. However, finding this optimal distribution seems troublesome since it involves the unknown values of P_f which is the quantity of interest. Hence, the idea of resorting to the design point, introduced in Section 3.2.2, seems promising to characterize the failure region in order to determine a suitable IS distribution (Au and Beck, 1999). As a result, one common way to select the IS distribution is to center it on the design point.

Subset Simulation (SS) is another popular simulation-based method that has been proposed to compute small probabilities of failure (Au and Beck, 2001, 2003). In this method, intermediate nested failure events are defined and the probability of failure is expressed as a product of conditional failure probabilities which have to be chosen sufficiently large to reduce the computational cost. The thresholds of the intermediate events are estimated from small samples. In this way, computing a small failure probability which may require a high computational cost with a pure MCS is replaced by computing a sequence of conditional probabilities with less computational effort. Performing MCS to evaluate the conditional probabilities is not a very efficient solution. For this reason, it is common to resort to a Markov Chain Monte Carlo (MCMC) based simulation method (Norouzi and Nikolaidis, 2012; Beck and Au, 2002). Au and Beck (2001) have proposed a modified version of the original Metropolis Hasting

algorithm to deal with high dimensional problems. Another way to efficiently perform the simulation is to perform subset simulation with splitting (Ching et al., 2005).

3.2.2 Approximation-based methods

Methods in this group are also called design point-based methods or Most Probable Point (MPP) based methods, since they are based on the MPP in the standard normal space (Huang et al., 2017; Melchers, 1999). For this reason, an isoprobabilistic transformation is required first to convert physical input variables from the input space $\mathbf{X}$ to uncorrelated Gaussian variables $\mathbf{U}$ with mean zero and standard deviation equal to 1. This U-space is called the standard normal space. The isoprobabilistic transformation conserves probabilities meaning that $F_X(\mathbf{x}) = \Phi_{\mathbf{U}}(\mathbf{u})$ where $\Phi_{\mathbf{U}}$ is the joint Cumulative Distribution Function (CDF) of $\mathbf{U}$ and its PDF is denoted by $\phi_{\mathbf{U}}$. Therefore, the probability of failure in the standard normal space can be formulated as:

$$P_f = \int ... \int_{H(\mathbf{u})\leq 0} \phi_{\mathbf{U}}(\mathbf{u}) \mathrm{d}\mathbf{u} \tag{3.12}$$

where $H(\mathbf{U})$ is the performance function expressed in the U-space.

The MPP of coordinates $\mathbf{u}^*$ results from the following constrained optimization problem:

$$\mathbf{u}^* = \underset{\mathbf{u}}{\operatorname{argmin}} \{ \| \mathbf{u} \| \, | H(\mathbf{u}) \leq 0 \} \tag{3.13}$$

Several methods have been proposed in literature to solve this optimization problem among which one can refer to HL-RF algorithm (Hasofer and Lind, 1974; Rackwitz and Flessler, 1978), Newton methods, and the sequential quadratic program (Wright and Nocedal, 1999). It can be seen from Equation 3.13 that the MPP belongs to the failure domain and it is the closest point to the origin in the U-space. Among all realizations in the failure domain, the MPP has the highest probability density. For this reason it is called most probable point or design point.

The Euclidean distance between the origin and MPP is called the reliability index β. The failure probability then can be approximated by Equation 3.14 where Φ is the

standard normal cumulative density function.

$$P_f \approx \Phi(-\beta) \tag{3.14}$$

The MPP can be considered as an optimal anchor point to locally approximate the limit state function $H(\mathbf{u}) = 0$. First Order Reliability Method (FORM) and Second Order Reliability Method (SORM) are among the most prevalent methods in this group. In FORM, the limit state is linearized using the first-order Taylor expansion around the MPP whilst in SORM, a second-order Taylor expansion is used. These approximations are used to replace the original limit state function at the design point in order to approximate the failure probability.

The FORM is widely used in structural reliability analysis due to its efficiency and simplicity. However, the accuracy of this method would drastically reduce when dealing with problems with highly nonlinear limit state functions, high dimensionality, and multiple design points. The SORM can be used to increase the accuracy for quadratic limit state functions. However, it requires the computation of the second order derivatives which leads to less efficiency than FORM in terms of computational cost. SORM has the same drawbacks as FORM when it comes to highly nonlinear performance functions, high dimensionality, and existence of several MPPs.

3.2.3 Meta-model based methods for time-independent reliability analysis

The underlying idea behind hybrid methods is to replace a costly-to-evaluate performance function by a meta-model. A meta-model emulates the behavior of an original function and which is expected to be less costly-to-evaluate than the original function. In this way, the number of calls to the original performance function should be reduced which can help to mitigate the computational burden in reliability analysis. Kriging (Williams, 1998) and Polynomial Chaos Expansion (PCE) (Blatman and Sudret, 2010) are among the most common used meta-models employed for reliability applications. Appendix B provides a short review of Kriging since it will be further used in this chapter.

Meta-models are calibrated from a numerical Design of Experiment (DoE). The selection of samples in DoE is of a paramount importance and they should be selected in a way to adequately cover the domain of variations of the input variables. In meta-modeling based approaches, it is a common practice to sample an initial DoE of reduced size and then to sequentially enrich it with an appropriate strategy. The initial DoE is prepared by sampling N_{DoE} realizations $\mathbf{x}^{(k)}, k = 1, ..., N_{DoE}$ from the input random vector $\mathbf{X}$ and evaluating the original performance function G on this primary sample. Different sampling approaches such as random sampling, Latin Hypercube Sampling (LHS), and Hammersley sampling can be used to efficiently generate the initial DoE from the input random vector (Hu and Du, 2015b). Meta-models can then reach a sufficient level of accuracy by enriching the initial DoE with additional samples and recalibrating the meta-models.

In reliability analysis it is sufficient to know properly the sign of the performance function response rather than knowing the exact value of the response. For instance, if the signs of the performance function responses for a MCS population are exactly known the probability of failure can be estimated by:

$$P_f^{MCS} = \frac{N^-}{N_{MCS}} \tag{3.15}$$

where N^- is the number of response values with negative sign and N_{MCS} corresponds to the size of the MCS population.

Echard et al. (2011) have proposed to replace the performance function G by a Kriging meta-model $\hat{G}$, and an active learning process is employed to efficiently classify a Monte Carlo population into positive (safe) and negative (failure) domains by analyzing the sign of $\hat{G}$. As Kriging meta-modeling provides a measure of uncertainty on the prediction of unforeseen points, the authors have proposed a learning function U (Equation 3.16) which measures the uncertainty on the estimation of the right sign of the performance response.

$$U(\mathbf{x}) = \frac{|\mu_{\hat{G}(\mathbf{x})}|}{\sigma_{\hat{G}(\mathbf{x})}} \tag{3.16}$$

where $\mu_{\hat{G}(\mathbf{x})}$ is the Kriging prediction and $\sigma^2_{\hat{G}(\mathbf{x})}$ is the Kriging variance at an unknown point $\mathbf{x}$. This learning function can be used to classify the points into two groups:

1. $\mathbf{x}$ such that $U(\mathbf{x}) \geq 2$: the sign of G is almost surely predicted
2. $\mathbf{x}$ such that $U(\mathbf{x}) < 2$: the predicted sign using $\hat{G}$ might be wrong, i.e. $\hat{G} \times G \leq 0$

This learning process has led to a group of reliability methods often called AK family which includes for example AK-MCS (Echard et al., 2011), AK-IS (Echard et al., 2013), AK-SS (Huang et al., 2016), AK-SSIS (Tong et al., 2015), AK-LS (Lv et al., 2015), etc. AK-MCS is the pioneer of those methods and it is briefly recalled here.

AK-MCS is an active learning reliability method that combines Kriging and MCS with the aim to efficiently assess the failure probability for problems involving costly-to-evaluate performance functions. The main steps of this method are:

1. Generating a Monte Carlo population of size N_{MCS}, $\mathbf{x}^{(i)},\ i = 1, ..., N_{MCS}$
2. Selecting an initial DoE of size N_{DoE}, $\{\mathbf{x}^{(i)}, G(\mathbf{x}^{(i)})\},\ i = 1, ..., N_{DoE}$
3. Calibrating and iteratively enriching the Kriging meta-model $\hat{G}$:
   - Calibrating the initial Kriging meta-model $\hat{G}$ from the initial DoE
   - Calculating the probability of failure with MCS by replacing G by $\hat{G}$
   - Evaluating the learning function U on the Monte Carlo population: $\mathbf{x}^{(i)},\ i = 1, ..., N_{MCS}$
   - Evaluating the stopping criterion $\min U(\mathbf{x}^{(i)}) \geq 2$ on $\mathbf{x}^{(i)},\ i = 1, ..., N_{MCS}$
   - Enriching the DoE by adding the best next point $\mathbf{x}^{(*)} = \underset{i=1,...,N_{MCS}}{\operatorname{argmin}}\ U(\mathbf{x}^{(i)})$ and re-calibrating the Kriging meta-model
   - Continuing the process until the stopping criterion is satisfied
4. Estimating the probability of failure P_f^{AK-MCS} using the Equation 3.15
5. Repeating the algorithm with a larger Monte Carlo population if $CoV_{P_f^{AK-MCS}} \geq CoV_{target}$ and stopping the algorithm otherwise.

One should note that the Monte Carlo population size should be chosen in a way that it guarantees a low COV of the failure probability. The stopping criterion ($\min U \geq 2$) is related to the probability of making mistake in predicting the sign of G at each unknown sample which is equal to 0.023. This value has been chosen to guarantee a high level of accuracy. The points $\mathbf{x}$ that are added to the DoE for the enrichment are the points where $U(\mathbf{x}) < 2$ since their mean value $\mu_{\hat{G}(\mathbf{x})}$ is close to zero or their standard deviation $\sigma_{\hat{G}(\mathbf{x})}$ is high. Therefore, it is probable to make mistake on predicting the sign of $G(\mathbf{x})$.

3.3 Time-dependent reliability analysis

Methods and formulations of reliability analysis presented in the previous section do not consider the time as an input parameter. However, time can be incorporated into a structural reliability problem through different input parameters such as loading, material properties, geometry, etc. With this respect, performing a time-dependent reliability analysis seems to be inevitable. Time can be involved in a reliability problem either explicitly as an input variable or implicitly through stochastic processes. The general form of a time-dependent, also named time-variant, performance function can be represented as $G(\mathbf{X}, \mathbf{Y}(t), t)$ where $\mathbf{X}$ is the vector of input random variables, $\mathbf{Y}(t)$ is the vector of input random processes, and t is the time parameter. Performance functions including random processes can be converted into an explicit form of performance function, $G(\mathbf{X}, t)$, by means of some appropriate random process representations such as Karhunen-Loeve (KL) expansion (Loeve, 1977) or spectral representation method (Li and Kiureghian, 1993).

Given the explicit version of a time-dependent performance function, two types of failure probability can be defined: the instantaneous and the cumulative probabilities of failure. The first one is formulated in Equation 3.17 and measures the probability of failure at a given time instant t_i. The cumulative failure probability corresponds to the probability of having at least one failure during a given period of time $[t_0, t_l]$, i.e. the lifetime of a system, see Equation 3.18. Figure 3.1 shows an illustration of these

two failure probabilities.

$$P_{f,i}(t_i) = \text{Prob}(G(\mathbf{X}, t_i) \leq 0) \tag{3.17}$$

$$P_{f,c}(t_0, t_l) = \text{Prob}(\exists \tau \in [t_0, t_l], G(\mathbf{X}, \tau) \leq 0) \tag{3.18}$$

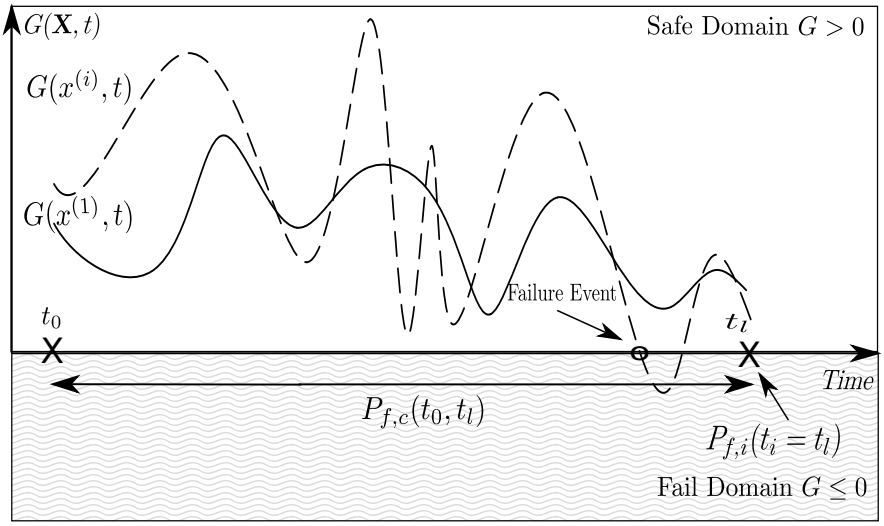

Figure 3.1: An illustration of instantaneous and cumulative probability of failure for a non-monotonic performance function

Instantaneous failure probability is, in fact, a time-independent reliability problem since it is calculated at a given time instant and thus it can be considered as a constant through reliability calculations. Accordingly, reliability methods such as MCS, IS, SS, AK-MCS etc. introduced in the previous section can be employed to evaluate the instantaneous probability of failure. It should be noted that for time-dependent problems with a monotonically increasing or decreasing performance functions with respect to time, the instantaneous and cumulative probabilities of failure are equal, see Equation 3.19. Therefore such problems are equivalent to time-independent reliability problems. Figure 3.2 illustrates the difference between the monotonic and non-monotonic performance functions.

$$P_{f,c}(t_0, t_l) = P_{f,i}(t_l), \text{ when G is non-monotonic} \tag{3.19}$$

The main goal of time-dependent reliability methods is then to calculate the cumulative probability of failure for problems with non-monotonic performance functions

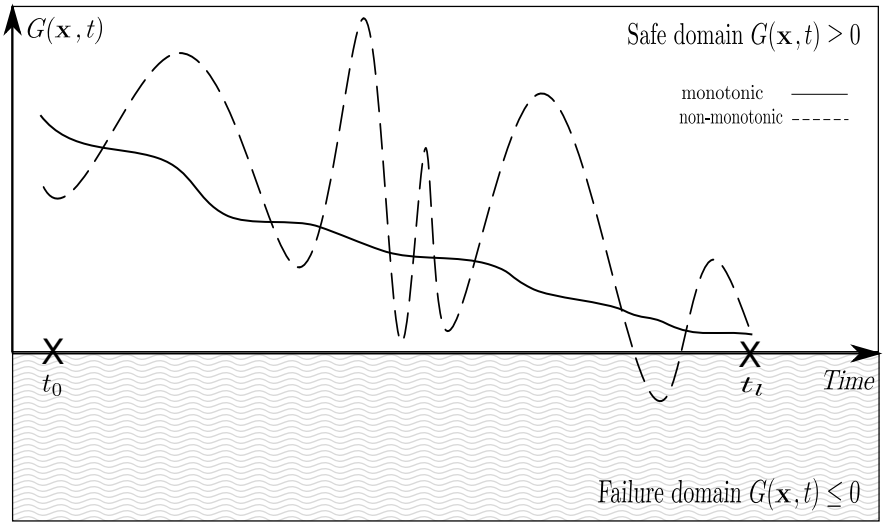

Figure 3.2: An illustration of the difference between the monotonic and non-monotonic performance functions with time

over time. Addressing time-dependent reliability problems remains challenging and a crude Monte Carlo approach is unaffordable due to the added complexity by time variable. Similar to time-independent reliability methods, finding a balance between efficiency and accuracy is always pursued especially for problems with low failure probabilities, high dimensionality, complex and computationally expensive performance functions, or a combination of them. Several methods have been developed so far for time-dependent reliability analysis and they can mainly be classified into two main groups namely Out-Crossing Based (OCB) methods and Extreme-Value Based (EVB) methods. The aim of the methods in the first group is to find the crossing rate of the performance function from the safe domain to the failure domain while methods in the second group are searching for the extreme values of the performance function (the extreme value here refers to the minimum value of the performance function). These methods are reviewed in the following.

3.3.1 Out-crossing based methods

The cumulative probability of failure, within the methods in OCB, is linked to the first-time-to-failure or the first passage t_f from the safe to the failure domain. The first-time-to-failure is a random variable and it corresponds to the first time instant

when the performance function crosses a given threshold. Hence, the formulation of $P_{f,c}(t_0, t_l)$ can be written as:

$$P_{f,c}(t_0, t_l) = \text{Prob}(t_f < t_l) \tag{3.20}$$

This equation implies that the cumulative probability of failure within $[t_0, t_l]$ is equal to the probability of having at least one out-crossing event from the safe to the failure domain within this time interval. If $N_{(t_0,t_l)}$ counts the number of out-crossing events over the desired time interval, the previous formulation for the cumulative probability of failure can be converted into the Equation 3.21.

$$P_{f,c}(t_0, t_l) = \text{Prob}(G(\mathbf{X}, 0) \leq 0 \cup N_{(t_0,t_l)} \geq 1) \tag{3.21}$$

It has been shown in (Shinozuka, 1964) that the cumulative failure probability can be bounded such as:

$$\max_{t\in[t_0,t_l]} P_{f,i}(t) \leq P_{f,c}(t_0, t_l) \leq P_{f,i}(0) + \mathbb{E}[N_{(t_0,t_l)}] \tag{3.22}$$

where $\mathbb{E}[N_{(t_0,t_l)}]$ is the mean value of out-crossings. The problem therefore lies in estimating the mean value of out-crossings during the desired period of time $[t_0, t_l]$. The mean value of out-crossings can be calculated by Equation 3.23 where $\nu(t)$ is the out-crossing rate which is formulated in Equation 3.24.

$$\mathbb{E}[N_{(t_0,t_l)}] = \int_{t_0}^{t_l} \nu(t)dt \tag{3.23}$$

$$\nu(t) = \lim_{\Delta t\to 0} \frac{\text{Prob}(N(t, t + \Delta t) = 1)}{\Delta t} \tag{3.24}$$

Calculating this rate is a complicated task. If the performance function can be expressed as a stationary and differentiable univariate process that is added to a constant threshold, then the Rice's formula can be used to find the out-crossing rate (Rice, 1944). By employing Rice's formula, asymptotic analytical formulations of out-crossing rate have been obtained for stationary Gaussian process in Lutes and Sarkani (2004) and also for a general Gaussian processes (stationary and non-stationary) in Lutes and Sarkani (2009); Sudret (2008).

Using some basic probability theories, it can be shown that $N_{[t_0,t_l]}$ follows a binomial distribution. For long-term reliability assessments the binomial distribution

tends to a Poisson distribution. Under this assumption and by neglecting the dependence between the out-crossing events, the out-crossing rate is equal to the rate for the first-time-to-failure (Ponte, 1985). However, ignoring the dependency between the out-crossing events for problems with high reliability levels (low probability of failure) can cause a big amount of error in calculations (Zhang and Du, 2011; Lutes and Sarkani, 2009; Sudret, 2008). Researchers have tried to mitigate this deficiency by using joint out-crossing rates (Hu and Du, 2013) and first order sampling approach (Hu and Du, 2015a).

One of the most popular methods among OCB methods is the PHI2 method (Andrieu-Renaud et al., 2004) that is extensively used because of its numerical efficiency. This method is based on system reliability analysis. A parallel system hence is considered for time instant t and $t + \Delta t$. The out-crossing happens if the system is in safe domain at time t and in the fail domain at time $t + \Delta t$. Accordingly, the out-crossing rate can be formulated as:

$$\nu(t) = lim_{\Delta t \to\ 0^+} \frac{\text{Prob}\big((G(\mathbf{X}, t) > 0) \cap (G(\mathbf{X}, t + \Delta t) \leq 0)\big)}{\Delta t} \tag{3.25}$$

PHI2 tries to approximate this out-crossing rate using FORM which is a time-independent reliability method. For this reason, two FORM analyses are required to estimate the probabilities of failure associated with $G(\mathbf{X}, t) > 0$ and $G(\mathbf{X}, t + \Delta t) \leq 0$ respectively. The input stochastic processes can be replaced by two random variables $Y(t)$ and $Y(t + \Delta t)$ for time instants t and $t + \Delta t$. Therefore, discretization of input stochastic processes is not required. PHI2 method provides an upper bound for the failure probability and thus underestimates the reliability level. The choice of the time increment Δt is crucial and affects the accuracy of this method. An approximation should be made on the choice of time increment, see (Sudret, 2008). Another drawback lies in employing FORM for problems with highly nonlinear performance functions which can lead to non-negligible errors. PHI2+ is an improvement of PHI2 that tries to stabilize the effect of the time increment Δt (Sudret, 2008). However, it should be noted that PHI2+ still may lead to significant errors in case of highly nonlinear limit states due to the use of FORM.

More recently, a method named mean value first passage method has been proposed in Zhang and Du (2011); Du (2012) for time-dependent reliability applications. Up-crossing rates are derived analytically under simplifying assumptions such as normality for random variables with small variance. The time-dependent reliability can be calculated by integrating those analytical equations. The integration process has been done using a numerical procedure proposed in this study. The applicability of this method for many of reliability problems that are far from its assumptions is questionable.

3.3.2 Extreme-value based methods

Methods in this category search for the extreme values of the performance function (global minimum here). The cumulative probability of failure then can be defined as the probability that the global minimum of the performance function becomes negative which is formulated by Equation 3.26.

$$P_{f,c}(t_0, t_l) = \text{Prob}(\min_{t\in[t_0,t_l]} G(\mathbf{X}, t) \leq 0) = \text{Prob}(G_{min}(\mathbf{X}) \leq 0) \tag{3.26}$$

where G_{min} is a random variable and the cumulative probability of failure can be accurately calculated if the probability distribution of this quantity is well known. However, determining this distribution is a difficult task especially for engineering applications with highly nonlinear performance functions. Moreover, structural analysis are usually performed over a long period of time and this can cause problem of dimensionality when stochastic processes are involved in a reliability problem.

Employing methods like MCS is not feasible to evaluate the cumulative failure probabilities because it can lead to a very huge computational cost especially when costly-to-evaluate performance functions are involved. Therefore, more advanced methods based on meta-modeling have been developed to reduce the computational cost. They are generally based on Kriging meta-modeling. In some studies, however, PCE is also used. Methods in this category are reviewed in the next section.

3.4 Review of meta-model-based methods for time-dependent reliability problems

3.4.1 t-PCE

t-PCE is a time dependent reliability method that combines Principle Component Analysis (PCA) and PCE to estimate the cumulative failure probability (Hawchar et al., 2017). KL expansion (Loeve, 1977) is used to represent input random processes which in turn allows one to transform the performance function into a function of only random variables and time, $G(\mathbf{X}, t)$. The first step in this method is to discretize the time interval $[t_0, t_l]$ into a finite number of time nodes N_t. Afterwards, an initial DoE of size N_{DoE} is considered and the time-dependent performance function is evaluated on the samples of DoE for all time nodes $t_i,\ i = 1, ..., N_t$ as:

$$\mathbf{G} = \begin{bmatrix} G(t_1)^{(1)} & \cdots & G(t_i)^{(1)} & \cdots & G(t_{N_t})^{(1)} \\ \vdots & \ddots & \vdots & \ddots & \vdots \\ G(t_1)^{(j)} & \cdots & G(t_i)^{(j)} & \cdots & G(t_{N_t})^{(j)} \\ \vdots & \ddots & \vdots & \ddots & \vdots \\ G(t_1)^{(N_{DoE})} & \cdots & G(t_i)^{(N_{DoE})} & \cdots & G(t_{N_t})^{(N_{DoE})} \end{bmatrix} \tag{3.27}$$

A PCA is performed on the covariance matrix of $\mathbf{G}$ which yields eigenvalues and eigenvectors of this matrix denoted by λ_i and $\mathbf{w}_i$ respectively, where $i = 1, ..., N_t$. Then only the first N_λ principle components are selected to represent the time dependent performance function with a polynomial meta-model as:

$$\hat{\mathbf{G}} = \bar{\mathbf{G}} + \sum_{i=1}^{N_\lambda} \hat{\mathbf{B}}_i \mathbf{w}_i^t \tag{3.28}$$

where $\bar{\mathbf{G}}$ is a matrix of size $N_{DoE} \times N_t$ in which all the components for a given row j is equal to the average value of the row, $\mathbf{B}_i$ is a non-physical vector and it is obtained by Equation 3.29. Since it is considered as a random variable, therefore, it can be estimated by PCE.

$$\mathbf{B}_i = (\mathbf{G} - \bar{\mathbf{G}})\mathbf{w}_i \tag{3.29}$$

The N_λ is chosen in a way to ensure a minimum deviation from the real problem by making the PCA error ε^{PCA} smaller than a target error ε_{tgt}^{PCA}. A PCE is then used to

provide a meta-model for the original performance function in which it is only required to build N_λ polynomial meta-models which helps to reduce the computational cost.

An enrichment procedure on the initial DoE is performed to ensure: a) the convergence of the covariance matrix of $\mathbf{G}$ which is used to determine eigenvalues and eigenvectors, and b) a sufficient accuracy of the PCE prediction. The first condition is evaluated by calculating the convergence criterion using Equation 3.30 between two consecutive PCA iterations k and $k-1$. Considering $\varepsilon^{\lambda}_{tgt} = 0.01$ ensures a good representation of the real covariance function.

$$\varepsilon^{\lambda}_i = |\frac{\lambda^{(k)}_i - \lambda^{(k-1)}_i}{\lambda^{(k)}_i}| < \varepsilon^{\lambda}_{tgt} \; i = 1, ..., N_\lambda \tag{3.30}$$

The final step is to check the polynomial approximation. The DoE is enriched if the determination coefficient Q^2 of the meta model defined by Equation 3.31 is higher than a target accuracy level Q^2_{tgt}.

$$Q^2(\hat{G}) = 1 - \frac{I^*(\hat{G})}{\frac{N}{N-1} Var(\hat{G})} \geq Q^2_{tgt} \tag{3.31}$$

where $I^*(\hat{G})$ is the mean square predicted residual, $Var()$ stands for the variance, and N is the number of samples used to construct the PCE model. The Q^2 takes values between 0 and 1 in which values closer to 1 indicate that the meta-model has a better accuracy of prediction.

In this approach, the cumulative probability of failure is approximated using a MCS in which the original performance function is replaced by a global polynomial meta-model. Even if performing PCA helps to reduce the number of polynomial meta-models to construct the meta-model, it should be noted that this can cause some deficiency in approximating the failure probability especially when dealing with problems involving weakly correlated performance functions and low failure probabilities.

3.4.2 Nested Extreme Response Surface

Nestd Extreme Response Surface (NERS) is a Kriging-based method which tries to efficiently construct a Nested Time Prediction Model (NTPM) to be able to properly

approximate the time when the performance function reaches its global extreme value (Wang and Wang, 2012). A double loop procedure is applied for such a purpose. In a first loop, the Efficient Global Optimization (EGO) procedure is used to obtain the extreme responses of the performance function and their associated times of occurrence $\{t_{min}^{(i)}, G_{min}^{(i)}\}, i = 1, ..., n_0$ on a reduced number of input samples, $\mathbf{x}^{(i)}, i = 1, ..., n_0$, of size n_0 where $G_{min}^{(i)}$ refers to $G_{min}(\mathbf{x}^{(i)})$. This sample is selected from a large Monte Carlo population of size N_{MCS}. The time, where the minimum response is reached, reads:

$$t_{min}^{(i)} = \underset{t \in [t_0, t_l]}{\operatorname{argmin}}\ G(\mathbf{x}^{(i)}, t) \tag{3.32}$$

A Kriging meta-model is then used to model the NTPM in a second loop using the sample $\{\mathbf{x}^{(i)}, t_{min}^{(i)}\}, i = 1, ..., n_0$. This meta-model serves to estimate the time where the extreme response happens for each sample of the Monte Carlo population. In this way, a time-dependent problem is converted into a time-independent one where any traditional method like FORM can be applied. The accuracy of the Kriging meta-model can be improved by adding an extra point $\{\mathbf{x}, t_{min}\}$ to the initial DoE. This has been done through an adaptive response prediction and model maturation process which relies on the mean square error of the current best prediction. It should be noted that the accuracy of this method for problems with highly nonlinear performance functions is questionable due to FORM application and the computational cost can still remain high because of the double loop procedure.

3.4.3 Mixed-EGO

This method is also a double loop procedure algorithm based on EGO and Kriging (Hu and Du, 2015b). This method is considered as an improvement of methods like NERS in which sampling on $\mathbf{X}$ and t is done on two nested and independent levels. In mixed-EGO, however, time is treated as a uniform random variable and samples from input random variables and time are simultaneously generated. In this way the training points required for calibrating the Kriging meta-model is reduced which can increase the efficiency of the method compared to NERS.

The algorithm of mixed-EGO starts with generating a large Monte Carlo population of size N_{MCS} from input random variables. In an inner loop, the initial DoE is defined by selecting N_{DoE} samples from the Monte Carlo population and generating N_{DoE} samples from the time random variable as $\{\mathbf{x}^{(i)}, \mathbf{t}^{(i)}\}, i = 1, ..., N_{DoE}$. The original performance function is evaluated on the initial DoE that yields the vector of $\mathbf{G}$ which is considered to be the primary approximation of the extreme responses and the initial Kriging meta-model $\hat{G}_{min}(\mathbf{X}, t)$ is calibrated on $\{[\mathbf{x}^{(i)}, \mathbf{t}^{(i)}]; \mathbf{G}(\mathbf{x}^{(i)}, \mathbf{t}^{(i)})\}, i = 1, ..., N_{DoE}$. Afterwards, the initial DoE is enriched to improve the extreme response prediction using $\hat{G}_{min}(\mathbf{X}, t)$. For this reason, the Expected Improvement (EI) function provided in Equation 3.33 is used

$$\mathrm{EI}(\mathbf{x}^{(i)}, t) = (\hat{\mu}(\mathbf{x}^{(i)}, t) - g_{min}^{(i)})\Phi(\frac{\hat{\mu}(\mathbf{x}^{(i)}, t) - g_{min}^{(i)}}{\hat{\sigma}(\mathbf{x}^{(i)}, t)}) + \hat{\sigma}(\mathbf{x}^{(i)}, t)\phi(\frac{\hat{\mu}(\mathbf{x}^{(i)}, t) - g_{min}^{(i)}}{\hat{\sigma}(\mathbf{x}^{(i)}, t)}) \quad (3.33)$$

where $\hat{\mu}(\mathbf{x}^{(i)}, t)$ and $\hat{\sigma}(\mathbf{x}^{(i)}, t)$ are the mean value and the standard deviation obtained by evaluating the Kriging meta-model, and $g_{min}^{(i)}$ is the current extreme value corresponding to the sample $\mathbf{x}^{(i)}$ which belongs to the DoE. The values of $\mathbf{x}^{new} \subset \{\mathbf{t}^{(i)}\}, i = 1, ..., N_{DoE}$ and $t^{new} \in [t_0, t_l]$ are determined by Equations 3.34 and 3.35 respectively. It should be noted that finding the new samples for enriching the DoE, in practice, requires to discretize the desired time interval $[t_0, t_l]$.

$$\mathbf{x}^{new} = \underset{\mathbf{x}^{(i)},\, i=1,...,N_{DoE}}{\mathrm{argmax}} \; (\max_{t \in [t_0, t_f]} \mathrm{EI}(\mathbf{x}^{(i)}, t)) \quad (3.34)$$

$$t^{new} = \underset{t \in [t_0, t_f]}{\mathrm{argmax}} \mathrm{EI}(\mathbf{x}^{new}, t) \quad (3.35)$$

In the second loop another Kriging meta-model is calibrated only on $\{\mathbf{x}^{(i)}; \mathbf{G}_{min}^{(i)}\}$, $i = 1, ..., N_{DoE}$. This Kriging meta-model is of course a time-independent function and the U-learning function of AK-MCS is here employed for training this meta-model. The U-learning function is evaluated on the Monte Carlo population to find the best training point $\mathbf{x}^{NEW}$. In order to find the extreme response for $G(\mathbf{x}^{NEW}, t)$, the previous iterative procedure is applied and so on. This procedure continues until the $\min U \geq 2$ and the failure probability is calculated in the same fashion as AK-MCS.

Even though mixed-EGO has a better efficiency than NERS, it still inherits the shortcomings of the double loop procedures. Two drawbacks can be identified for

double loop methods. First, the accuracy of meta-model depends on the accuracy of optimization in the inner loop. Then, the inner loop process can be very time consuming when stochastic processes are involved. This, in fact, would require the discretization of stochastic processes which can significantly increase the dimension of the problem and consequently reduces the efficiency of the method.

3.4.4 SILK

SILK is a SIngle-Loop Kriging meta-modeling for time-dependent reliability evaluation. This method is proposed by Hu and Mahadevan (2016) to tackle the efficiency problem in double-loop procedure methods. In this method the time-dependent performance function $G(\mathbf{X}, t)$ is replaced with a single Kriging meta-model $\hat{G}(\mathbf{X}, t)$. The desired time interval $[t_0, t_l]$ is discretized into N_t time nodes such as $t^{(j)},\ j = 1, ..., N_t$. The time parameter is treated as a uniform random variable. The Kriging meta-model $\hat{G}(\mathbf{X}, t)$ is then calibrated on an initial DoE $\{\mathbf{x}^{(i)}, t^j\},\ i = 1, ..., N_{DoE},\ j = 1, ..., N_t$ in which samples from random variables and time are generated simultaneously.

The enrichment of the DoE and training the Kriging meta-model is done using the U-learning function that is modified for time dependent problems, see Equation 3.36 .

$$U(\mathbf{x}^{(i)}, t^{(j)}) = \frac{|\hat{\mu}(\mathbf{x}^{(i)}, t^{(j)})|}{\hat{\sigma}(\mathbf{x}^{(i)}, t^{(j)})} \tag{3.36}$$

where $\hat{\mu}(\mathbf{x}^{(i)}, t^{(j)})$ and $\hat{\sigma}(\mathbf{x}^{(i)}, t^{(j)})$ are respectively the Kriging prediction and variance for a given input $\{\mathbf{x}^{(i)}, t^{(j)}\}$. The learning function is evaluated on a Monte Carlo population of size N_{MCS} samples. Accordingly, for $i = 1, .., N_{MCS}$ trajectories of the time-dependent performance function estimated by the Kriging meta-model can be classified into three groups as following:

1. Surely safe: if $\forall j = 1, ..., N_t,\ \hat{\mu}(\mathbf{x}^{(i)}, t^{(j)}) > 0$ and $U(\mathbf{x}^{(i)}, t^{(j)}) \geq 2$. The number of trajectories in this category is denoted by N_{safe}

2. Surely failure: if $\exists j = 1, ..., N_t,\ \hat{\mu}(\mathbf{x}^{(i)}, t^{(j)}) \leq 0$ and $U(\mathbf{s}^{(i)}, t^{(j)}) \geq 2$. Their number is pointed out by N_{fail}

3. Unsure: otherwise. Their number is denoted by $N^* = N_{MCS} - (N_{safe} + N_{fail})$ in which N^*_{fail} of them are potentially failing where $\exists j = 1, ..., N_t$, $\hat{\mu}(\mathbf{x}^{(i)}, t^{(j)}) \leq 0$

The cumulative probability of failure, therefore, can be estimated by Equation 3.37.

$$P^{SILK}_{f,c} = \frac{N_{fail} + N^*_{fail}}{N_{MCS}} \tag{3.37}$$

The maximum percentage error of this failure probability defined in Equation 3.38 is used to decide whether or not the Kriging meta-model is well trained. Hence, the enrichment process stops when ε^{max}_r is lower than a given target value. Otherwise, a new point $\{\mathbf{x}^{new}, t^{new}\}$ will be added to the DoE.

$$\varepsilon^{max}_r = \max_{N^*_f \in [0, N^*]} \{\frac{|N^*_{fail} - N^*_f|}{N_{fail} + N^*_f}\} \tag{3.38}$$

The new training point is determined by minimizing the U_{min} which for $i = 1, ..., N_{MCS}$ reads:

$$U_{min}(\mathbf{x}^{(i)}) = \begin{cases} u_e \quad if\ \hat{G}(\mathbf{x}^{(i)}, t^{(j)}) \leq 0,\ and\ U(\mathbf{x}^{(i)}, t^{(j)}) \geq 2,\ \exists j = 1, ..., N_t \\ \min\limits_{j=1,...,N_t} U(\mathbf{x}^{(i)}, t^{(j)}) \qquad \text{Otherwise} \end{cases} \tag{3.39}$$

and u_e is any real number greater than 2. For each realization, the corresponding time instant to the $U_{min}(\mathbf{x}^{(i)})$ is identified by Equation 3.40. The new training point is then identified by Equation 3.41:

$$t_{min}(i) = \underset{j=1,...,N_t}{\text{argmin}} U(\mathbf{x}^{(i)}, t^{(j)}) \tag{3.40}$$

$$\{\mathbf{x}^{new}, t^{new}\} = \{\mathbf{x}^{(i_{min})}, t_{min}(i_{min})\} \tag{3.41}$$

where

$$i_{min} = \underset{i=1,...,N_{MCS}}{\text{argmin}}\ U_{min}(\mathbf{x}^{(i)}) \tag{3.42}$$

SILK proposes a single loop procedure that does not involve EGO for finding extreme responses of the performance function which leads to a higher efficiency in terms of computational cost rather than NERS or mixed-EGO. This method is surely an efficient time-dependent reliability method for many problems but may face some problems when the performance function involves weakly correlated stochastic processes such as fatigue loading.

3.4.5 Adaptive Extreme Response Surface

Adaptive Extreme Response Surface (AERS) is another recent Kriging-based time-dependent reliability method which can be used for problems involving weakly correlated stochastic processes (Wang and Chen, 2017). The first step in this method is to properly discretize the desired time interval into N_t time nodes. Afterwards, a Kriging meta-model is calibrated for each instantaneous performance function associated with a time node. The idea here is to identify the extreme responses of the time-dependent performance function from the prediction of Kriging meta-models evaluated on samples of a simulated Monte Carlo population.

Before calculating the probability of failure, an adaptive learning process is used to improve separately the accuracy of N_t meta-models. The learning process tries to correctly classify the sample points between the failure and safe domains. Using the Kriging features, one can show that the probability of a correct classification P_c for point $\{\mathbf{x}^{(i)}, t_j\}$ for $i = 1, ..., N_{MCS}$ and $j = 1, ..., N_t$ can be calculated by:

$$P_c(\mathbf{x}^{(i)}, t_j) = \Phi(\frac{|\hat{G}(\mathbf{x}^{(i)}, t_j)|}{\sqrt{\hat{e}(\mathbf{x}^{(i)}, t_j)}}) \tag{3.43}$$

where $\hat{e}$ is the mean square error of prediction using Kriging. The new point for the enrichment process is defined by calculating an importance measure ψ over the Monte Carlo population.

$$\psi(\mathbf{x}^{(i)}, t_j) = (1 - P_c(\mathbf{x}^{(i)}, t_j)) \times f_w(\mathbf{x}^{(i)}) \times \hat{e}(\mathbf{x}^{(i)}, t_j) \tag{3.44}$$

where $f_w(\mathbf{x}^{(i)})$ is the probability density function value at $\mathbf{x}^{(i)}$. For a given time node t_j the point $\mathbf{x}^{(i)},\ i = 1, ..., N_{MCS}$ that has the maximum importance measure will be added to the associated DoE. The calibration of Kriging meta-models continues until the confidence levels of instantaneous reliability approximations meet the confidence target CL_t, see Equation 3.45.

$$CL(t_j) = \frac{1}{N_{MCS}} \sum_{i=1}^{N_{MCS}} P_c(\mathbf{x}^{(i)}, t_j) > CL_t \tag{3.45}$$

The idea of calibrating a meta-model for instantaneous performance functions

at each time node (like AERS) seems to be the most general way to evaluate time-dependent reliability problems involving stochastic processes (especially for those that are weakly correlated) as a replacement for crude MCS. However, dealing with the meta-models separately is not the best strategy to tackle computationally expensive problems. For instance, recalibrating only those meta-models that have a significant contribution to the system's failure can help to reduce the computational burden.

It can be shown that an EVB approach can be seen as a serially connected system problem in which each component represents a time node in the time dependent problem. Therefore, efficient system reliability methods can be used to address time-dependent reliability problems. On that account, a new approach named AK-SYS-t, that relies on AK-SYS (Fauriat and Gayton, 2014), is introduced in Section 3.5. The motivation here is to propose an alternative approach to AERS and SILK that can deal with problems involving weakly correlated performance functions while it remains efficient in terms of computational burden, accurate, and it can be simply implemented.

3.5 Proposed Methodology: AK-SYS-t

In many of time-dependent reliability methods, discretizing the time interval of interest into a finite number of time nodes is one way to tackle the complexity that is imposed by considering the time. One can, therefore, introduce an instantaneous performance function for each time node after discretization. Failure at one node implies the failure of the structure. This is equivalent to finding the probability of failure in a serially connected system in which each component represents a time node after discretization. This brings up the idea to employ an efficient system reliability method to address time-dependent reliability problems. Accordingly, a new time-dependent approach is proposed in this section based on AK-SYS (Fauriat and Gayton, 2014). The new method is called AK-SYS-t which is described in details in the following.

3.5.1 From time-dependent to system reliability

As mentioned previously, the aim of EVB methods is to identify the extreme responses of time-dependent performance functions. The cumulative probability of failure therefore can be formulated by Equation 3.46. In most of the cases, approximating this failure probability requires the discretization the desired time interval $[t_0, t_l]$ into N_t time nodes as $\{t_1, t_2, ..., t_{N_t} = t_l\}$. Considering an instantaneous performance function for each time node $G_j(\mathbf{X}) = G(\mathbf{X}, t_j),\ j = 1, ..., N_t$, the Equation 3.46 can be approximated by Equation 3.47.

$$P_{f,c}(t_0, t_l) = \text{Prob}(\exists t \in [t_0, t_l],\ G(\mathbf{X}, t) \leq 0) = \text{Prob}(\min_{t \in [t_0, t_l]} G(\mathbf{X}, t) \leq 0)$$
$$= \text{Prob}(G_{min}(\mathbf{X}) \leq 0) \quad (3.46)$$

$$P_{f,c}(t_0, t_l) \simeq \text{Prob}(\exists j \in \{1, ..., N_t\}, G(\mathbf{X}, t_j) \leq 0) = \text{Prob}(\exists j \in \{1, ..., N_t\}, G_j(\mathbf{X}) \leq 0) \quad (3.47)$$

Equation 3.47 can be reformulated by Equation 3.48 by defining failure events such as $E_j = \{G_j(\mathbf{X}) \leq 0\},\ j = 1, ..., N_t$ on time nodes. Figure 3.3 presents an illustration of time discretization.

$$P_{f,c}(t_0, t_l) \simeq \text{Prob}(\exists j \in \{1, ..., N_t\},\ G_j(\mathbf{X}) \leq 0) = \text{Prob}(\cup_{j=1}^{N_t} E_j) \quad (3.48)$$

This definition is strictly equivalent to the failure probability of a serially connected system with N_t components (Royset et al., 2006; Son and Savage, 2007). It should be noted that, in this case, a correlation is likely to exist between the limit state functions of components. This situation may also occur for system problems too, e.g. for limit states that are resulted from the same finite element computations.

It should be highlighted that the discretization strategy has a significant effect on the accuracy and efficiency of the corresponding method. Hence, the time interval Δt between time nodes should be chosen very carefully since it defines the required number of meta-models. In one hand, a small Δt leads to a big number of time nodes N_t which leads to high computational cost if the original performance function is costly-to-evaluate. On the other hand, by selecting a large Δt, some failure events might be avoided which can cause underestimation of the cumulative probability of failure.

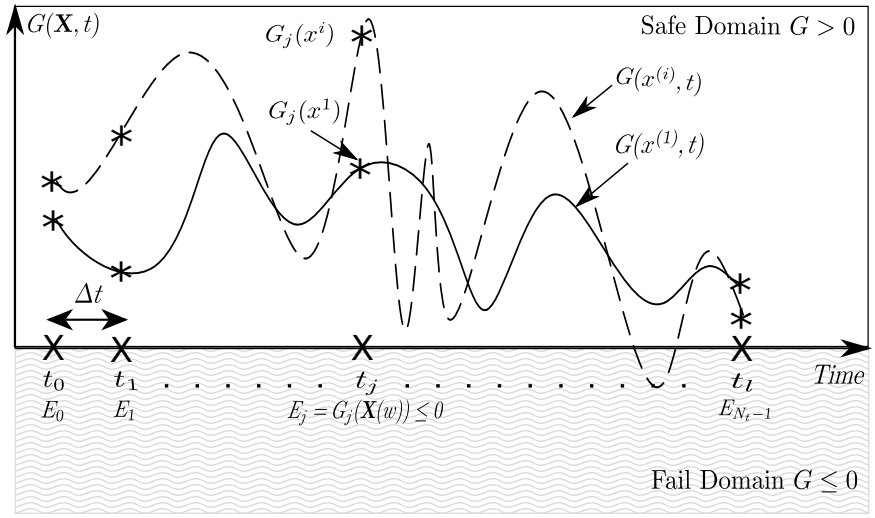

Figure 3.3: A representation of discretizing the time interval into N_t time nodes

The system reliability problem can be converted into a component reliability problem by using composite limit state function that searches for the extreme values of the system's performance function such as $G_{min}(\mathbf{X}) = \min_{j\in\{1,\ldots,N_t\}} G_j(\mathbf{X})$. System's failure probability can then be calculated as:

$$\text{Prob}(\cup_{j=1}^{N_t} E_j) = \text{Prob}(G_{min}(\mathbf{X}) \leq 0) \tag{3.49}$$

However, the final limit state based on G_{min} can be very complex which prevents the use of conventional component reliability methods like FORM, SORM, etc.

One way to tackle this issue is to approximate instantaneous performance functions $G_j(\mathbf{X})$ with meta-models and use an active learning process for the enrichment procedure. This strategy seems promising for system reliability problems accompanied by costly-to-evaluate performance functions. With this respect, Fauriat and Gayton (2014) have proposed a new reliability method for systems using Kriging meta-modeling and an active learning process. This method is called AK-SYS and has been successfully validated for system problems. AK-SYS is described with more details in the following section and will be employed for time-dependent reliability analysis.

3.5.2 AK-SYS method

AK-SYS is a reliability method related to the AK family developed for system reliability analysis. This method aims at reducing the computational cost for system problems (especially series and parallel systems) by making less calls to the expensive-to-evaluate original performance function. It is a Kriging-based method using an active learning process for the enrichment process (Fauriat and Gayton, 2014). The learning process introduced in this method makes it possible to enrich only the meta-models that contribute the most to the system's failure.

In this method, Kriging meta-models $\hat{G}_j, j = 1, ..., p$ are used to replace the original performance functions $G_j, j = 1, ..., p$ for a system with p components. Like other methods in the AK family, AK-SYS tries to classify samples of a Monte Carlo population in the safe or failure domains based on their signs predicted by Kriging meta-models. Updating all Kriging meta-models in each step of enrichment can be a very time consuming task. Accordingly, the main feature of AK-SYS is its learning process since it searches for the weakest component in the system to only recalibrate the associated meta-model. The learning process is an adaptation of the original U learning function for component problems. The algorithm of the AK-SYS is recalled hereafter.

• Generating an initial Monte-Carlo population of size N_{MCS}: $\mathbf{x}^{(i)}, i = 1, ..., N_{MCS}$.
• Selecting an initial DoE of size N_{DoE} from the Monte Carlo population and evaluating each performance function $G_j, j = 1, ..., p$ on samples of the DoE: $\mathbf{x}_a^{(i)},\ i = 1..., N_{DoE}$.
• Calibrating the initial Kriging meta-models, one per component using $\{\mathbf{x}_a^{(i)}; G_j(\mathbf{x}_a^{(i)})\},\ i = 1..., N_{DoE}$.
• Identifying the weakest component of the system $s^{(i)} \in \{1, ..., p\}$ for each sample of the Monte Carlo population $\mathbf{x}^{(i)}, i = 1, ..., N_{MCS}$. For a serially connected system, for example, it can be found by Equation 3.50:

$$s^{(i)} = \underset{j=1,...,p}{\operatorname{argmin}}\ \hat{G}_j(\mathbf{x}^{(i)}) \tag{3.50}$$

• Evaluating the learning function $U(\mathbf{x}^{(i)})$ for each couple $\{\mathbf{x}^{(i)}; s^{(i)}\},\ i = 1, ..., N_{MCS}$

as:

$$U(\mathbf{x}^{(i)}) = \frac{|\mu_{\hat{G}_{s^{(i)}}}(\mathbf{x}^{(i)})|}{\sigma_{\hat{G}_{s^{(i)}}(\mathbf{x}^{(i)})}} \tag{3.51}$$

where $\mu_{\hat{G}_{s^{(i)}}}(\mathbf{x}^{(i)})$ and $\sigma_{\hat{G}_{s^{(i)}}(\mathbf{x}^{(i)})}$ are respectively the mean prediction and variance of Kriging meta-models $\hat{G}_{s^{(i)}}$ computed for each $\mathbf{x}^{(i)},\ i = 1, ..., N_{MCS}$.

• Identifying the training point $\mathbf{x}_a^{(*)}$ for enriching the DoE using Eq.3.52. The new sample is added to the DoE of $\hat{G}_s$ which is the weakest component in the system. It should be noted that $\hat{G}_s$ is the only meta-model that is re-calibrated at a given iteration.

$$\mathbf{x}_a^{(*)} = \underset{i=1,...,N_{MCS}}{\operatorname{argmin}}\ U(\mathbf{x}^{(i)}) \tag{3.52}$$

• Terminating the process when the minimum value of U becomes greater than 2 over the Monte Carlo population and then calculating the probability of failure in the same fashion as crude MCS.

It has been shown that AK-SYS is a very efficient system reliability method due to the composite criterion learning function used for the enrichment process. It recalibrates only the components that have the biggest contribution to the system's failure. Moreover, this method does not make any presumptions on the shape of the limit state. Therefore, it can be seen as a general approach that can be applied on problems with different kinds of performance functions. This approach is hereafter used for time-variant reliability analysis.

3.5.3 AK-SYS-t: an extension of AK-SYS for time-dependent reliability

AK-SYS-t is a new time-dependent reliability method which exploits the advantages of AK-SYS to address time-dependent reliability problems especially when non-monotonic and costly-to-evaluate performance functions are involved. This method is inspired by the equivalence between system and time-dependent reliability analyses as explained in Section 3.5.1. According to what has been described before, following steps can be pursued to perform time-dependent reliability analysis with AK-SYS-t which are explained in details in the sequel.

1. Discretizing the time interval $[t_0, t_l]$ into N_t nodes
2. Calibrating an initial Kriging meta-model for each instantaneous performance function $G_j(\mathbf{x}), j \in \{0, ..., N_t - 1\}$
3. Recalibrating meta-models using the AK-SYS enrichment strategy
4. Computing the cumulative failure probability

1- Discretizing the time interval is here the first step of AK-SYS-t method. The desired lifetime of a system $[t_0, t_l]$ is discretized into N_t time nodes, see Figure 3.3. By evaluating the original time-dependent performance function at each time node $t_j,\ j = 1, ..., N_t$, one can allocate an instantaneous performance function $G_j(\mathbf{x}) = G(\mathbf{x}, t_j)$ per time node. The region where $G_j(\mathbf{x}) \leq 0$ defines the failure domain for each instantaneous performance function. As mentioned before, the choice of the time distance Δt between two consecutive time nodes is crucial. It should be chosen in a way to ensure the detection of all failure events. For problems involving stochastic processes, the smallest autocorrelation length can be used to decide about the time interval Δt. It has been shown that $\Delta t = l_{low}/4$ ensures the detection of failures, where l_{low} is the smallest autocorrelation length of random processes (Sudret, 2008). For other situations a trade-off between the accuracy and computational cost should be considered, even not easily managable.

2- Calibration of the initial Kriging meta-models is performed next. Kriging meta-models replace the original instantaneous performance functions. Kriging meta-models $\hat{G}(\mathbf{X}, t_j),\ j = 1, ..., N_t$ are prepared first using an initial DoE for which samples in the DoE are chosen from a Monte Carlo population of size N_{MCS} generated from the input random vector $\mathbf{X}$. The instantaneous performance functions $G_j(\mathbf{X})$ are evaluated on samples of the DoE and initial Kriging meta-models $\hat{G}_j(\mathbf{X}),\ j =, ..., N_t$ are calibrated on $\{\mathbf{x}^{(i)}; G_j(\mathbf{x}^{(i)})\},\ i = 1, ..., N_{DoE}$. One should note that the size of DoE should be chosen in a way that it involves the least possible experiments since, in one hand, the aim of a meta-model is to replace a costly-to-evaluate performance function. Hence, the cost of calibrating the meta-model is expected to be far lower than the one induced

by using the original performance function. In the other hand, most meta-modelling methods like Kriging become less efficient and intractable when the size of the DoE is very large Dubourg (2011). Accordingly, different sampling approaches such as random sampling, LHS, and Hammersley sampling can be used to generate an efficient initial DoE from the input random vector (Hu and Du, 2015b).

3- Enrichment process is the key step of AK-SYS-t. The aim of this step is to increase the accuracy of the Kriging surrogates to be able to properly classify the samples of the Monte Carlo population $\mathbf{x}^{(i)}, i = 1, ..., N_{MCS}$ of size N_{MCS} between the safe and failure domains. As mentioned previously, updating all meta-models, i.e for all time nodes, is not the smartest strategy since it can be very time consuming if costly-to-evaluate performance functions are involved. For this reason, the learning process of AK-SYS is employed. Therefore, for each sample $\mathbf{x}^{(i)}$ the Kriging meta-model $G_{s^{(i)}}$ is first identified with

$$s^{(i)} = \underset{j=1,...,N_t}{\operatorname{argmin}} \hat{G}_j(\mathbf{x}^{(i)}) \tag{3.53}$$

The learning function $U(\mathbf{x}^{(i)})$ is then assessed for each couple $\{\mathbf{x}^{(i)}; G_{s^{(i)}}\},\ i = 1, ..., N_{MCS}$ and the point $\mathbf{x}_a^{(*)}$ that minimizes U will be added to the DoE of the corresponding instantaneous performance function $\hat{G}_s$. As in time-dependent framework, the computation of $\hat{G}_s$ may sometimes require the computation of G_j for $j \leq s$, and all $\hat{G}_j$, $j = 0, ..., s$ are simultaneously re-calibrated which requires extra computational cost. This process continues until the minimum value of U for all samples in the Monte Carlo population is greater than 2.

4- Computing the cumulative failure probability is the final step of the proposed methodology. After adequately training the Kriging meta-models $\hat{G}_j(\mathbf{X})$, they can be employed to approximate the cumulative probability of failure in the same way as MCS by replacing the original instantaneous performance functions in MCS with Kriging surrogates. The cumulative failure probability is then equal to the ratio of the failed realizations $\hat{N}_{fail}(t_0, t_l)$ predicted by Kriging meta-models over the total number of trajectories, N_{MCS}, of the time-dependent performance function prepared by Kriging meta-models, see Equation 3.54.

$$\hat{P}_{f,c}(t_0, t_l) = \frac{\hat{N}_{fail}(t_0, t_l)}{N_{MCS}} \tag{3.54}$$

The final stopping criterion can be based on the COV of $\hat{P}_{f,c}$, see Equation 3.55. If the COV is greater than a target value, the initial size of Monte Carlo population N_{MCS} is augmented. This can be done by adding samples to the initial Monte Carlo population. This is expected to ensure an adequate accuracy of the estimated cumulative failure probability for a given initial COV. The algorithm of the proposed approach is illustrated in Figure 3.4.

$$COV_{\hat{P}_{f,c}} = \sqrt{\frac{1 - \hat{P}_{f,c}(t_0, t_l)}{N_{MCS} \times \hat{P}_{f,c}(t_0, t_l)}} \tag{3.55}$$

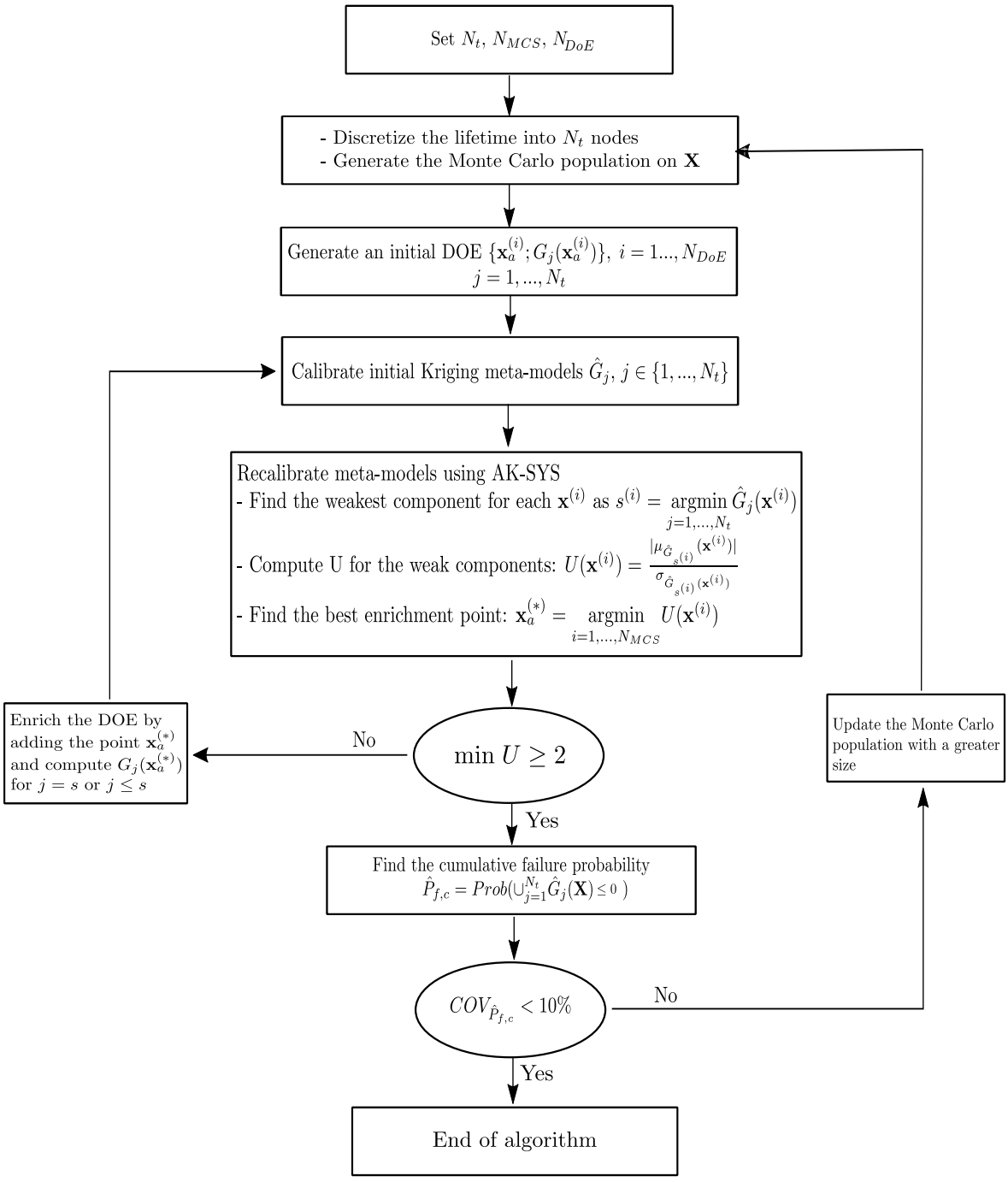

Figure 3.4: General algorithm for AK-SYS-t

3.6 Validation of AK-SYS-t on two numerical case studies

The goal of this section is to examine the efficiency and accuracy of the proposed methodology on two academic cases taken from the literature and compare the results with some competing methods if possible.

To evaluate the efficiency and accuracy of AK-SYS-t some indicators are employed. The Number of calls N_{calls} to the original performance function is considered first to evaluate the efficiency of the new approach. It is obvious that the efficiency increases if N_{calls} decreases. Moreover, two indicators are used to measure the accuracy of the algorithm. The first indicator is the relative percentage error on the failure probability which is formulated in Equation 3.56. The second indicator is the number of miss-classified realizations of the performance function calculated using Equation 3.57. It should be mentioned that the number of miss-classified realizations can be greater than zero even if the percentage of error is zero due to compensation effects. Hence, the second indicator is more sever than the relative percentage error to check the accuracy of meta-modeling for reliability analysis.

$$\epsilon(\%) = \frac{|P_{MCS} - \hat{P}_{f,c}|}{P_{MCS}} \times 100 \tag{3.56}$$

$$N_{misclass} = \sum_{n=1}^{N_t} \sum_{i=1}^{N_{MCS}} I(\mathbf{x}^{(i)}, t_n) \tag{3.57}$$

where

$$I(\mathbf{x}^{(i)}, t_n) = \begin{cases} 1 \quad if \quad \hat{G}(\mathbf{x}^{(i)}, t_n) \times G(\mathbf{x}^{(i)}, t_n) < 0 \\ 0 \qquad\qquad\qquad\qquad\qquad \text{Otherwise} \end{cases} \tag{3.58}$$

3.6.1 Numerical case 1: a nonlinear model time-dependent performance function

The first numerical case considered here is a simple model since it involves only one random variable. The performance function is nonlinear with an explicit relationship between the random variable X and time t (Hu and Du, 2015b). The random variable X follows a normal distribution with $X \sim N(10, 0.5^2)$. The performance function for this case is formulated in Equation 3.59 and the aim here is to calculate the cumulative probability of failure during the time interval $t \in [1, 2.5]$, see Equation 3.60.

$$G(X,t) = 0.014 - \frac{1}{X^2+4}\sin(2.5X)\cos(t+0.4)^2 \tag{3.59}$$

$$P_{f,c}(1, 2.5) = \text{Prob}(\exists\tau \in [1, 2.5],\ G(X,\tau) \leq 0) \tag{3.60}$$

To evaluate this failure probability using AK-SYS-t, a Monte Carlo population of size $N_{MCS} = 10^6$ is generated first. This population is considered for all instantaneous performance functions after the discretization of the desired time interval into N_t time nodes. Thus, the total size of the Monte Carlo population (in terms of evaluations of G) is equal to $N_{MCS} \times N_t$ for all performance functions. A LHS is performed to prepare initial DoEs of size $N_{DoE} = 10$, to calibrate N_t initial Kriging meta-models. All N_t initial DoEs are considered identical in the beginning. However, after the enrichment process the final DoEs might differ from each other.

Several discretization scenarios are considered to emphasize its importance on the final results. Table 3.1 provides some results for this case using MCS and AK-SYS-t. It can be seen that by increasing N_t the estimated cumulative failure probability converges to its real value. The results for this case are promising since the estimation of the cumulative failure probability using AK-SYS-t and MCS are exactly the same for each discretization scenario. The relative percentage error and the number of misclassified realizations are zero. Moreover, it should be noted that AK-SYS-t provides this result only by making few calls to the original performance functions.

The SILK method has also been applied on this case study by Hu and Du (2015b).

Therefore, one can compare the results provided by both methods. As said before, AK-SYS-t leads to zero percentage error regarding to the failure probability for this problem while SILK computes this probability of failure with an error of $\epsilon(\%) = 0.92$. Number of calls to the original performance function in SILK is $N_{calls} = 18.35$ (in average) which is much less than AK-SYS-t ($N_{calls} = 1,051$). It should be mentioned that the nature of N_{calls} in AK-SYS-t is different from SILK since in SILK only one Kriging meta-model is calibrated for the time-dependent performance function while in AK-SYS-t N_t Kriging meta-models are prepared. The number of calls in Table 3.1 therefore refers to the total number of calls to all meta-models: $N_{calls} = N_t \times N_{doe} + N_e$ where N_e is the enrichment iterations. When the performance function is not very complex, as it is the case here, see Fig. 3.5, SILK can be a suitable alternative. However, for highly nonlinear performance functions SILK might face some difficulties.

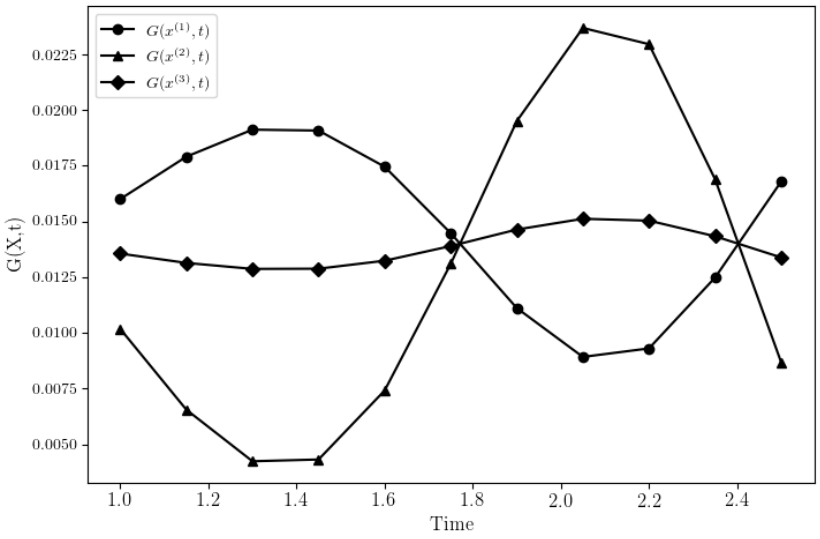

Figure 3.5: Some realizations of the performance function for the first case study

3.6.2 Numerical case 2: a general case time-dependent performance function

The second numerical case is a more general performance function involving random variables and stochastic processes. This case is related to a simply supported corroding beam of length 5 m with a rectangular cross section ($b_0 \times h_0$). A uniform corrosion with

Table 3.1: AK-SYS-t and MCS results for the first case study for several discretization scenarios

	MCS		AK-SYS-t			
N_t	P_f	N_{calls}	P_f	N_{calls}	$N_{misclas}$	ϵ (%)
10	0.0	10×10^6	0.0	117	0	0.0
20	$9.1e^{-5}$	20×10^6	$9.1e^{-5}$	222	0	0.0
50	$1.06e^{-4}$	50×10^6	$1.06e^{-4}$	534	0	0.0
100	$1.08e^{-4}$	100×10^6	$1.08e^{-4}$	1,051	0	0.0

a constant corrosion coefficient $c = 0.05\ mm/year$ is degrading all faces of the beam. The corrosion starts at time $t = 0$ and a pinpoint stochastic load $F(t)$ is applied at the midspan of the beam in addition to its own weight $W = \gamma_{st} b_0 h_0$ where γ_{st} is the steel mass density. Figure 3.6 shows an illustration of this beam. The load $F(t)$ is assumed to be a Gaussian process with mean of 5,500 N and 20% of COV. The autocorrelation function for this process is defined by $exp[-(\Delta t/l)^2]$ where the correlation length l is equal to one year. This beam has already been studied in Andrieu-Renaud et al. (2004); Hu and Mahadevan (2016), and Hawchar (2017).

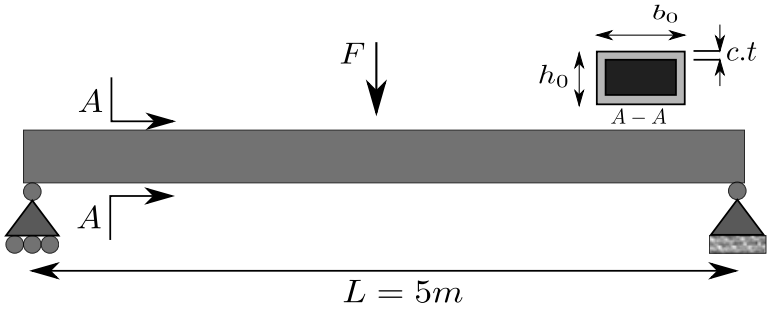

Figure 3.6: A schematic view of the simply supported steel beam

The time-dependent performance function for this case is formulated in Equation 3.61. $G(f_y, b_0, h_0, F(t), t) \leq 0$ indicates the failure of the system which means the maximum bending moment at the midspan of the beam exceeds the ultimate bending moment.

$$G(f_y, b_0, h_0, F(t), t) = \frac{(b_0 - 2ct)(h_0 - 2ct)^2}{4} f_y - [\frac{F(t)L}{4} + \frac{\gamma_{st} b_0 h_0 L^2}{8}] \tag{3.61}$$

f_y, b_0, and h_0 are random variables and their distribution and parameters are provided

in Table 3.2.

Table 3.2: Input random variables for case 2

Parameter	Mean	COV	Distribution
f_y	240 MPa	10%	Lognormal
b_0	0.2 m	5%	Lognormal
h_0	0.04 m	10%	Lognormal

The random process $F(t)$ is discretized into 12 random variables using Karhunen-Loeve expansion method. The dimension of the problem is then equal to $n = 15$. A Monte Carlo population of $N_{MCS} = 10^6$ is used to evaluate the cumulative probability of failure over $t \in [0, 10]$ years using MCS, AK-SYS-t, and t-PCE. It should be noted that MCS is used for validation purposes and errors for the other two methods are provided according to MCS results. According to the information provided in the first step of the AK-SYS-t in Section 3.5.3, the desired time interval is discretized into $N_t = 41$ time nodes since the correlation length of the $F(t)$ is one year. Therefore, 41 identical initial DoEs of size $N_{DoE} = 50$ are provided in order to calibrate the initial Kriging meta-models.

The results of AK-SYS-t, t-PCE, and MCS for this case are provided in Table 3.3. The total number of calls to the performance function for AK-SYS-t is calculated similar to the previous example. The values of failure probability and error for t-PCE are taken from (Hawchar, 2017). Even though the performance function here is more complicated with a higher dimension AK-SYS-t provides promising results. AK-SYS-t works more efficiently and accurately compared to t-PCE for this example. It is important to remind that PCA is used to reduce the computational burden in t-PCE when the number of time nodes after discretization is large. However, this can affect the accuracy of the methodology. AK-SYS-t searches through the most vulnerable time nodes thank to its efficient learning process and it is not necessary to reduce the number of meta-models for this case.

In the end, it should be noted that one common challenge for methods like AK-

Table 3.3: Results for the second case study compared to MCS and t-PCE

Method	N_t	P_f	N_{calls}	ϵ (%)	$N_{misclass}$
MCS	41	0.0137	41×10^6	-	-
t-PCE	11	0.0136	7380	0.18	-
AK-SYS-t	41	0.0137	5194	0.015	8

SYS-t is related to providing the evolution of the cumulative probability of failure with time which is crucial in the context of structural maintenance and inspection planning. For instance, it has been shown in Hawchar (2017) that t-PCE prediction for intermediate time nodes of the second numerical example can reach just over 10% of relative error. Figure 3.7 illustrates the evolution of cumulative failure probability for this example provided by MCS and AK-SYS-t which shows a small difference between AK-SYS-t predictions and MCS results for the intermediate time nodes. With this respect, Figure 3.8 illustrates the relative percentage error for each time node. It can be seen from this figure that the maximum relative percentage error is around 4% which is quite acceptable. For the cases with highly nonlinear performance functions, however, we believe this level of accuracy is hard to reach. Hence, a first approach to construct the whole curve of cumulative probability of failure over time using AK-SYS-t is proposed in the next section.

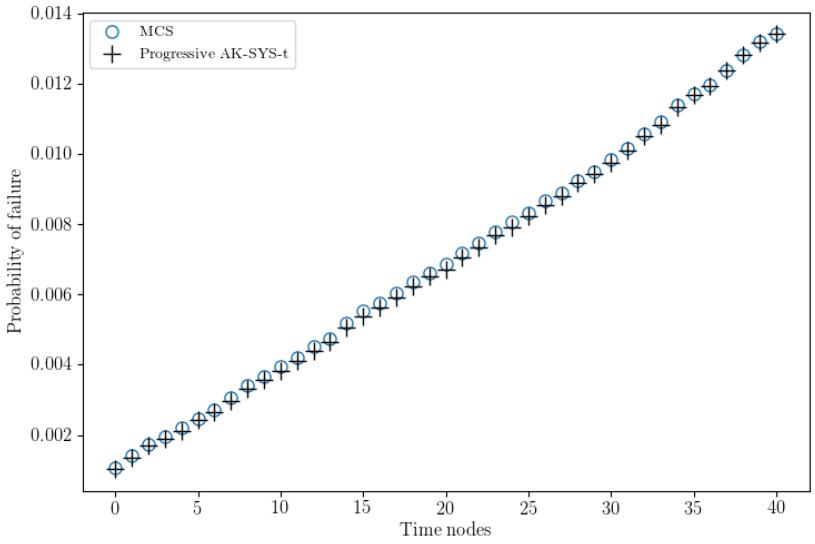

Figure 3.7: Full curve of cumulative probability of failure for the 2nd numerical example

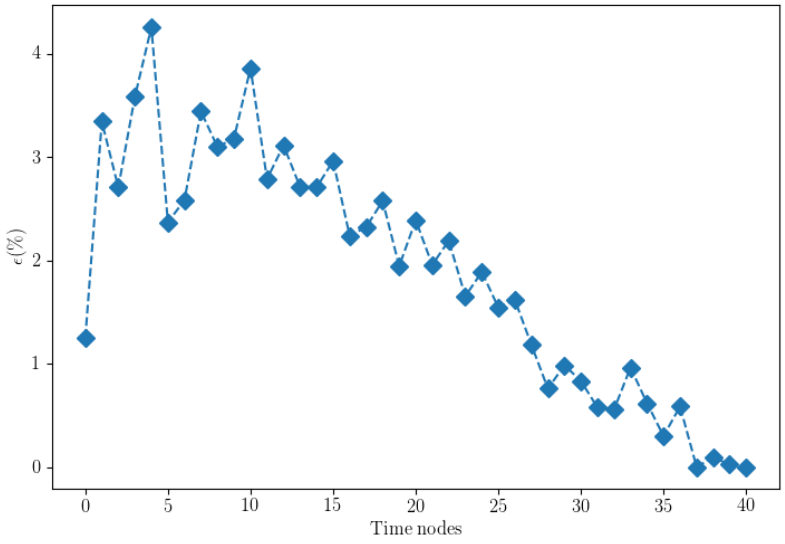

Figure 3.8: The relative percentage error of AK-SYS-t prediction for different time nodes

3.7 Towards cumulative probability of failure evolving with time using AK-SYS-t

Providing the evolution of the cumulative probability of failure with time is crucial in the context of structural maintenance and inspection planning. Given that the time interval of interest $[t_0, t_l]$ for a time-dependent reliability analysis is discretized into N_t time nodes, it has been observed from previous examples that AK-SYS-t provides an accurate approximation of cumulative probability of failure at the final time node N_t. However, AK-SYS-t calculations for a given time interval cannot be used to accurately approximate the cumulative probability of failure for intermediate time nodes $j = 1, ..., N_t - 1$. This is can be explained according to the learning process that is used for enriching the Kriging meta-models. As previously mentioned, in each enrichment step AK-SYS-t only recalibrates the Kriging meta-model associated tho the most vulnerable time node which has the most contribution to the system's failure within the time interval $[t_0, t_l]$. However, for sub intervals $[t_0, t_i] \in [t_0, t_l]$ the most vulnerable time node might be different. Therefore, one cannot resort to the AK-SYS-t calculations for $[t_0, t_l]$ to accurately compute the cumulative failure probability for sub intervals $[t_0, t_i]$. For this reason, a crude approach is proposed here in order to better estimate the cumulative probability of failure for intermediate time nodes $j = 1, ..., N_t - 1$ which enables us to construct the whole curve of cumulative failure probability more precisely within a given time interval, e.g. the structural service life.

Assuming that the structural service life is $N_{service}$ years, one can divide this time period into N_s smaller sub intervals. The idea here is to implement N_s simulations of AK-SYS-t progressively from the first sub interval to the last one. More precisely, AK-SYS-t is performed on the same N_{MCS} realizations of input random variables $\mathbf{X}$ for all sub intervals. In this way, one can update the information about the cumulative probability of failure for a given time interval $j = 1, ..., N_s$ according to the results of AK-SYS-t performed on the previous time intervals $[1, ..., j-1]$. Each sub interval $j = 1, ..., N_s$ is discretized into $N_{t_{s_j}}$ time nodes the failed realizations of size $N_{fail,j}$ in the jth AK-SYS-t are recorded. Hence, the failed realizations in the $(j+1)$th AK-SYS-t

is counted by the following equation:

$$N_{fail,(j+1)} = N_{fail,j} + N_{fail_{new}} \; j = 1, ..., (N_s - 1) \tag{3.62}$$

where $N_{fail_{new}}$ are the failed realizations in the $(j+1)$th AK-SYS-t that have not been recalled in the previous ones. This progressive process starts from the first time interval and continues until the last one, $j = 1, ..., N_s$. Accordingly, the cumulative probability of failure in the end of each time interval can be calculated by Equation 3.63 and the number of calls to the original performance function can be calculated by Equation 3.64 where N_e is the number of enrichment iterations before the algorithm stops.

$$P_{f,c_j} = \frac{N_{fail,j}}{N_{MCS}}, \; j = 1, ..., N_s \tag{3.63}$$

$$N_{calls} = N_s \times N_{t_s} \times N_{DoE} + N_e \tag{3.64}$$

This progressive procedure is applied on the second numerical case in this paper. For this reason, the time interval $[0, 10]$ years is divided into four equidistant sub intervals. The first sub interval is discretized into 11 time nodes while the others are discretized into 10 time nodes. Similar to the second numerical case, a Monte Carlo population of $N_{MCS} = 10^6$ is used to perform the progressive AK-SYS-t. The initial Kriging meta-models for each time node are calibrated on an initial DoE of size $N_{DoE} = 50$. MCS results are then used to evaluate the accuracy of the proposed approach.

The results for this approach show a significant improvement in terms of accuracy compared to the primary results in the second numerical example. Accordingly, Figure 3.9 illustrates the full curves of cumulative failure probability provided by the proposed approach and MCS. Figure 3.10 provides the prediction error on the cumulative failure probability for each time node. It can be seen from this figure that the maximum value of error is reduced from almost 4%, see Figure 3.8, to almost 0.4% which is a significant improvement. This can be explained according to the progressive approach which provides some check points $j = 1, ..., N_s$ within the time interval $[t_0, t_l]$ for which the cumulative failure probability is accurately approximated. This can help

to reduce the uncertainty on estimating the cumulative failure probability for other intermediate time nodes. Regarding the efficiency, the total number of calls to the original performance function in this approach is equal to $N_{calls} = 4792$ which also shows an improvement compared to the original approach in the second numerical case. It should be noted that increasing the number of AK-SYS-t procedures (sub intervals), leads to a higher prediction accuracy. This, however, can have a negative effect on the efficiency of this approach. Hence, it is important to divide the system's service life into a reasonable number of time sub intervals.

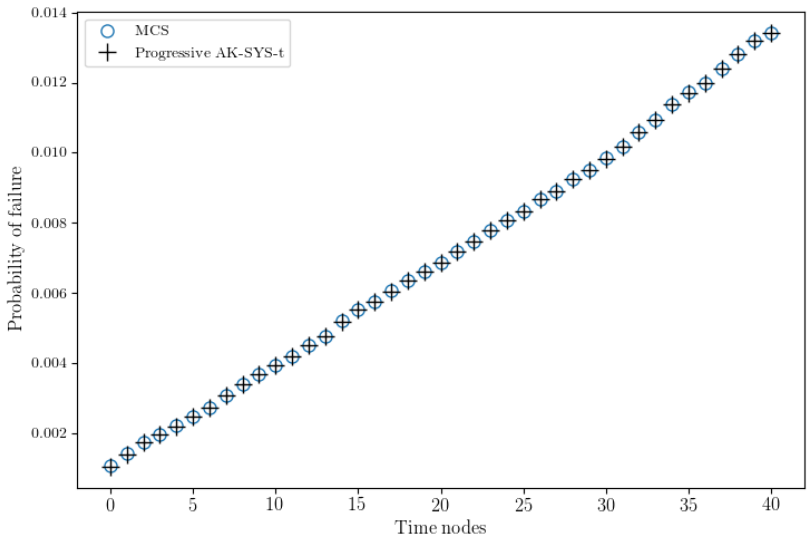

Figure 3.9: Full curve of cumulative probability of failure for the second numerical example provided by the progressive approach and MCS

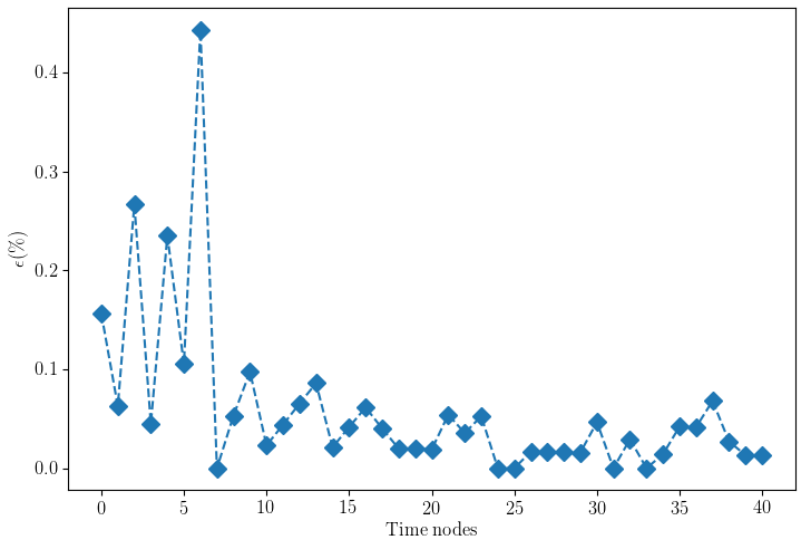

Figure 3.10: The relative percentage error after applying the progressive AK-SYS-t for different time nodes for the second numerical case

3.8 Conclusion and perspectives

This chapter was devoted to a new time-dependent reliability method developed during this thesis. The new approach is called AK-SYS-t which tries to relate time-dependent reliability problems to system reliability problems by taking advantage of efficient methods that have been already developed for system reliability analysis. With this respect, AK-SYS which is a system reliability method is employed for time-dependent reliability analysis. The name AK-SYS-t, in fact, refers to the extension of AK-SYS toward time-dependent reliability problems.

Time discretization is the first step of AK-SYS-t. In this way, an instantaneous performance function is defined for each time node. Kriging is then applied to prepare a meta-model for each instantaneous performance function and the composite criterion learning function developed for AK-SYS is hired to train the Kriging surrogates. This helps to implement the advantages of AK-SYS method in time-dependent reliability assessment. As said before, the advantages of AK-SYS are related to its efficiency thanks to its learning process and generality which means it can be applied on any

kind of performance functions since it does not make any assumptions on the limit state.

The accuracy and efficiency of AK-SYS-t have been tested on two illustrative examples from the literature. The first example is a nonlinear performance function with one random variable and the second one involves a stochastic process and 3 random variables. Results from both case studies show that the new methodology is very promising in terms of accuracy and efficiency. The results are compared with some recently developed methods in literature also such as SILK and t-PCE and it can be concluded that AK-SYS-t is a possible alternative for those methods.

In the last step of this study, a crude approach has been proposed in order to accurately provide the full curve of the cumulative failure probability using AK-SYS-t which has a crucial role in the field of structural maintenance and inspection planning. With this respect, it has been proposed to divide the time interval into few sub intervals. AK-SYS-t can then be applied progressively in order to evaluate the cumulative failure probability and to construct a more precise profile for the evolution of the cumulative failure probability.

One remaining issues associated with time-dependent reliability methods like AK-SYS-t can be related to providing appropriate strategies for time discretization. Time discretization strategy has a great influence on the accuracy and efficiency of the method since a small number of time nodes can cause lack of accuracy and large number of them can cause a huge computational cost. Therefore, a proper discretization strategy should be able to optimize the required number of time nodes in order to have a reasonable trade-off between accuracy and efficiency.

Chapter 4: Deterministic crack initiation and propagation analysis for characterizing bridge repair projects

4.1 Introduction

Fatigue of steel structures leads to the initiation and propagation of cracks. If not treated appropriately, fatigue cracks can grow until they put the structure under a very critical situation. Maintenance and repair strategies dealing with fatigue of structures generally aim at extending their fatigue life by controlling the fatigue crack growth in critical locations. In order to investigate proper maintenance actions for fatigue, one should first identify the critical fatigue prone locations within the structure. A crack propagation analysis is then required to study the influence of various parameters (e.g. loading condition and geometry) on the rate and the direction of the crack propagation. Identifying the most influential parameters is crucial to mitigate their impact on structural safety and to identify appropriate maintenance actions, when necessary.

If available, structural inspections can be used to identify the fatigue prone locations where the crack initiation and propagation is likely to occur. Otherwise, a FEA is required to identify the fatigue hot zones within the structure. Fatigue cracking behaviour then can be investigated for those locations using a crack propagation analysis associated with Paris's law for example. This requires a precise approximation of the SIF which is the driving force for crack propagation. For structures with simple geometries the SIF can be estimated by analytical solutions. For complex geometries, however, this needs employing advanced methods. In particular, this chapter considers

the XFEM method that makes it possible to deal with discontinuities like fatigue cracks within the structure.

The goal in this chapter is therefore to illustrate the application of the XFEM advanced method to investigate the fatigue problem on a real case study and to characterize the effectiveness of some possible repair solutions. The case study is a real bridge with an Orthotropic Steel Deck (OSD) system. The root of a fillet weld where stiffeners are welded to the deck plate is a crucial fatigue detail in OSDs since performing inspections for such locations is restricted. Cracks in this location can grow towards the deck plate without being inspected and put the structure in a very critical situation. This is particularly the case when transversal tension exists within the deck plate which can change the crack propagation direction. One main objective herein is to show that the mentioned location is a fatigue prone location and to investigate under which condition (transversal tension values) a crack that initiates at this location can grow towards the deck plate. In the end, some possible repair solutions are compared for this problem in order to extend the structural service life.

Accordingly, this chapter is organized as follows: OSD systems and the bridge case study are introduced in Sections 4.2 and 4.3, respectively. Section 4.4 shortly reviews the XFEM method. Section 4.5 is related to the crack initiation evaluation and the loading and boundary conditions. A strategy for crack propagation analysis is proposed in Section 4.6 and two repair solutions are compared in Section 4.7 to extend the service life of the structure. In the end, some conclusions are provided in Section 4.8.

4.2 Orthotropic steel plate systems

Orthotropic steel plate systems have become a fundamental element in many modern bridge structures. The goal of such systems is to increase the stiffness of thin plates in compression and to diffuse the traffic loads in the deck plate. OSDs have been firstly used by German engineers for bridge construction in 1930's. However, stiffened

steel plates have been employed before in different applications like marine industry or hydraulic applications.

OSDs are generally made from a flat and thin steel plate strengthened by a series of longitudinal stiffeners (ribs) that are supported by orthogonal transverse floor beams (Huang et al., 2019; Zhu et al., 2019). Figure 4.1 illustrates OSD types and their components. An OSD is considered as anisotropic structure since the stiffness features of the deck are significantly different in longitudinal and transverse directions. The OSD can be considered as a top flange for both crossbeams and longitudinal girders. Crossbeams are used to transfer the loads transversely to longitudinal girders which are the main load carrying system.

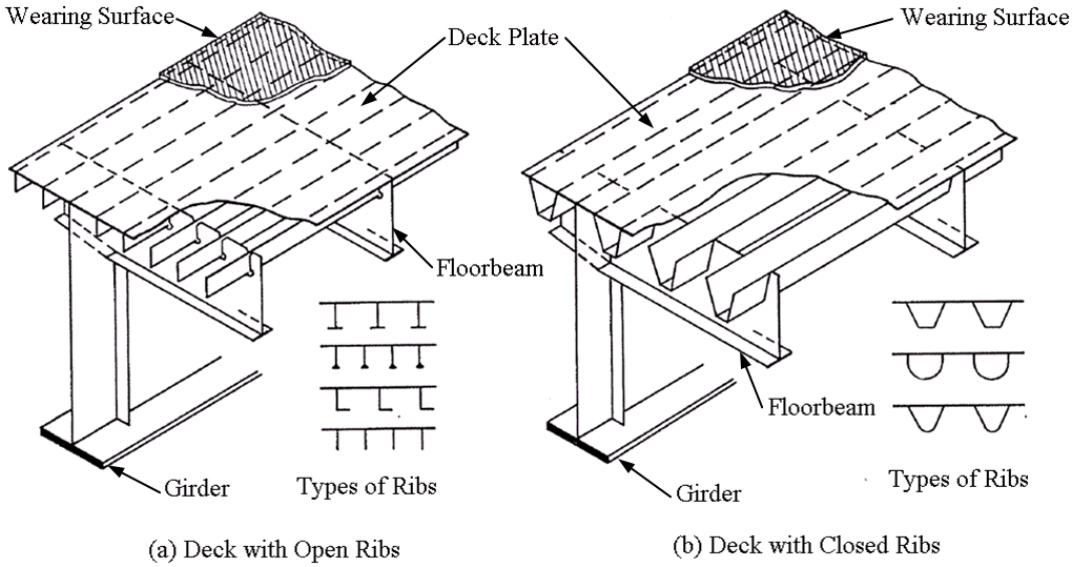

Figure 4.1: Components of bridges with OSD showing (a) Open ribs and (b) Closed ribs (Kozy et al., 2011)

OSDs are extensively used for long-span bridges due to some characteristics like light weight, high strength and durability, and fast construction (since most of the components are pre-fabricated) (Connor, 2012; Kainuma et al., 2016). One can refer to Runyang South in China, Great Belt East in Denmark, Akashi-Kaikyo in Japan as longest bridges of this type with the spans of 1490m, 1624m, and 1991m respectively. Application of OSDs also has a great potential in short to medium span bridges especially when they are located on roads with a high volume of traffic for which a fast

construction and high durability is required.

Welding is used to connect different components and to form an integrated OSD. As a result, compared to other conventional bridge construction methods, bridges constructed using OSDs present a distinctive challenge related to more frequent fatigue cracking. This indicates that in many elements of OSDs working under fluctuating loading, fatigue cracking can be considered as the main limit state (Huang et al., 2019; Maljaars et al., 2018; Zhu et al., 2018). Figure 4.2 depicts the typical fatigue cracks observed near the welding area in OSDs.

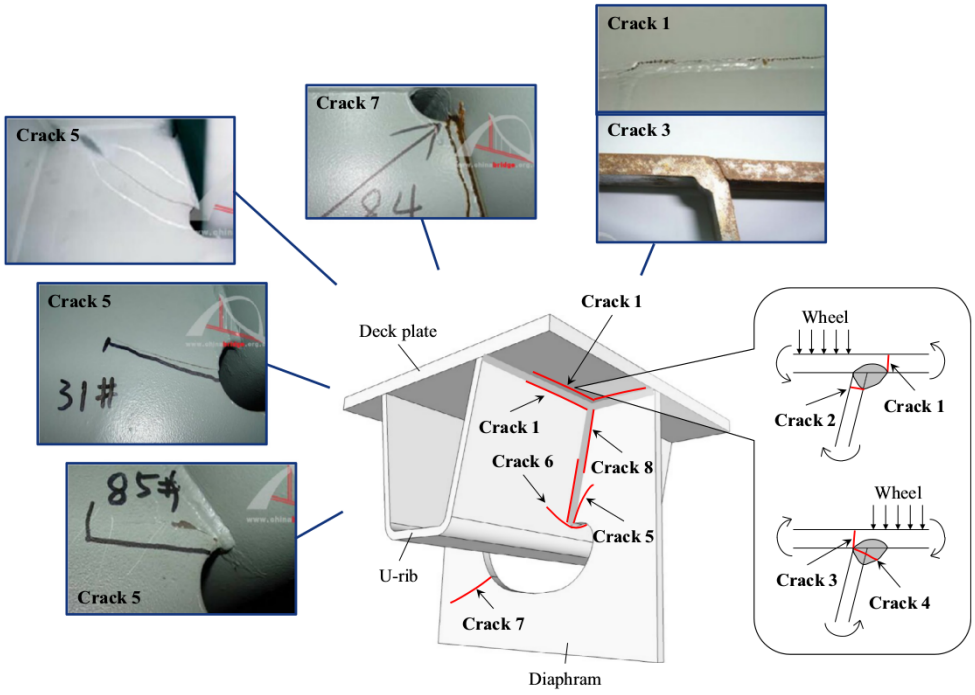

Figure 4.2: Typical fatigue cracks in OSD details (Cheng et al., 2017)

One of the most critical fatigue-prone locations in OSDs is the rib-to-deck welded joint since: 1) the total length of the welded joint is very long; 2) the welding penetration in single-sided fillet weld joints is generally insufficient; 3) direct loading from vehicles cause large local bending stresses; and 4) the values of stress concentration and residual welding stress are high. Fatigue cracks 1 to 4 in Figure 4.2 occur within this region (Cheng et al., 2017).

Depending on their locations, cracks can be either easy to detect and treat or

difficult to detect, like crack type 3 in Figure 4.2 that happens in the root of the fillet weld in a rib-to-deck weld joint. As a result, this kind of cracks can develop until they put the structure in a critical situation. Traffic loading and weight of the cantilever arms of the bridge in addition to residual stresses (after the first repair for instance) can cause a transversal tension within the deck plate which can govern the crack propagation direction and cause cracks of type 3.

4.3 Presentation of the bridge case study

The fatigue analysis is performed in this chapter on a fatigue detail of a real structure constructed in France from 1969 to 1972. Inspection results carried out on the metallic part of the structure indicate that the structure has insufficient fatigue resistance. Some of the inspected fatigue cracks on this bridge are illustrated in Figure 4.3. The overall length of the structure is 875 m where 300 m of this viaduct is constructed by steel box bridge with orthotropic deck supported by two inclined legs. The deck consists of an orthotropic slab of 30 m wide which carries the two pavements of 14 m. The metal structure is completed on both sides by pre-stressed concrete access viaducts. These concrete access viaducts were strengthened from 2012 to 2014 by additional pre-stressing. Figure 4.4 illustrates a cross-section of the bridge constructed by an orthotropic deck and Figure 4.5 presents a cross-section of a stiffener welded to the deck plate.

(a) Fatigue crack #1

(b) Fatigue crack #2

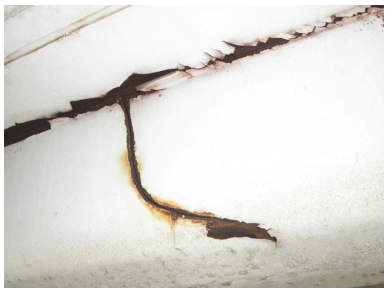

(c) Fatigue crack #3

(d) Fatigue crack #4

Figure 4.3: Observed fatigue cracks on the bridge case study

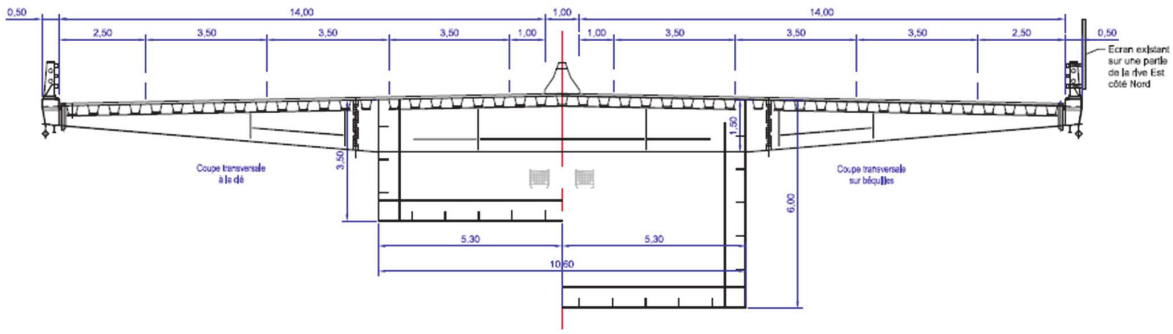

Figure 4.4: Functional cross-section of the steel structure

4.4 The Extended Finite Element Method (XFEM)

The XFEM is an extension of the classical FEM for problems involving discontinuities (e.g. fatigue cracks). Many approaches have already been proposed to address crack propagation in the context of FEM such as: the Lemaitre model using the continuum damage mechanics models (Lemaitre and Desmorat, 2005), the GTN (Gurson-Tvergaard-Needleman) model using the micro-mechanical damage model (Osovski et al., 2015), and the cohesive zone model (Cendón et al., 2017) among others.

One of the major disadvantage of such methods is that capturing the crack propagation path is highly influenced by the mesh structure. The XFEM method hence enables to deal with the discontinuity of the displacement field over the crack surface and singularity near the crack tip without needing to re-mesh the structure (Li et al., 2018).

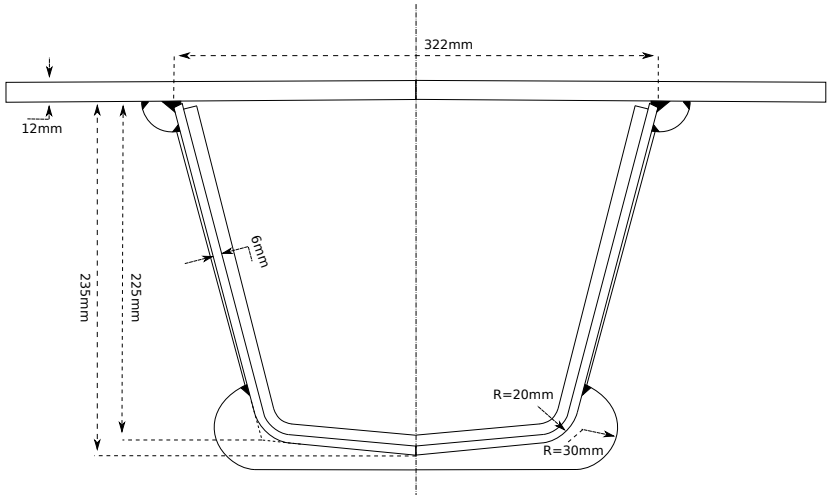

Figure 4.5: Cross-section of a rib of the motorway viaduct

The basic goal of any finite element method is to properly represent the stress and displacement fields within a loaded solid. On that account and for crack propagation analysis, XFEM employs the level set method to introduce cracks in addition to an enrichment process to be able to deal with the discontinuities and singularities within the crack region. With this respect, mesh nodes within the mesh grid for which their support is cut by the crack (see Figure 4.7) are enriched with an additional set of degrees of freedom $\mathbf{q}_i$. Therefore, classical XFEM approximates the displacement field $\mathbf{u}(\mathbf{x})$ using Equation 4.1

$$\mathbf{u}(\mathbf{x}) = \underbrace{\sum_{i \in I} N_i(\mathbf{x})\mathbf{u}_i}_{\text{standard FEM}} + \underbrace{\sum_{i \in I^*} N_i^*(\mathbf{x})(\psi(\mathbf{x}) - \psi(\mathbf{x}_i))\mathbf{q}_i}_{\text{XFEM enrichment}} \tag{4.1}$$

where $\mathbf{u}_i$ represents the traditional degrees of freedom, I^* represents the enriched nodes which is a subset of all nodes I, N_i and N_i^* are FEM shape functions, $\psi(\mathbf{x})$ is the enrichment function, and $\psi(\mathbf{x}_i)$ is a shifting term used to cancel the effect of $\mathbf{q}_i$ to ensure the compatibility among the elements. It should be noted that N_i^* has the

partition of unity property which means

$$\sum_{i \in I^*} N_i^* = 1 \tag{4.2}$$

As previously mentioned, the role of the enrichment process is to introduce the discontinuities and singularities to the displacement field. Using the LEFM, Belytschko and Black (1999) have proposed the enrichment function formulated in Equation 4.3 to deal with the singular displacement in the crack tip in which r and θ are the polar coordinates where the origin is the crack tip, see Figure 4.6.

$$\psi_{tip}(\mathbf{x}) = \sqrt{r}\left\{\cos(\frac{\theta}{2}),\ \sin(\frac{\theta}{2}),\ \sin(\theta)\sin(\frac{\theta}{2}),\ \sin(\theta)\cos(\frac{\theta}{2})\right\} \tag{4.3}$$

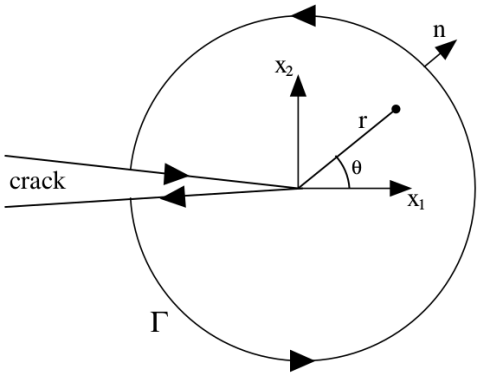

Figure 4.6: Coordinates and geometry of the crack tip

For cases where the plastic zone at the crack tip is not small, LEFM is not an appropriate assumption and this enrichment function becomes ineffective. Therefore, Elguedj et al. (2006) have proposed the following enrichment function to overcome this issue where n is the hardening exponent of the material. One should note that the plasticity zone, for this case, remains limited to the vicinity of the crack tip.

$$\psi_{tip}(\mathbf{x}) = r^{\frac{1}{n+1}}\left\{\sin(\frac{\theta}{2}),\ \cos(\frac{\theta}{2}),\ \sin(\theta)\sin(\frac{\theta}{2}),\right.$$
$$\left.\sin(\theta)\cos(\frac{\theta}{2}),\ \sin(3\theta)\sin(\frac{\theta}{2}),\ \cos(3\theta)\sin(\frac{\theta}{2})\right\} \tag{4.4}$$

Another enrichment process is also used to obtain the displacement of the nodes along the crack surface but far from the crack tip. The idea of using this enrichment is to

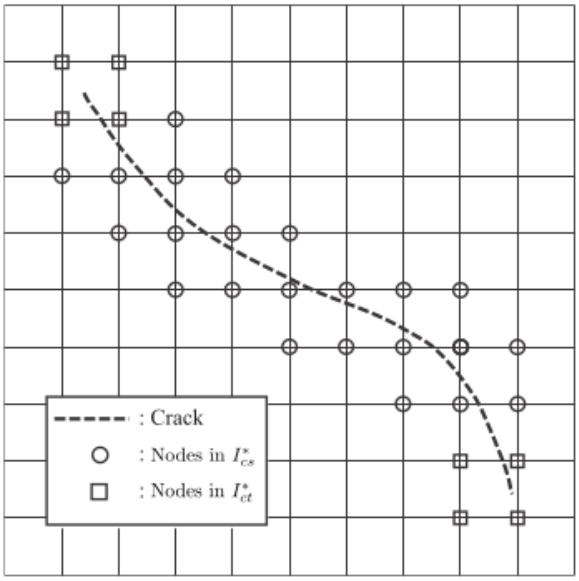

Figure 4.7: An illustration of enriched nodes by XFEM

reduce the amount of the required mesh elements. The Heaviside or sign functions can be used to define the new enrichment function as:

$$\psi_{step}(\mathbf{x}) = H(\mathbf{x}) = \begin{cases} 1 & above\ the\ crack \\ -1 & below\ the\ crack \end{cases} \tag{4.5}$$

The enrichment functions for the crack tip and crack surface can be used to obtain the stress and displacement fields. Therefore, Equation 4.1 can be reformulated as Equation 4.6 where I^* is divided into I^*_{ct} and I^*_{cs} which respectively represent sets of nodes near the crack tip and crack surface, see Figure 4.7. The additional degrees of freedom $\mathbf{q}_i$ are also divided into $\mathbf{b}_i$ for those around the crack tip and $\mathbf{a}_i$ for the remaining nodes.

$$\mathbf{u}(\mathbf{x}) = \sum_{i \in I} N_i(\mathbf{x})\mathbf{u}_i + \sum_{i \in I^*_{cs}} N^*_i(\mathbf{x})[\psi_{step}(\mathbf{x}) - \psi_{step}(\mathbf{x}_i)]\mathbf{a}_i + \sum_{i \in I^*_{ct}} \sum_j N^*_i(\mathbf{x})[\psi^j_{ct}(\mathbf{x}) - \psi^j_{ct}(\mathbf{x}_i)]\mathbf{b}^j_i \tag{4.6}$$

It also should be noted that the XFEM method uses the maximal tangential stress as a criterion to decide about the direction of the crack propagation. With this respect, the angle of the propagation is calculated as a function of K_I and K_{II} which are the stress intensity factors for crack opening modes I and II, see Chapter 2 Section 2.6.

4.5 Crack initiation analysis

The goal of this section is to identify the most critical locations on the structure where fatigue cracks are most likely to initiate. Accordingly, the finite element model, loading conditions, and crack initiation analysis are respectively presented in the following.

4.5.1 Finite element model

Crack initiation analysis is carried out on a 3D finite element model representing a small part of the bridge with the length of 4 m containing 3 ribs that is restricted between two transversal floor beams. It is assumed that the structural movement in the location of the transversal floor beams is fixed in all directions. The cross-section of the model is provided in Figure 4.8 where $l1 = 0.322$ m. To identify the critical locations for crack initiation analysis, it is necessary to execute the finite element analysis on a full 3D model to be able to compare the fatigue damage for all feasible locations. Figure 4.9 shows the full 3D model for the crack initiation study. The finite element model includes 11338 linear triangular and 2806 linear rectangular elements for 2D meshing and 317464 linear prismatic for 3D meshing. It is worth to mention that Gmsh (Geuzaine and Remacle, 2009) is used for finite element mesh generating, both for crack initiation and crack propagation.

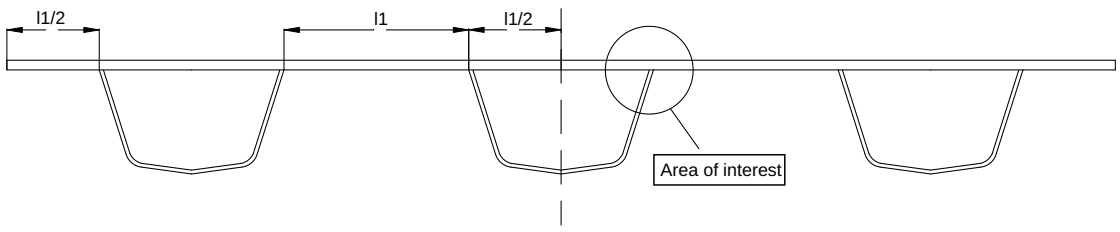

Figure 4.8: Cross section of the modeled part

Another issue that needs to be taken into consideration for crack initiation is the local stress calculation in the root or toe of the fillet weld. This is important since the notch root stress is the dominant influencing parameter for fatigue strength of welded structures. Effective notch stress method is one way that is recommended for such locations. In this approach (Fricke, 2007), the weld root or toe is modeled with a reference radius ρ_f, see Figure 4.10. The local stresses (von Mises stress for example) can be calculated then and evaluated against the corresponding S-N curves for fatigue damage assessment. Figure 4.11 shows the root and the toe of the fillet weld that is modeled with a reference radius of 0.1 mm.

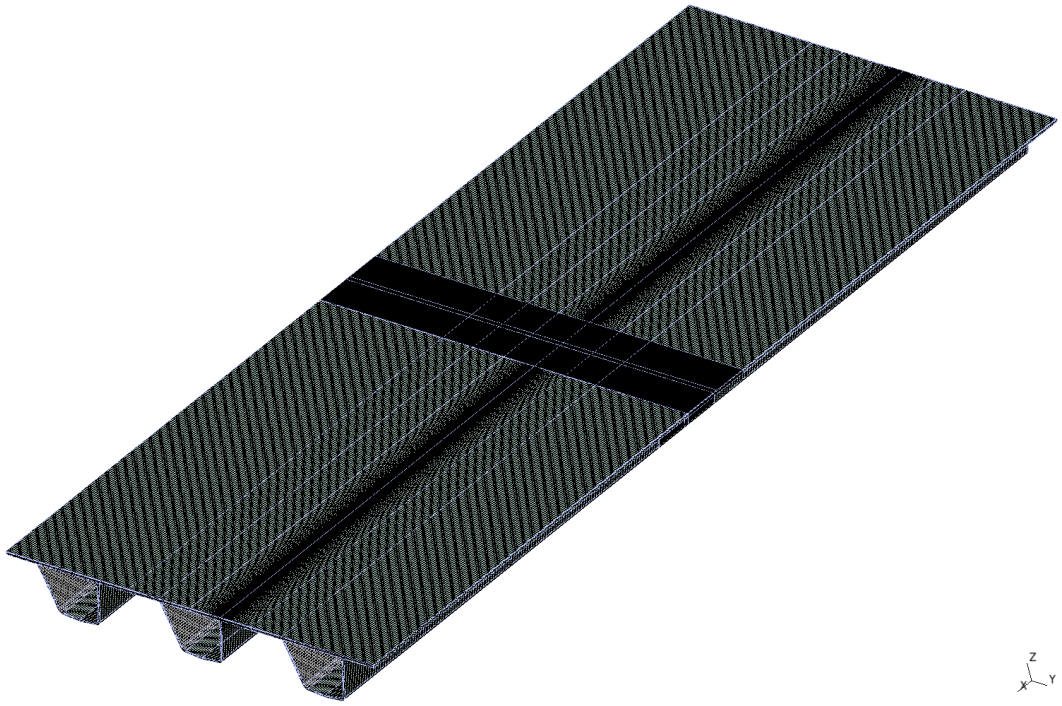

Figure 4.9: 3D finite element model for crack initiation analysis

4.5.2 Loading and boundary conditions

Two loading conditions are considered for this study, see Figure 4.12. In the first loading case, the load of the wheel is directly applied on a rib, while in the second case, the wheel is assumed to be located between two ribs. The worst bending condition is created when such loading conditions are caused by heavy vehicles and applied repeatedly on the structure. Figure 4.13 shows an illustration of the heavy vehicle.

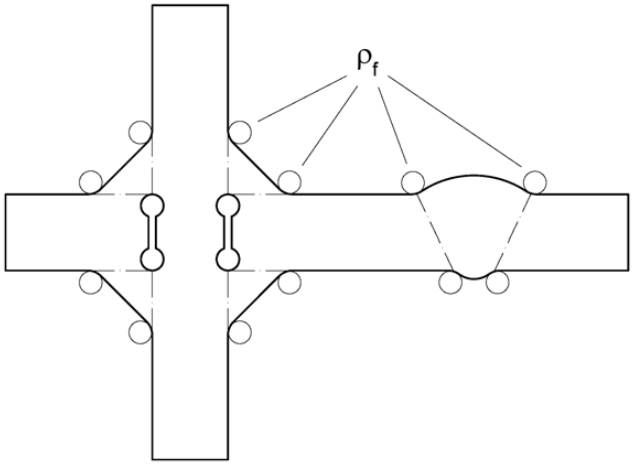

Figure 4.10: Fictitious notch rounding ρ_f

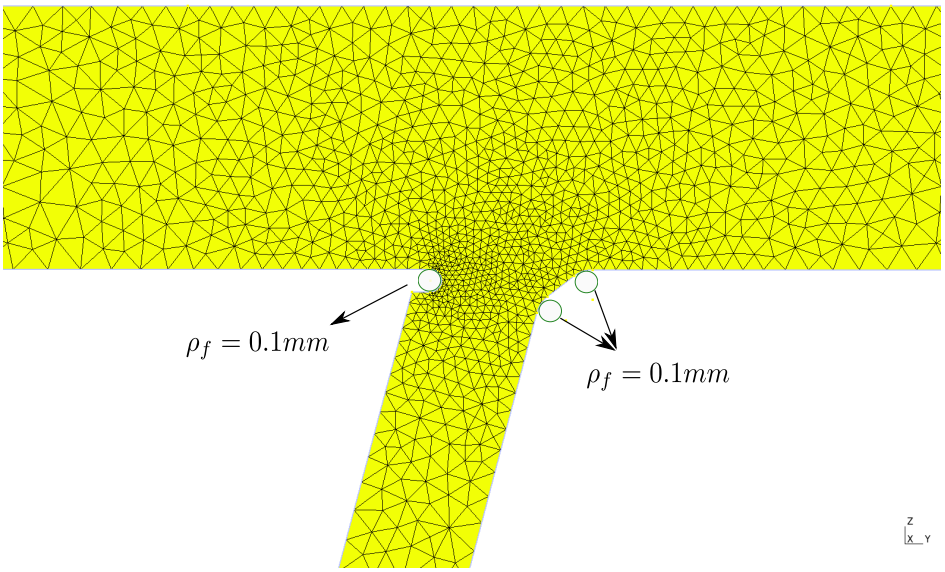

Figure 4.11: Effective notch with $\rho_f = 0.1$mm for the toe and the root of welding detail

The weight of the vehicle is considered to be 45t where the applying load under each wheel is 4.5t. Considering the dimensions of the model, maximum 3 wheels can be applied at the same time for the load cases 1 or 2 separately (see Figure 4.14).

As previously mentioned, it is assumed that the structural movement is fixed in the locations where the floor beams are installed. Therefore, in the finite element analysis the movements of the structure in those locations for X, Y, and Z directions are fixed to zero. Accordingly, a static analysis is performed under given boundary conditions

and load case 2 (applying 4.5t on the locations of the load case 2 illustrated in Figure 4.14). Figure 4.15 shows the displacements within the structure after applying the load. It can be seen that the deflection is symmetric longitudinally and that the maximum deflection happens under the wheel in the center of the model which seems reasonable.

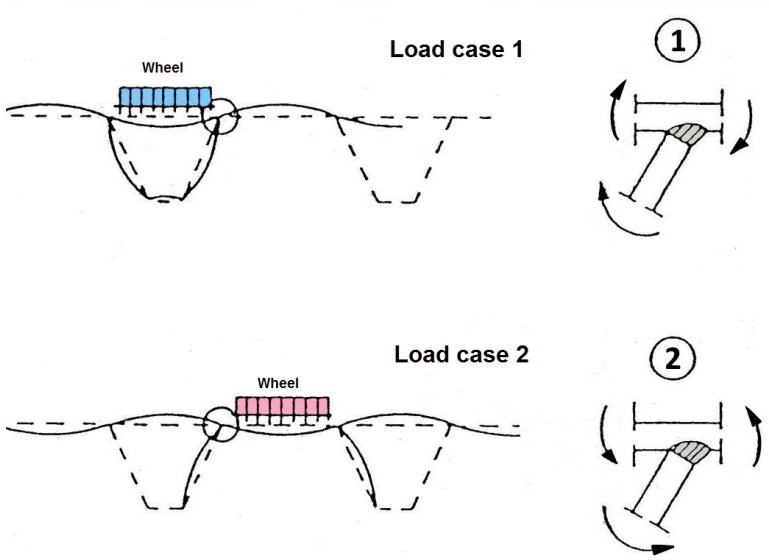

Figure 4.12: Loading conditions for crack initiation analysis

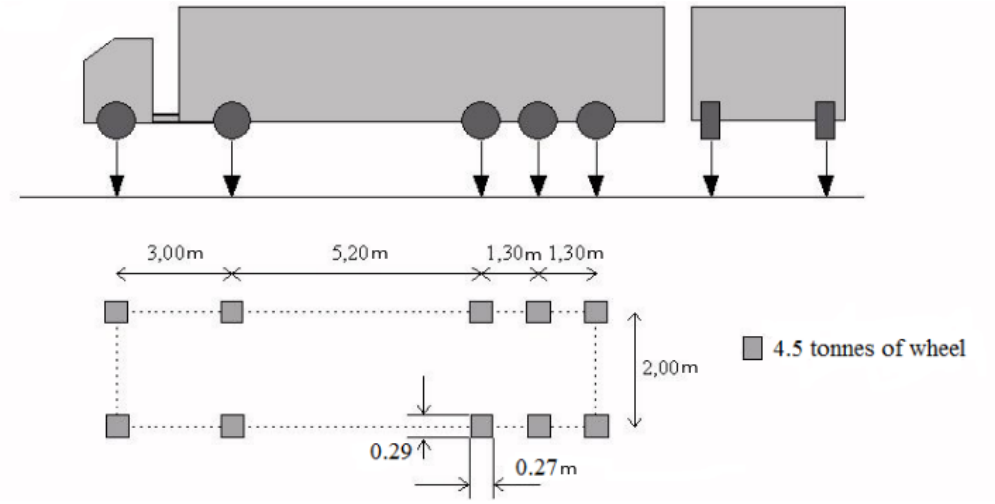

Figure 4.13: A schematic view of the heavy vehicle

4.5.3 Crack initiation

Crack initiation analysis is performed on the provided 3D finite element model by applying a cyclic loading composed of load cases 1 and 2 illustrated in Figure 4.12.

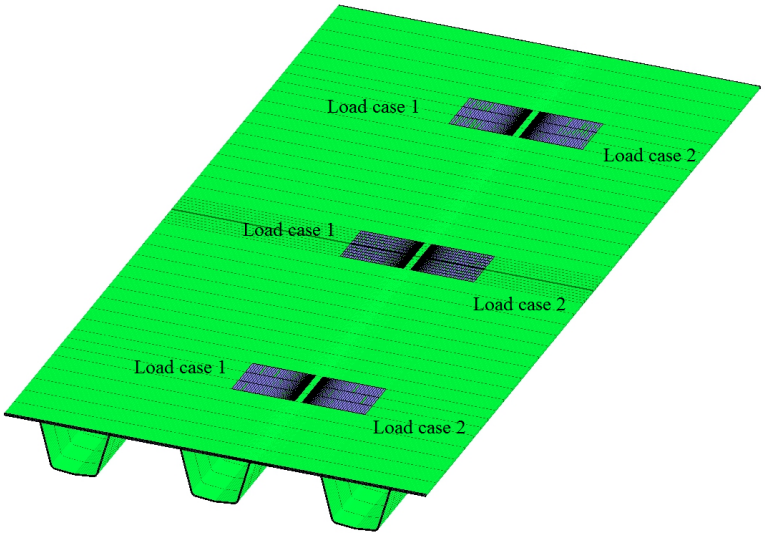

Figure 4.14: Location of applied loads (load cases 1 and 2) on the model

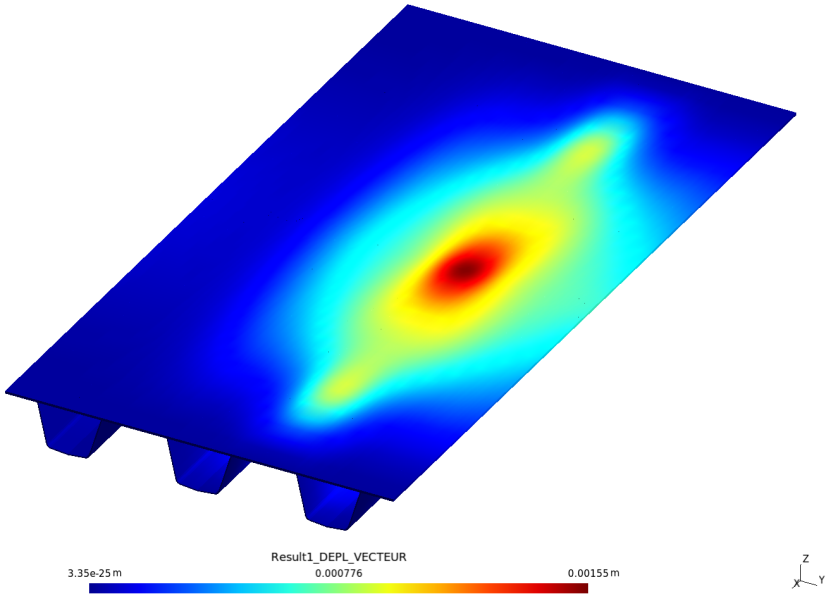

Figure 4.15: Results of the static analysis of the 3D model under load case 2

Figure 4.16 shows how this cyclic loading is changing over time. Code_Aster which is a free software for numerical simulation in structural mechanics (Electricité de France, 2017) is used to perform a static FEA on the structure for a small number of load cycles (only 12 load cycles) due to the computational limitations. In this way one can calculate the value of stresses in different locations of the structure which can be used for evaluating the cumulative fatigue damage by Miner's rule. The material that is

considered for this model is steel with Young modulus of 210 GPa and the welding class for the fatigue details is assumed to be class 125. The S-N curves for this welding class are used to calculate the cumulative fatigue damage under the given cyclic loading, see Figure 4.17. Accordingly, Figure 4.18 illustrates the cumulative fatigue damage in different locations of the fatigue detail which is located in the center of the structure that has maximum displacement, see figure 4.15. It can be seen that, under the given loading and boundary conditions, the root of the fillet weld is a fatigue prone location since the maximum fatigue damage occurs in this location (equals to 2.32×10^{-5}), which reads that the fatigue cracks are most likely to develop at this place. Subsequently, a crack propagation analysis is performed in the following section to evaluate the loading conditions for which the crack starts propagating towards the deck plate.

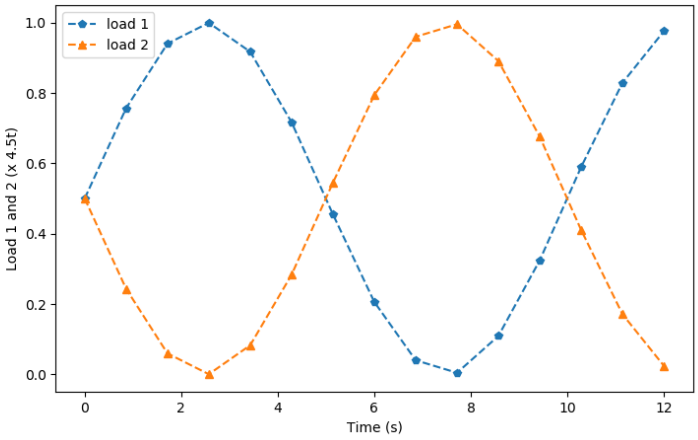

Figure 4.16: Cyclic loading applied for crack initiation analysis

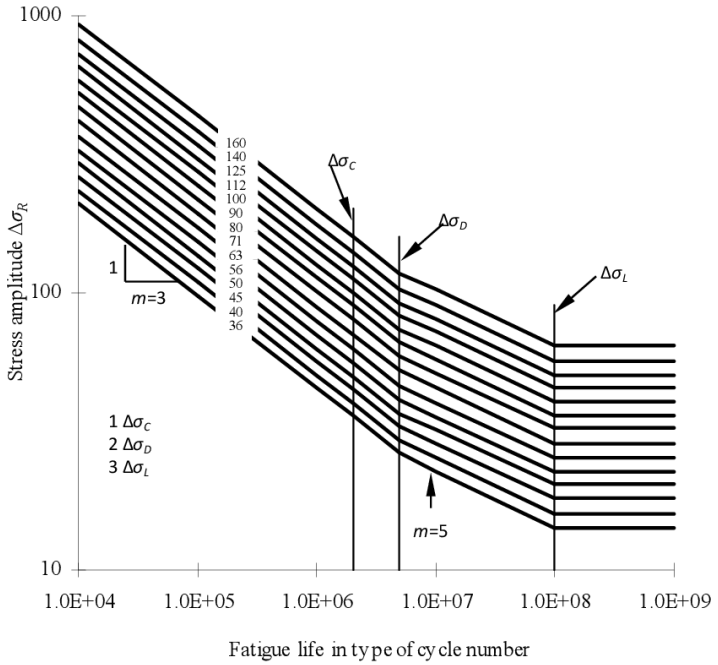

Figure 4.17: S-N curves for several welding classes used in orthotropic decks (Wang and Song, 2017)

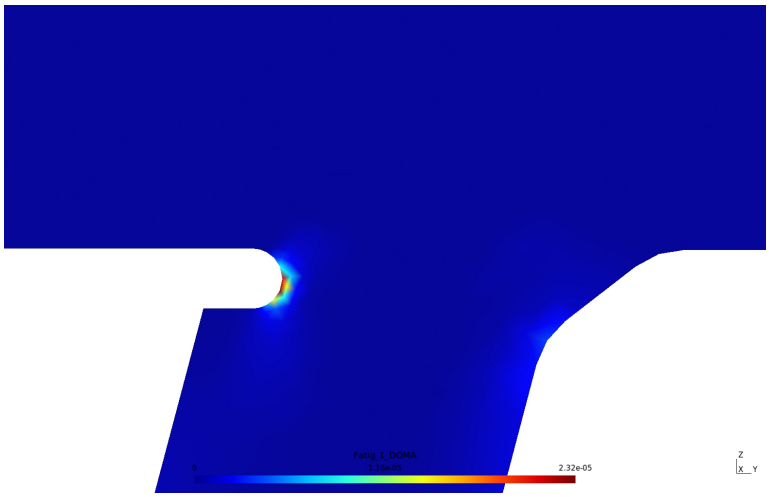

Figure 4.18: Cumulative fatigue damage in different locations of the fatigue detail

4.6 Deterministic crack propagation with XFEM

After identifying the crack initiation location, a crack propagation analysis is required to investigate the fatigue crack behavior. This can help to search closely for the loading conditions causing the sever conditions in order to come up with relevant maintenance actions. An unwanted situation for the cracks initiated in the root of the fillet weld in

a rib-to-deck welding joint occurs when cracks are tending to grow towards the deck plate. Transversal tension within the deck plate can be considered as the governing force that creates this situation. On that account, a deterministic crack propagation analysis is performed in this section to study the influence of the transversal tension on the crack propagation direction.

This analysis is performed on a 2D finite element model using the XFEM method (Moës et al., 1999). In this method the maximum circumferential stress criterion introduced by Erdogan and Sih (1963) for elastic materials is used to approximate the crack propagation direction. One difficulty at this stage can be related to properly introducing the loading and boundary conditions on the 2D finite element model. For this reason, we propose a strategy in which the effects of applied loads on the structure are investigated independently using separate 3D FEA for each load. This strategy can help to properly identify the load effects at the boundaries of the 2D model and it is introduced in Section 4.6.2.

4.6.1 Finite element model

As mentioned earlier, a 2D finite element model is considered to perform the crack propagation analysis. One reason to choose this model is to obtain more consistent results for approximation of SIFs that leads to a better estimation of crack propagation rate and crack propagation direction. It should be noted that SIFs are usually evaluated by interaction integral that is mostly used for 2 dimensional problems. Using the interaction integral can pose some difficulties and uncertainties in 3 dimensional cases (Baydoun and Fries, 2012). Another reason is due to the computational limitations of the computer used for the finite element analysis which is a DELL laptop with an Intel Core i5 processor running at 2.7 GHz using 16 GB of Random Access Memory (RAM).

The 2D finite element model is illustrated in Figure 4.19 in which the applied mesh on this area includes 11776 triangular elements. The area of the crack propagation is prepared with a higher mesh concentration that enables us to calculate the SIF more precisely in this region which is necessary to shorten the crack propagation steps

in order to predict the propagation direction properly. As already said before, the difficulty here is related to properly identifying the loading and boundary conditions on the 2D model. On that account, an appropriate strategy is proposed in next section in order to translate the load effects from the 3D model to the 2D model.

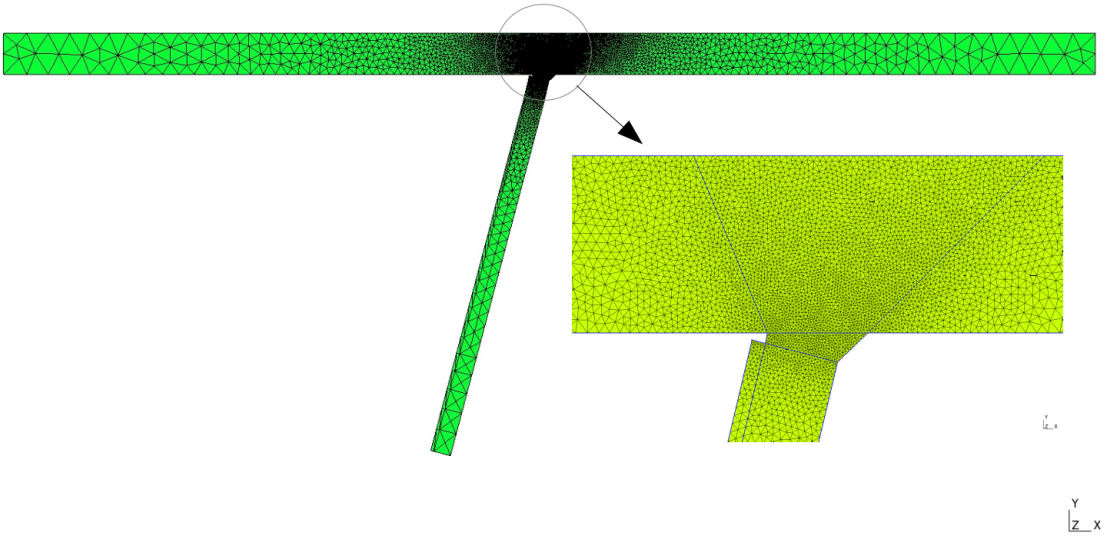

Figure 4.19: 2D finite element model used for crack propagation

4.6.2 Loading and boundary conditions

For the crack propagation analysis it is assumed that the structure is working under the second loading case introduced in Section 4.5.2 in which the load of the wheel is applied between stiffeners. Additionally, it is assumed that a local transversal tension exists near the cracking area and the goal here is to study the influence of this transversal tension on the direction of crack propagation in this location.

Identifying the loading and boundary conditions for the 2D model requires a proper strategy since it is not a straightforward task. Hence, in order to simplify transforming the loading and boundary conditions from the 3D to the 2D model, corresponding load effects (displacements and rotations) are measured on the 3D model and they are directly introduced on the 2D model. On that account, assuming that the 2D model is fixed in the left edge, see Figure 4.20, the goal here is to identify the relative displace-

ments and rotations in the right edge $(\Delta X_r, \Delta Y_r, R_r)$ and bottom edge $(\Delta X_b, \Delta Y_b, R_b)$ of the model.

Displacements and rotations in the right edge and bottom edge of the model result from the vertical load and the transversal tension and it is assumed herein that they are acting independently on the structure. Therefore, the strategy here is composed of two 3D finite element analyses: one measuring the load effects caused by the vertical load and the other one measuring the displacements and rotations caused by the transversal tension. An illustration of this strategy is provided in Figure 4.21.

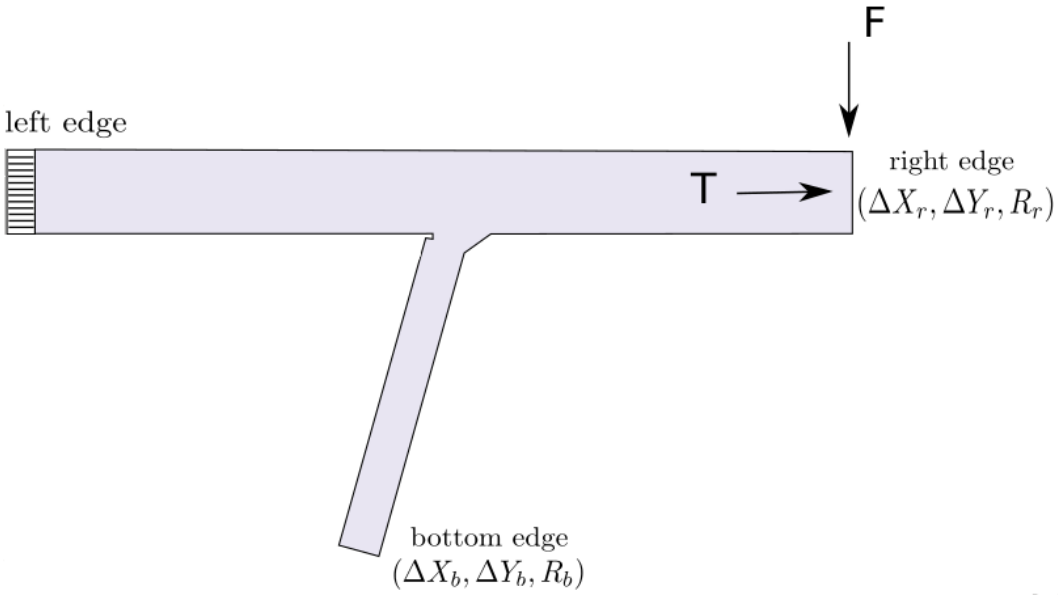

Figure 4.20: An illustration of load effects in the 2D model

The first FEA aims at measuring the relative displacements and the rotations caused by the vertical load F in the right edge $(\Delta X_{F_r}, \Delta Y_{F_r}, R_{F_r})$ and the bottom edge $(\Delta X_{F_b}, \Delta Y_{F_b}, R_{F_b})$ of the 2D model. For this reason, this analysis considers the 3D finite element model used for crack initiation which is subjected to the second loading case introduced in Section 4.5.2. Assuming that the 2D model is fixed at the left edge, Table 4.1 summarizes the relative displacements and rotations at the boundaries of the 2D model caused by the mentioned loading case. It should be noted that the amount of rotations caused by the vertical load in the right and bottom edges is negligible.

The second FEA is performed on a local 3D finite element model to measure the

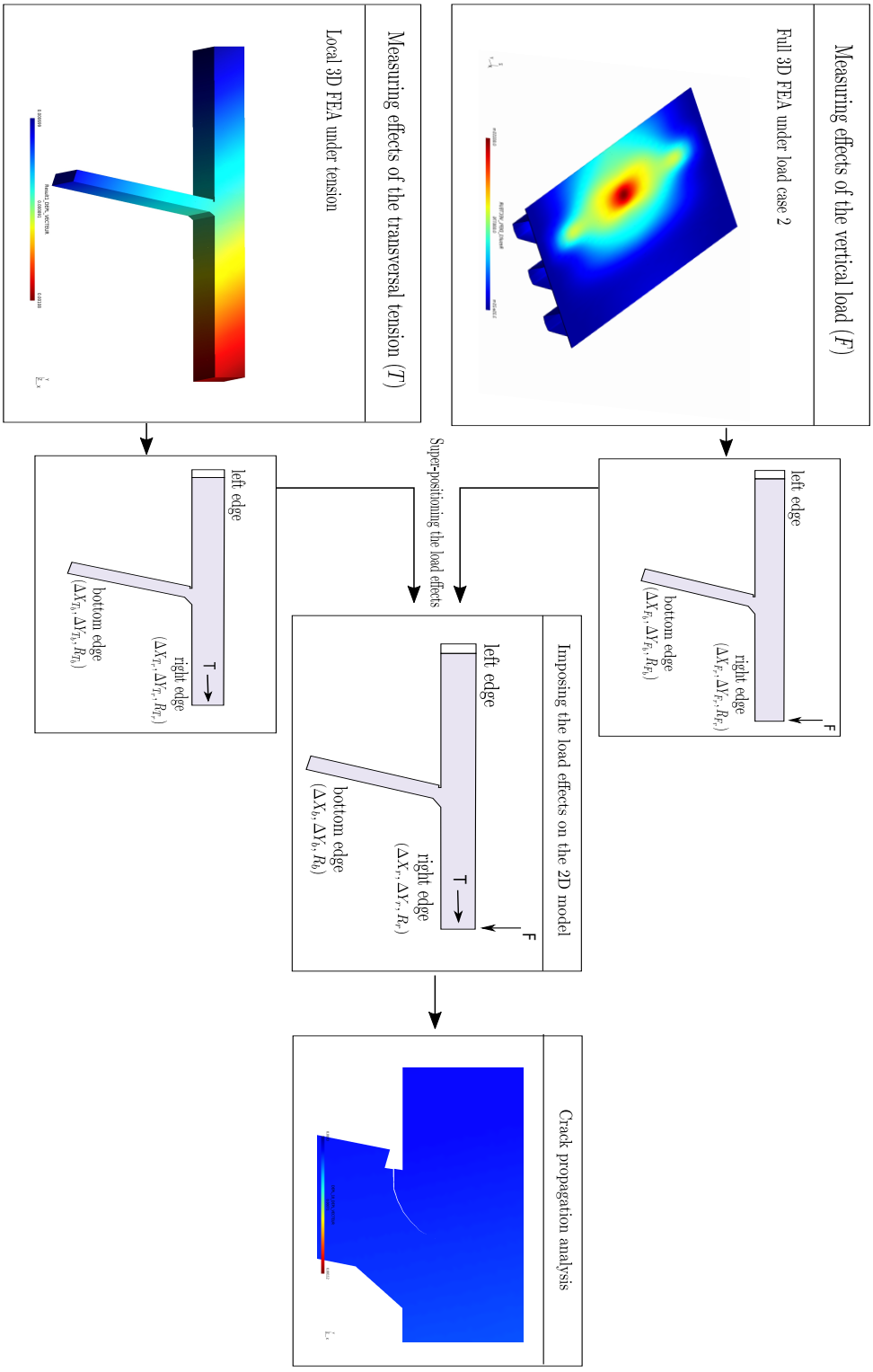

Figure 4.21: An illustration of the strategy to extract the load effects from 3D finite element models for 2D finite element analysis

Table 4.1: Relative displacements and rotations in 2D model due to the vertical load

Location	Rotation	Displacement	
Right edge	R_{F_r}	ΔX_{F_r}(mm)	ΔY_{F_r}(mm)
	0.0	0.00	-0.858
Bottom edge	R_{F_b}	ΔX_{F_b}(mm)	ΔY_{F_b}(mm)
	0.0	-0.045	-0.314

displacements and rotations caused by the transversal tension near the area where the crack initiates and propagates. Figure 4.22 illustrates the 3D finite element model and its loading and boundary conditions. Displacements and rotations are measured for different levels of transversal tension. Results of FEA show that the amount of rotation caused by the transversal tension in different locations of this model is also negligible. Hence, Table 4.2 presents the tension levels and their corresponding displacements at the right edge (ΔX_{T_r}, ΔY_{T_r}) and the bottom edge (ΔX_{T_b}, ΔY_{T_b}) of the structure. It should be mentioned that, this study will not discuss about the sources of this transversal tension. As mentioned previously, traffic loading, weight of the structure, and existing residual stresses in the deck plate (after repair for instance) can be counted as some of the sources for this tension.

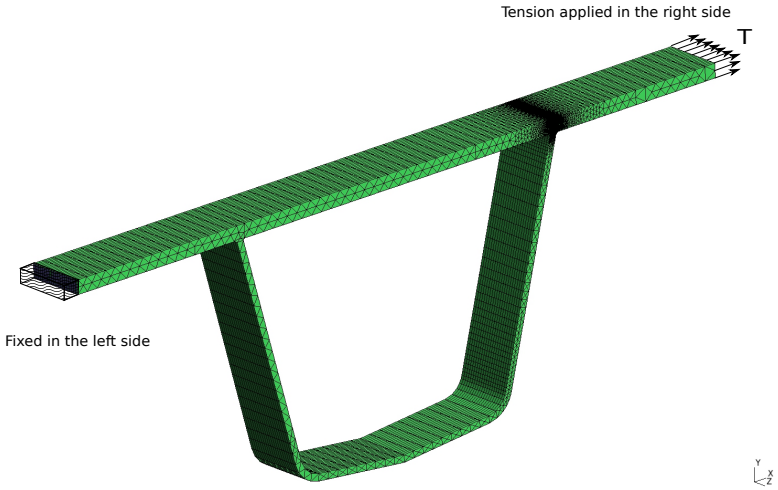

Figure 4.22: An illustration of applied tension in the 3D model

In the end, by assuming that the vertical load and the transversal tension are acting

Table 4.2: Applied tension levels and corresponding displacements

Level	1	2	3	4	5	6	7	8
Tension (MPa)	0.0	70	140	210	227.5	245	262.5	280
ΔX_{T_r} (mm)	0.0	0.054	0.108	0.161	0.175	0.188	0.202	0.215
ΔY_{T_r} (mm)	0.0	-0.057	-0.114	-0.17	-0.184	-0.198	-0.213	-0.227
ΔX_{T_b} (mm)	0.0	0.0011	0.0022	0.0032	0.0035	0.0038	0.0040	0.0043
ΔY_{T_b} (mm)	0.0	-0.017	-0.034	-0.050	-0.054	-0.058	-0.063	-0.067

independently on the structure, Equations 4.7 and 4.8 can be used to calculate the displacements in the right edge and the bottom edge respectively by super-positioning the load effects.

$$\begin{cases} \Delta X_r = \Delta X_{F_r} + \Delta X_{T_r} \\ \Delta Y_r = \Delta Y_{F_r} + \Delta Y_{T_r} \end{cases} \tag{4.7}$$

$$\begin{cases} \Delta X_b = \Delta X_{F_b} + \Delta X_{T_b} \\ \Delta Y_b = \Delta Y_{F_b} + \Delta Y_{T_b} \end{cases} \tag{4.8}$$

It is observed that the displacements in the bottom edge show a linear relationship with ΔY_{F_r} and ΔX_{T_r}. Therefore, Equation 4.9 can be used to approximate the displacements in the bottom edge. Coefficients in this equation are derived from the results of previous finite element analyses. This formulation will be further used in Chapter 5 which it covers a time-dependent reliability assessment on the fatigue detail of interest.

$$\begin{cases} \Delta X_b = 0.05\Delta Y_{F_r} + 0.02\Delta X_{T_r} \\ \Delta Y_b = 0.33\Delta Y_{F_r} - 0.31\Delta X_{T_r} \end{cases} \tag{4.9}$$

4.6.3 Crack propagation

After introducing the boundary and loading conditions into the 2D finite element model, a 2D crack propagation analysis is performed for different levels of transversal tension. Crack propagation analysis is carried out using Code_Aster by employing Paris' law and introducing a horizontal initial crack of 1 mm length in the root of the fillet weld. Material properties considered for Paris' law are: $C = 1.4 \times 10^{-11}$ and

$m = 3.75$. Figure 4.23 depicts results of the crack propagation when the transversal tension is equal to $T = 140$ MPa. Figures in the left side show the crack progress (0.6 mm in each step when the initial crack is 1 mm), and figures in the right side illustrate the stress field for the corresponding crack propagation. It can be seen from the stress fields that the stress values around the crack tip are higher compared to other locations of the structure and that they can reach 324 MPa in this case.

Figure 4.24 illustrates the results of the crack propagation for several transversal tension levels provided in Table 4.2. The initial crack size for all cases is equal to 1 mm and the propagation is performed for 10 steps where in each step crack moves for 0.3 mm. It can be seen that by increasing the transversal tension, crack propagation direction changes gradually until it starts propagating upwards for tensions greater than 210 MPa. Results here clearly highlight the influence of transversal tension on the crack propagation direction. Observing cracks within the deck plates of structures with OSDs indicates that the transversal tension can exceed this threshold ($T > 210$ MPa for this study) which forces the cracks to grow towards the deck plate.

Crack propagation in previously mentioned weld detail towards the deck plate is an unwanted situation. Difficulties in inspecting those cracks due to the crack location and the asphalt layer on the deck plate can lead to a late identification of such cracks. Hence, they can reach a critical length and put the structure in a critical situation for which prompt repair interventions are required to keep this situation under control. Repair actions for such problems are aiming at controlling the load effects and increasing the fatigue life of the weld detail. Accordingly, the effectiveness of two repair actions are compared in the next section.

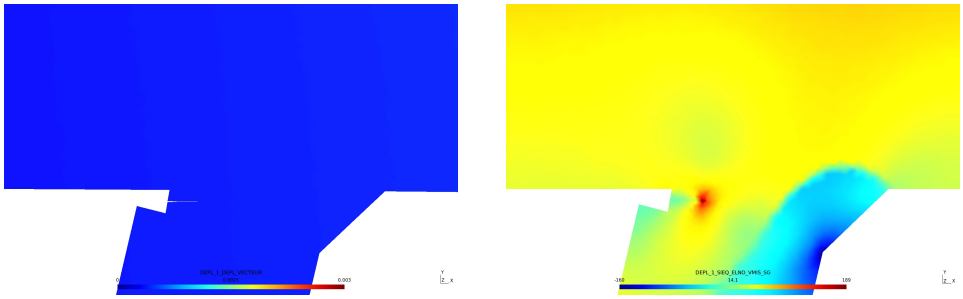

(a) Propagation #1: 1 mm

(b) Stress field for propagation #1

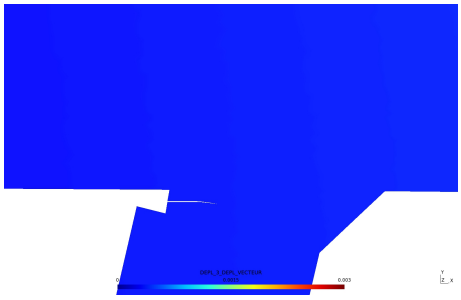

(c) Propagation #2: 1.6 mm

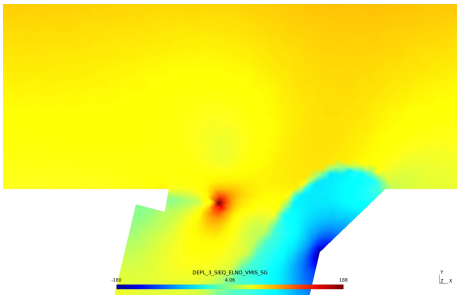

(d) Stress field for propagation #2

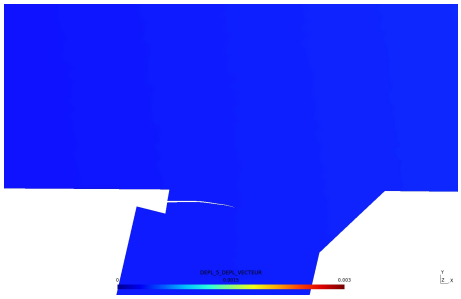

(e) Propagation #3: 2.2mm

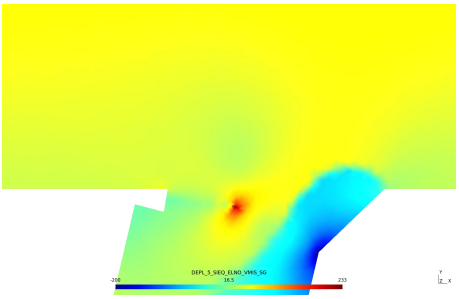

(f) Stress field for propagation #3

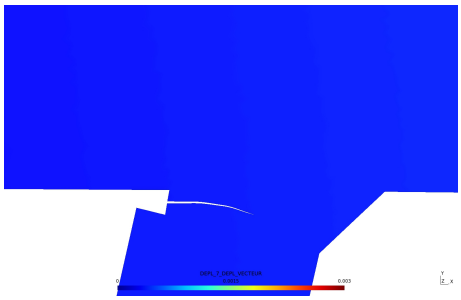

(g) Propagation #4: 2.8mm

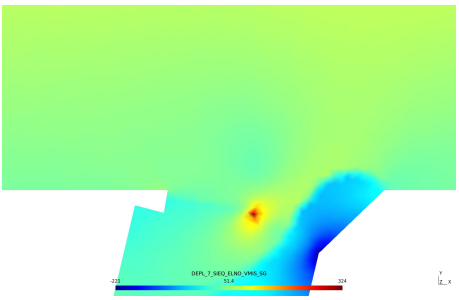

(h) Stress field for propagation #4

Figure 4.23: Some propagation steps and their corresponding stress field for T= 140 MPa

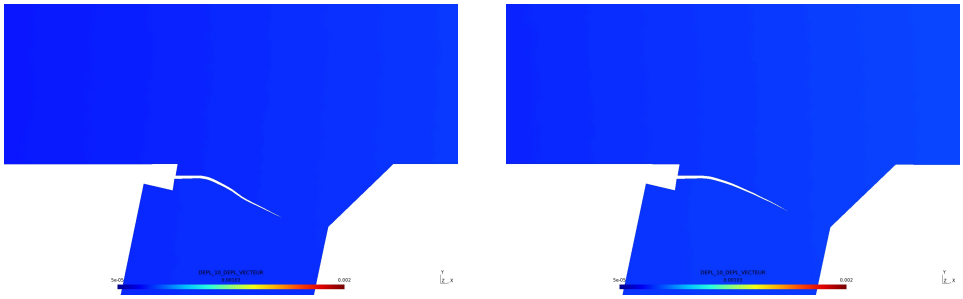

(a) Propagation #1: T= 0.0

(b) Propagation #2: T= 70 MPa

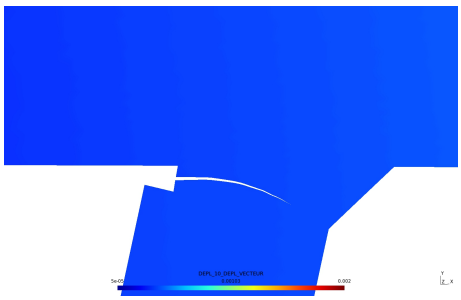

(c) Propagation #3: T= 140 MPa

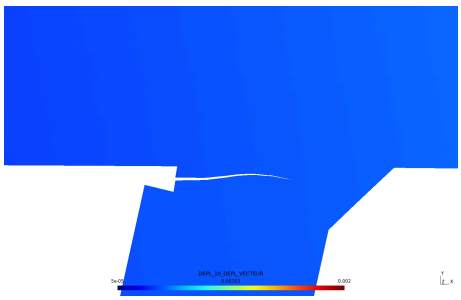

(d) Propagation #4: T= 210 MPa

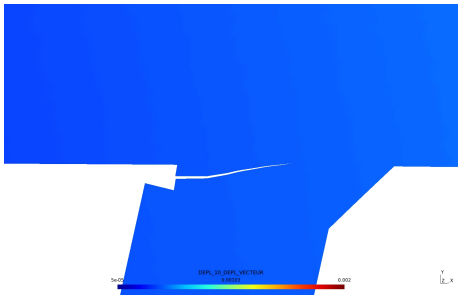

(e) Propagation #5: T= 227.5 MPa

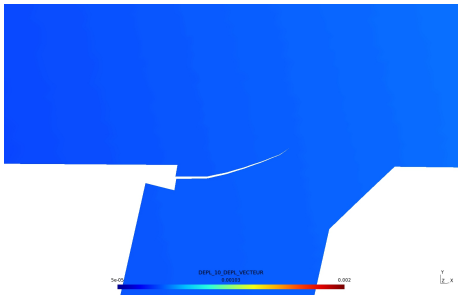

(f) Propagation #6: T= 245 MPa

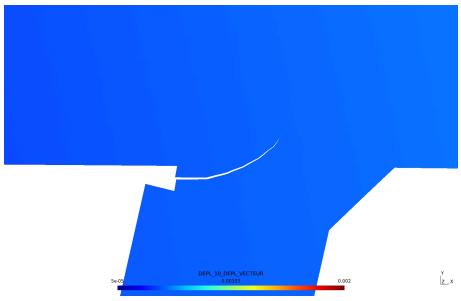

(g) Propagation #7: T= 262.5 MPa

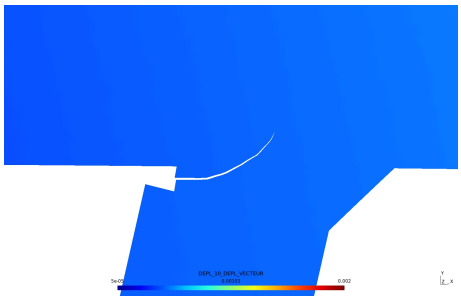

(h) Propagation #8: T= 280 MPa

Figure 4.24: Propagation direction for different levels of transversal tension

4.7 Repair strategies to control the crack propagation

The crack initiation analysis in Section 4.5 has indicated the possibility of crack initiation in the root of the fillet weld where a rib is welded to the deck plate. Moreover, it has been observed that the transversal tension can change the crack growth direction towards the deck plate, in Section 4.6, which can put the structure in a very critical situation. Repair actions can be applied to eliminate or at least reduce the damage caused by such cracks. Repair strategies for such a problem are expected to control the crack propagation by alleviating the SIF within the crack region which in turns can increase the fatigue life of a structure. The effectiveness of two repair solutions is looked over in the sequel.

Before investigating the influence of the repair actions on the fatigue problem of the desired welding detail, a sensitivity analysis is performed to study the influence of acting loads (the transversal tension and the load of the vehicle) on the SIF in the crack region. This can help to identify which load has a higher impact on the SIF which is important to make decisions on selecting better repair actions.

4.7.1 Sensitivity analysis on load effects

Sensitivity analysis is an advantageous tool to study the influence of various independent variables on a given dependent variable under a set of assumptions (Orta and Bartlett, 2020; Abbiati et al., 2021). Therefore, the goal here is to determine what are the impacts of vertical force and transversal tension on the SIFs in the vicinity of the crack tip. Hence, the best repair solution will be the one that better controls the effect of the load with the largest impact. For this reason, the 2D model introduced in Section 4.6 is reused here to perform finite element analyses in order to measure the SIFs at the crack tip.

To perform the sensitivity analysis, one force (vertical load or transversal tension) is considered to be fixed while the other one varies. In this way, one can study the effect of the varying force on the magnitude of the SIF at the crack tip which is already

introduced into the 2D model using XFEM. It should be noted that for all conditions of the sensitivity analysis, the same crack of length 3mm and crack angle of $\theta = 25°$ is introduced to the model using XFEM method. An illustration of this crack is provided in Figure 4.25

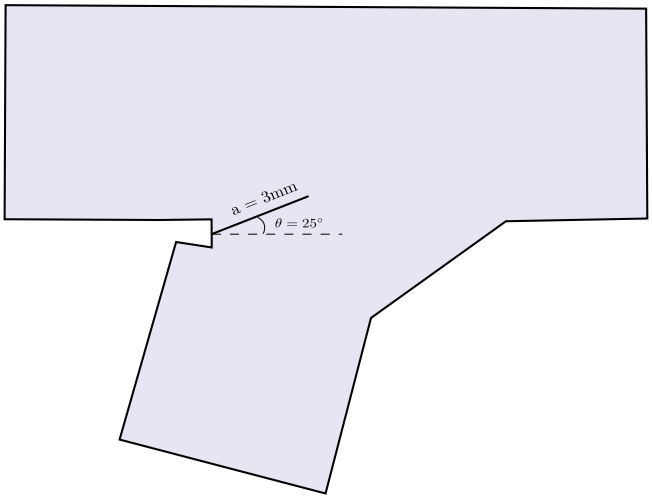

Figure 4.25: An illustration of the fatigue crack used for sensitivity analysis

Three different conditions for the sensitivity analysis are provided in Table 4.3 (conditions 0, 1, and 2). The condition 0 is used as the reference condition in which the load effects imposed on the right edge of the structure are: $\Delta X_{T_r} = 0.161mm$, $\Delta Y_{T_r} = -0.17mm$, and $\Delta Y_{F_r} = -0.858mm$ where ΔX_{T_r} and ΔY_{T_r} are the displacements imposed by the transversal tension and ΔY_{F_r} is the displacement imposed by the vertical load. The ultimate displacements in the right edge and the bottom edge of the model can be calculated by Equations 4.7 and 4.9 respectively. For condition 1, the load effects of transversal tension ΔX_{T_r} and ΔY_{T_r} are increased up to 50% with a step of 10%, while the load effect of vertical load ΔY_{F_r} does not change. For condition 2, however, ΔX_{T_r} and ΔY_{T_r} remain the same as the reference condition while ΔY_{F_r} is increased up to 50% with a step of 10%. Equation 4.10 is used to measure the percentage of change in SIF (K) after changing the load effects.

$$\%\text{change of } K = \frac{|K - K_{ref}|}{K_{ref}} \times 100 \tag{4.10}$$

Figures 4.26 and 4.27 present the results of this sensitivity analysis. Figures 4.26a and 4.27a illustrate that SIFs have a linear relationship with the associated load effects.

Table 4.3: Sensitivity analysis conditions

Condition	Description
Condition 0	ΔX_{T_r}= 0.161mm, ΔY_{T_r} = -0.170mm, ΔY_{F_r}= -0.858mm
Condition 1	ΔX_{T_r} and ΔY_{T_r} are increased up to 50%
Condition 2	ΔY_{F_r} is increased up to 50%

It can be seen in both conditions that K_I has greater values than K_{II}. Figures 4.26b shows that increasing the effect of transversal tension has a significant impact on K_{II} while it does not have a big impact on K_I. However, it can be seen from Figure 4.27b that increasing the effect of vertical load has considerable effects on both K_I and K_{II}.

The results of this sensitivity analysis provide important information for selecting appropriate repair actions to tackle the fatigue problem in the root of the fillet weld. According to those results, one can conclude that repair solutions should concentrate more on reducing the load effects caused by the vertical load. However, it should be reminded that the transversal tension has a non-negligible impact on K_{II} which can be a determining factor for fatigue life and the crack propagation direction. On that account, two repair actions are considered for this fatigue problem in the following. The first solution suggests to locally apply a cement or metal-based layer on the deck plate to reduce the effect of the transversal tension while the second solution proposes to place vertical plates between the stiffeners to reduce their movements which is mostly caused by the vertical load. These repair actions are investigated more thoroughly in the following.

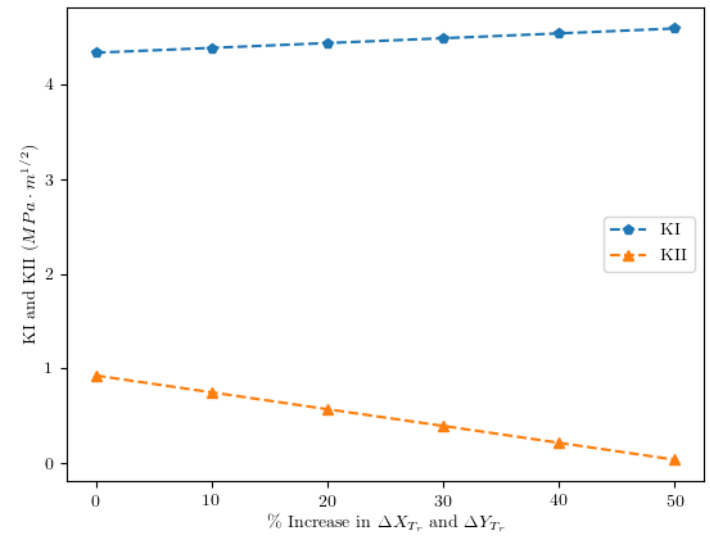

(a) Values of SIFs for condition 1

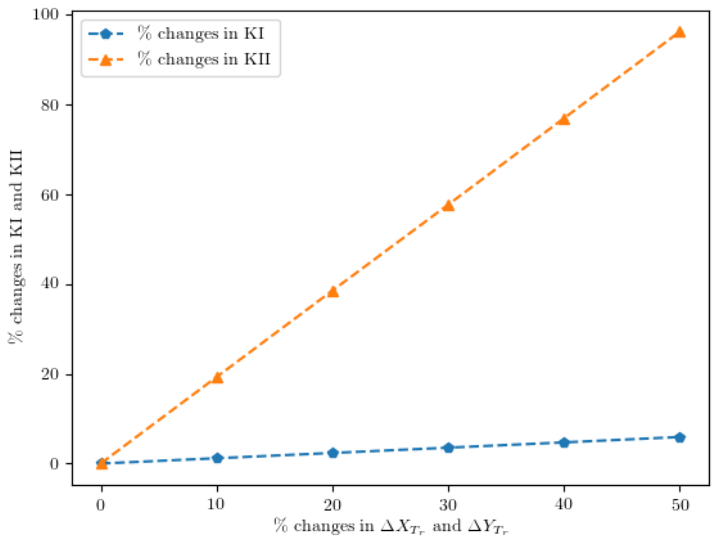

(b) Percentage changes of SIFs for condition 1

Figure 4.26: Changes in SIFs for condition 1 of sensitivity analysis

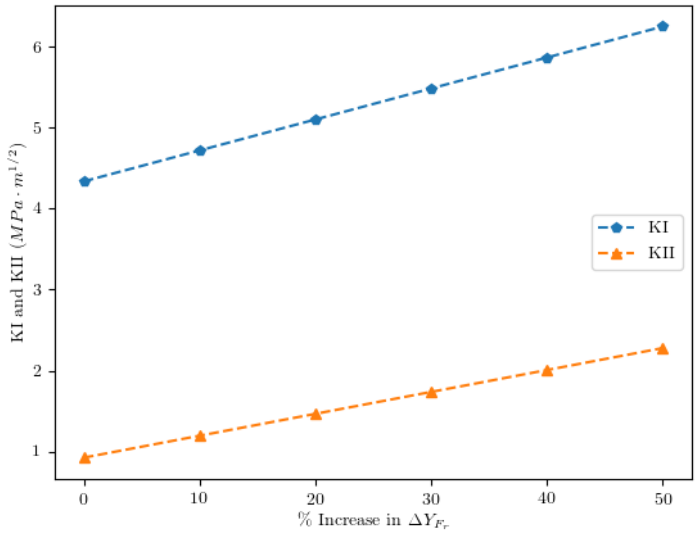

(a) Values of SIFs for condition 2

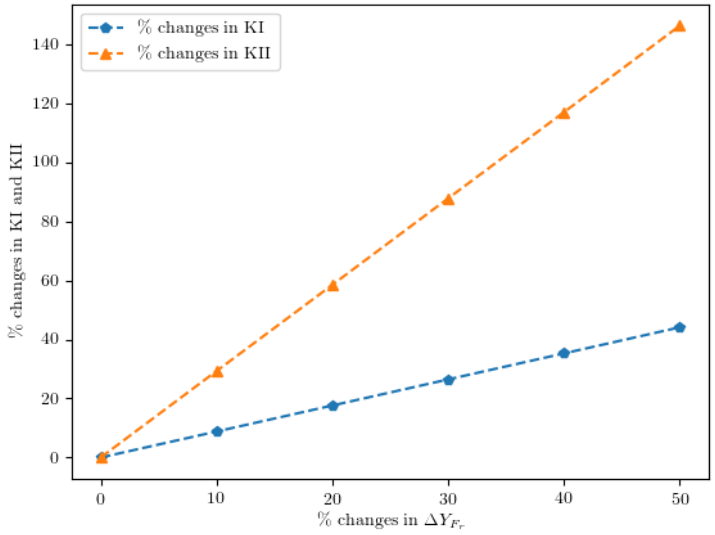

(b) Percentage changes of SIFs for condition 2

Figure 4.27: Changes in SIFs for condition 2 of sensitivity analysis

4.7.2 Repair I: applying a horizontal overlay on the deck plate

One common practice to tackle the fatigue problem in bridges with an OSD is to locally apply a cement or metal-based horizontal overlay on the deck plate, referred as repair I henceforward (Battista and Pfeil, 2000; Buitelaar, 2002; Buitelaar et al., 2003; Walter et al., 2007). Figure 4.28 provides an illustration of repair I. Such application helps to increase the transverse bending resistance by reducing the stress values in hot regions. Walter et al. (2007) have also studied the influence of increasing the thickness of the deck plate from 8 to 20 mm and they show a substantial reduction in von Mises stresses within the crack region.

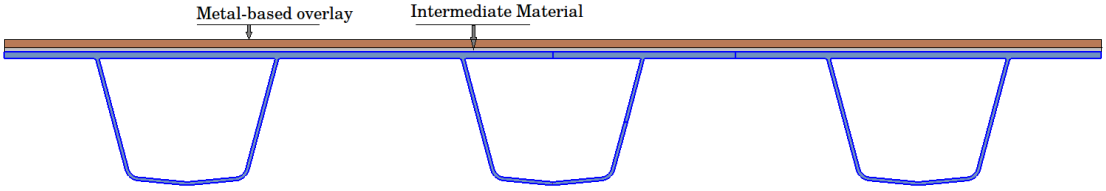

Figure 4.28: Applying a cement-based horizontal overlay

The problem with repair I can be related to the bonding between the horizontal plate and the deck plate. In case of applying a cement-based overlay, vibration of the overlay might cause water to separate from the mix, which might result in a weak interface. In case of the metal-based overlay, however, welding or bolting the overlay to the deck plate can create new hot zones for crack initiation. It should be noted that in both cases the added weight to the structure is significant (Walter et al., 2007). Moreover, the application of such action requires stopping the traffic flow which causes some economical loss for the owner and inconvenience for the road users.

4.7.3 Repair II: applying vertical plates between stiffeners

An alternative repair solution, noted repair II, is considered herein to increase the fatigue life of the given weld detail. This repair action is composed of placing some vertical plates (timber or metallic) between the stiffeners to control their movements, see Figure 4.29. According to the results of the sensitivity analysis in Section 4.7.1, it

can be realized that the vertical load has a significant influence on the SIF in the crack region. The movement of the stiffeners is mostly originated by the vertical loading which causes a bending moment in the crack region, see Figure 4.12. This bending can have a significant influence on propagation of the cracks initiated in the root of the fillet weld. Therefore, the proposed repair action tries to reduce the effects of the vertical load within the crack region by reducing the movements of the stiffener. In the same time, the new repair action is easy to apply and does not need to stop the traffic flow. The following section provides a comparison for the effectiveness of both repair solutions.

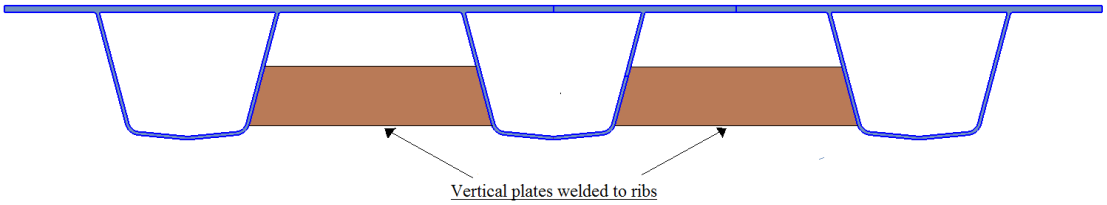

Figure 4.29: Placing vertical plates between stiffeners

4.7.4 Investigating the effectiveness of the repair solutions

The influence of repair solutions on the fatigue life of the welding detail is studied by performing separate 2D crack propagation analysis for each repair action. For this reason, the 2D finite element model used in Section 4.6 is employed. Identifying the loading and boundary conditions on the 2D model is done by performing the same strategy in Section 4.6. As mentioned before, two 3D finite element analyses are performed separately in order to identify the load effects caused by the vertical load and the transversal tension, see Figure 4.21. The difference here is that associated 3D finite element models are enhanced with repair actions. Similar to the crack propagation analysis in Section 4.6, the vertical load has a fixed value while different values are assigned to the transversal tension in order to study the influence of the transversal tension on the crack propagation after repair and also to be able to compare the results with the case without repair.

Repair I is modelled by increasing the thickness of the deck plate in order to

simplify the finite element model. Accordingly, two scenarios are considered for repair I by increasing the thickness of the deck plate from 12mm to 15mm and 18mm. These changes are applied on the 3D model presented in Section 4.5 and the local 3D model presented in Section 4.6. Accordingly, these finite element models are used to calculate relative displacements at the boundaries of the 2D finite element model due to the vertical load and different levels of transversal tension. It should be noted that rotations in different locations still remain very small, hence, they can be ignored. Table 4.4 summarizes the relative displacements due to the vertical load and Table 4.5 presents relative displacements in the right and bottom edges of the 2D model for different levels of transversal tension.

Table 4.4: Relative displacements and rotations on the boundaries of the 2D model due to the vertical loading after applying repair I

Thickness	R_r	ΔX_{F_r}(mm)	ΔY_{F_r}(mm)	R_b	ΔX_{F_b}(mm)	ΔY_{F_b}(mm)
t = 15mm	0.00	0.00	-0.611	0.00	-0.024	-0.257
t = 18mm	0.00	0.00	-0.473	0.00	-0.024	-0.226

Table 4.5: Relative displacements at the boundaries of the 2D model for given tension levels after applying repair I

Thickness	t = 15mm				t = 18mm			
Tension(MPa)	ΔX_{T_r}	ΔY_{T_r}	ΔX_{T_b}	ΔY_{T_b}	ΔX_{T_r}	ΔY_{T_r}	ΔX_{T_b}	ΔY_{T_b}
192.5	0.143	-0.111	0.011	-0.030	0.141	-0.083	0.0170	-0.020
227.5	0.169	-0.131	0.013	-0.035	0.166	-0.098	0.020	-0.023
262.5	0.195	-0.151	0.016	-0.041	0.192	-0.113	0.023	-0.027
297.5	0.221	-0.172	0.018	-0.046	0.218	-0.128	0.026	-0.030
332.5	0.247	-0.192	0.020	-0.052	0.243	-0.143	0.029	-0.034

For repair II, a 3D finite element model including the vertical plates is prepared in order to calculate the displacements caused by the vertical loading. The 3D finite element model is presented in Figure 4.30 in which the boundary conditions are similar to the one given in Section 4.5.2. Figure 4.31 illustrates the displacements in the

structure before and after applying the repair which shows a significant decrease of the displacement in different regions of the structure. Table 4.6 summarizes the relative displacements at the boundaries of the 2D model caused by the vertical load. Regarding transversal tension, it is assumed that the second repair action does not have a significant influence on the structural resistance against transversal tension since this tension is developed within the deck plate because of some local residual stresses and bending moments. Accordingly, it is expected that the load effects due to the transversal tension will not change significantly after applying this repair action. Therefore, the local 3D finite element model used in Section 4.6 is used to approximate the transversal tension effects at the boundaries of the 2D model which are provided in Table 4.7.

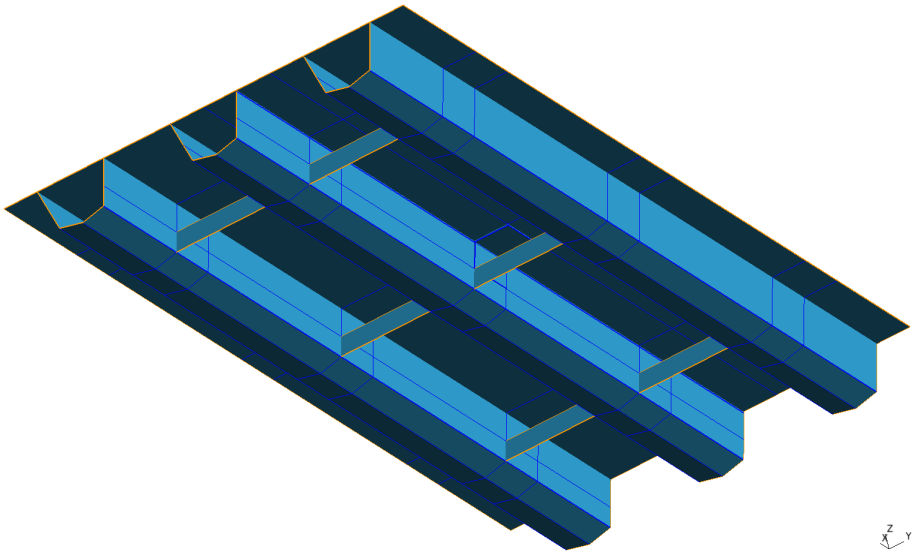

Figure 4.30: 3D finite element model for the proposed repair solution

After identifying the load effects at the boundaries of the 2D finite element model for the two given repair solutions, one can perform a crack propagation analysis to evaluate the effectiveness of each repair action. In all cases, the crack is propagated for 3mm for different levels of transversal tension. The initial crack length is 1mm, and the crack advances 0.03 mm at each step of propagation. On that account, Figure 4.32 presents the required load cycles to propagate the crack from 1mm to 4mm under

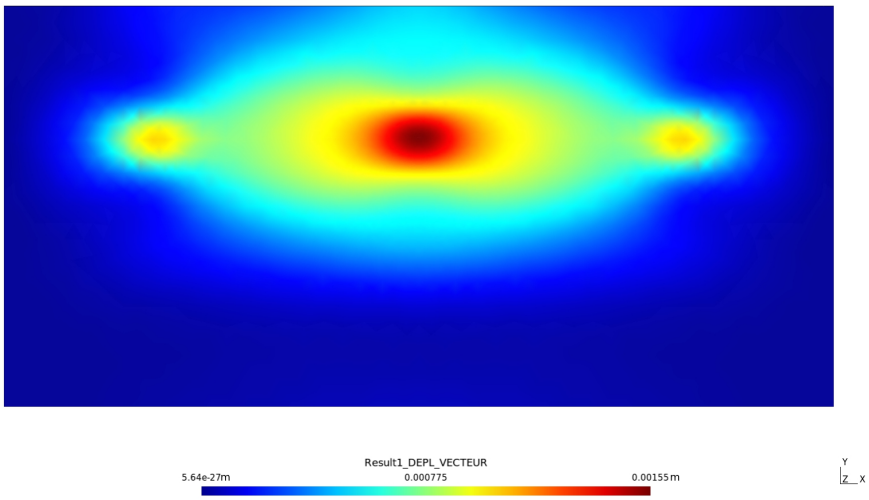

(a) Displacement field for initial structure

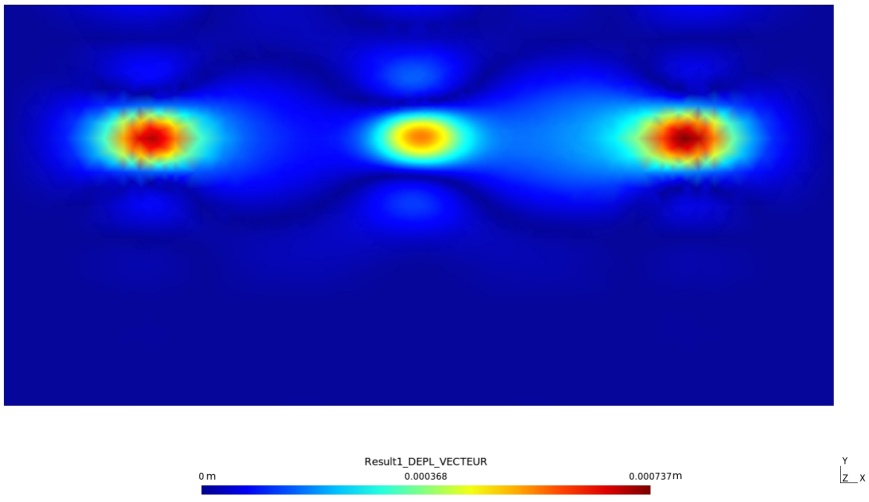

(b) Displacement field after repair

Figure 4.31: Displacement fields before and after applying the vertical plates (repair I)

Table 4.6: Relative displacements and rotations at the boundaries 2D model caused by the vertical load after applying repair II

Location	Rotation	Displacement	
Right edge	R_{F_r}	ΔX_{F_r}(mm)	ΔY_{F_r}(mm)
	0.00	0.00	-0.661
Bottom edge	R_{F_b}	ΔX_{F_b}(mm)	ΔY_{F_b}(mm)
	0.00	-0.050	-0.182

Table 4.7: Relative displacements at the boundaries of the 2D model for given tension levels for applying repair II

Tension(MPa)	ΔX_{T_r}(mm)	ΔY_{T_r}(mm)	ΔX_{T_b}(mm)	ΔY_{T_b}(mm)
192.5	0.148	-0.157	0.003	-0.046
227.5	0.175	-0.184	0.0035	-0.054
262.5	0.202	-0.213	0.004	-0.063
297.5	0.229	-0.242	0.0046	-0.071
332.5	0.256	-0.271	0.005	0.079

different levels of the transversal tension for the given repair actions. Regarding repair I, one shows that increasing the thickness of the deck plate improves the fatigue life of the welding detail. Repair II shows a significant improvement compared to the structure without repair and also compared to the case with repair I especially for lower levels of tension. It also can be seen that for high levels of transversal tension ($>$ 262.5 MPa), the fatigue life after applying repair II is almost two times higher than the fatigue life of structure supported by repair I.

In addition to adding extra fatigue life, repair II offers some other advantages. For instance, it can be easily realized that the added weight to the structure after repair II is much lower than repair I. Moreover, implementing the repair I requires some traffic interruptions over the bridge while repair II can be applied with minimum traffic disruption. Regarding to the crack propagation direction, it should be pointed out that for both repair actions the crack still clearly propagates towards the deck plates, see

Figure 4.33. This is one disadvantage of these two repair actions highlighted by the XFEM approach which needs to be balanced with the significant gain in number of cycles to failure.

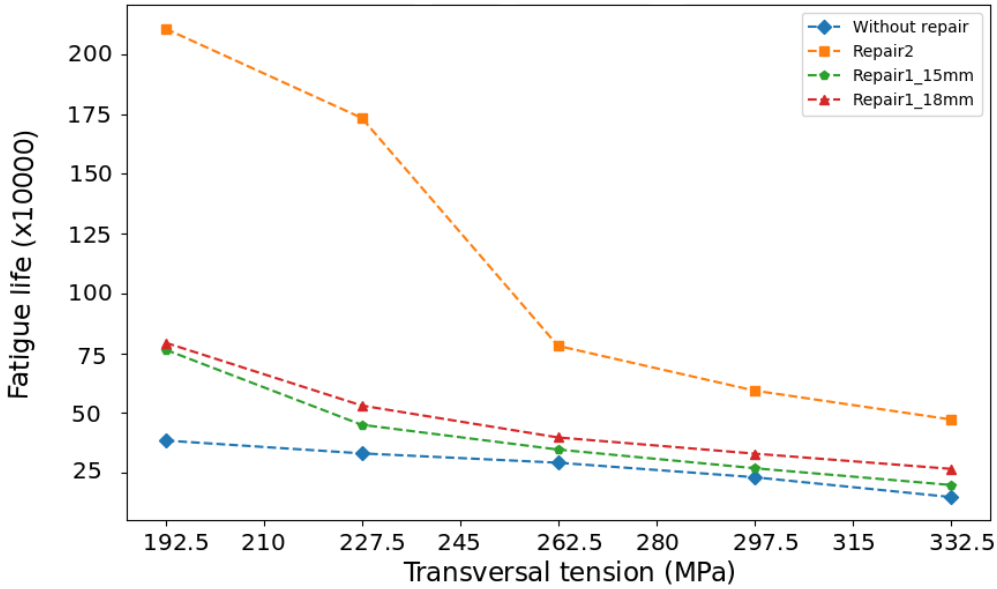

Figure 4.32: Required fatigue load cycles to reach a crack of length 3mm for different transversal stress levels for given repair solutions

In the end, it is necessary to highlight some important issues about repair II that need to be studied more carefully such as 1) the connection of vertical plates to ribs, 2) the materials, and 3) the configuration of vertical plates. Regarding to the first issue, it should be noted that connecting the plates to the ribs by welding may establish some new hot zones which may cause other crack initiations within the structure. Hence, some other strategies such as gluing or bolting might eliminate this issue. Blind bolts for instance can be used since they produce a strong connection without adding residual stresses (Liu et al., 2018; Hosseini et al., 2020). Figure 4.34 shows an illustration of how the vertical plates can be connected to the stiffeners using blind bolts. Concerning the second issue, it should be noted that alternative materials to steel can be used such as timber which is lighter and has high resistance under tension and compression. This is helpful to reduce the extra weight added to the structure after applying the repair action. The last issue is also important since lots of configurations can be considered

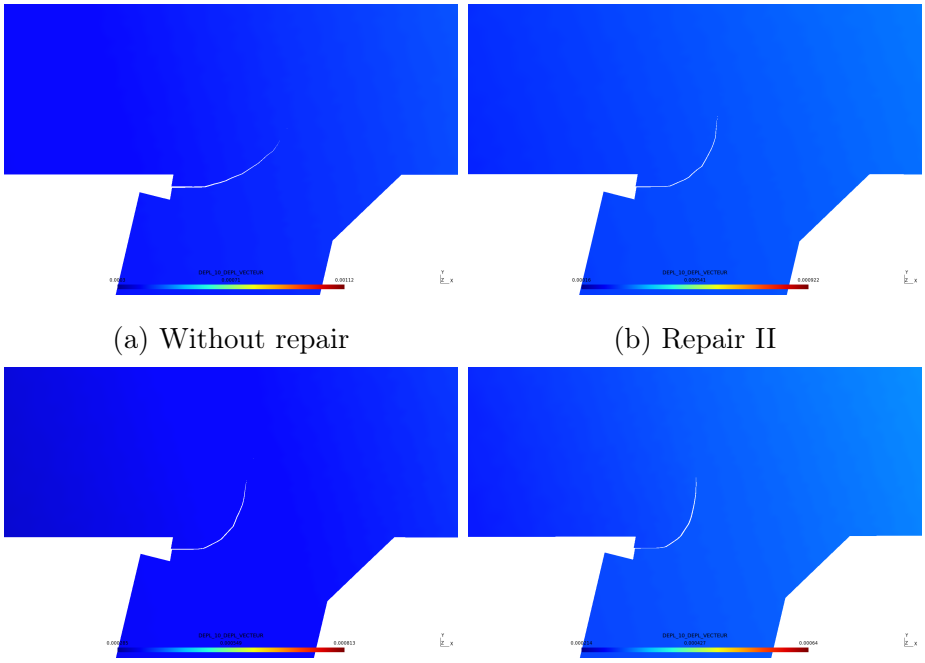

(a) Without repair (b) Repair II

(c) Repair I: thickness = 15 (d) Repair I: thickness = 18

Figure 4.33: Crack propagation direction before and after repair for $T = 297.5$ MPa

for this repair action. Therefore, it is important to find the best configuration related to the number and the location of applied plates.

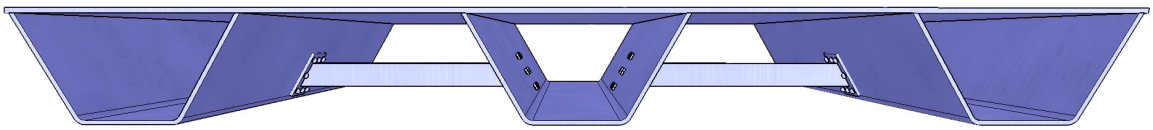

Figure 4.34: Connecting the vertical plates to the stiffeners with blind bolts

4.8 Conclusions

In this chapter, some analyses on fatigue cracking such as identification of the crack initiation location and crack propagation have been performed using some advanced methods, in particular XFEM. This investigation has been performed on a real bridge case study with an orthotropic deck system on which the inspections data already indicated fatigue issues on the structure.

Accordingly, a crack initiation analysis has been performed on the structure to identify the fatigue prone locations. This analysis has been done using a finite element analysis incorporating Miner's rule in order to calculate the cumulative fatigue damage for different locations of the structure. Crack initiation results show that the root of the fillet weld where longitudinal stiffeners are welded to the deck plate is a critical fatigue location.

The XFEM is then used to study the influence of the transversal tension on the crack propagation direction on the pre-identified critical fatigue location within a 2D finite element analysis framework. A strategy composed of two 3D FEA is proposed to translate the loading and boundary conditions from 3D to 2D model. The crack propagation analysis is then performed for different levels of the transversal tension and the results verify that with higher levels of transversal tension, cracks in this location tend to propagate upwards which can put the structure in a critical situation.

A sensitivity analysis has then been performed in order to identify which parameter has a greater effect on the crack propagation. This can be helpful for the decision making process in order to identify the appropriate repair solutions. The results of the sensitivity analysis show that both the vertical loading caused by vehicles and the transversal tension have a significant influence on the SIF within the crack region. Repair actions can be used to reduce the intensity of the load effects and to increase the fatigue life of the structure.

Two repair actions have been investigated next in order to reduce the severity of

the crack propagation problem. A comparison between the repair actions has been done by performing a crack propagation using XFEM for each case. It has been shown that placing some vertical plates between stiffeners is more effective for increasing the fatigue life of the structure even though both repair solutions may increase the risk of crack direction towards the deck plate. Such simulations illustrate how the use of advanced methods for crack initiation and propagation (XFEM herein) can be an effective decision making tool for practitioners when analyzing the effect of some repair actions.

In the end, it should be noted that the studies in this chapter have considered deterministic loading conditions. However, as mentioned in Chapter 2, fatigue phenomenon is associated with uncertainties. Hence, performing studies like fatigue crack propagation under a probabilistic framework which takes into account the associated uncertainties seems more realistic. This can be done through a fatigue reliability assessment that aims at finding the fatigue failure probability for a given period of time. This is a challenging task since, in one hand, it requires a cycle-by-cycle calculations of the SIF which is a computationally expensive process. In the other hand, the associated performance function in fatigue reliability analysis can be highly nonlinear which can cause trouble to achieve a reasonable level of accuracy using traditional reliability methods. That being the case, AK-SYS-t appears to be a promising time-dependent reliability method that can be employed to address such problems even though its application for fatigue reliability assessment can still be computationally expensive. Hence, some simplification steps would be required to make this application computationally affordable. One goal of the following chapter is therefore to identify such steps through two applicational case studies.

Chapter 5 : Time-dependent reliability approach for crack propagation models

5.1 Introduction

As mentioned in Chapter 2 fatigue crack propagation models are suitable tools to evaluate the fatigue life of existing structures. However, performing reliability analysis on crack growth models can be challenging. One reason is that it requires a cycle-by-cycle evaluation of SIFs which is a computationally demanding process. It can be even more computationally expensive for cases in which SIFs must be calculated by a FEA. Moreover, underlying performance functions can be highly irregular which may cause troubles for fatigue reliability assessment.

This chapter, therefore, aims at resorting to the proposed time-dependent reliability method in Chapter 3 for fatigue crack growth based reliability problem. The objective is to highlight how AK-SYS-t can be applied for such problems and how it can be a useful practice in the field of structural maintenance planning. For this reason, a short discussion is provided in Section 5.2 to review the common approaches used for fatigue time-dependent reliability assessment. Implementing AK-SYS-t is then illustrated on two applications. This, however, requires some simplification steps in order to keep a reasonable computational cost which are described herein.

The first applicational example in this chapter is taken from the literature and it considers a mode I crack growth problem in an aluminum alloy subjected to a stochastic loading. The SIF in this example is estimated using an analytical formula-

tion and the failure happens when the SIF becomes greater than the fracture toughness which leads to an unstable crack propagation. The aim of this example is to emphasize the challenges related to dealing with a cycle-by-cycle calculation of the SIF and appropriately introducing the performance function. A strategy is defined to provide the instantaneous performance functions for the corresponding time nodes. This example is presented in Section 5.3 more extensively and the results are compared with MCS, for validation purpose.

The second applicational case considers a mixed-mode fatigue crack propagation concerning the fatigue detail of interest introduced in Chapter 4. This fatigue detail is supposed to be subjected to random loading and the goal here is also to calculate the cumulative probability of failure using AK-SYS-t. The challenge in this case can be related to the calculation of SIFs and implementing them into the time-dependent reliability analysis. On that account, Code_Aster associated with XFEM method is used to calculate the SIFs for a set of input samples. In order to reduce the computational cost, Kriging meta-modelling is used to provide meta-models for SIFs in order to incorporate them into AK-SYS-t algorithm. This example is presented in Section 5.4.

5.2 Common approaches for fatigue crack growth reliability problems

Methods and approaches for fatigue assessment of steel structures have been shortly introduced in Chapter 2 Section 2.6. It has been noted that a probabilistic fracture mechanism based approach for fatigue analysis can be used in order to assess the degradation of fatigue reliability of existing structures which is of a great importance for structural inspection and maintenance planning. Depending on the objectives of the problem, various types of performance functions can be formulated for a fracture based fatigue reliability problem. In many studies, the performance function of a fatigue crack growth problem is formulated according to the required time of reaching a critical crack length a_{cr} (Hashemi et al., 2017; He et al., 2015; Huang et al., 2013; Riahi et al., 2011;

Feng et al., 2012). This performance function is recalled in the following equation:

$$G(\mathbf{X}, t) = a_{cr} - a(\mathbf{X}, t) \tag{2.21}$$

This formulation is valid under LEFM assumptions and until the crack propagation occurs within the Paris' law region, see Figure 2.7. Addressing such a problem does not necessarily require the application of time-dependent reliability methods since this performance functions is monotonically decreasing by time. Hence, time-independent reliability methods like FORM, IS, MCS (Melchers, 1999), AK-MCS (Echard et al., 2011), etc. can be used for the final time instant of the desired time interval in order to evaluate the cumulative failure probability. This performance function can sometimes be reformulated according to the number of cycles instead of time (He et al., 2015).

The crack propagation does not always remain within the Paris' law region and the LEFM assumptions are not always valid. Therefore, some other criteria can be used to formulate the failure for a crack growth problem. Accordingly, Equations 2.18, 2.19, and 2.20 can be used to formulate the performance function for a fatigue crack growth reliability problem. Time-dependent reliability approaches should be used to address such performance functions since they are not monotonically increasing or decreasing with time anymore. Most of the studies in this domain use out-crossing based approaches to address fatigue time-dependent reliability (Engelund et al., 1995; Zayed et al., 2013). With this respect, Dong et al. (2020) have employed the PHI2 method to perform a time-dependent reliability analysis on a T-plate welded joint which is subjected to a stochastic loading. In order to reduce the computational cost, polynomial regression and Kriging interpolation are used to measure the crack size at any time instant instead of a cycle-by-cycle calculation. PHI2 method has been also used in another study by Dong et al. (2018) to evaluate the fatigue time-dependent reliability where response surface models are used to measure the crack size under a stochastic loading. Marley and Moan (1992) have proposed an out-crossing formulation for fatigue degradation based on fracture mechanism. They have proposed a conservative approximation based on time-independent methods to avoid the numerical instability and intensive computation for the time-dependent model. Guedes Soares and Garbatov (1996) have presented a model to evaluate the time-dependent fatigue reliability of a

hull girder through an up-crossing analysis by considering a random number of cracks with different crack sizes. Afterwards, Wang et al. (2007) have improved the work of Guedes Soares and Garbatov (1996) by employing the PHI2 method to calculate the time-variant reliability of ship structure subjected to fatigue and corrosion.

It can be realized form this review that meta-model based approaches like AERS, t-PCE, mixed-EGO, etc. in the context of time-dependent reliability analysis have not received enough attention in the field of fracture based fatigue time-dependent reliability analysis. This can be related to the difficulty of dealing with such performance functions in which a cycle-by-cycle calculation of the SIF is required that leads to a huge computational cost. Hence, a strategy is proposed in this chapter to reformulate the associated performance function in order to be able to adopt AK-SYS-t for fatigue time-dependent reliability analysis within the limited computational resources.

5.3 Time-dependent reliability assessment of a tensile opening crack model

5.3.1 Fatigue detail and input parameters

The first example focuses on the crack growth of a Center Crack Tension (CCT) specimen made of a Al 2024-T3 aluminum alloy with a width of $W = 152.4$mm and a thickness of $t = 2$mm. Figure 5.1 provides an illustration for the test specimen in this case where an initial crack of length $2a_0$ is introduced in the center of the fatigue detail. The SIF is estimated using an analytical solution formulated in Equation 5.1 in which a is the semi-crack length and σ is the applied remote tensile stress.

$$K(\sigma, a) = \frac{1 - 0.025(\frac{a}{W})^2 + 0.06(\frac{a}{W})^4}{\sqrt{\cos(\pi \frac{a}{W})}} \sigma \sqrt{\pi a} \tag{5.1}$$

The crack opening mode for this example is assumed to be the tensile opening or mode I. Given the initial crack size a_0, the Paris' law, introduced in Chapter 2 Equation

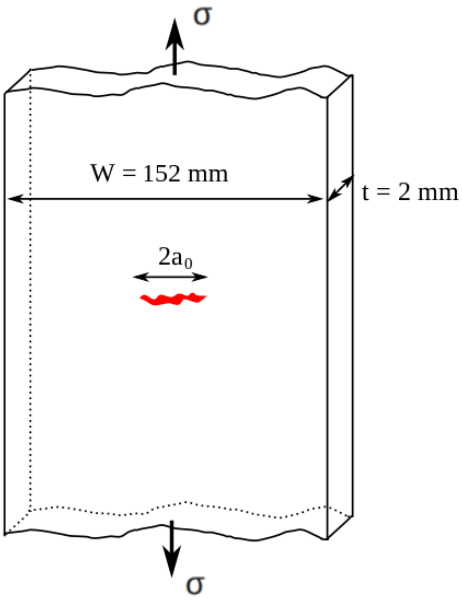

Figure 5.1: An illustration of the test specimen for the tensile opening crack model (Mattrand, 2011)

2.11, is chosen to propagate the crack. The crack propagation become unstable when the SIF exceeds the fracture toughness. Therefore, it is reasonable to employ this condition as the failure criterion which is expressed by the Equation 5.2 where K_c is the fracture toughness and σ_{max} is the highest load value for a given fatigue load cycle.

$$K(\sigma_{max}, a) \geq K_c \tag{5.2}$$

The initial crack length a_0 and material parameters C and m in Paris' law are assumed to be random here. For the sake of illustration, it is arbitrarily assumed that the initial crack length follows a lognormal distribution with mean of 9 mm and coefficient of variation of 20%. Randomness in the crack growth properties for Al 2024-T3 aluminum alloy are characterized according to the Virkler data (Virkler et al., 1979) in which from 68 individual crack growth curves, one may find that lnC and m are normally distributed such as: $lnC \sim N(-26.056, 0.972)$, $m \sim N(2.855, 0.166)$ and highly correlated: $\rho_{lnC,m} = -0.99795$, see (Bourinet and Lemaire, 2008). According to Ditlevsen and Olesen (1986), the linear regression of lnC on m here allows one to

express lnC as:

$$lnC = \varepsilon_{lnC} - 5.847m - 9.362 \tag{5.3}$$

where ε_{lnC} follows a Gaussian distribution with mean of -5.479×10^6 and standard deviation of 0.062 and it is uncorrelated with m. This representation facilitates generating random samples of C and m. Table 5.1 summarizes the first set of random variables involved in this problem and their associated parameters.

Table 5.1: Input random variables for the first applicational case

Parameter	Mean	Standard deviation	Distribution
$a_0(mm)$	9	0.18	Lognormal
m	2.855	0.166	Normal
ε_{lnC}	-5.479×10^{-6}	0.062	Normal

In this example, the structure is also assumed to be subjected to a random fatigue load $\sigma(t)$ which is here modelled by a stationary Gaussian process. A spectral representation is used to define this process (Li and Kiureghian, 1993). For this reason, one needs to know the mean function and the power spectral density function of the process. Hereafter, it is arbitrarily assumed that the process has a constant mean value of $m_{\sigma(t)} = 100$ MPa where its power spectral density function is defined by the following equation:

$$S_\sigma(\lambda) = 500e^{\frac{1}{2}(\frac{\lambda - 0.5\pi}{0.5})^2} \tag{5.4}$$

where λ is the natural frequency. Figure 5.2 illustrates a realization of this stochastic load on the test specimen. It can be seen from this figure that the applied load is very noisy due to the weakly correlated stochastic process which would lead to a highly nonlinear performance function according to Equation 5.2.

5.3.2 Fatigue crack growth performance function

It is worthy to recall that the objective of a time-dependent reliability assessment is to evaluate the cumulative probability of failure for a given time interval $[t_0, t_l]$. For a fatigue crack growth problem this time interval may involve a huge number of load

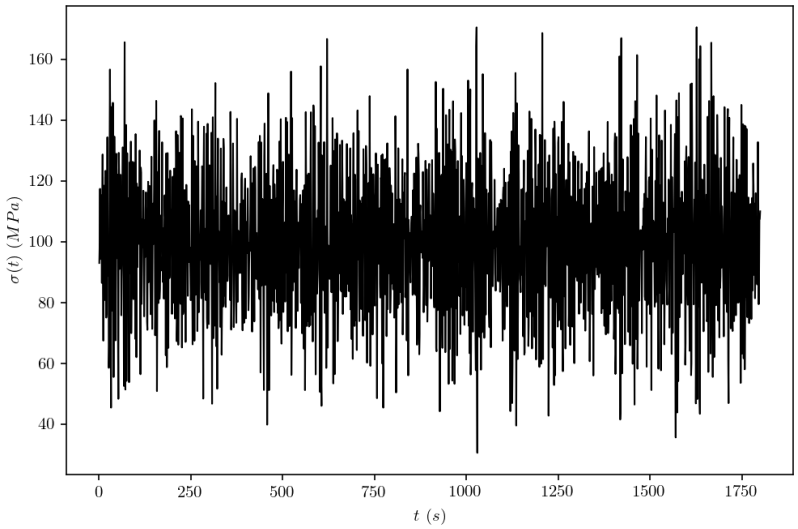

Figure 5.2: A realization of the stochastic loading applied on the test specimen

cycles N_{cycles} and the SIF evaluated at each load cycle can possibly lead to a failure, see Equation 5.2. This makes it difficult to simply discretize the desired time interval into N_t time nodes as required for most of time-dependent reliability methods. On that account, some simplifications are required first to resort to time-dependent reliability methods like AK-SYS-t.

Before that, let us remark that after time discretization the crack length at the end of each given time sub interval obviously reaches its maximum value since the crack length increases monotonically with the number of load cycles within each time sub interval. However, this is not the case for the maximum value of load cycles associated with those time intervals for a variable amplitude loading. Theoretically, Equation 5.2 should therefore be evaluated at each cycle of any given time sub interval for an exact reliability assessment but, as said before, this is intractable in practice and simplifying assumptions should be considered. Hence, to overcome the issue of cycle-by-cycle evaluation of Equation 5.2 in a reliability approach the following procedure is proposed and can be followed to define the instantaneous performance functions for each time node before applying AK-SYS-T:

1. Discretize the desired time interval $[t_0, t_l]$ into N_t equidistant time intervals
2. Propagate the crack from t_0 to t_l using Paris' law and measure the corresponding crack lengths for each time node as: $a_j,\ j = 1, ..., N_t$
3. Identify the maximum load value within each sub interval and denote them as: $S_j,\ j = 1, ..., N_t$
4. Evaluate the $K_j = K(a_j, S_j),\ j = 1, ..., N_t$ using Equation 5.1
5. Prepare the instantaneous performance function for each time node as: $G(\mathbf{X}, t_j) = K_c - K_j$ and $j = 1, ..., N_t$

This approach leads to a certain degree of conservatism but is still better than considering a unique maximum stress over the load sequence to assess $G(\mathbf{X}, t)$

5.3.3 AK-SYS-t to approximate the cumulative probability of failure

Before applying AK-SYS-t to estimate the cumulative probability of failure, the previously introduced procedure is applied on this example. Time-series of 30 minutes are sampled at 1 Hz from the spectral representation which leads us to about 500 load cycles on average per sequence. Time is then scaled by 250 and 40 time-series are generated in order to simulate final load sequences for 5,000 hours. 20,000 load cycles are in mean obtained after post-processing final time-series into sequences of turning-points.

The desired time interval here is discretized into $N_t = 40$ equidistant time nodes where each time interval is a sequence of turning points of 125 hours. Crack lengths $a_j,\ j = 1, ..., 40$, are computed on each time node from a cycle-by-cycle calculation procedure using the Paris' law. The maximum load stress within each time interval S_j, $j = 1, ..., 40$ and the crack lengths $a_j,\ j = 1, ..., 40$ are used to evaluate the associated SIF as $K(a_j, S_j),\ j =, ..., 40$ and the performance function for each time node therefore

can be expressed by the following equation:

$$G(\mathbf{X}, t_j) = K_c - K_j \; and \; j = 1, ..., 40 \tag{5.5}$$

where K_c is arbitrarily fixed to $K_c = 1284 \; MPa\sqrt{mm}$ which leads to a failure probability p_f of 10^{-2}. This enables us to validate the results obtained by AK-SYS-t with those obtained by MCS. It should be noted that the calculated cumulative probability of failure using the aforementioned performance function provides an upper bound for the cumulative probability of failure of the original problem since the associated SIF for a given time interval is overestimated.

Figure 5.3 illustrates two realizations of the time-dependent performance function. As we can see, the behavior of this performance function is very complex. According to our point of view, evaluating the time-dependent reliability for this performance function using competing methods such as t-PCE and SILK might be challenging even though not tried in this study. The problem in t-PCE can be related to the computational cost. This method uses a PCA to reduce the computational cost by reducing the required number of meta-models to calibrate. This, however, can not be very helpful when the performance function is highly irregular since reducing the number of required meta-models would seriously jeopardise the accuracy of the methodology. On the contrary, calibrating a high number of meta-models would also drastically reduce the efficiency of the t-PCE algorithm. Estimating such time-dependent performance function that is highly nonlinear by a single Kriging meta-model would not lead to a very accurate approximation of cumulative probability of failure. Therefore, SILK method which pursues such procedure might face serious challenges to accurately estimate the cumulative failure probability for this kind of problems.

Accordingly, the goal here is to employ AK-SYS-t to estimate the failure probability for this problem. A Monte Carlo population of size $N_{MCS} = 10^4$ is generated for all time nodes $j = 1, ..., 40$. The parameters a_0, m, C as well as load sequences are used to calculate the crack length a_j for each given time node $j = 1, ..., 40$. For this reason, the Paris' law is used to calculate the crack length a_i cycle-by-cycle using Equation

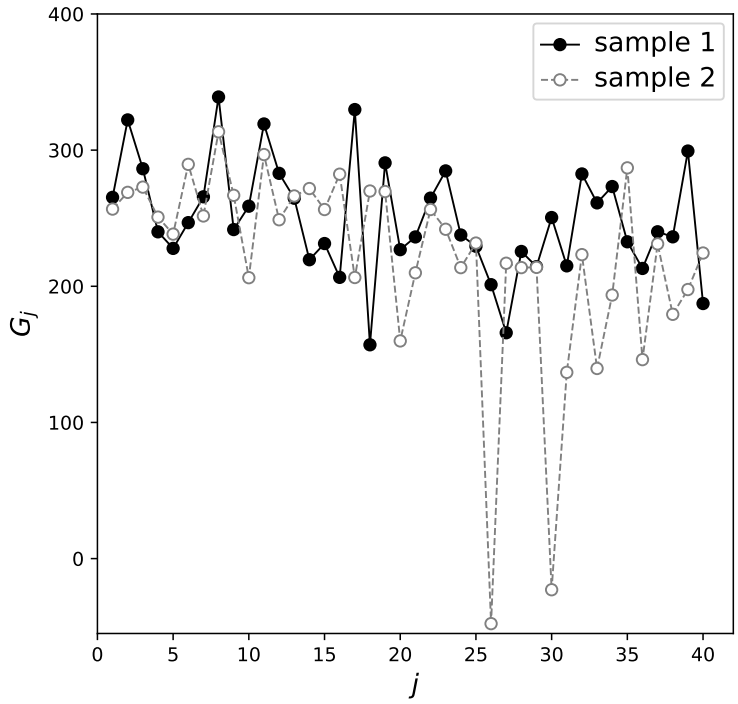

Figure 5.3: Two realizations of the performance function for the tensile opening crack model

5.6. Equation 5.7 can then be used to calculate a_j at each time node.

$$a_i = C(\Delta K_i)^m + a_{i-1},\ i = 1, ..., N_{cycles} \tag{5.6}$$

$$a_j = a_i\ for\ i = j * \frac{N_{cycles}}{N_t},\ and\ j = 1, ..., 40 \tag{5.7}$$

where $N_{cycles} = 20000$, and $\Delta K_i = \sigma_{max,i} - \sigma_{min,i}$ for each i^{th} cycle.

AK-SYS-t starts with calibrating $N_t = 40$ initial meta-models, one per each time node. For this reason, $N_t = 40$ DoEs of size $N_{DoE} = 50$ are considered first as:

$$DoE_j : \{(\mathbf{x}^{(i)}, S_{j,i}); K_{j,i}\}, \quad j = 1, ..., N_t\ and\ i = 1, ..., N_{DoE} \tag{5.8}$$

Due to the cycle-by-cycle calculation procedure of a_j, the enrichment process for this case is slightly different compared to the numerical examples proposed in Chapter 2. The enrichment process for this case study relies on recalibrating all performance functions before the weakest component identified by the algorithm $\hat{G}_s$, see Chapter

3 Section 3.5.3. In order to obtain a_s, $a_i, i = 1, ..., s$ should be computed first and therefore $G_i, i = 1, ..., s$ can also be assessed. The number of calls to the original performance function can finally be computed using the following equation.

$$N_{calls} = N_t \times N_{DoE} + \sum_{i=1}^{N_e} N_{s_i} \tag{5.9}$$

where N_e is the number of iterations until the algorithm reaches the stopping criterion and N_{s_i} is the number of meta-models that are enriched at each i^{th} iteration. Similarly to examples in Chapter 3, two indicators are used to compare the obtained results with the MCS: the relative percentage error $\epsilon(\%)$ (see Equation 3.56) and the number of miss-classified realizations $N_{misclass}$ (see Equation 3.57).

Considering the relative percentage error criterion, results in Table 5.2 indicate that AK-SYS-t here exactly predicts the cumulative probability of failure. However, it should be pointed out that even if the relative percentage error for this example is equal to zero, AK-SYS-t fails to properly classify 2 realizations of the performance function. This can be due to a false identification of a failed realization as a safe one and a false identification of a safe realization as a failed one. However, assuming that both realizations are classified properly the percentage error will be equal to $\epsilon = 0.02\%$.

Table 5.2: Results for the tensile remote crack problem

Method	N_t	P_f	N_{calls}	N_e	ϵ (%)	$N_{misclass}$
AK-SYS-t	40	0.0101	4726	90	0	2
MCS	40	0.0101	40×10^4	-	-	-

Performing the MCS requires evaluations of the original performance functions for the whole Monte Carlo population. Hence, for this example with $N_t = 40$ instantaneous performance functions it requires a huge number of calls to the original performance functions, $N_{calls} = 40 \times 10^4$. AK-SYS-t, on the contrary, calculates the same failure probability with only 4,726 calls to the original performance function. This highlights the efficiency of AK-SYS-t to drastically reduce the computational burden for crack propagation problems compared to MCS.

Figures 5.4 and 5.5 illustrate the convergence of the cumulative failure probability and min$U$ respectively. One can realize from these figures that in the beginning of the algorithm when the value of min$U$ is very small, the approximation of the cumulative failure probability is not accurate. However, in the end of the algorithm and by training the meta-models the value of min$U$ reaches the stopping criterion and the cumulative probability of failure converges to the final approximation which is the same as the MCS approximation. Figure 5.6 shows how many times a time node is identified as the weak node before AK-SYS-t converges. It can be seen from this figure that time nodes in the tail of the time interval have been counted as weak nodes more than others. This seems reasonable since by increasing the crack length, the SIF for such nodes tends to be higher, even though it is not systematic, hence they contribute more to the system's failure.

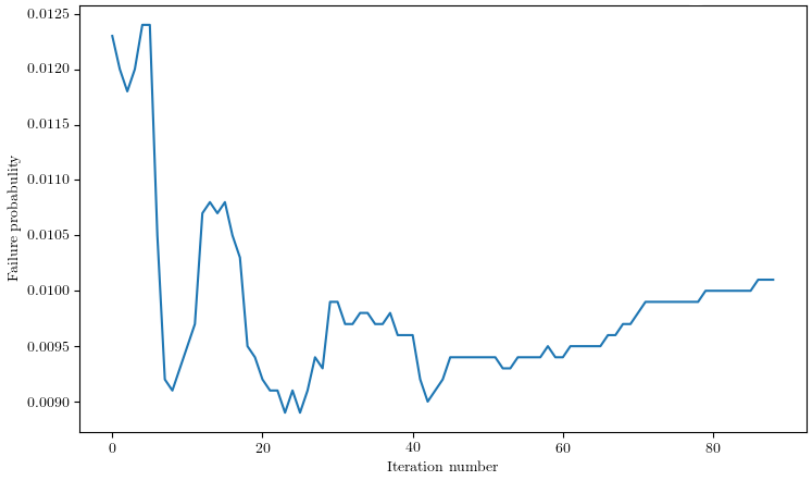

Figure 5.4: Evolution of the cumulative failure probability estimation for the tensile remote crack problem during the learning process

This example shows the importance of developing methods like AK-SYS-t to evaluate the cumulative probability of failure for fatigue crack growth reliability problems. The performance functions for such problems can be highly irregular due to weakly correlated random loads which can make most of time-dependent reliability methods inaccurate. However, dealing with crack growth based performance functions in time-dependent reliability approaches that require to discretize the time, such as AK-SYS-t,

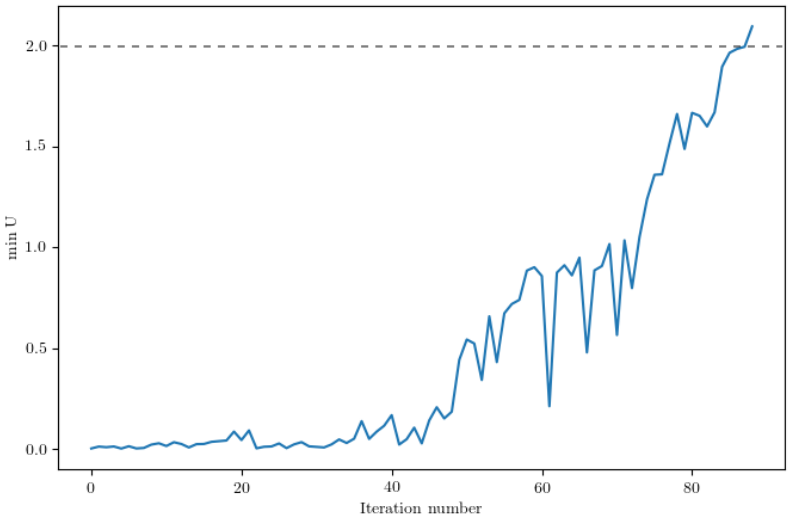

Figure 5.5: Evolution of min$U$ for the tensile remote crack problem during the learning process

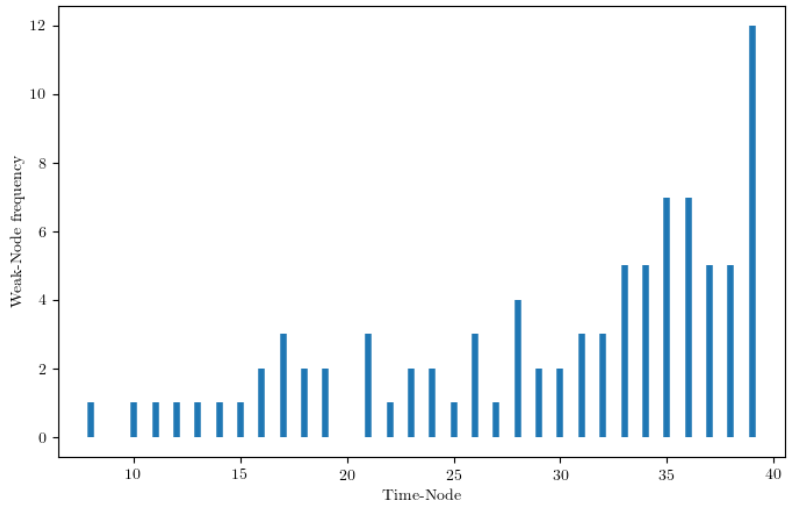

Figure 5.6: Frequency of the weak nodes for the tensile remote crack problem

still remains challenging. An exact evaluation of the failure probability becomes too computationally expensive due to the cycle-by-cycle calculation of the SIF, and thus of the performance function. Hence, some simplifications have been done on the frequency of performance function evaluation in order to be able to implement methods like AK-SYS-t.

The SIF calculation in this example, based on an analytical formulation, does not add any computational time. In most of the cases in real world, however, the SIF is calculated through a FEA which can lead to a non-negligible additional computational cost. Accordingly, a Kriging-based approach is proposed in the next section to deal with this issue for a mixed-mode crack growth problem.

5.4 Time-dependent reliability assessment of a mixed mode (I/II) crack propagation problem

The previous applicational case considers a one dimensional crack propagation in which the SIF is calculated analytically. However, crack propagation problems in most of the real world cases are mixed-mode and multi-dimensional in which calculating the SIFs is a challenging task. Hence, a more complex crack propagation problem is considered in this section.

For such purpose, the second applicational case here aims at assessing the time-dependent reliability for the fatigue detail of interest in Chapter 4 which involves a mixed-mode (I/II) two-dimensional crack growth problem. Performing such reliability assessment is quite challenging and computationally demanding since calculation of SIFs requires performing FEA. On that account, a proper approach is needed in order to reduce the computational cost to be able to deal with low failure probabilities in reliability analysis.

Providing an affordable model to calculate the SIFs is one of the main goals here. For this reason, FEA associated with the XFEM method is used to evaluate the SIFs for a reduced set of input variables. This enables one to employ Kriging meta-modelling in order to approximate the SIFs. Employing Kriging meta-model instead of performing the FEA for calculating the SIFs is expected to considerably reduce the computational cost. This is on prime importance since a structure generally experiences a huge number of load cycles during its service life and fatigue crack propagation analysis requires a cycle-by-cycle calculation of SIFs.

Applying the proposed approach makes it possible to employ AK-SYS-t to evaluate fatigue reliability in a crack propagation context in the same fashion as the previous applicational case. Since the accuracy and efficiency of AK-SYS-t has been approved in previous examples, results from this example are not going to be compared with other methods like MCS due to the huge required computational time. This allows us to calculate failure probabilities lower than 10^{-2} using AK-SYS-t for crack propagation problems. Accordingly, the following steps are going to be followed in this section.

1. Introducing the mixed-mode fatigue crack growth phenomenon, Section 5.4.1
2. Introducing the fatigue detail, loading conditions, and input variables, Section 5.4.2.
3. Introducing the proposed approach for approximating the SIFs, Section 5.4.3.
4. Implementing AK-SYS-t to evaluate the cumulative failure probability, Section 5.4.4.

5.4.1 Mixed-mode fatigue crack propagation

Fatigue crack propagation analysis for many of engineering problems have been focused on mode I or tensile opening mechanism during past decades. However, in most of real world fatigue problems, fatigue crack propagation occurs in a mixed-mode behaviour rather than just a tensile opening mechanism in which the direction of the loads is normal to the crack plane. Mixed-mode fatigue crack growth can be caused due to several reasons such as multi-axial loading conditions, different combinations of boundary conditions, and non-perpendicular orientations of crack surfaces regarding a global uni-axial loading (Demir et al., 2018). In such a mechanism, the crack propagation direction can be defined according to the mode mixity.

Equation 5.10 represents a modification of the Paris' law proposed by Tanaka (1974) that is widely used to model mixed-mode fatigue crack propagation. In a mixed-mode (I/II) fatigue crack growth problem, this law correlates the crack growth rate

with the equivalent stress intensity factor ΔK_{eq} which is a function of ΔK_I in mode I and ΔK_{II} in mode II.

$$\frac{da}{dN} = C(\Delta K_{eq})^m \tag{5.10}$$

Several formulations have been proposed in the literature to calculate the equivalent stress intensity factor ΔK_{eq}. For instance, Tanaka (Tanaka, 1974) has proposed two following formulations to approximate ΔK_{eq} which are widely used to perform numerical fatigue propagation analyses.

$$\Delta K_{eq} = (\Delta K_I^2 + 2\Delta K_{II}^2)^{1/2} \tag{5.11}$$

$$\Delta K_{eq} = (\Delta K_I^4 + 8\Delta K_{II}^4)^{1/4} \tag{5.12}$$

Another way to estimate the equivalent SIF is the Irwin's model expressed by Equation 5.13. (Irwin, 1957)

$$\Delta K_{eq} = (\Delta K_I^2 + \Delta K_{II}^2)^{1/2} \tag{5.13}$$

One can also refer to the Yan's model (Xiangqiao et al., 1992) and the Hussain's (Hussain et al., 1974) model among others to calculate the equivalent SIF in a mixed mode crack propagation.

Accurately predicting the crack propagation direction has a very crucial impact on the accuracy of the fatigue life estimation. Erdogan and Sih (1963) have proposed the the Maximum Tangential Stress (MTS) criterion which is widely used for mixed-mode (I/II) crack propagation. This criterion expresses that the crack propagation direction is the radial direction from the crack tip for which the tangential stress is maximum. On that account, Equation 5.14 can be used to approximate the crack propagation direction θ_c measured in the anticlockwise direction regarding the initial crack orientation direction (Alegre et al., 2007; Chen et al., 2019).

$$\begin{cases} \theta_c = 2\tan^{-1}\left[\frac{1}{4}\frac{K_I}{K_{II}} - \frac{1}{4}\sqrt{(\frac{K_I}{K_{II}})^2 + 8}\right] & for\ K_{II} > 0 \\ \theta_c = 2\tan^{-1}\left[\frac{1}{4}\frac{K_I}{K_{II}} + \frac{1}{4}\sqrt{(\frac{K_I}{K_{II}})^2 + 8}\right] & for\ K_{II} < 0 \end{cases} \tag{5.14}$$

In a mixed-mode fatigue crack growth process, crack propagation becomes unstable if $\Delta K_{eq_{max}}$ is greater than the fracture toughness (Sajith et al., 2020; Demir et al., 2018).

Therefore, a failure criterion can be formulated for the mixed mode crack propagation as Equation 5.15. This criterion will be further used to define the performance function for the reliability evaluation of the mixed-mode fatigue crack growth problem.

$$\Delta K_{eq_{max}} \geq K_c \tag{5.15}$$

5.4.2 Fatigue detail, loading conditions, and input parameters

The fatigue reliability analysis is performed on the fatigue detail introduced in Section 4.6. The geometry of this 2D fatigue detail and its loading and boundary conditions are recalled in Figure 5.7 in which crack propagation takes place in the root of the fillet weld. As explained previously in Chapter 4 Section 4.6.2, instead of applying the transversal tension T and the vertical load F, their corresponding load effects are super-positioned and applied in the right edge and the bottom edge of the 2D model as $(\Delta X_r, \Delta Y_r, R_r)$ and $(\Delta X_b, \Delta Y_b, R_b)$ respectively using Equations 4.7 and 4.9. Accordingly, knowing the values of ΔY_{F_r} (vertical displacement caused by the vertical load at the right edge of the model) and ΔX_{T_r} (transversal displacement caused by the transversal tension at the right edge of the model) is sufficient to identify the loading conditions on the structure. It should be noted that by resorting to the calculations in Chapter 4 Section 4.6.2, it is assumed that the amount of rotations in the right edge and the bottom edge is negligible.

It is assumed that the fatigue detail is subjected to random loading. For this reason, the load effects ΔY_{F_r} and ΔX_{T_r} are imposed as lognormal random white noises. ΔY_{F_r} follows a lognormal distribution with mean of 0.7 mm and standard deviation of 0.25 mm, and ΔX_{T_r} follows a lognormal distribution with mean of 0.58 mm and standard deviation of 0.15 mm.

The fatigue detail is made of steel with Young modulus of 210 GPa and the crack propagation occurs at the root of the fillet weld. The initial crack length a_0, initial crack angle θ_0, and material properties m and C are assumed to be random here. The initial crack length follows an arbitrary lognormal distribution with mean 1 mm and standard

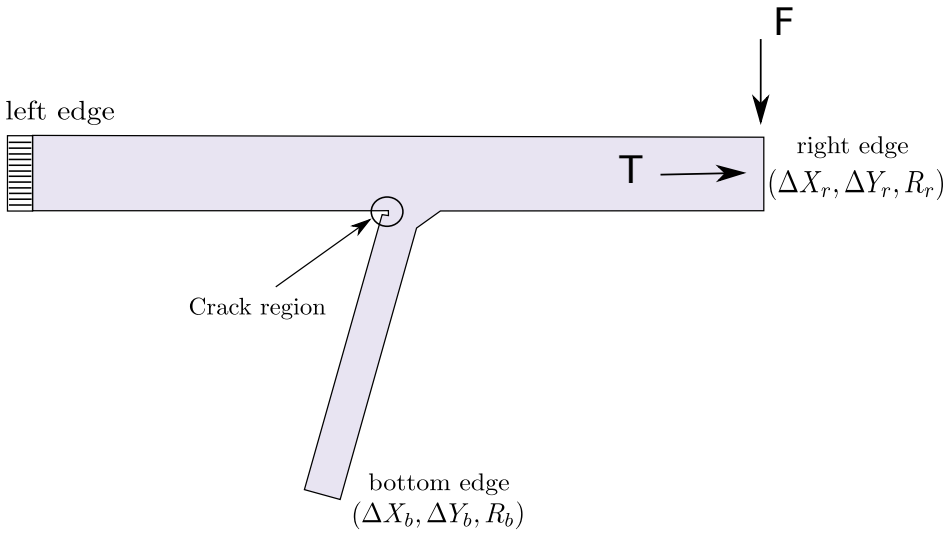

Figure 5.7: An illustration of loading and boundary conditions on the 2D finite element model

deviation of 0.1 mm while the initial crack angle follows a uniform distribution bounded between 0.0 to 30 degrees. Parameters of the Paris' law are assumed to be highly correlated here as well even though we have no data for the fatigue detail material. It is assumed that m and lnC are following normal distributions and with a correlation coefficient of 0.989. The parameter m is considered to follow a normal distribution with mean 3.75 and coefficient of variation of 0.06, and lnC follows a normal distribution with mean -25 and coefficient of variation of 0.04. A similar approach as in Section 5.3.1 is followed here to generate correlated samples from m and C.

5.4.3 Evaluation of the SIFs using Kriging meta-modeling

Proper approximation of the SIFs is a crucial task in fatigue crack propagation analysis. For simple geometries like in the previous case, analytical formulations can be derived from test results with different stress levels. For more complex geometries, however, providing an analytical formulation is not always possible. In such cases, one solution is to calculate the SIFs through a FEA. However, for fatigue reliability analysis this is not really feasible since cycle-by-cycle calculation of the SIFs by means of the FEA leads to a huge computational cost.

In order to illustrate the computational cost of fatigue crack propagation associated with FEA for SIF approximation, a prior crack propagation analysis has been performed on the fatigue detail of interest in this section. The information about the finite element model and the computer used for this calculation has been already introduced in Chapter 4 Section 4.6.1. This analysis involves the propagation of 10 cracks where each crack is propagated for 1000 cycles. The XFEM method implemented in Code_Aster is used for cycle-by-cycle calculations of SIFs. The results show that the required time for this crack propagation analysis is equal to 4 hours 33 minutes and 11 seconds which is very long and intractable for real case studies. This emphasises the need of a faster method to approximate the SIFs.

The goal in this section is to provide a strategy to approximate the SIFs with less computational cost. The proposed strategy tries to alleviate the computational cost by combining a FEA with Kriging meta-modeling. Accordingly, FEA associated with XFEM method are used to provide adequate information about the SIFs (K_I and K_{II}) over the input domain. Kriging meta-modeling is then used to prepare two surrogates for the evaluation of the SIFs, hereafter named $\hat{K}_I$ and $\hat{K}_{II}$. In order to reduce the calculation time to prepare the Kriging meta-models, one can start by calibrating the initial Kriging meta-models on a small DoE and then use the coefficient of determination R^2 as the stopping criterion whilst iteratively recalibrating the meta-models. Hence, the initial Kriging meta-models will be trained until the stopping criterion reaches a given target value R^2_{target}. It should be noted that R^2 provides a measure of how well observed outcomes are approximated by the model according to the proportion of total variation of outcomes explained by the model (Kurz-Kim and Loretan, 2014). Accordingly the following procedure can be considered for the proposed strategy:

1. Evaluating the SIF on N samples of input parameters $\mathbf{x}^{(i)}, i = 1, ..., N$ using FEA. The input parameters are defined subsequently.

2. Preparing the initial DoEs based on N_{DoE} pairs of input parameters and SIFs as: $\{\mathbf{x}^{(i)}, K_l(\mathbf{x}^{(i)})\}$, $i = 1, ..., N_{DoE}$ and $l = I or II$

3. Calibrating the initial Kriging meta-models $\hat{K}_I$ and $\hat{K}_{II}$ on the initial DoEs
4. Evaluating the R^2 on $N - N_{DoE}$ samples of input variables
5. If $R^2 < R^2_{target}$: adding the input sample with the maximum Kriging variance $\sigma^2_{\hat{K}_l(\mathbf{x})}$ to the corresponding DoE and recalibrating the Kriging meta-model $\hat{K}_l$, $l = I or II$
6. Stopping the algorithm otherwise and using the final Kriging meta-models $\hat{K}_l$, $l = I or II$ for further calculations

The input variables $\mathbf{x}$ for the crack propagation in the fatigue detail of interest in this section are the crack length a, crack angle θ, vertical load effect ΔY_{F_r}, and transversal tension effect ΔX_{T_r}. A set of experiments are simulated by means of Code_Aster associated with XFEM method in the first step in order to measure the values of K_I and K_{II} for different levels of input variables. Samples for these independent variables are drawn from uniform distributions provided in Table 5.3. The upper and lower bounds of the uniform distributions are chosen in a way to cover a wide range of possible values for each variable. An optimized space-filling Latin Hyper-cube Sampling (LHS) is employed to generate 1000 samples of the input variables in order to perform the simulation-based tests. This sampling technique helps to adequately cover the domain of variation of the input variables. The values of K_I and K_{II} are evaluated on the generated samples using FEA.

Table 5.3: Input random variables for the simulation-based experiments

Parameter	Low	High	Distribution
$a(mm)$	0.5	5.0	Uniform
θ°	-10	60	Uniform
$\Delta X_{T_r}(mm)$	0.1	0.4	Uniform
$\Delta Y_{F_r}(mm)$	0.2	2.0	Uniform

In the second step, two DoEs of size $N_{DoE} = 100$ are prepared for $\hat{K}_I$ and $\hat{K}_{II}$ meta-models. The samples of the DoEs are randomly selected from the generated samples

in previous step as $\{\mathbf{x}^{(i)}, K_I(\mathbf{x}^{(i)})\}$, $\{\mathbf{x}^{(i)}, K_{II}(\mathbf{x}^{(i)})\}$, $i = 1, ..., 100$. Afterwards, the initial Kriging meta-models $\hat{K}_I$ and $\hat{K}_{II}$ are calibrated on the initial DoEs. The initial meta-models are required to be trained in order to reach an adequate level of accuracy for further applications. For this reason, the samples with the largest Kriging variance are identified for each Kriging meta-model and they are added to the corresponding DoE. This process continues until each meta-model reaches the stopping criterion. The stopping criterion here is arbitrarily fixed at $R^2_{target} = 0.98$. The enrichment process for the Kriging meta-model $\hat{K}_I$ requires 135 extra iterations, and for the Kriging meta-mdel $\hat{K}_{II}$ it requires 95 extra iterations. Figures 5.8 and 5.9 respectively present the original values vs. the meta-model predictions for 100 randomly selected samples not used during the learning process, which indicate a good level of prediction accuracy for each Kriging meta-model $\hat{K}_I$ and $\hat{K}_{II}$.

In the end, the same prior crack propagation analysis has been performed on the fatigue detail of interest in order to highlight how cost-effective this approach is compared to directly employing the FEA. Similarly, 10 cracks are propagated for 1000 cycles. Kriging meta-models $\hat{K}_I$ and $\hat{K}_{II}$ are used to approximate the SIFs for this problem. The results show that the required time for constructing the Kriging meta-models is about 510 seconds and the crack propagation part takes less than 5 seconds. This highlights the efficiency of the proposed approach in terms of computational cost.

5.4.4 Time-dependent reliability analysis based on AK-SYS-t

The final step of this applicational case is related to the evaluation of the cumulative probability of failure using AK-SYS-t. As previously mentioned in Section 5.4.1, a mixed-mode crack growth can be modelled by Equation 5.10 and the failure criterion can be formulated by Equation 5.15. As it was discussed previously in Section 5.3.2, it is necessary to make some assumptions on the performance function in order to be able to apply AK-SYS-t. The simplification steps for this example are similar to the previous applicational case with small differences since we are dealing with a mixed-mode (I/II) crack growth problem, as explained subsequently.

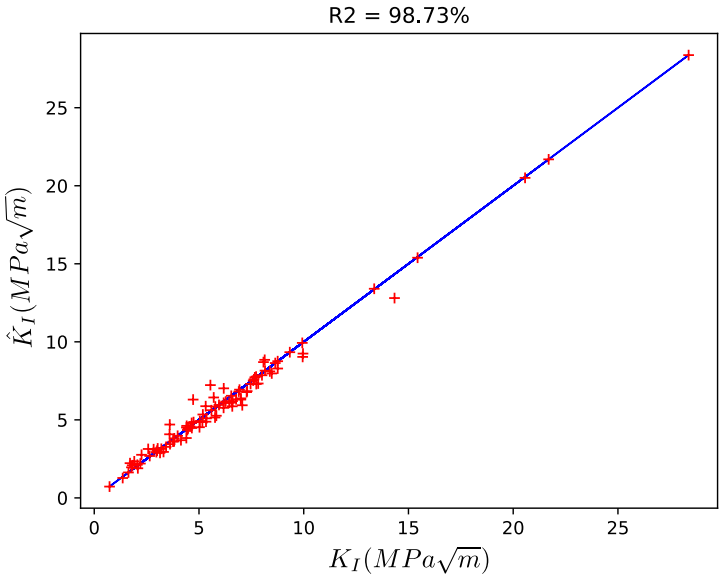

Figure 5.8: Validation results of the Kriging meta-model for K_I

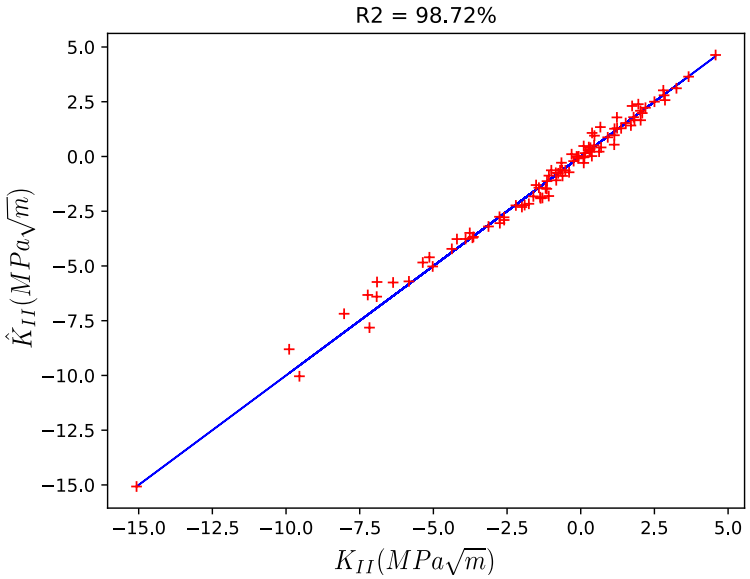

Figure 5.9: Validation results of the Kriging meta-model for K_{II}

In this example, initial crack are only propagated for 1000 load cycles and the expected order of magnitude of failure probability is of $P_f = 10^{-4}$. The objective here is to show that AK-SYS-t can also be applied for low failure probabilities. Figure 5.10 illustrates some probabilistic crack growth paths under given realizations of random parameters $(a_0, \theta_0, m, C, \Delta X_{T_r}, \Delta Y_{F_r})$. The time period is discretized into 10 time

nodes and it is assumed that each sub interval between the time nodes involves in mean 100 load cycles. Paris' law for mixed mode crack propagation (Equation 5.10) is used to propagate the crack.

An upper bound for the maximum value of the equivalent stress intensity factor for each time interval $\Delta K_{eq_{max_j}},\ j = 1, ..., 10$ is here formulated as:

$$\Delta K_{eq_{max_j}} = \Delta K_{eq}(a_j, \theta_j, \Delta X_{T_{max_j}}, \Delta Y_{F_{max_j}}) \tag{5.16}$$

where a_j and θ_j are the crack length and crack angle at the given time node $j = 1, ..., 10$. The parameters $\Delta X_{T_{max_j}}$ and $\Delta Y_{F_{max_j}}$ respectively correspond to the ΔY_{F_r} and ΔX_{T_r} values for a given time interval where the equivalent load effect $L_{eq} = (\Delta Y_{F_r}^2 + \Delta X_{T_r}^2)^{1/2}$ is maximum. The instantaneous performance functions $G_j,\ j = 1, ..., 10$ can then be formulated by the following equation:

$$G_j = K_c - \Delta K_{eq_{max_j}},\ j = 1, ..., 10 \tag{5.17}$$

The value K_c is arbitrarily fixed to $K_c = 30\ MPa\sqrt{m}$ to have $p_f \simeq 10^{-4}$. Figure 5.11 illustrates three realizations of this performance function which has a nonlinear behavior.

AK-SYS-t is used to evaluate the cumulative failure probability. The MCS population size is 10^6 and Equation 5.18 is used to provide initial DoEs of size $N_{DoE} = 50$ for each performance function in order to calibrate initial Kriging meta-models, one per time node.

$$DoE_j : \{(\mathbf{x}^{(i)}, \Delta X_{T_{max_{j,i}}}, \Delta Y_{F_{max_{j,i}}}); K_{j,i}\}, \quad j = 1, ..., N_t \text{ and } i = 1, ..., N_{DoE} \tag{5.18}$$

During the enrichment process the weakest time node is identified and the Kriging meta-model corresponding to this time node in addition to all Kriging meta-models before it are enriched (by adding the sample point that minimizes the U learning function to their corresponding DoE). This process continues until $\min U$ becomes greater than 2 which is the convergence criterion for AK-SYS-t.

The cumulative probability of failure is estimated by AK-SYS-t which is equal to $P_{f,c}^{AK-SYS-t} = 2.19 \times 10^{-4}$. This requires to make only 709 calls to original performance

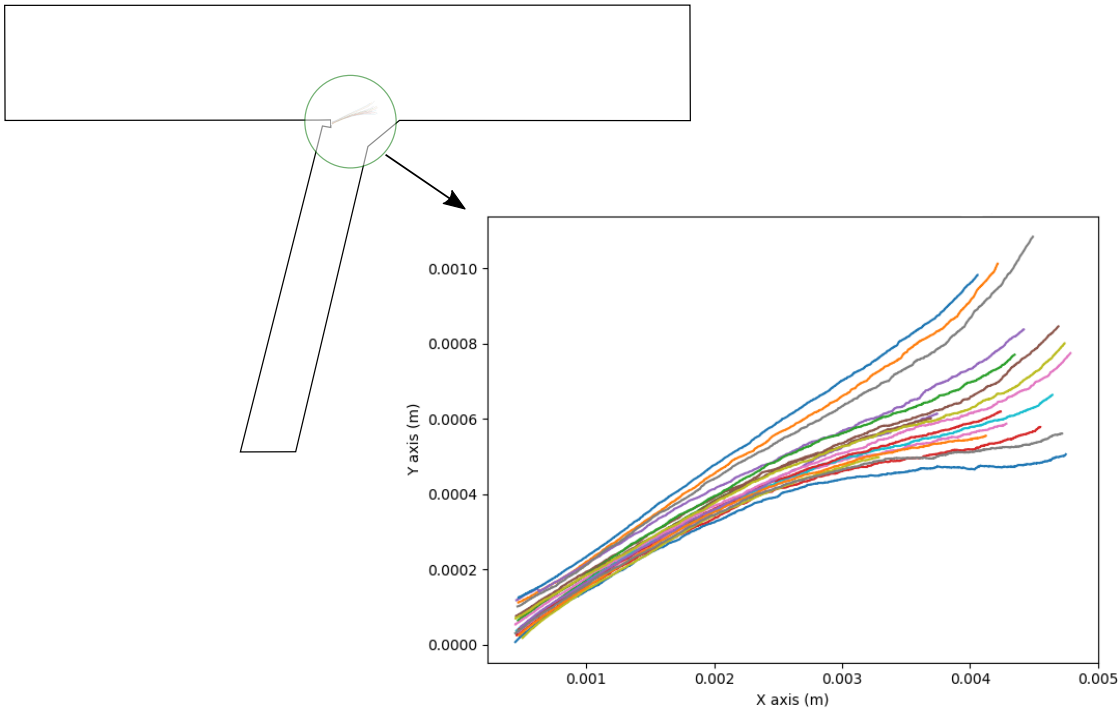

Figure 5.10: Some realizations of the crack propagation path using the approximated SIF computations

functions. The coefficient of variation for the estimated failure probability is equal to 0.067. Additionally, Figure 5.12 illustrates the convergence of the cumulative probability of failure where in the beginning of the algorithm, the estimation is not very accurate due to the lack of accuracy of the meta-models. This estimation converges to its final value after 32 iterations of enrichment, see Figure 5.13. Figure 5.14 provides information about how many time a time node has been considered as a weak node during the enrichment procedure. This figure shows almost the same behaviour as the one in previous example in which the final time node has the most contribution within the enrichment process.

To conclude, it has been tried to establish a framework within this example to employ AK-SYS-t for a finite element based mixed-mode crack growth problems in order to approximate the cumulative probability of failure over a given period of time and with a reasonable computational cost. On that account, we have proposed a Kriging-based approach to estimate the SIFs which leads us to a less computational

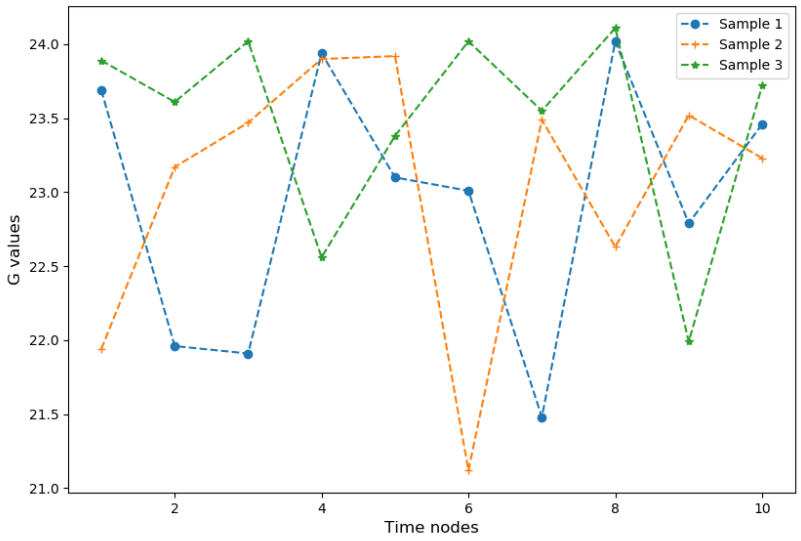

Figure 5.11: Some realizations of the performance function for the mixed mode crack propagation

cost compared to FEA. In addition, simplification assumptions due to the discretization of the time interval have been done for the time-dependent performance function. The results in this section show the usefulness of the proposed approaches in this context and AK-SYS-t estimates the cumulative probability of failure with a reasonable number of calls to the performance functions. It should be mentioned that the results in this section are not compared with MCS in order to save some time for other duties during this PhD.

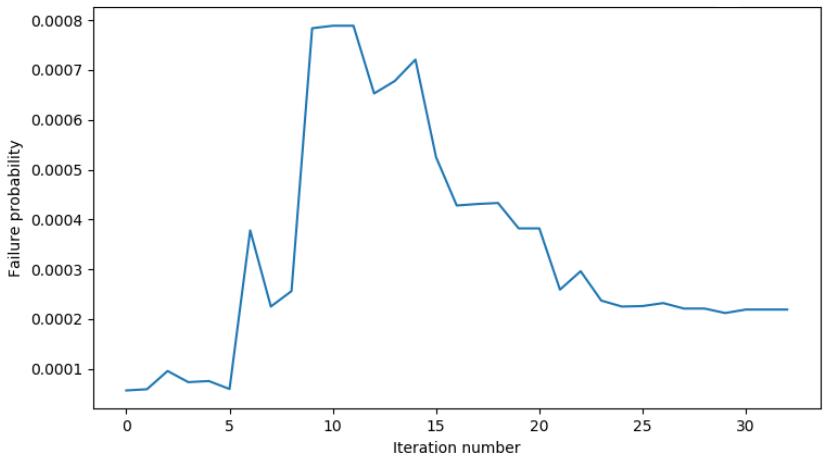

Figure 5.12: Evolution of the cumulative failure probability for the mixed mode crack growth problem

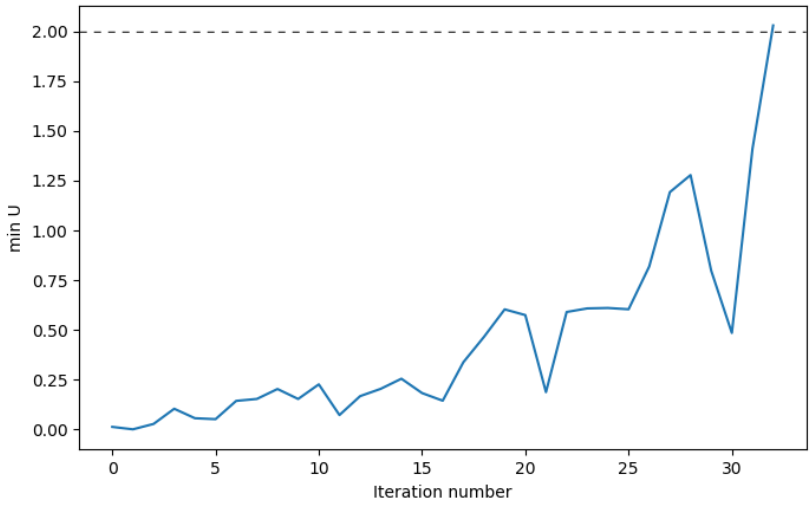

Figure 5.13: Evolution of min$U$ for the mixed mode crack growth problem

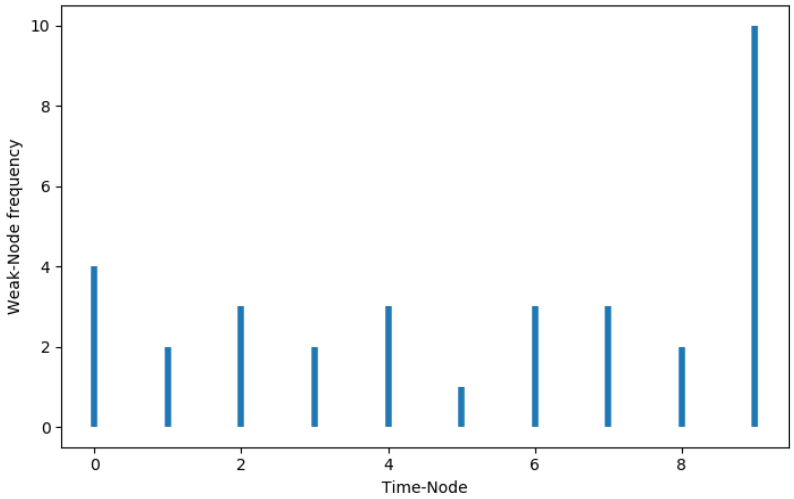

Figure 5.14: Frequency of the weak nodes for the mixed mode crack growth problem

5.5 Conclusion

It has been tried in this chapter to illustrate which are the required steps and strategies to implement AK-SYS-t on fatigue crack growth time-dependent reliability problems. The first case considers a Mode I crack propagation in an aluminum alloy subjected to a stochastic loading in which the SIF is approximated by an analytical formulation. In the second case, a mixed-mode (I/II) crack propagation is studied in which the fatigue detail is subjected to two random loading. The SIFs are approximated with Kriging meta-models which are calibrated on input samples provided by XFEM in Code_Aster.

The comparison of the results of AK-SYS-t versus MCS for the first example indicates that AK-SYS-t can be considered as an accurate and efficient approach for such problems. The results in the second case, however, are provided without making such comparison (which requires huge computational resources) in order to be able to evaluate low cumulative failure probabilities. It has been concluded that the enrichment process for such problems makes more calls to the original performance functions compared to the numerical examples in Chapter 3 since all Kriging meta-models before the weak node are required to be re-calibrated as well. However, performing the time-dependent reliability analysis for crack propagation models using AK-SYS-t requires

much less computational resources compared to methods like MCS in terms of number of calls to the performance function.

One remaining step related to this chapter is to illustrate the application of provided approaches and strategies within the structural LCM. Accordingly, it is necessary to provide the whole curve of cumulative probability of failure. With this respect, one can resort to the proposed strategy in Chapter 3 Section 3.7 to provide the profile of the cumulative failure probability over time. This curve provides a valuable decision indicator to decide about the maintenance and inspection allocation. As mentioned in Chapter 2, this can be done through an optimization framework which, for instance, aims at finding the best maintenance and inspection plan with the minimum cost. For this, however, one must need to know how the repair actions will change the profile of the cumulative failure probability.

Chapter 6 : Conclusions and future works

6.1 General Conclusion

In the overall scope of INFRASTAR, this thesis aimed at bringing contributions to the research field of optimal maintenance planning of existing structures that are vulnerable to fatigue. Optimal maintenance planning can be counted as a global objective of the structural LCM. It is composed of several steps in which each step plays a role in order to accomplish this objective. This, however, is a comprehensive task for which different challenges and difficulties are required to be addressed properly. For this reason, the studies performed within this thesis were trying to improve the capabilities of the structural LCM by providing approaches and strategies to address challenges related to: time-variant fatigue reliability assessment, crack propagation modelling using advanced tools for characterizing repair solutions, and processing the long-term monitoring data for fatigue analysis. The main outputs of this study were divided in four chapters that are summarised hereafter. It should be mentioned that we have devoted the Chapter 2 in the beginning of this thesis to introduce the common practices within structural LCM to cope with fatigue problem. It was highlighted in this chapter that the structural LCM is an extensive task that needs mastering in many other fields such as structural analysis, reliability assessment, data analysis, etc.

A new time-dependent reliability approach was proposed in Chapter 3 that is called AK-SYS-t. An extensive review of currently available time-dependent reliability methods was performed in this chapter. It was pointed out that methods in this domain try to estimate the cumulative probability of failure with a reasonable trade-off between ef-

ficiency and accuracy. This can be a challenging task for problems with non-monotonic and costly-to-evaluate performance functions. Discretizing the desired time interval into finite number of time nodes makes it possible to connect the time-dependent reliability problems with system reliability problems. Accordingly, AK-SYS-t aims at taking advantage of AK-SYS which is a recent and effective system reliability method towards time-dependent reliability assessment. AK-SYS is a Kriging based system reliability method in which the performance functions of components are replaced by Kriging meta-models and an active learning process is employed for enriching the DoEs. The learning process identifies the most vulnerable components during the enrichment process to update the DoEs which makes AK-SYS very efficient. Consequently, this learning process has been used in AK-SYS-t in order to address time-dependent reliability problems. The efficiency and accuracy of the proposed approach was tested on two numerical examples from literature. The first example is a simple numerical case with only one input random variable while the second example considers a more general performance function involving random variables and stochastic processes. For both cases, it was observed that AK-SYS-t successfully approximates the cumulative failure probability with a very good level of accuracy and efficiency. Moreover, an approach was proposed for accurately providing the evolution profile of the cumulative failure probability with time which is a crucial tool for structural maintenance planning.

Chapter 4 of this thesis was dedicated to incorporating advanced methods like FEM and XFEM for evaluating fatigue issues like crack initiation and propagation on real structures. For that reason, fatigue analyses were performed on a real bridge with an Orthotropic Steel Deck (OSD). The results of finite element analysis have shown that under given loading conditions the root of the fillet weld, where longitudinal stiffeners are connected to the deck plate, has the highest risk of crack initiation. The XFEM method was used afterwards to perform the 2D crack propagation in this location. The goal was to figure out the influence of the transversal tension on the crack propagation direction. One challenge here was related to translating the loading and boundary conditions from the 3D model (exposed to a vertical loading and the transversal tension) into the 2D model. To overcome this challenge, it has been assumed

that the vertical load and the transversal tension are acting independently on the structure. Therefore, two separate 3D FEA were performed in order to measure their effects (displacements and rotations) and introduce them on the 2D model. The results of the crack propagation indicated that cracks tend to propagate towards the deck plate for transversal tensions higher than $T = 210$ MPa. Such cracks can put the structure in a very unfavorable situation since they can reach their critical length without being inspected. Therefore, repair actions are necessary in this circumstance in order to reduce the severity of the problem. On that account, the usefulness of two repair solutions was investigated using XFEM method. The first repair action involves applying a horizontal overlay on the deck plate and the second one suggests placing vertical plates between the stiffeners. The crack propagation results using XFEM method indicated that the second repair solution leads to a significant improvement on the fatigue life of the structure.

The objective of Chapter 5 was to illustrate the required simplification steps and strategies in order to integrate AK-SYS-t for fatigue fracture based time-dependent reliability problems. Performing a time-dependent reliability analysis on crack growth performance functions is very challenging since it relies on a cycle-by-cycle calculation of SIF which makes the process too computationally expensive especially for cases in which the SIF is calculated through a FEA. Accordingly, AK-SYS-t was implemented on two applicational cases. The first application was related to a mode I fatigue crack growth in an aluminum alloy subjected to a stochastic loading where the SIF is calculated by an analytical formulation. The lifetime of the test specimen was discretized into a finite number of time nodes and a simplifying strategy was proposed to provide the instantaneous performance functions for the corresponding time nodes before applying AK-SYS-t. The cumulative probability of failure is then approximated using AK-SYS-t and MCS. The results show that AK-SYS-t approximate this failure probability as accurate as MCS with a higher efficiency with respect to the number of calls to the original performance function. The second application was a mixed mode (I/II) crack propagation where the SIFs have to be computed by the XFEM method. It has been highlighted that directly employing the XFEM within AK-SYS-t is exceed-

ingly time consuming. Hence, a Kriging based approach was proposed to calculate the SIFs in order to reduce the computational cost. Then, the instantaneous performance functions for AK-SYS-t were provided in the same manner that was followed in the first case. It has been observed in this applicational case that AK-SYS-t can estimate a lower magnitude of failure probability $P_f = 10^{-4}$ with a reasonable number of calls to the original performance function.

An additional contribution of this thesis is introduced in Appendix A which is related to processing the long-term monitoring data for fatigue analysis. One challenge here can be related to dealing with the seasonality effect available within the long-term monitoring data. The seasonality effect in time series is related to the presence of variations that happen at specific regular intervals. With this respect, time series methods such as seasonal ARIMA can be used to deal with the seasonality effect. However, the huge size of long-term monitoring data leads to another difficulty for this application. Accordingly, an approach is proposed to deal with this issue by transforming the large-sized monitoring data to a small set of observations. For this reason, the monitoring duration is divided into smaller time intervals first. Afterwards, one can fit a distribution to the monitoring data for each time interval. The parameters of the associated distributions can then replace the observations in each time interval. In this way, the entire monitoring data can be replaced by a time series with fewer observations for which the seasonal ARIMA can be employed easily. This approach is applied on the long-term monitoring data of Chillon viaduct. The data is collected for almost two years using strain gauges with the frequency of 50, 100, or 200 Hz.

6.2 Future works

It has been tried in this thesis to add contributions to different aspects of structural LCM for structures that are vulnerable to fatigue. This, however, opens windows to more studies and additional improvements that can be followed in the future. Some of the ideas that can be considered for further development are enumerated in the following:

(I) In Chapter 3, the time discretization has been performed uniformly using a constant discretization step. The discretization strategy is likely to have a noticeable impact, even not fully quantified yet, on the efficiency of the algorithm since it defines the required number of meta-models. Therefore, a more convenient strategy would be proposed based on an adaptive variable step time discretization strategy with smaller steps where the extreme responses of the performance functions are likely to happen and wider steps elsewhere. This would help to control the computational cost especially for cases that require a long-term reliability evaluation.

(II) The crack propagation analysis in Chapter 4 was performed under deterministic loading conditions where the vertical load was assumed to be constant and the value of transversal tension was changing in a deterministic manner. However, it is obvious that loading on structures have a probabilistic nature. Therefore, this study can be improved by performing a probabilistic fatigue crack growth analysis. SHM data can help to identify the parameters of such probabilistic input variables.

(III) Another issue that can be further investigated regarding the study in Chapter 4 is related to identifying the contribution of different parameters on the magnitude of the transversal tension such as residual stresses, traffic loading, and structural weight. This can be very helpful in order to locally approximate the real values of the transversal tension.

(IV) Numerical simulation results in Chapter 4 have shown that the second repair action has promising results regarding the fatigue life extension of the desired fatigue detail. It would be interesting to lead some experimental studies to support the provided results in this chapter. Also, to find out if the new repair action does not lead to new hot zones for fatigue crack initiation.

(V) Another related future work can be related to employing the provided approach in Appendix A within structural LCM which makes it possible to deal with long-term monitoring data involving seasonality effect. The proposed approach can be used to update the loading parameters based on the monitoring data and it can be easily incorporated within S-N curve or fracture mechanism based approaches.

Bibliography

Abbiati, G., Marelli, S., Tsokanas, N., Sudret, B., and Stojadinović, B. (2021). A global sensitivity analysis framework for hybrid simulation. *Mechanical Systems and Signal Processing*, 146:106997. 118

Akiyama, H., Teshigawara, M., and Fukuyama, H. (2000). A framework of structural performance evaluation system for buildings in japan. In *proceedings 12 th World Conference on Earthquake Engineering, January*, volume 30. 11

Alegre, J., Preciado, M., and Ferreño, D. (2007). Study of the fatigue failure of an anti-return valve of a high pressure machine. *Engineering Failure Analysis*, 14(2):408 – 416. Papers presented at the 22nd meeting of the Spanish Fracture Group (Almargro, Spain, March 2005). 148

Anastasopoulos, A., Kourousis, D., Botten, S., and Wang, G. (2009). Acoustic emission monitoring for detecting structural defects in vessels and offshore structures. *Ships and Offshore Structures*, 4(4):363–372. 37

Andrieu-Renaud, C., Sudret, B., and Lemaire, M. (2004). The phi2 method: a way to compute time-variant reliability. *Reliability Engineering and System Safety*, 84(1):75 – 86. Selected papers from ESREL 2002. 63, 84

Antonaci, P., Bocca, P., and Masera, D. (2012). Fatigue crack propagation monitoring by acoustic emission signal analysis. *Engineering Fracture Mechanics*, 81:26 – 32. Fracture and Damage Analysis in Design. 40

Au, S. and Beck, J. (1999). A new adaptive importance sampling scheme for reliability calculations. *Structural Safety*, 21(2):135 – 158. 53, 54

Au, S. and Beck, J. (2003). Important sampling in high dimensions. *Structural Safety*, 25(2):139 – 163. 53, 54

Au, S.-K. and Beck, J. L. (2001). Estimation of small failure probabilities in high dimensions by subset simulation. *Probabilistic Engineering Mechanics*, 16(4):263 – 277. 53, 54

Augusto, O. B., Bennis, F., and Caro, S. (2012). A new method for decision making in multi-objective optimization problems. *Pesquisa Operacional*, 32:331 – 369. 43

Barone, G. and Frangopol, D. M. (2014). Reliability, risk and lifetime distributions as performance indicators for life-cycle maintenance of deteriorating structures. *Reliability Engineering and System Safety*, 123:21 – 37. 15, 19, 21, 22, 23, 24, 33

Basquin, O. H. (1910). The exponential law of endurance tests. In *American Society for Testing and Materials Proceedings*, volume 10, pages 625–630. 25

Battista, R. and Pfeil, M. (2000). tranghening fatigue cracked orthotropic decks with composite layers. In *Annual Technical Sesseion, and Meetin, Structural Stability Research Council*, page 376–389. 123

Baydoun, M. and Fries, T. (2012). Crack propagation criteria in three dimensions using the xfem and an explicit-implicit crack description. *International journal of fracture*, 178(1-2):51–70. 109

Beck, J. L. and Au, S.-K. (2002). Bayesian updating of structural models and reliability using markov chain monte carlo simulation. *Journal of Engineering Mechanics*, 128(4):380–391. 54

Belytschko, T. and Black, T. (1999). Elastic crack growth in finite elements with minimal remeshing. *International Journal for Numerical Methods in Engineering*, 45(5):601–620. 100

Benasciutti, D. and Tovo, R. (2007). On fatigue damage assessment in bimodal random processes. *International Journal of Fatigue*, 29(2):232 – 244. 30

Blatman, G. and Sudret, B. (2010). An adaptive algorithm to build up sparse polynomial chaos expansions for stochastic finite element analysis. *Probabilistic Engineering Mechanics*, 25(2):183 – 197. 56

Bocchini, P., Frangopol, D. M., Ummenhofer, T., and Zinke, T. (2014). Resilience and sustainability of civil infrastructure: Toward a unified approach. *Journal of Infrastructure Systems*, 20(2):04014004. 10

Bourinet, J.-M. and Lemaire, M. (2008). Form sensitivities to correlation : application to fatigue crack propagation based on virkler data. *4th International ASRANet Colloquium*. 137

Broek, D. (1986). *Elementary engineering fracture mechanics*. Springer Netherlands, 4th edition edition. 27

Brühwiler, E. and Bastien Masse, M. (2015). Strengthening the chillon viaducts deck slabs with reinforced UHPFRC. *IABSE Conference Geneva 2015 'Structural Engineering: Providing Solutions to Global Challenges'*, pages 1171–1178. 196

Buitelaar, P. (2002). Ultra thin heavy reinforced high performance concrete overlays. In *6th International Symposium on Utilization of High Strength / High Performance Concrete, Leipzig, Germany*, page 1577–1590. 123

Buitelaar, P., Braam, C., and Kaptaijn, N. (2003). Reinforced high performance concrete overlay system for steel bridges. In *5th International CROW-Workshop on Fundamental Modelling of the Design and Performance of Concrete Pavements, Istanbul, Turkey*. 123

Byers, W. G., Marley, M. J., Mohammadi, J., Nielsen, R. J., and Sarkani, S. (1997). Fatigue reliability reassessment procedures: State-of-the-art paper. *Journal of Structural Engineering*, 123(3):271–276. 32

Cai, G. and Mahadevan, S. (2016). Big data analytics in online structural health monitoring. 36

CDOT (1998). *Pontis Bridge Inspection Coding Guide*. Colorado Department of Transportation. xxvii, 20

Cendón, D., Jin, N., Liu, Y., Berto, F., and Elices, M. (2017). Numerical assessment of gray cast iron notched specimens by using a triaxiality-dependent cohesive zone model. *Theoretical and Applied Fracture Mechanics*, 90:259 – 267. 98

Chang, K.-H. (2015). Chapter 19 - multiobjective optimization and advanced topics. In Chang, K.-H., editor, *e-Design*, pages 1105 – 1173. Academic Press, Boston. 43

Chen, H., Wang, Q., Zeng, W., Liu, G., Sun, J., He, L., and Bui, T. Q. (2019). Dynamic brittle crack propagation modeling using singular edge-based smoothed finite element method with local mesh rezoning. *European Journal of Mechanics - A/Solids*, 76:208 – 223. 148

Cheng, B., Ye, X., Cao, X., Mbako, D. D., and Cao, Y. (2017). Experimental study on fatigue failure of rib-to-deck welded connections in orthotropic steel bridge decks. *International Journal of Fatigue*, 103:157 – 167. xxv, 96

Cheng, F. Y. (1999). Multiobjective optimum design of structures with genetic algorithm and game theory: Application to life-cycle cost design. In Cheng, F. Y. and Gu, Y., editors, *Computational Mechanics in Structural Engineering*, pages 1 – 16. Elsevier Science Ltd, Oxford. 43

Ching, J., Beck, J., and Au, S. (2005). Hybrid subset simulation method for reliability estimation of dynamical systems subject to stochastic excitation. *Probabilistic Engineering Mechanics*, 20(3):199 – 214. 55

Ciang, C. C., Lee, J.-R., and Bang, H.-J. (2008). Structural health monitoring for a wind turbine system: a review of damage detection methods. *Measurement Science and Technology*, 19(12). 37, 38

Connor, R. (2012). Manual for design, construction, and maintenance of orthotropic steel deck bridges. *FHWA-IF-12-027*. 95

Connor, R. J. and Lloyd, J. B. (2017). *Maintenance Actions to Address Fatigue Cracking in Steel Bridge Structures: Proposed Guidelines and Commentary*. West Lafayette, IN: Purdue University. 40

Cremona, C. and Santos, J. (2018). Structural health monitoring as a big-data problem. *Structural Engineering International*, 28(3):243–254. 36

Demir, O., AYHAN, A. O., IRIC, S., and LEKESIZ, H. (2018). Evaluation of mixed mode-i/ii criteria for fatigue crack propagation using experiments and modeling. *Chinese Journal of Aeronautics*, 31(7):1525 – 1534. 147, 148

Demsetz, L. A. (1996). *Inspection of Marine Structures*. Ship Structure Committee. 39

Ditlevsen, O. and Olesen, R. (1986). Statistical analysis of the virkler data on fatigue crack growth. *Engineering Fracture Mechanics*, 25(2):177 – 195. 137

Dong, Y., Frangopol, D. M., and Saydam, D. (2013). Time-variant sustainability assessment of seismically vulnerable bridges subjected to multiple hazards. *Earthquake Engineering & Structural Dynamics*, 42(10):1451–1467. 10

Dong, Y., Teixeira, A., and Guedes Soares, C. (2018). Time-variant fatigue reliability assessment of welded joints based on the phi2 and response surface methods. *Reliability Engineering and System Safety*, 177:120 – 130. 135

Dong, Y., Teixeira, A., and Guedes Soares, C. (2020). Application of adaptive surrogate models in time-variant fatigue reliability assessment of welded joints with surface cracks. *Reliability Engineering and System Safety*, 195:106730. 135

Dowling, N. (1971). Fatigue failure predictions for complicated stress-strain histories. 30

Du, X. (2012). Toward time-dependent robustness metrics. *Journal of Mechanical Design*, 134:011004–8. 64

Dubourg, V. (2011). *Adaptive surrogate models for reliability analysis and reliability-based design optimization*. PhD thesis, Université Blaise Pascal Clermont II. 78

Echard, B., Gayton, N., and Lemaire, M. (2011). AK-MCS: An active learning reliability method combining Kriging and monte carlo simulation. *Structural Safety*, 33(2):145 – 154. 57, 58, 135

Echard, B., Gayton, N., Lemaire, M., and Relun, N. (2013). A combined importance sampling and kriging reliability method for small failure probabilities with time-demanding numerical models. *Reliability Engineering and System Safety*, 111:232 – 240. 58

Electricité de France (1989–2017). Finite element *code_aster*, analysis of structures and thermomechanics for studies and research. Open source on www.code-aster.org. 106

Elguedj, T., Gravouil, A., and Combescure, A. (2006). Appropriate extended functions for x-fem simulation of plastic fracture mechanics. *Computer Methods in Applied Mechanics and Engineering*, 195:501–515. 100

Ellyin, F. (1997). *Fatigue Damage, Crack Growth and Life Prediction*. Springer Netherlands, 1st edition. 24

Engelund, S., Rackwitz, R., and Lange, C. (1995). Approximations of first-passage times for differentiable processes based on higher-order threshold crossings. *Probabilistic Engineering Mechanics*, 10(1):53 – 60. 135

Erdogan, F. and Sih, G. C. (1963). On the Crack Extension in Plates Under Plane Loading and Transverse Shear. *Journal of Basic Engineering*, 85(4):519–525. 109, 148

Estes, A. C. and Frangopol, D. M. (2001). Minimum expected cost-oriented optimal maintenance planning for deteriorating structures: application to concrete bridge decks. *Reliability Engineering and System Safety*, 73(3):281 – 291. 14

Fauriat, W. and Gayton, N. (2014). AK-SYS: An adaptation of the AK-MCS method for system reliability. *Reliability Engineering and System Safety*, 123:137 – 144. 6, 50, 72, 74, 75

Feng, G., Garbatov, Y., and Guedes Soares, C. (2012). Fatigue reliability of a stiffened panel subjected to correlated crack growth. *Structural Safety*, 36-37:39 – 46. 135

Ferchichi, A., Boulila, W., and Farah, I. R. (2017). Propagating aleatory and epistemic uncertainty in land cover change prediction process. *Ecological Informatics*, 37:24 – 37. 18

FHWA (2013). *Manual for Repair and Retrofit of Fatigue Cracks in Steel Bridges*. U.S. Department of Transportation, Washington, DC. 40

Fisher, J. W., Kulak, G. L., and Smith, I. (1998). *A Fatigue Primer for Structural Engineers*. National Steel Bridge Alliance, American Institute of Steel Construction. 24, 25, 38, 39, 40

Frangopol, D. M. (2011). Life-cycle performance, management, and optimisation of structural systems under uncertainty: accomplishments and challenges. *Structure and Infrastructure Engineering*, 7(6):389–413. xxv, 12, 16, 36, 43

Frangopol, D. M. (2018). *Structures and Infrastructure Systems: Life-Cycle Performance, Management, and Optimization*. CRC Press, 1st edition edition. 16

Frangopol, D. M., Bocchini, P., Decò, A., Kim, S., Kwon, K., M.Okasha, N., and Saydam, D. (2012). Integrated life-cycle framework for maintenance, monitoring, and reliability of naval ship structure. *Naval Engineers Journal*, 124(1):89–99. 12

Frangopol, D. M. and Kim, S. (2019). *Life-Cycle of Structures Under Uncertainty: Emphasis on Fatigue-Sensitive Civil and Marine Structures*. CRC Press, 1st edition edition. 16, 19

Frangopol, D. M., Lin, K.-Y., and Estes, A. C. (1997). Life-cycle cost design of deteriorating structures. *Journal of Structural Engineering*, 123(10):1390–1401. 41, 42

Frangopol, D. M. and Liu, M. (2007). Maintenance and management of civil infrastructure based on condition, safety, optimization, and life-cycle cost. *Structure and Infrastructure Engineering*, 3(1):29–41. 42

Frangopol, D. M. and Soliman, M. (2016). Life-cycle of structural systems: recent achievements and future directions. *Structure and Infrastructure Engineering*, 12(1):1–20. 16

Frangopol, K. K. D. M. (2012). System reliability of ship hull structures under corrosion and fatigue. *Journal of Ship Research*, 95(4):234–251. 12

Fricke, W. (2007). Round-robin study on stress analysis for the effective notch stress approach. *Welding in the World*, 51:68–79. 103

Gallagher, J., Giesslar, F., Berens, A., Engle, R., Command, U. S. A. F. S., (U.S.), A. F. F. D. L., and Laboratories, A. F. W. A. (1984). *USAF Damage Tolerant Design Handbook: Guidelines for the Analysis and Design of Damage Tolerant Aircraft Structures*. Number pt. 1 in AFWAL-TR. Flight Dynamics Laboratory, Air Force Wright Aeronautical Laboratories, Air Force Systems Command. 31

Geuzaine, C. and Remacle, J.-F. (2009). Gmsh: a three-dimensional finite element mesh generator with built-in pre- and post-processing facilities. *International Journal for Numerical Methods in Engineering*, 79:1309–1331. 102

Ghosn, M., Dueñas-Osorio, L., Frangopol, D. M., McAllister, T. P., Bocchini, P., Manuel, L., Ellingwood, B. R., Arangio, S., Bontempi, F., Shah, M., Akiyama, M., Biondini, F., Hernandez, S., and Tsiatas, G. (2016). Performance indicators for structural systems and infrastructure networks. *Journal of Structural Engineering*, 142(9):F4016003. 18

Guedes Soares, C. and Garbatov, Y. (1996). Fatigue reliability of the ship hull girder accounting for inspection and repair. *Reliability Engineering and System Safety*, 51(3):341 – 351. Maintenance and reliability. 135, 136

Harrison, R., Loosemore, K., and Milne, I. (1977). *Assessment of the Integrity of Structures Containing Defects: Hauptbd.* Central Electricity Generating Board, Research Division. Central Electricity Generating Board. 34

Hashemi, B., Maljaars, J., Leonetti, D., and Snijder, H. B. (2017). Compatibility of s-n and crack growth curves in the fatigue reliability assessment of a welded steel joint. *Procedia Structural Integrity*, 5:959 – 966. 2nd International Conference on Structural Integrity, ICSI 2017, 4-7 September 2017, Funchal, Madeira, Portugal. 134

Hasofer, A. M. and Lind, N. C. (1974). Exact and invariant second-moment code format. *Journal of the Engineering Mechanics Division*, 100(1):111–121. 55

Hawchar, L. (2017). *Development of Metamodeling Methods for Time-Dependent Structural Reliability Analysis*. PhD thesis, Université de Nantes. 84, 85, 86

Hawchar, L., Soueidy, C.-P. E., and Schoefs, F. (2017). Principal component analysis and polynomial chaos expansion for time-variant reliability problems. *Reliability Engineering and System Safety*, 167:406 – 416. Special Section: Applications of Probabilistic Graphical Models in Dependability, Diagnosis and Prognosis. 65

He, W., Liu, J., and Xie, D. (2015). Probabilistic life assessment on fatigue crack growth in mixed-mode by coupling of kriging model and finite element analysis. *Engineering Fracture Mechanics*, 139:56 – 77. 134, 135

Hellier, C. J. (2012). *Handbook of Nondestructive Evaluation*. McGraw-Hill, 2nd edition edition. 39

Hosseini, S. M., Mamun, M. S., Mirza, O., and Mashiri, F. (2020). Behaviour of blind bolt shear connectors subjected to static and fatigue loading. *Engineering Structures*, 214:110584. 129

Hu, Z. and Du, X. (2013). Time-dependent reliability analysis with joint upcrossing rates. *Structural and Multidisciplinary Optimization*, 48(5):893–907. 63

Hu, Z. and Du, X. (2015a). First order reliability method for time-variant problems using series expansions. *Structural and Multidisciplinary Optimization*, 51(1):1–21. 63

Hu, Z. and Du, X. (2015b). Mixed efficient global optimization for time-dependent reliability analysis. *Journal of Mechanical Design*, 137:051401–9. 57, 67, 78, 82

Hu, Z. and Mahadevan, S. (2016). A single-loop kriging surrogate modeling for time-dependent reliability analysis. *Journal of Mechanical Design*, 138:061406–061406–10. 69, 84

Huang, C., Hami, A. E., and Radi, B. (2017). Overview of structural reliability analysis methods-part i: Local reliability methods. *Uncertainties and Reliability of Multiphysical Systems*, 1(Optimization and Reliability). 55

Huang, W., Garbatov, Y., and Guedes Soares, C. (2013). Fatigue reliability assessment of a complex welded structure subjected to multiple cracks. *Engineering Structures*, 56:868 – 879. 134

Huang, X., Chen, J., and Zhu, H. (2016). Assessing small failure probabilities by ak–ss: An active learning method combining kriging and subset simulation. *Structural Safety*, 59:86 – 95. 58

Huang, Y., Zhang, Q., Bao, Y., and Bu, Y. (2019). Fatigue assessment of longitudinal rib-to-crossbeam welded joints in orthotropic steel bridge decks. *Journal of Constructional Steel Research*, 159:53 – 66. 95, 96

Hussain, M., Pu, S., and Underwood, J. (1974). Strain energy release rate for a crack under combined mode i and mode ii. In *Proceedings of the 1973 National Symposium on Fracture Mechanics (West Conshohocken, PA: ASTM International, 1974)*. 148

Hyndman, R. and Athanasopoulos, G. (2018). *Forecasting: principles and practice*. OTexts. 196

Irwin, G. R. (1957). Analysis of stresses and strains near the end of a crack traversing a plate. *Journal of Applied Mechanics-Transactions of the ASME*, 24:351–369. 148

ITSEOA (1979). *Instruction technique pour la surveillance et l'entretien des ouvrages d'art*. Direction Departementale de l'Equipement (DDE) Ministere des Transport, Paris, France. xxvii, 38, 39

Kainuma, S., Yang, M., Jeong, Y.-S., Inokuchi, S., Kawabata, A., and Uchida, D. (2016). Experiment on fatigue behavior of rib-to-deck weld root in orthotropic steel decks. *Journal of Constructional Steel Research*, 119:113 – 122. 95

Karanki, D., Rahman, S., Dang, V., and Zerkak, O. (2017). Epistemic and aleatory uncertainties in integrated deterministic and probabilistic safety assessment: Tradeoff

between accuracy and accident simulations. *Reliability Engineering & System Safety*, 162:91 – 102. 18

Khosrovaneh, A. and Dowling, N. (1990). Fatigue loading history reconstruction based on the rainflow technique. *International Journal of Fatigue*, 12(2):99 – 106. 192

Kim, S. and Frangopol, D. M. (2011a). Cost-based optimum scheduling of inspection and monitoring for fatigue-sensitive structures under uncertainty. *Journal of Structural Engineering*, 137(11):1319–1331. 12

Kim, S. and Frangopol, D. M. (2011b). Inspection and monitoring planning for rc structures based on minimization of expected damage detection delay. *Probabilistic Engineering Mechanics*, 26(2):308–320. 12

Kim, S. and Frangopol, D. M. (2011c). Optimum inspection planning for minimizing fatigue damage detection delay of ship hull structures. *International Journal of Fatigue*, 33(3):448 – 459. 12, 44

Kim, S. and Frangopol, D. M. (2012). Probabilistic bicriterion optimum inspection/-monitoring planning: applications to naval ships and bridges under fatigue. *Structure and Infrastructure Engineering*, 8(10):912–927. 12

Kim, S. and Frangopol, D. M. (2017). Efficient multi-objective optimisation of probabilistic service life management. *Structure and Infrastructure Engineering*, 13(1):147–159. 43

Kim, S. and Frangopol, D. M. (2018a). Decision making for probabilistic fatigue inspection planning based on multi-objective optimization. *International Journal of Fatigue*, 111:356 – 368. 43, 44

Kim, S. and Frangopol, D. M. (2018b). Multi-objective probabilistic optimum monitoring planning considering fatigue damage detection, maintenance, reliability, service life and cost. *Structural and Multidisciplinary Optimization*, 57(1):39–54. 44

Kong, J. S. and Frangopol, D. M. (2003a). Evaluation of expected life-cycle maintenance cost of deteriorating structures. *Journal of Structural Engineering*, 129(5):682–691. 15

Kong, J. S. and Frangopol, D. M. (2003b). Life-cycle reliability-based maintenance cost optimization of deteriorating structures with emphasis on bridges. *Journal of Structural Engineering*, 129(6):818–828. 15

Kozy, B. M., Connor, R. J., Paterson, D., and Mertz, D. R. (2011). Proposed revisions to aashto-lrfd bridge design specifications for orthotropic steel deck bridges. *Journal of Bridge Engineering*, 16(6):759–767. xxv, 95

Krenk, S. and Gluver, H. (1989). A markov matrix for fatigue load simulation and rainflow range evaluation. *Structural Safety*, 6(2):247 – 258. 30, 192

Kunz, P. (1992). Probabilistisches verfahren zur beurteilung der ermüdungssicherheit bestehender brücken aus stahl. page 216. 35

Kurz-Kim, J.-R. and Loretan, M. (2014). On the properties of the coefficient of determination in regression models with infinite variance variables. *Journal of Econometrics*, 181(1):15 – 24. Heavy Tails and Stable Paretian Distributions. 151

Kwon, K. and Frangopol, D. M. (2011). Bridge fatigue assessment and management using reliability-based crack growth and probability of detection models. *Probabilistic Engineering Mechanics*, 26(3):471–480. 12

Kwon, K. and Frangopol, D. M. (2012). Fatigue life assessment and lifetime management of aluminum ships using life-cycle optimization. *Journal of Ship Research*, 56(2):91–105. 12

Leemis, L. (1995). *Reliability, Probabilistic Models and Statistical Methods*. Prentice Hall, New Jersey. 22

Lemaire, M., Chateauneuf, A., and Mitteau, J. (2009). *Structural Reliability*. Wiley. 52

Lemaitre, J. and Desmorat, R. (2005). *Engineering damage mechanics: ductile, creep, fatigue and brittle failures*. Springer Science & Business Media. 98

Li, C. and Kiureghian, A. D. (1993). Optimal discretization of random fields. *Journal of Engineering Mechanics*, 119(6):1136–1154. 59, 138

Li, H., Li, J., and Yuan, H. (2018). A review of the extended finite element method on macrocrack and microcrack growth simulations. *Theoretical and Applied Fracture Mechanics*, 97:236 – 249. 99

Li, H., O'Hara, P., and Duarte, C. (2019). A two-scale generalized fem for the evaluation of stress intensity factors at spot welds subjected to thermomechanical loads. *Engineering Fracture Mechanics*, 213:21 – 52. 27

Ling, Y., Shantz, C., Mahadevan, S., and Sankararaman, S. (2011). Stochastic prediction of fatigue loading using real-time monitoring data. *International Journal of Fatigue*, 33(7):868 – 879. 29, 30, 192

Liu, M. and Frangopol, D. M. (2005). Multiobjective maintenance planning optimization for deteriorating bridges considering condition, safety, and life-cycle cost. *Journal of Structural Engineering*, 131(5):833–842. 42

Liu, M., Frangopol, D. M., and Kwon, K. (2010). Fatigue reliability assessment of retrofitted steel bridges integrating monitored data. *Structural Safety*, 32(1):77 – 89. 33

Liu, Y., Chen, J., Zhang, X., and Tan, D. (2018). Fatigue behaviour of blind bolts under tensile cyclic loads. *Journal of Constructional Steel Research*, 148:16 – 27. 129

Liu, Y. and Mahadevan, S. (2009). Probabilistic fatigue life prediction using an equivalent initial flaw size distribution. *International Journal of Fatigue*, 31(3):476 – 487. 31

Loeve, M. (1977). *Probability theory I.* Springer-Verlag. 59, 65

Long, L., Thöns, S., and Döhler, M. (2018). The effects of shm system parameters on the value of damage detection information. *EWSHM; European workshop on structural health monitoring, Manchester, United Kngdom.* 191

Lukic, M. (1999). *Evaluation et maintenance probabilistes des assemblages soudes vis-a-vis de la fatigue et de la rupture application aux ponts mixtes.* PhD thesis. Thèse de doctorat dirigée par BROZZETT, JACQUES Sciences et techniques École nationale des ponts et chaussées (France) 1999. 25, 26, 27

Lukic, M. and Cremona, C. (2001). Probabilistic assessment of welded joints versus fatigue and fracture. *Journal of Structural Engineering*, 127(2):211–218. 44

Lutes, L. D. and Sarkani, S. (2004). Random vibrations. Butterworth-Heinemann, Burlington. 62

Lutes, L. D. and Sarkani, S. (2009). Reliability analysis of systems subject to first-passage failure. Butterworth-Heinemann, Burlington. 62, 63

Lv, Z., Lu, Z., and Wang, P. (2015). A new learning function for kriging and its applications to solve reliability problems in engineering. *Comput. Math. Appl.*, 70(5):1182–1197. 58

Maljaars, J., Bonet, E., and Pijpers, R. J. (2018). Fatigue resistance of the deck plate in steel orthotropic deck structures. *Engineering Fracture Mechanics*, 201:214 – 228. 96

Marley, M. J. and Moan, T. (1992). Time variant formulation for fatigue reliability. 135

Marquis, G. (2011). 8 - fatigue assessment methods for variable amplitude loading of welded structures. In Macdonald, K. A., editor, *Fracture and Fatigue of Welded Joints and Structures*, Woodhead Publishing Series in Welding and Other Joining Technologies, pages 208 – 238. Woodhead Publishing. 26

Martin-Sanz, H., Dertimanis, V., Avendaño-Valencia, L., Chatzi, E., and Brühwiler, E. (2018). Monitoring of the chillon viaduct after strengthening with uhpfrc. *Proceedings of the Ninth International Conference on Bridge Maintenance, Safety and Management (IABMAS 2018) : Maintenance, Safety, Risk, Management and Life-Cycle Performance of Bridges*, pages 968–975. 196

Masciotta, M. G., RAMOS, L. F., LOURENÇO, P. B., and MATOS, J. A. (2016). Development of key performance indicators for the structural assessment of heritage buildings. In *8th European Workshop On Structural Health Monitoring (EWSHM 2016), 5-8 July, Spain, Bilbao*. 19

Matheron, G. (1973). The intrinsic random functions and their applications. *Advances in Applied Probability*, 5(3):439–468. 203

Mattrand, C. (2011). *Approche probabiliste de la tolérance aux dommages*. Theses, Université Blaise Pascal - Clermont-Ferrand II. xxvi, 137

Melchers, R. E. (1999). *Structural Reliability Analysis and Prediction*. John Wiley and Sons. 33, 53, 55, 135

Merati, A. and Eastaugh, G. (2007). Determination of fatigue related discontinuity state of 7000 series of aerospace aluminum alloys. *Engineering Failure Analysis*, 14(4):673 – 685. 31

Miner, M. (1945). Cumulative damage in fatigue. *Journal of Applied Mechanics*, 3:159–164. 26

Minguez, J. (1994). Foreman's crack growth rate equation and the safety conditions of cracked structures. *Engineering Fracture Mechanics*, 48(5):663 – 672. 32

Miyamoto, A. and Motoshita, M. (2015). Development and practical application of a bridge management system (j-bms) in japan. *Civil Engineering Infrastructures Journal*, 48(1):189–216. 12

Moan, T. (2005). Reliability-based management of inspection, maintenance and repair of offshore structures. *Structure and Infrastructure Engineering*, 1(1):33–62. 38

Moreno, B., Zapatero, J., and Domínguez, J. (2003). An experimental analysis of fatigue crack growth under random loading. *International Journal of Fatigue*, 25(7):597 – 608. 30

Moës, N., Dolbow, J., and Belytschko, T. (1999). A finite element method for crack growth without remeshing. *International Journal for Numerical Methods in Engineering*, 46(1):131–150. 109

Neves, L. A. C., Frangopol, D. M., and Petcherdchoo, A. (2006). Probabilistic lifetime-oriented multiobjective optimization of bridge maintenance: Combination of maintenance types. *Journal of Structural Engineering*, 132(11):1821–1834. 15

Norouzi, M. and Nikolaidis, E. (2012). Efficient random vibration analysis using markov chain monte carlo simulation. *SAE Int. J. Mater. Manf.*, 5:77–86. 54

Okasha, N. M. and Frangopol, D. M. (2009a). Lifetime-oriented multi-objective optimization of structural maintenance considering system reliability, redundancy and life-cycle cost using ga. *Structural Safety*, 31(6):460 – 474. Optimization under Uncertainty with Emphasis on Structural Applications. 45

Okasha, N. M. and Frangopol, D. M. (2009b). Time-variant redundancy of structural systems. *Structure and Infrastructure Engineering*, 6(1-2):279–301. 23

Okasha, N. M. and Frangopol, D. M. (2010a). Advanced modeling for efficient computation of life-cycle performance prediction and service-life estimation of bridges. *Journal of Computing in Civil Engineering*, 24(6):548–556. 10

Okasha, N. M. and Frangopol, D. M. (2010b). Novel approach for multicriteria optimization of life-cycle preventive and essential maintenance of deteriorating structures. *Journal of Structural Engineering*, 136(8):1009–1022. 12, 15

Okasha, N. M. and Frangopol, D. M. (2010c). Redundancy of structural systems with and without maintenance: An approach based on lifetime functions. *Reliability Engineering and System Safety*, 95(5):520 – 533. 19

Okasha, N. M. and Frangopol, D. M. (2011). Computational platform for the integrated life-cycle management of highway bridges. *Engineering Structures*, 33(7):2145 – 2153. 10

Orcesi, A. D. and Frangopol, D. M. (2011a). Optimization of bridge maintenance strategies based on structural health monitoring information. *Structural Safety*, 33(1):26 – 41. 12, 42, 44

Orcesi, A. D. and Frangopol, D. M. (2011b). Use of lifetime functions in the optimization of nondestructive inspection strategies for bridges. *Journal of Structural Engineering*, 137(4):531–539. 10, 23

Orcesi, A. D., Frangopol, D. M., and Kim, S. (2010). Optimization of bridge maintenance strategies based on multiple limit states and monitoring. *Engineering Structures*, 32(3):627 – 640. 44

Orta, L. and Bartlett, F. (2020). Sensitivity analysis of restrained shrinkage stresses of concrete deck overlays. *Engineering Structures*, 210:110396. 118

Osovski, S., Srivastava, A., Williams, J., and Needleman, A. (2015). Grain boundary crack growth in metastable titanium alloys. *Acta Materialia*, 82:167 – 178. 98

Paris, P. and Erdogan, F. (1963). A Critical Analysis of Crack Propagation Laws. *Journal of Basic Engineering*, 85(4):528–533. 27

Park, Y.-S., Han, S.-Y., and Suh, B.-C. (2005). Fatigue reliability analysis of steel bridge welding member by fracture mechanics method. *Structural Engineering and Mechanics*, 19(3):347–359. 34

Ponte, R. M. (1985). The theory of statistics of extremes and el niño phenomena : a stochastic approach. 63

Qian, J. and Long, Y. (1992). Sub-region mixed fem for calculating stress intensity factor of antiplane notch in bi-material. *Engineering Fracture Mechanics*, 43(6):1003 – 1007. 27

Rackwitz, R. and Flessler, B. (1978). Structural reliability under combined random load sequences. *Computers and Structures*, 9(5):489 – 494. 55

Rahman, S., Karanki, D., Epiney, A., Wicaksono, D., Zerkak, O., and Dang, V. (2018). Deterministic sampling for propagating epistemic and aleatory uncertainty in dynamic event tree analysis. *Reliability Engineering & System Safety*, 175:62 – 78. 18

Rausand, M. and Høyland, A. (2003). *System Reliability Theory: Models, Statistical Methods, and Applications, 2nd Edition*. John Wiley & Sons, New York, 2nd edition edition. 22

Riahi, H., Bressolette, P., Chateauneuf, A., Bouraoui, C., and Fathallah, R. (2011). Reliability analysis and inspection updating by stochastic response surface of fatigue cracks in mixed mode. *Engineering Structures*, 33(12):3392 – 3401. 134

Rice, S. (1944). Mathematical analysis of random noise. *The Bell System Technical*, 23(3):282–332. 62

Ritchie, R. and Knott, J. (1973). Mechanisms of fatigue crack growth in low alloy steel. *Acta Metallurgica*, 21(5):639 – 648. 27

Ritchie, R. O. (1999). Mechanisms of fatigue-crack propagation in ductile and brittle solids. *International Journal of Fracture*, 100:55–83. 28

Royset, J. O., Kiureghian, A. D., and Polak, E. (2006). Optimal design with probabilistic objective and constraints. *Journal of Engineering Mechanics*, 132(1):107–118. 73

Sahu, M., Chattopadhyay, J., and Dutta, B. (2019). Hybrid approach for calculation of j-r curve using r6. *Engineering Fracture Mechanics*, 215:16 – 35. xxv, 35

Sajith, S., Shukla, S., Murthy, K., and Robi, P. (2020). Mixed mode fatigue crack growth studies in aisi 316 stainless steel. *European Journal of Mechanics - A/Solids*, 80:103898. 148

Sankararaman, S., Ling, Y., and Mahadevan, S. (2011). Uncertainty quantification and model validation of fatigue crack growth prediction. *Engineering Fracture Mechanics*, 78(7):1487 – 1504. 31

Sankararaman, S., Ling, Y., Shantz, C., and Mahadevan, S. (2009). Uncertainty quantification in fatigue damage prognosis. *Annual Conference of the Prognostics and Health Management Society*. xxvii, 29, 31, 32

Shinozuka, M. (1964). Probability of structural failure under random loading. *Journal of the Engineering Mechanics division*, 90(5):147–170. 62

Soliman, M., Frangopol, D. M., and Kim, S. (2013). Probabilistic optimum inspection planning of steel bridges with multiple fatigue sensitive details. *Engineering Structures*, 49:996 – 1006. 44

Soliman, M., Frangopol, D. M., and Mondoro, A. (2016). A probabilistic approach for optimizing inspection, monitoring, and maintenance actions against fatigue of critical ship details. *Structural Safety*, 60:91 – 101. 38, 39, 41, 44

Son, Y. K. and Savage, G. J. (2007). Set theoretic formulation of performance reliability of multiple response time-variant systems due to degradations in system components. *Quality and Reliability Engineering International*, 23(2):171–188. 73

Strauss, A., MandićIvanković, A., Matos, J. C., and Casas, J. R. (2017). Performance indicators for road bridges: overview of findings and future progress. In *The Value of Structural Health Monitoring for thereliable Bridge Management 2-3 March*. University of Zagreb. 19

Sudret, B. (2008). Analytical derivation of the outcrossing rate in time-variant reliability problems. *Structure and Infrastructure Engineering*, 4(5):353–362. 62, 63, 77

Susmel, L. (2009). Three different ways of using the modified wöhler curve method to perform the multiaxial fatigue assessment of steel and aluminium welded joints. *Engineering Failure Analysis*, 16(4):1074 – 1089. Papers presented at the Third International Conference on Engineering Failure Analysis (Sitges, Spain, 13-16 July 2008). 25

Susmel, L., Sonsino, C., and Tovo, R. (2011). Accuracy of the modified wöhler curve method applied along with the rref=1mm concept in estimating lifetime of welded joints subjected to multiaxial fatigue loading. *International Journal of Fatigue*, 33(8):1075 – 1091. Multiaxial Fatigue Models. 25

Swartz, R. A. and Lynch, J. P. (2009). Damage characterization of the z 24 bridge by transfer function pole migration. 38

Szerszen, M. M., Nowak, A. S., and Laman, J. A. (1999). Fatigue reliability of steel bridges. *Journal of Constructional Steel Research*, 52(1):83 – 92. 33

Tanaka, K. (1974). Fatigue crack propagation from a crack inclined to the cyclic tensile axis. *Engineering Fracture Mechanics*, 6(3):493 – 507. 147, 148

Tong, C., Sun, Z., Zhao, Q., Wang, Q., and Wang, S. (2015). A hybrid algorithm for reliability analysis combining kriging and subset simulation importance sampling. *Journal of Mechanical Science and Technology*, 29:3183–3193. 58

Transportation Research Board and National Academies of Sciences Engineering and Medicine (2007). Bridge inspection practices. Technical report. 38

Treacy, M. A. (2014). The use of monitored data in the verification of structural and fatigue safety of existing post-tensioned concrete highway bridges. 193, 196

van der Toorn, A. (1994). The maintenance of civil engineering structures. *Heron*, 39(2):3–34. 14, 17

Virkler, D. A., Hillberry, B. M., and Goel, P. K. (1979). The statistical nature of fatigue crack propagation. *Journal of Engineering Materials and Technology*, 101:148–153. 137

Walter, R., Olesen, J. F., Stang, H., and Vejrum, T. (2007). Analysis of an orthotropic deck stiffened with a cement-based overlay. *Journal of Bridge Engineering*, 12(3):350–363. 123

Wang, S., Shi, X., and He, J. (2007). Time-variant reliability analysis of ship structure subjected to fatigue and corrosion. *Key Engineering Materials - KEY ENG MAT*, 348-349:153–156. 136

Wang, Y. and Song, Y. S. (2017). Monitoring and analysis of stress field for orthotropic steel deck of dashengguan yangzte river bridge (eccomas congress 2016). xxvi, 108

Wang, Z. and Chen, W. (2017). Confidence-based adaptive extreme response surface for time-variant reliability analysis under random excitation. *Structural Safety*, 64:76 – 86. 71

Wang, Z. and Wang, P. (2012). A nested extreme response surface approach for time-dependent reliability-based design optimization. *Journal of Mechanical Design*, 134:121007–14. 67

Weertman, J. (1984). Crack growth for the double slip plane crack model-i. the r-curve. *Acta Metallurgica*, 32(4):563 – 573. 32

Williams, C. K. I. (1998). *Prediction with Gaussian Processes: From Linear Regression to Linear Prediction and Beyond*, pages 599–621. Springer Netherlands, Dordrecht. 56

Wirsching, P. H. (1984). Fatigue reliability for offshore structures. *Journal of Structural Engineering*, 110(10):2340–2356. 31, 32

Wright, S. and Nocedal, J. (1999). *Numerical Optimization*. Berlin: Springer. 55

Xiangqiao, Y., Shanyi, D., and Zehua, Z. (1992). Mixed-mode fatigue crack growth prediction in biaxially stretched sheets. *Engineering Fracture Mechanics*, 43(3):471 – 475. 148

Yang, S.-I., Frangopol, D. M., and Neves, L. C. (2004). Service life prediction of structural systems using lifetime functions with emphasis on bridges. *Reliability Engineering & System Safety*, 86(1):39 – 51. 23

Ye, X. W., Su, Y. H., and Han, J. P. (2014). A state-of-the-art review on fatigue life assessment of steel bridges,. *Mathematical Problems in Engineering*, pages 1–13. 24, 34

Yusof, M. (2014). Building investigation: Material or structural performance. volume 10. 11

Zapatero, J., Moreno, B., González-Herrera, A., and Domínguez, J. (2005). Numerical and experimental analysis of fatigue crack growth under random loading. *International Journal of Fatigue*, 27(8):878 – 890. Cumulative Fatigue Damage Conference - University of Seville 2003. 30

Zayed, A., Garbatov, Y., and Guedes Soares, C. (2013). Time variant reliability assessment of ship structures with fast integration techniques. *Probabilistic Engineering Mechanics*, 32:93 – 102. 135

Zhang, J. and Du, X. (2011). Time-dependent reliability analysis for function generator mechanisms. *Journal of Mechanical Design*, 133:031005–9. 63, 64

Zhu, A., Li, M., Zhu, H., Xu, G., Xiao, H., and Ge, H. (2018). Fatigue behaviour of orthotropic steel bridge decks with inner bulkheads. *Journal of Constructional Steel Research*, 146:63 – 75. 96

Zhu, B. and Frangopol, D. M. (2013a). Incorporation of structural health monitoring data on load effects in the reliability and redundancy assessment of ship cross-sections using bayesian updating. *Structural Health Monitoring*, 12(4):377–392. 37

Zhu, B. and Frangopol, D. M. (2013b). Reliability assessment of ship structures using bayesian updating. *Engineering Structures*, 56:1836 – 1847. 37

Zhu, Z., Xiang, Z., Li, J., Huang, Y., and Ruan, S. (2019). Fatigue behavior of orthotropic bridge decks with two types of cutout geometry based on field monitoring and fem analysis. *Engineering Structures*, page 109926. 95

Appendices

Annex A : Application of time series methods on long-term structural monitoring data for fatigue analysis

***Abstract*:** Structural health monitoring (SHM) can be employed to reduce uncertainties in different aspects of structural analysis such as: load modeling, crack development, corrosion rates, etc. Fatigue is one of the main degradation processes of structures that causes failure before the end of their design life. Fatigue loading is among those variables that have a great influence on uncertainty in fatigue damage assessment.

Conventional load models such as Rain-flow counting and Markov chains work under stationarity assumption, and they are unable to deal with the seasonality effect in fatigue loading. Time series methods, such as ARIMA (Auto-Regressive Integrated Moving Average), are able to deal with this effect in the data; hence, they can be helpful for fatigue load modelling. The goal of this study is to implement seasonal ARIMA to prepare a load model for long-term fatigue loading that can capture more details of the loading scenario regarding the seasonal effects in traffic loading.

A.0.1 Introduction

Structural Health Monitoring (SHM) plays an important role for the maintenance and inspection of existing structures. It helps in understanding the structure's condition for a better allocation of maintenance funding by reducing the uncertainties in degradation processes, like fatigue and corrosion among others (Long et al., 2018). Motorized traffic loading introduces large uncertainties due to its stochastic nature.

An appropriate load model is necessary for realistic structural analysis. Therefore, the main objective of this study is to provide the fatigue load model on the basis of long-term monitoring data by means of ARIMA (Auto-regressive integrated moving average).

SHM can be utilized to provide different types of information about the structure, and the monitoring duration is crucial. Monitoring of a longer duration can provide more precise information on the structure thanks to capturing the extreme events, seasonal effects in structural loading, etc. But the gaps due to limited lifetime of gauges, power outages and computer errors are difficult to avoid. On the other hand, processing and utilizing the data is another issue as its size can be enormous. The proposed method can help in dealing with these problems.

Several approaches can be identified in the literature to prepare a load model for structural fatigue analysis among which: cycle counting methods, like rain-flow counting; and random process methods, like Markov chain method, are most utilized (Khosrovaneh and Dowling, 1990). It should be noted that the load amplitudes are discretized into different levels in both approaches (Krenk and Gluver, 1989). Frequency domain-based and time domain-based methods can be used to provide the load model as a random process with a continuous state space. Application of the frequency domain-based methods for fatigue load modeling is complicated since all operations against fatigue, such as risk assessment, maintenance and inspection planning are performed in the time domain. Hence, time series methods that are defined in time domain can provide a more suitable load model. The prediction accuracy of ARMA (Auto Regressive Moving Average) as a time series method was compared with rain-flow counting and Markov chain methods (Ling et al., 2011). All the methods have acceptable performance based on Bayesian hypothesis testing, however ARMA performs better than the other methods.

It is worthy to mention that all previous methods are applicable on stationary data. However, in reality the fatigue loading might have a non-stationary behavior, especially because of seasonality in traffic and environmental loadings. Seasonality

refers to a seasonal pattern that can occur because of seasonal factors, such as the day of the week or time of the year. For instance, fatigue loading can experience a seasonality because of weekends when, the heavy traffic is reduced (Treacy, 2014). Among different time series methods, seasonal ARIMA is a strong tool that can be used for fatigue load modeling, and it is capable of dealing with seasonality. The goal of this research is to employ seasonal ARIMA to prepare a better load model for fatigue analysis being able to capture the seasonality effect. However, applying the seasonal ARIMA is not very straightforward on long-term loading data due to many observations within the seasonal window, understood as a period when the seasonal pattern occurs.

The reminder of this article is organized as following: in Section A.0.2 time series methods are reviewed; Section A.0.3 is related to the long-term monitoring data used in this study; the proposed approach for load modelling using long-term monitoring data is introduced in Section A.0.4 and a short conclusion is provided in Section A.0.5.

A.0.2 Time series methods: ARIMA

ARIMA

ARIMA is a time series method that combines Auto-Regressive (AR) and Moving Average (MA) models integrated with differencing. AR predicts the current value of a desired variable by a linear combination of the past values of that variable. The following equation shows an AR model of order p

$$y_t = c + \varphi_1 y_{t-1} + ... + \varphi_p y_{t-p} + \varepsilon_t \tag{A.1}$$

where: y_t is the predicted value of the desired variable, c is a constant value, ε_t is white noise, and $\varphi_i : i = 1, ..., p$ are the coefficients of AR model of order p.

The MA model uses the errors ε of the past values regarding to the mean value

of the data μ in a regression-like model to predict the current value for the desired variable according to Equation A.2.

$$y_t = \mu + w_1\varepsilon_{t-1} - ... - w_q\varepsilon_{t-q} \tag{A.2}$$

where $w_i : i = 1, ..., q$ are the coefficients of the MA model of order q.

An ARIMA model of order (p, d, q) (Equation A.3) is constructed by combining an AR of order p with MA of order q, where d is the degree of differencing.

$$y_t^{(d)} = c + \varphi_1 y_{t-1}^{(d)} + ... + \varphi_p y_{t-p}^{(d)} + \varepsilon_t + w_1\varepsilon_{t-1} - ... - w_q\varepsilon_{t-q} + \varepsilon_t \tag{A.3}$$

Seasonal ARIMA

Seasonal ARIMA can be constructed by adding the extra seasonal term into the non-seasonal ARIMA and it can be formulated as follows:

$$\text{seasonal ARIMA} = \underbrace{(p, d, q)}_{\text{non-seasonal part}} + \underbrace{(P, D, Q)}_{\text{seasonal part}} \tag{A.4}$$

P, D, and Q represent the parameters for the ARIMA model of seasonal behavior with m observations for each seasonal window. By removing the seasonal behavior, a non-seasonal ARIMA model with parameters p, d and q can be fitted to the residuals. In fact, the seasonal effect is removed from the data for sake of stationarizing, and the seasonal pattern can be modeled with another ARIMA.

Identification of the best ARIMA model

The first step to construct the ARIMA model is to find the orders p, q and the differencing degree d. The main purpose of application of the differencing is to stationarize the data. Hence, the best value for d is such that gives a stationary residual after differencing the data d-many times. Akaike's Information Criterion (AIC) is used to identify the orders p and q of an ARIMA model. AIC criteria can be formulated as:

$$AIC = -2Log(L) + 2(p + q + k + 1) \tag{A.5}$$

where L is the likelihood of the time series and $k = 0$ if $c = 0$, otherwise $k = 1$ (see Equation A.3).

Parameter estimation using maximum likelihood

After identifying the order of an ARIMA model, associated parameters (c; p_i; w_i; $i = 1, ..., p$; $j = 1, ..., q$) need to be approximated. One of the most common methods to estimate the parameters is Maximum Likelihood Estimation (MLE). MLE tries to approximate the parameters in a way such that the probability to obtain the observed data is maximized. MLE for ARIMA models is similar to least squares estimates that tries to minimize the square error between the observed and approximated data.

Model validation

One common way to test the model is to divide the available data into two parts: training and test data. Training data is used to fit the ARIMA and to estimate the model parameters. After defining the ARIMA model, it will be validated on test data to evaluate the accuracy of the model. More details about time series methods can be

found in (Hyndman and Athanasopoulos, 2018).

Figure A.1: Scheme of training and test data concept

A.0.3 Long-term monitoring data

In this study, the long-term monitoring data of Chillon viaducts was used. The Chillon viaducts are two parallel post-tensioned concrete structures in the Geneva lake region, Switzerland. The monitoring was commenced in 2016, after upgrading the structure with UHPFRC (Ultra High- Performance Fiber Reinforced Cementitious composite) (Brühwiler and Bastien Masse, 2015; Martin-Sanz et al., 2018). In this paper, the data coming from the strain gauges installed on the transversal rebars was used. The data is available for almost two years with some gaps. During the monitoring campaign, the signals from the strain gauges have been recorded with the frequency of 50, 100, or 200 Hz, depending on period.

Figure A.2 A shows an example of the raw data from one full day. The wave in data comes from the difference in temperature between day and night. Figure A.2 B shows the data after removing this thermal effect (Treacy, 2014). Additionally, only strain-reversal points of cycles bigger than 1 micro-strain were kept to reduce the size of data.

In the next section seasonal ARIMA is going to be used to prepare the load model utilizing the data from Autumn 2016. The reason of choosing this period was small amount of the monitoring interruptions. Since there is a linear relationship between the strain and stress values based on the Hook's law, the ARIMA model has been directly applied on the observed strains.

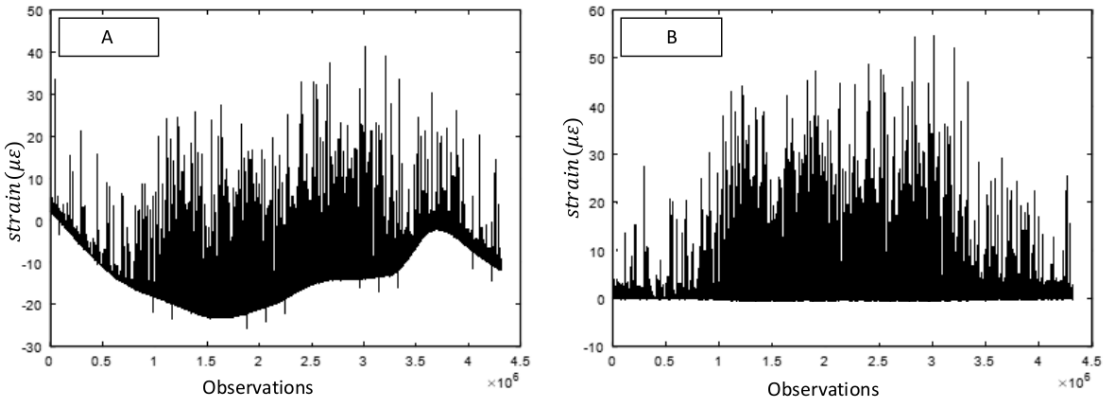

Figure A.2: A: raw data from the strain gauge from midnight to midnight, B: processed data from the strain gauge from same period.

A.0.4 Applying ARIMA to long-term strain data

Challenge

As it was mentioned before employing the ARIMA method on long-term monitoring data is not very straightforward. The difficulty is that the number of observations within a seasonal window is very large. If we consider that the seasonality window for traffic loading is one week (since there is a big difference between the loading experienced during the weekdays and weekends), the number of load cycles recorded in this period would be considerable (more than 10,000 cycles). This makes the process of applying seasonal ARIMA on the long-term load monitoring very difficult as the allowable observations within a seasonal window in conventional applications is around 350. However, in practice, for seasonal window larger than 200 observations available models in R and Python run out of memory. Hence, in the following part the data is treated differently to apply the seasonal ARIMA.

Proposed solution

To tackle the issue of a long seasonality window, the long-term monitoring data needs to be treated differently. For this reason, instead of considering each maximum or minimum value in the load data as a sample for time series analysis, the monitoring period was divided into shorter periods, such as monthly, weekly or daily. The aim is to define a probability distribution for the load cycles within each time interval. The parameters of the distributions will be used to replace the observations in the time series analysis. Hence, a few values (like mean value and standard deviation) can be employed to represent the big amount of observations in each period. Finally, time series analysis can be performed on the parameters of the distributions.

This transformation is well represented in Figures A.3 and A.4 where the former shows the strain values recorded for autumn 2016 and the latter shows the mean values for days and nights during autumn. The time interval used for this study is 12 hours, which divide the monitoring period into days and nights. This discretization strategy is used as the traffic flow during the day and night is different, and it is a reasonable period where there is no seasonality effect in the observations. Seasonal ARIMA can be used to prepare a load model for the monitoring data after this transformation.

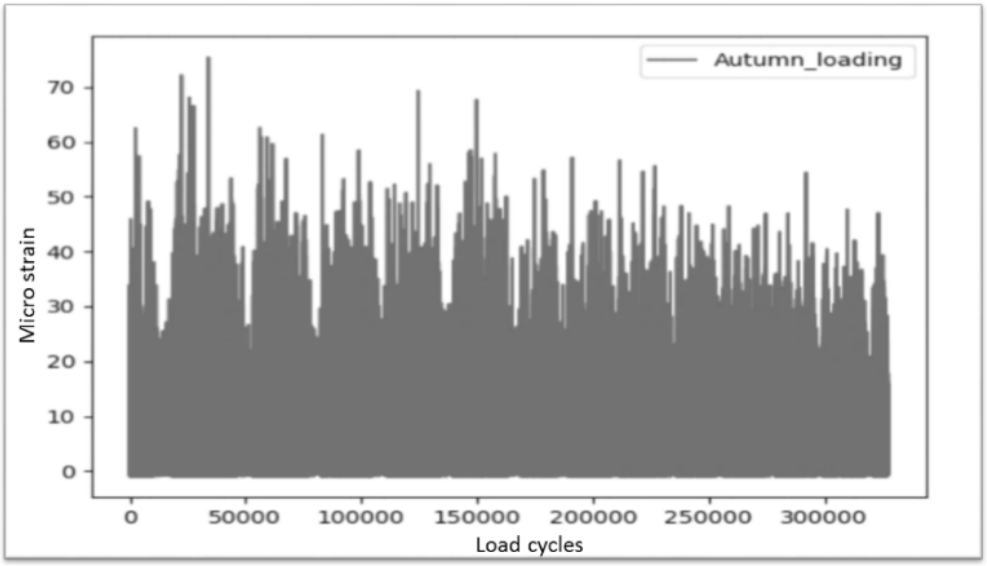

Figure A.3: Strain values recorded for autumn 2016

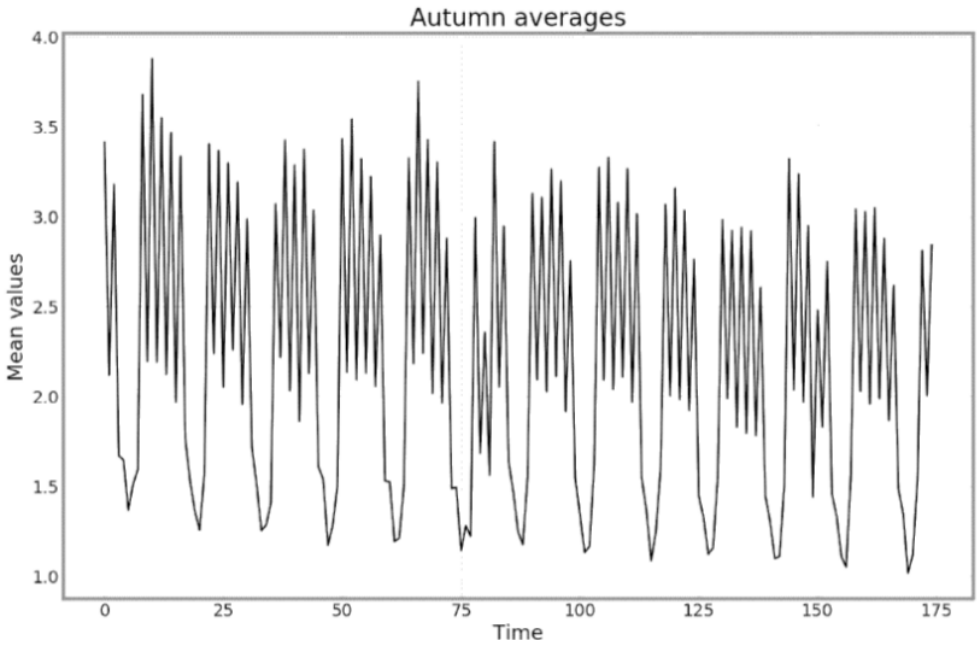

Figure A.4: Mean values for days and nights for autumn 2016

Seasonal ARIMA results

After the data transformation according to the previous section, seasonal ARIMA was applied on the mean values of the monitoring data for each 12 hours. As explained before, in seasonal ARIMA, the seasonal part of the data is removed first. It can be done by seasonal differencing as in the following equation, where m is the seasonality window. For our data it is equal to 14 (nights and days in a week).

$$y'_t = y_t - y_{t-m} \tag{A.6}$$

Two ARIMA models are fitted to the seasonal data and the residuals (as in Equation A.4). Figure A.5 illustrates the Q-Q plot and the correlogram on the residuals, showing that the seasonality is well removed and the residuals are fairly stationarized. KPSS (Kwiatkowski-Philips-Schmidt- Shin) stationarity test has been used to check the stationarity of the residuals. P-value of 0.79 confirms the good level of stationarity while the null hypothesis in KPSS is that the data is stationary. Table A.1 shows the

best ARIMA order that has the minimum AIC among other orders, and Table A.2 show the calculated parameters for the model using maximum likelihood estimation.

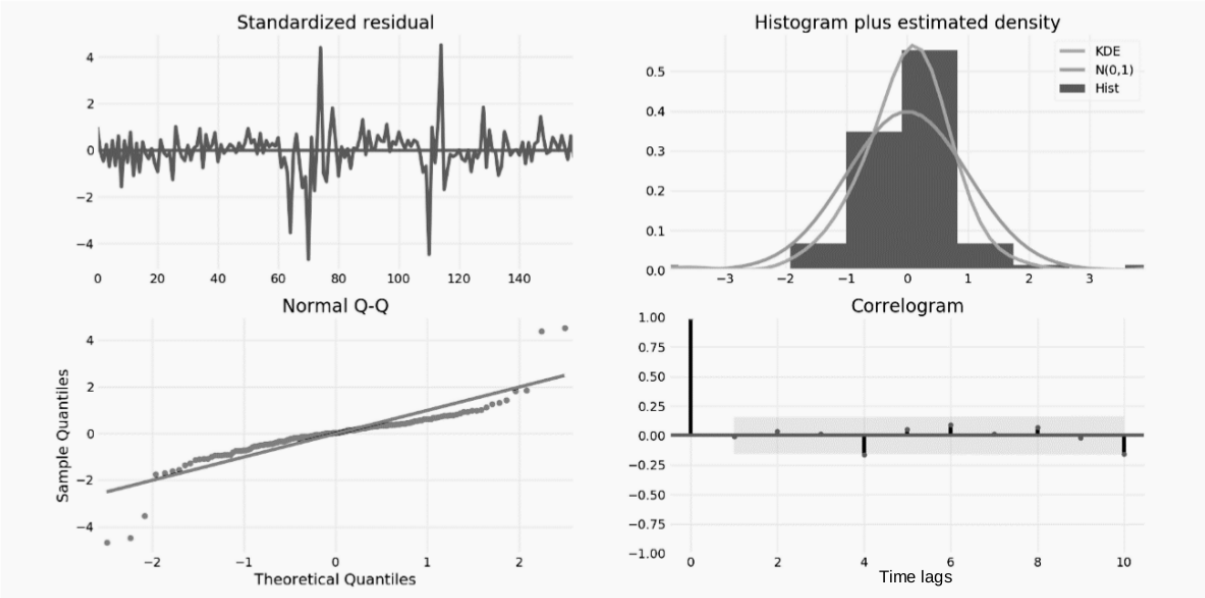

Figure A.5: Mean values for days and nights for autumn 2016

Table A.1: Best order for seasonal ARIMA using the minimum AIC

p	d	q	P	D	Q	m	AIC
2	0	1	1	0	1	14	86.2

Table A.2: Parameters for best seasonal ARIMA

φ_1	φ_2	w_1	φ_{1s}	w_{1s}
-0.38	0.62	0.99	0.96	-0.11

The last step is related to the model validation. As illustrated in Figure A.6, some part of the data is used as the training data and the rest as test data. The seasonal ARIMA prepared for this data and then this model is used to provide predictions for the test data. Comparison between the test data and the model predictions is provided by means of the 90% confidence interval for one step ahead forecasting (the shaded area). The one step ahead forecasting uses the previous observations to predict y_{t+1} . It can be seen that all the predictions are close enough to the test data and all of them are within the desired confidence interval.

The suggested seasonal ARIMA model in this section can provide a useful tool to reproduce the loading scenario on different structures for further applications such as structural fatigue life assessment. What makes this model different from previous models is that it can capture the seasonality effect in the loading and is easy to employ on the long-term monitoring data. On the other hand, this model can be used to deal with the missing monitoring data and to predict the future loading, since the seasonality effect is implemented inside this model.

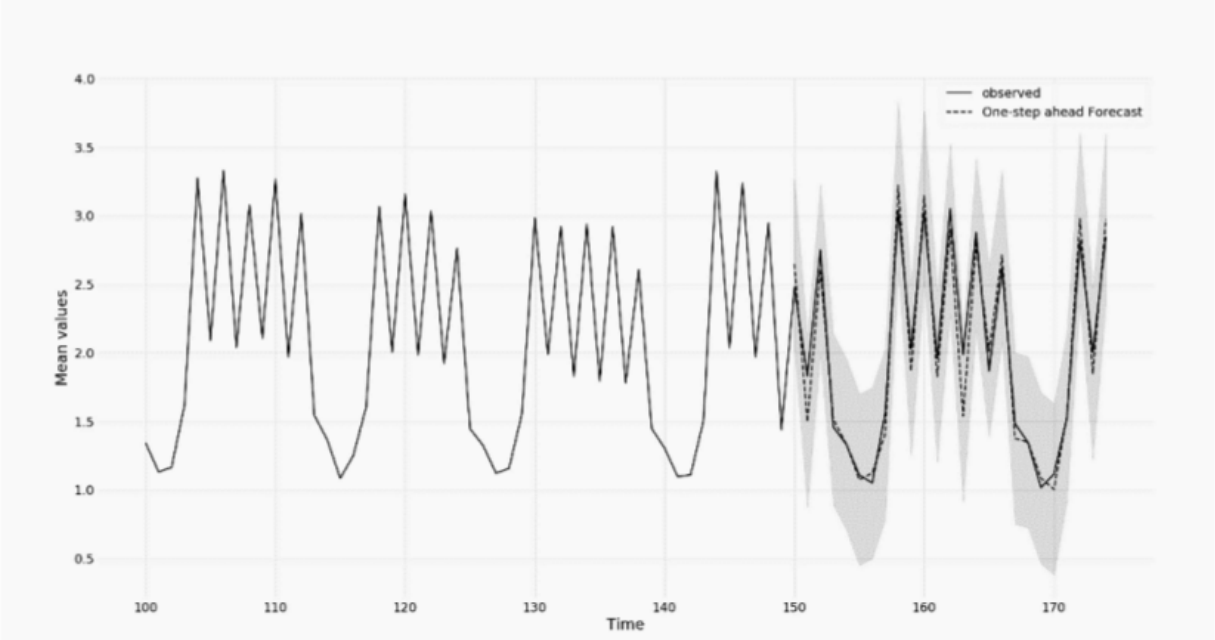

Figure A.6: Model validation

A.0.5 Conclusion and perspectives

Application of seasonal ARIMA on long-term monitoring data of traffic load effects is studied in this paper. It can help in understanding the seasonal behavior of the structure under motorized traffic. The difficulty related to the seasonality window on long-term loading data is its big size, which makes it very difficult to apply the seasonal ARIMA. The data transformation has been introduced in this study to tackle this difficulty. The new approach has been implemented on the long-term monitoring data on Chillon viaduct. Part of monitoring data was used for the model calibration, while the remaining for verification. A very good agreement between foreseen and measured values was obtained.

The proposed algorithm for load model preparation can be used not only for the fatigue life assessment, but also to deal with the missing monitoring data and to predict the future loading scenarios. To achieve this, the metamodels to transform the distribution time series into the load cycles should be further developed.

Annex B : Kriging meta-modeling

Kriging meta-modeling (Matheron, 1973) is based on the idea that any function $G(\mathbf{x})$ can be seen as a realization of a stationary process $Y(\mathbf{x}, w) \equiv Y(\mathbf{x})$ which can be expressed by a regression model $\mathbf{f}(\mathbf{x})^T\boldsymbol{\beta}$ and a stationary Gaussian process $Z(\mathbf{x})$. Accordingly, the desired function can be described by:

$$G(\mathbf{x}) = \mathbf{f}(\mathbf{x})^T\boldsymbol{\beta} + Z(\mathbf{x}) \tag{B.1}$$

where $\mathbf{f}(\mathbf{x}) = \{f_1(\mathbf{x}), ..., f_K(\mathbf{x})\}$ are the basis functions, $\boldsymbol{\beta}^t = \{\beta_1, ..., \beta_K\}$ are the regression coefficients in which K is the size of the set of the regression functions; $Z(\mathbf{x})$ is assumed to be a stationary Gaussian process with mean zero and its covariance between two points of space $\mathbf{x}$ and $\mathbf{w}$ is defined by:

$$Cov(Z(\mathbf{x}), Z(\mathbf{w})) = \sigma_z^2 R(\boldsymbol{\theta}, \mathbf{x}, \mathbf{w}) \tag{B.2}$$

in which σ_z^2 and R are respectively the variance and correlation function of the process. The correlation function is defined by its set of unknown parameters $\boldsymbol{\theta}$. Several types of correlation functions are available in the literature such as square exponential function, generalized exponential or Matern kernel. Square exponential function, also called as the Gaussian correlation function is one of the most used correlation functions which is formulated by Equation B.3

$$R(\boldsymbol{\theta}, \mathbf{x}, \mathbf{w}) = \exp(-\sum_{k=1}^{d} \theta_k(\mathrm{x}_k - \mathrm{w}_k)^2) \tag{B.3}$$

where x_k and w_k are the kth coordinates of the evaluation point $\mathbf{x}$ and the reference point $\mathbf{w}$ and θ_k is a scalar parameter that provides the multiplicative inverse of the correlation length in the ith direction.

According to the regression part, three types of Kriging are usually identified in the literature: the simple Kriging, ordinary Kriging, and universal Kriging. In simple Kriging, it is assumed that the trend of the regression is a known constant. In ordinary Kriging, the trend is still constant, however, its value is unknown. In universal Kriging, as it is formulated in Equation B.1, the regression trend is a sum of predefined functions $f_i(\mathbf{x})$, $i = 1, ..., K$ multiplied with unknown coefficients β_i which are required to be determined. It should be noted that simple and ordinary Kriging are simplified versions of the universal Kriging.

To provide the Kriging meta-model $\hat{G}$ for a given function G of dimension d, one requires to define the parameters: σ and $\boldsymbol{\beta}$. According to the information provided by design of experiment $\{\mathbf{X}, \mathbf{G}\}$ of size N_{DoE} where $\mathbf{X} = [\mathbf{x}^{(1)}, ..., \mathbf{x}^{(N_{DoE})}]$ and $\mathbf{G} = [G(\mathbf{x}^{(1)}), ..., G(\mathbf{x}^{(N_{DoE})})]$, and the given correlation function, the desired parameters can be obtained by following equations:

$$\hat{\boldsymbol{\beta}}(\boldsymbol{\theta}) = (\mathbf{F}^T\mathbf{R}^{-1}\mathbf{F})^{-1}(\mathbf{F}^T\mathbf{R}^{-1}\mathbf{G}) \tag{B.4}$$

$$\hat{\sigma}^2(\boldsymbol{\theta}) = \frac{1}{N_{DoE}}(\mathbf{G} - \mathbf{F}\hat{\boldsymbol{\beta}})^T\mathbf{R}^{-1}(\mathbf{G} - \mathbf{F}\hat{\boldsymbol{\beta}}) \tag{B.5}$$

where $\mathbf{F}$ is defined as: $F_{ij} = f_j(\mathbf{x}^{(i)})$, $i = 1, ..., N_{DoE}$, $j = 1, ..., K$, and $\mathbf{R}$ is the correlation matrix of size $N_{DoE} \times N_{DoE}$ which defines the correlation between each pair of points of the design of experiments determined by equation B.3. It should be noted that the vector of correlation coefficients $\hat{\boldsymbol{\beta}}$ and the process variance $\hat{\sigma}^2$ depend on the vector of correlation parameters $\boldsymbol{\theta}$ through he correlation matrix $\mathbf{R}$. The optimal values for the correlation parameters θ_k, $k = 1, ...d$ can be identified using maximum likelihood estimation as:

$$\boldsymbol{\theta}^{opt} = \underset{\boldsymbol{\theta}}{\operatorname{argmin}}(\frac{1}{N_{DoE}}(\mathbf{G} - \mathbf{F}\boldsymbol{\beta})^T\mathbf{R}^{-1}(\mathbf{G} - \mathbf{F}\boldsymbol{\beta})(\det\mathbf{R})^{1/N_{DoE}}) \tag{B.6}$$

The next step after identifying the Kriging parameters is to predict the value of the performance function for an unmeasured sample $\mathbf{x}^*$. At such point, the Best Linear Unbiased Predictor (BLUP) $\hat{G}(\mathbf{x}^*)$ of $G(\mathbf{x}^*)$ is calculated by the following equation:

$$\hat{G}(\mathbf{x}^*) = \mathbf{f}(\mathbf{x}^*)^T\boldsymbol{\beta} + \mathbf{r}(\mathbf{x}^*)^T\mathbf{R}^{-1}(\mathbf{G} - \mathbf{F}\boldsymbol{\beta}) \tag{B.7}$$

where $\mathbf{r}(\mathbf{x}^*)$ is the correlation vector between the desired sample point and other points calculated by Equation B.3.

The Kriging variance $\sigma^2_{\hat{G}}(\mathbf{x}^*)$ is defined as the minimum of the mean squared error between $\hat{G}(\mathbf{x}^*)$ and $G(\mathbf{x}^*)$ and it can be formulated by the following Equation:

$$\sigma^2_{\hat{G}}(\mathbf{x}^*) = \sigma^2 \left(1 - \langle \mathbf{f}(\mathbf{x}^*)^T \mathbf{r}(\mathbf{x}^*)^T \rangle \begin{bmatrix} \mathbf{0} & \mathbf{F}^T \\ \mathbf{F} & \mathbf{R} \end{bmatrix}^{-1} \begin{bmatrix} \mathbf{f}(\mathbf{x}^*) \\ \mathbf{r}(\mathbf{x}^*) \end{bmatrix} \right) \tag{B.8}$$

This is a very important feature of Kriging meta-modelling since for each new model approximation $\hat{G}(\mathbf{x}^*)$, it also provides a measure of the local epistemic uncertainty of prediction $\sigma^2_{\hat{G}}(\mathbf{x}^*)$. It should be noted that the calculation of the Kriging variance is done at the same level as $\hat{G}(\mathbf{x}^*)$ and it does not require additional computational time. Another great characteristic of Kriging meta-modeling is that it is an exact interpolation. It means that the prediction of the meta-model for the sample points of DoE is exact and the Kriging variance for such points is null.